Live-Load Response of In-Service Bridge Constructed with Precast, Prestressed Self-Consolidating Concrete Girders

by

David Eric Miller

A thesis submitted to the Graduate Faculty of
Auburn University
in partial fulfillment of the
requirements for the Degree of
Master of Science

Auburn, Alabama
December 14, 2013

Key words: Self-Consolidating Concrete, SCC, Live-Load Test

Approved by

Robert Barnes, Chair, Associate Professor of Civil Engineering
Anton Schindler, Professor of Civil Engineering, Director of Highway Research Center
Michael Stallings, Professor of Civil Engineering

Abstract

In order to assess the viability of a bridge constructed with precast, prestressed, self-consolidating concrete (SCC) bridge girders in the state of Alabama, the Alabama Department of Transportation (ALDOT) sponsored an investigation to be performed by the Auburn University Highway Research Center. Researchers instrumented twenty-eight bulb-tee girders in a replacement bridge constructed on State Route 22 over Hillabee Creek in Tallapoosa County, Alabama. Two spans of the bridge were constructed using girders composed of SCC while two companion spans were constructed using girders composed of vibrated concrete (VC). The bridge was subjected to two live-load tests—one shortly before the bridge was opened to traffic and one after a year of bridge service. A finite-element model (FEM) of the bridge was also created using CSiBridge. Bridge test results and FEM predictions were analyzed in order to evaluate the acceptability and predictability of in-place SCC girder performance when subjected to design-level service loads.

In addition, the accuracy of superstructure analysis techniques—including AASHTO LRFD distribution factors as well as refined analysis (FEM)—were evaluated using the measured flexural response of the prestressed concrete bridge girders subjected to truck loads. Furthermore, adjusted FEMs were used to assess the effects of cast-in-place traffic barriers and intermediate diaphragm alignment on the distribution of service-level truck loads to individual bridge girders.

Based on experimental observations, it was concluded that the service-level live-load behavior of SCC girders is acceptably similar to that of VC girders. The bridge response to service loads experienced no significant deterioration after one year of service conditions. AASHTO LRFD Bridge Design Specifications (2012) methods for determining load distribution to girders within a span were determined to be generally accurate, but overly conservative in some instances and slightly *unconservative* in others. The inclusion of traffic barriers in analysis tended to make a significant difference in the behavior of exterior bridge girders. Intermediate webwall orientation was found to have only a small effect on transverse load distribution.

Acknowledgements

I would like to thank my committee chair, Dr. Robert Barnes, for his countless hours of wisdom and guidance provided throughout the data collection and thesis writing process. Without his help this project would not have been possible. I would also like to thank my fellow graduate students for assisting in performing the load tests including Tyler Neal, Brandon Johnson, Dave Mante, Andric Hofrichter, Zach Skinner, and Patrick Koch. A special thank you to Sam Keske for his long hours logged at the bridge and in the lab in preparation for load tests. I would also like to thank the Auburn University Highway Research Center and the Alabama Department of Transportation. Finally, I would like to thank my family and friends, my fiancé, Heather, for her unwavering patience and support during my most stressful moments as a student, and my parents, David and Lisa, who instilled the discipline and educational foundation necessary for me to complete this thesis. Words cannot describe how much I appreciate their years of endless love and support.

Table of Contents

List of Tables

List of Figures

Abbreviations

AASHTO	American Association of State Highway and Transportation Officials
ALDOT	Alabama Department of Transportation
BT-54	Bulb-tee girder 54 inches in height
BT-72	Bulb-tee girder 72 inches in height
FEM	Finite-element modeling
LRFD	Load and Resistance Factor Design
PCI	Precast/Prestressed Concrete Institute
SCC	Self-consolidating concrete
VC	Vibrated concrete
VWSG	Vibrating-wire strain gauge

Chapter 1 Introduction

1.1 Background

Precast, prestressed girders are currently used in bridges across the state of Alabama. New concrete materials are being introduced for girder construction including self-consolidating concrete (SCC). SCC girders have been tested in laboratory conditions for several parameters including transfer length, development length and flexural behavior (Boehm 2010), service load performance (Zia et al. 2005), and in comparison with vibrated concrete (VC) girders (Ozyildirim 2008; Trejo et al. 2008) but have not been tested under truck loads in a full-scale, beam-slab bridge. In order to assess the viability of a bridge constructed with precast, prestressed, SCC bridge girders in the state of Alabama, the Alabama Department of Transportation (ALDOT) sponsored an investigation to be performed by Auburn University researchers. Staff from the Auburn University Highway Research Center attached deformation sensors to twenty-eight bulb-tee girders in a replacement bridge constructed on State Route 22 over Hillabee Creek in Tallapoosa County, Alabama (Figure 1.1). Two of the spans of the bridge were constructed using girders composed of self-consolidating concrete (SCC) while the remaining two spans were constructed using girders composed of vibrated concrete (VC). The bridge was subjected to two subsequent live-load tests, allowing for the performance of spans containing SCC girders to be compared to that of spans containing VC girders.

Figure 1.1. *Load trucks on Span 2 (SCC Girders) of the Hillabee Creek Bridge during testing.*

AASHTO LRFD Bridge Design Specifications introduced a live-load distribution equation for beam-slab bridges as a result of the NCHRP 12-26 project (Zokaie, Osterkamp, and Imbsen 1991). This equation is based on elastic finite-element analyses. It is considered to be a good representation of bridge behavior. However, Sotelino et al. (2004) point out the finite-element model used in developing the LRFD distribution factor equation did not include some important features of bridges which may affect lateral load distribution such as webwalls (diaphragms) and barriers. A simplified method of finite element analysis could be used to more accurately predict the effects of diaphragms and webwalls for service-load design in beam-slab bridges.

Huo, Wasserman, and Zhu (2004) point out that simplified, efficient finite-element modeling techniques may be needed when bridges fall outside of the parameters outlined for distribution factor design aides in the AASHTO LRFD Bridge Design Specifications (2012) and agree with previous research (Barr, Eberhard, and Stanton 2001) suggesting that finite-element-based distribution factors are less conservative than those set forth in AASHTO LRFD (2012), leading to reduced construction costs.

Barnes, Stallings, and Porter (2003) also determined that the AASHTO LRFD (2012) distribution factor methods were conservative, especially for exterior girders, when compared to

load-testing data. The researchers suggested further research be conducted for bridges with barriers acting compsitely with the deck under service loads. They also proposed that more complex finite-element analyses be utilized to determine the effect of in-span diaphragms on transverse load distribution in beam-slab bridges.

1.2 Research Objectives

Specific objectives of the research described in this thesis are stated below:

1. Analyze and evaluate the acceptability and predictability of in-place SCC girder performance when subjected to design-level service loads.
2. Evaluate the effectiveness of modern superstructure analysis techniques for determining the flexural response of prestressed concrete bridge girders when subjected to truck loads.
3. Assess the effects of cast-in-place barriers and webwalls on the distribution of service-level truck loads to individual bridge girders.

1.3 Research Scope

Bottom-surface flexural strains and midspan deflections, resulting from an applied live-load were measured for each of the twenty-eight girders and utilized to compare the performance of spans with SCC girders to that of spans with VC girders. The applicability of the principle of superposition to service-level bridge behavior was verified. Live-load strains and deflections were predicted for each of the twenty-eight girders utilizing CSiBridge modeler and were compared to measured field results. The expected distribution of lane load was computed using AASHTO LRFD Bridge Design Specifications (2012) and compared to service-load distribution observed during bridge load testing.

1.4 Organization of Thesis

Chapter two contains project-applicable topics previously completed by others. This research includes the AASHTO LRFD Bridge Design Specifications requirements for an accurate finite-element bridge model as well as a description of the finite-element program used to complete a portion of the required research for this project. The chapter also contains an overview of AASHTO LRFD Bridge Design Specifications manual requirements pertaining to the transverse distribution of load to each of the girders within each span of the bridge.

Chapter three includes the placement and orientation of all surface and vibrating-wire strain gauges used in each of the load tests and also gives an overall description of the in-situ bridge that was tested. It also contains information pertaining to the devices used to measure the deflection of the bridge during the load tests. Finally, chapter three describes the devices used to record the load test data and the notation used to distinguish each strain gauge and deflectometer.

Chapter four is an outline of the load testing procedures used for both of the load tests. It includes the load truck configuration and the resulting weight per axle. It also details the truck placement and procedures as well as the ambient conditions and traffic control measures that were necessary during either of the load tests.

The steps and procedures for constructing the finite-element bridge models utilizing the CSiBridge program are presented in Chapter five. This chapter addresses the three different models constructed for analysis and comparison to the experimental results from the bridge.

Chapter six comprises the results from this project. It begins with a discussion of how the measured strains from the vibrated concrete girders were modified to simulate having a modulus of elasticity equivalent to those of their SCC counterparts. A confirmation of the hypothesis that superposition is appropriate to use on the bridge is then presented with

comparisons of the behavior of SCC girders versus the CVC girders following. The measured field results are compared to results garnered from models of the bridge constructed utilizing CSiBridge modeler software. Lastly, the transverse behavior of the bridge under live load is presented and discussed.

Chapter seven concludes the document, reiterating the discussion and results and providing final conclusions from the study.

Chapter 2 Literature Review

2.1 Introduction

This chapter contains a review of previously published research and methods pertinent to the objectives of this research including previous service-load testing of SCC girders, transverse live-load distribution in beam-slab bridges with precast concrete girders, AASHTO LRFD Bridge Design Specifications (2012) finite-element modeling requirements, and a review of the CSiBridge modeling program.

2.2 Previous Service Load Testing of SCC Girders

Laboratory research on SCC girders has been conducted on a small scale for both fresh and hardened properties (Keske, Schindler, and Barnes 2013; Zia et al. 2005; Naito et al. 2005), time-dependent deformations (Erkmen, French, and Shield 2008), and compared to VC girder ultimate flexural behavior (Kim 2008) as well as the full range of flexural behavior with a composite, cast-in-place deck (Boehm, Barnes, and Schindler 2010). SCC girders have also been tested under field conditions for time-dependent deformations prior to placement (Johnson 2012) and for time-dependent performance after placement and deck casting (Ozyildirim and Davis 2008; and Zia et al. 2005).

2.2.1 Laboratory Comparison of SCC Girders to VC Girders under Service Loads

Zia et al. (2005) studied two SCC girders and one VC girder cast from a set of five girders (three VC) being produced for a multispan, beam-slab bridge in eastern North Carolina. The researchers loaded two separate precast, prestressed SCC AASHTO Type III girders. The 54.8 ft long AASHTO Type III girders were initially loaded to 12.4 kips as a point load at

midspan, and increased incrementally by 6.2 kips up to 55.8 kips. At each load increment, midspan girder deflection was measured. No girder cracking was observed and full girder deflection recovery occurred after the removal of the applied load. This result indicated that the SCC girders remained fully elastic under service loading (Zia et al. 2005). The researchers determined that when subjected to service loads, the SCC and VC girders "exhibited virtually identical" load-deflection relationships thus clearing the SCC girders to be placed in the bridge.

2.2.2 Laboratory Comparison of SCC Girders to VC Girders with Composite Decks

Boehm, Barnes, and Schindler (2010) tested two SCC high-strength, two SCC moderate-strength and two VC moderate-strength AASHTO Type I, precast, prestressed girders 40 ft in length with a composite, 3.5 in. thick by 48 in. wide deck under laboratory conditions. The girders were subjected to flexural testing in the three configurations shown in Figure 2.1. Each girder was tested once on each end of the girder for a total of twelve tests. For each group of two girders, the west end of the first was tested in the first condition displayed in the figure. The east end was then tested in the second configuration from the figure. The second beam was tested on both ends in the third figure configuration. This sequence was repeated for the remaining four girders. Under service loads, deflections were well predicted for the most flexural test configuration for each type of concrete. A slightly higher and more accurately predicted stiffness was apparent for the two SCC girders when compared to the VC girder.

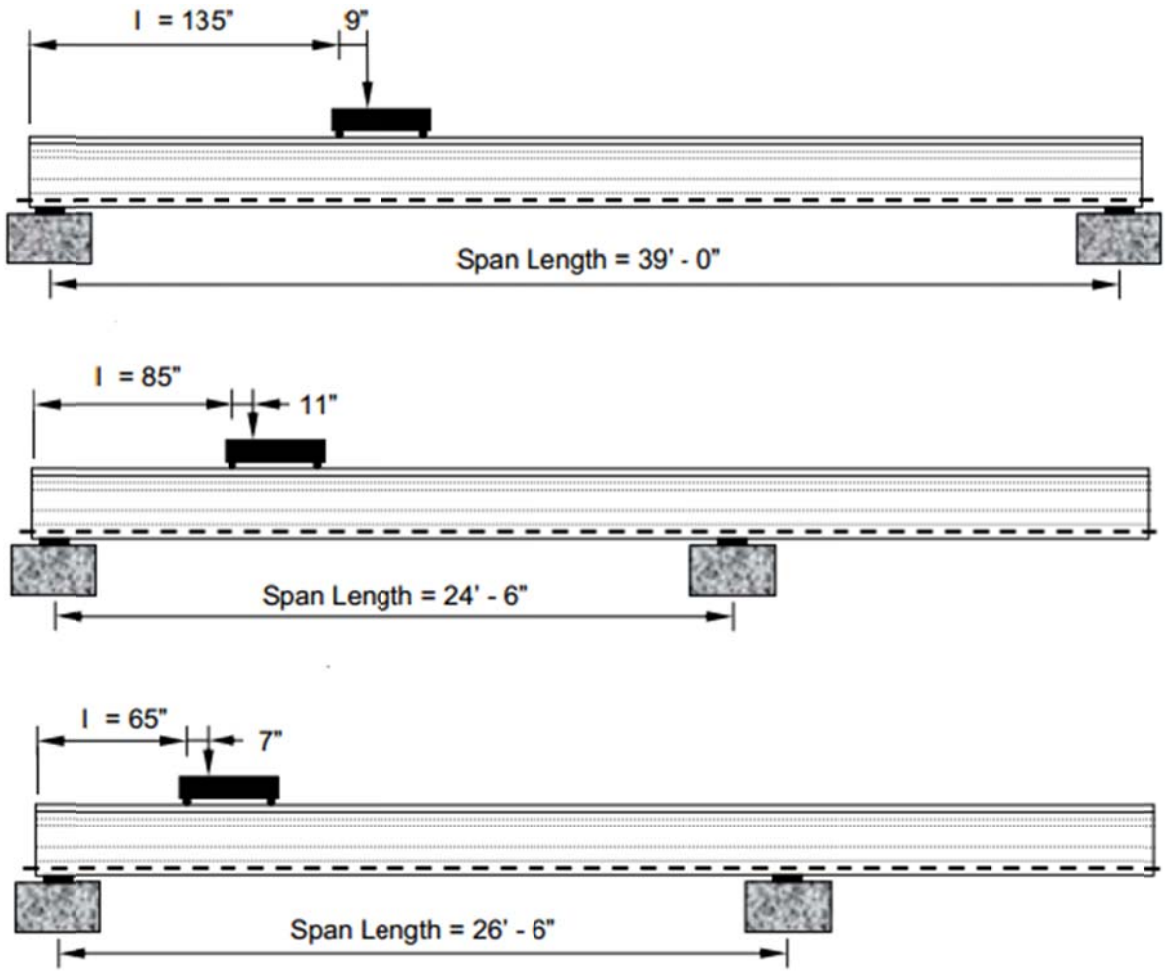

Figure 2.1. *Boehm, Barnes, and Schindler (2010) flexural testing configuration.*

Trejo et al. (2008) tested two SCC and two VC, precast, prestressed, 28 in. deep, Texas DOT Type A girders 40 ft in length and containing a deck applied to the girders at a girder age of approximately seven weeks. The deck for each girder was 64 in. wide and 8 in. thick and were cast-in-place directly onto the girders. The girders were tested flexurally as depicted in Figure 2.2. The researchers determined the measured nominal moments for all girders were as much as 12% larger than the predicted values utilizing the proper AASHTO expression that utilized actual compressive strength values. The SCC girder-deck systems had slightly higher nominal moment values relative to the companion conventional concrete girder-deck systems.

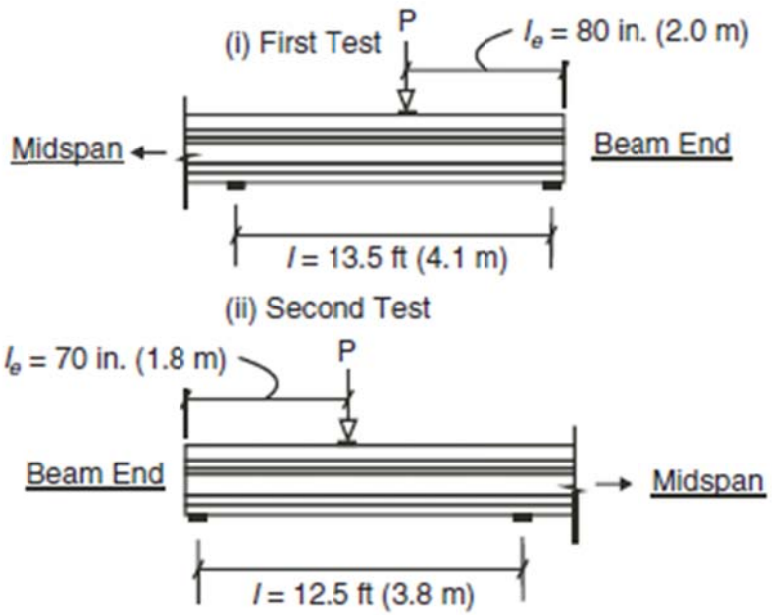

Figure 2.2. *Flexural test setup for precast, prestressed SCC beams* (Trejo et al. 2008)

2.2.3 Laboratory Testing of the Flexural and Shear Strength of SCC Girders

Ozyildirim and Davis (2008) found through testing of two, 45 in. bulb-tee, precast, prestressed beams, 60 feet in length, that the girders performed as expected in flexure and shear. The beams were tested in four combinations of moment and shear to induce various shear, flexure, and flexure-shear failures. Strand development failure was never realized and strand slip was minimal. The team concluded the results indicated the test beams could reach nominal flexural capacity as determined by sectional analysis. This conclusion led the team to propose the use of eight SCC girders in a span in the Virginia Route 33 Bridge over the Pamunkey River. The two center girders in that span as well as the two center VC girders in an adjacent span were instrumented with VWSGs and utilized in the bridge. The researchers reported that the averaged performance for all four instrumented beams have been similar in service (Figures 2.3 and 2.4).

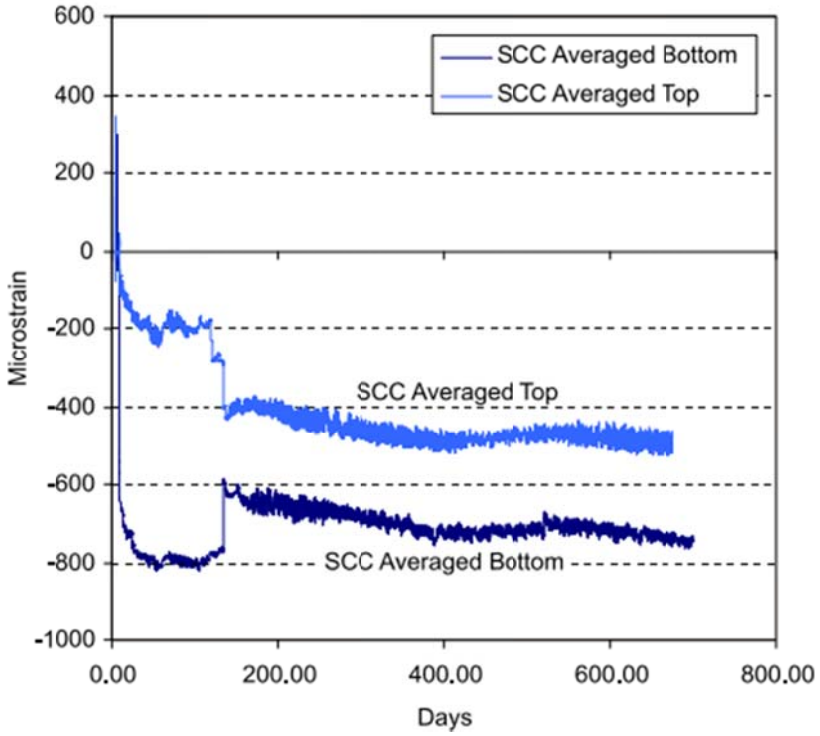

Figure 2.3. Averaged SCC girder strains from tensioning through service (Ozyildirim and Davis 2008).

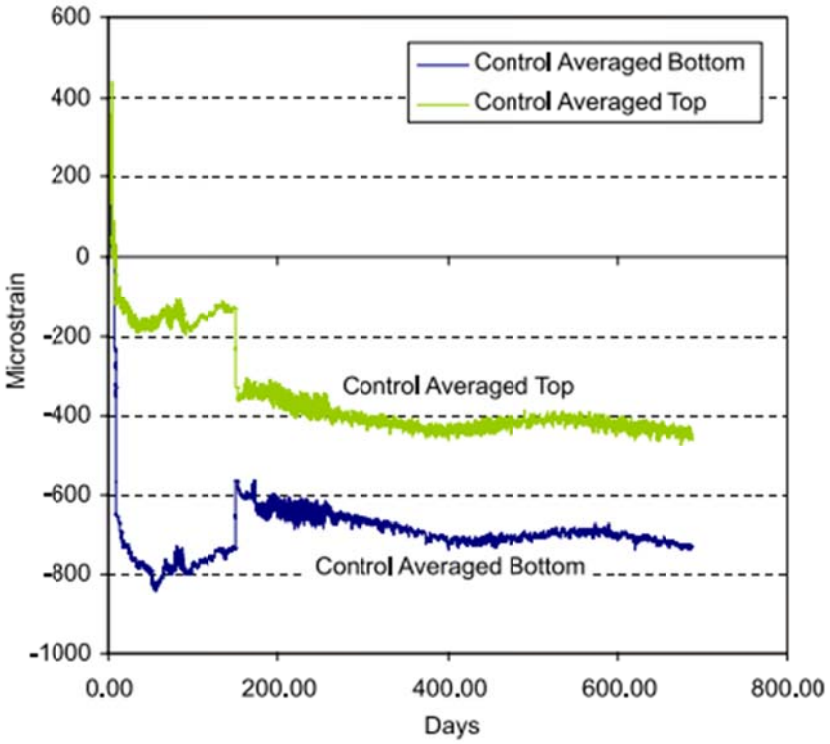

Figure 2.4. Averaged VC girder strains from tensioning through service (Ozyildirim and Davis 2008).

While previous research compared SCC girders to VC girders, it was done so under lab conditions, not to the scale of the Hillabee Creek bridge (volume, span length, or prestressing demand) and did not include in-situ live-load testing. Large-scale, in situ load-testing is crucial to the evaluation of SCC girders in bridges with precast, prestressed girders because they represent direct load-response comparisons of in-service SCC and VC girders.

2.3 Transverse Live-Load Distribution in Beam-Slab Bridges with Precast Concrete Girders

Transverse load distribution between girders reflects a bridge's response to applied truck loads. Load distribution is a function of many parameters such as bridge geometry, relative stiffness of bridge components, static or dynamic loading, and load state (service versus ultimate strength) (Cai 2005). Transverse load distribution is used for design purposes to determine the critical load effects for design of each girder. A critical girder is a girder that experiences the most critical load effects and therefore usually controls the design of the other girders in bridge span. A load distribution factor is the maximum portion of one-lane loading that is resisted by a single girder and is determined for the critical girder of a span. The following discussion is limited to static load distribution factors for moment effects only on a beam-slab bridge with precast, prestressed girders.

2.3.1 LRFD Transverse Load Distribution Research

Huo, Wasserman, and Zhu (2004) point out that the live load distribution factors found in AASHTO LRFD Bridge Design Specifications (2012) have been verified with finite-element analyses and have been calibrated against a database of real bridges with certain ranges of properties such as span length, moment of inertia of beams, and beam spacing (Zokaie, Osterkamp, and Imbsen 1991). The key parameters considered for live load distribution in AASHTO LRFD Bridge Design Specifications (2012) are beam spacing, span length, skew,

longitudinal beam stiffness, and slab thickness. Longitudinal beam stiffness integrates the beam area, beam moment of inertia, and beam eccentricity with respect to the deck. However, this method does not include effects for unequal span lengths for continuous bridges or intermediate diaphragms. The LRFD distribution factor method is considered to be most accurate when the bridge has uniform beam stiffness and equal spans. In order to use AASHTO LRFD Bridge Design Specifications (2012) distribution factor equations, several bridge parameters must fall within a specified range of applicability. Though the equations are accurate within this range, additional refined analysis must be performed by the engineer when any of the parameters fall outside of the applicable range (Huo, Wasserman, and Zhu 2004). This limitation results in the need for a fast, accurate, and efficient way for the engineer to model a bridge that falls outside of these aforementioned parameters or may contain intermediate diaphragms or uneven span lengths.

Barr, Eberhard, and Stanton (2001) determined the effect of several parameter variations in prestressed concrete girder bridges. Lifts, or haunches, were found to slightly lower the live-load distribution factor in critical girders. The researchers determined that intermediate diaphragms had little to no effect on distribution factors for both interior and exterior girders. End diaphragms were found to affect distribution factors in two ways. The first was through inhibiting end rotation of the critical girder, distributing rotation to adjacent girders, thus reducing the distribution factor. The second mechanism applied to skewed bridges. The skewed end diaphragms created an end moment condition when girders were loaded at midspan, reducing distribution factors increasingly as skew increased. The researchers also found that as the skew of the bridge increased, distribution factors tended to decrease for both interior and exterior girders. Research from Huo, Wasserman, and Zhu (2004) was consistent with Barr,

Eberhard, and Stanton (2001) in concluding that utilizing finite element techniques to determine distribution factors over AASHTO LRFD Bridge Design Specifications techniques would have resulted in fewer required strands, reduced concrete strength required at prestress transfer, or allowed for an increase in span length.

2.3.2 AASHTO LRFD Bridge Design Specifications (2012) Distribution Factor Requirements for Beam-Slab Bridges

In order to use the AASHTO LRFD Bridge Design Specifications (2012) distribution factor process for bridge design, the bridge must meet several geometric requirements (AASHTO LRFD 4.6.2.2.2):

- The bridge must be either straight or horizontally curved
- Deck thickness must be between 4.5 in. and 12 in.
- The roadway part of the deck overhang must not exceed 3.0 ft
- The bridge may have no less than four beams
- Beams must be parallel and have approximately the same stiffness
- Deep, rigid end diaphragms must be provided
- Beam-stem spacing must be between 3.5 ft and 16 ft to avoid refined analysis requirements
- Span length must be between 20 ft and 240 ft while the longitudinal flexural stiffness of the span must be between 10,000 in.^{4} and 7,000,000 in.^{4}
- Bridge cross-section must be consistent with one of the cross-section types shown in Table 4-6.2.2.1-1 (AASHTO 2012)

The loads applied to the bridge must also conform to certain specifications. The bridge must be analyzed for a single lane of loading or multiple lanes of live load yielding

approximately the same force effect per lane. It also specifies that multiple presence factors shall not be used with the approximate load assignments due to the fact that they are already accounted for in the distribution factor equations. An exception to this requirement occurs when the statical moment or lever arm methods are used. The stiffness parameters for area, moments of inertia, and torsional stiffness shall be taken as those of the cross section to which traffic is applied, i.e., the composite section (AASHTO 2012).

2.3.3 Utilizing AASHTO LRFD Bridge Design Specifications 2012 to Determine Live-Load Distribution

The AASHTO LRFD process for determining distribution factors for design is described in this section. Interior girder requirements are discussed first followed by exterior girders and the exterior girder alternate method. Application of this process is limited to bridge superstructures that satisfy the conditions listed in the previous section.

2.3.3.1 Multiple Presence of Live Load in Bridge Design

Multiple presence of live load is addressed in 3.6.1.1.2 of the AASHTO LRFD Bridge Design Specifications manual. Multiple Presence Factors (MPFs) are displayed in Table 3.6.1.1.2.1 (AASHTO 2012). MPFs address the probability that heavy trucks may appear on a highway bridge span in one or more lanes simultaneously (Fu, Liu, and Bowman 2013). Most codes set one lane loaded as the reference load case. However, AASHTO LRFD specifications set two lanes loaded as a reference with an MPF value of 1.0. Kulicki et al. (2007) explain that the one-lane loaded load effects then need to be factored higher to account for real load effects possibly higher than the notional HL93 load truck. MPFs are already incorporated in AASHTO LRFD equations for calculating distribution factors *except* when the lever rule and alternate

exterior girder method in C4.6.2.2.2d are required. When the lever rule or alternate exterior girder method is employed, the result must be multiplied by the correct MPF.

2.3.3.2 Interior Girders

Section 4.6.2.2.1 of AASHTO LRFD Bridge Design Specifications 2012 gives equation 4.6.2.2.1-1 for longitudinal stiffness as:

$$K_g = n\left(I + Ae_g^2\right) \qquad (2-1)$$

in which:

$$n = \frac{E_B}{E_D} \qquad (2-2)$$

where:

E_B= modulus of elasticity of beam material (ksi)

E_D= modulus of elasticity of deck material (ksi)

I= moment of inertia of beam (in.^{4})

e_g= distance between the centers of gravity of the basic beam and deck (in.)

A= area of beam (in.^{2})

K_g, known as the longitudinal stiffness parameter, was introduced in AASHTO LRFD by Zokaie, Osterkamp, and Imbsen (1991) to increase the accuracy of the distribution factor equations. The parameter is the area moment of inertia of the girder taken with respect to the centroid of the deck transformed to the equivalent of the entire composite section being composed of deck concrete. Table 4.6.2.2.1-1 provides typical cross-sections and supporting component material choices for the bridge. Once the appropriate cross section is selected, section 4.6.2.2.2b and table 4.6.2.2.2b-1 give the following equations for the distribution of lane live load:

One Design Lane Loaded:

$$g = 0.06 + \left(\frac{S}{14}\right)^{0.4}\left(\frac{S}{L}\right)^{0.3}\left(\frac{K_g}{12.0Lt_s^3}\right)^{0.1} \quad (2-3)$$

Two or More Design Lanes Loaded:

$$g = 0.075 + \left(\frac{S}{9.5}\right)^{0.6}\left(\frac{S}{L}\right)^{0.2}\left(\frac{K_g}{12.0Lt_s^3}\right)^{0.1} \quad (2-4)$$

where:

g=distribution factor

K_g= longitudinal stiffness as defined above (in.)

S= center to center girder spacing (ft)

L= length of the span (ft)

t_s= thickness of the deck (in.)

2.3.3.3 Exterior Girders

Table 4.6.2.2.2d-1 gives the equations for distribution of live loads per lane to exterior girders as:

One Design Lane Load:

Use Lever Rule. The Lever Rule is addressed in the commentary of section 4.6.2.2.1. Within that commentary, AASHTO LRFD Bridge Design Specifications 2012 describes that "the lever rule involves summing moments about one support to find the reaction at another support by assuming that the supported component is hinged at interior supports" (see Figure 2.5). The resulting "reaction" on the exterior girder divided by the applied lane load between the assumed hinge and the barrier gives the portion of the lane load distributed to the exterior girder.

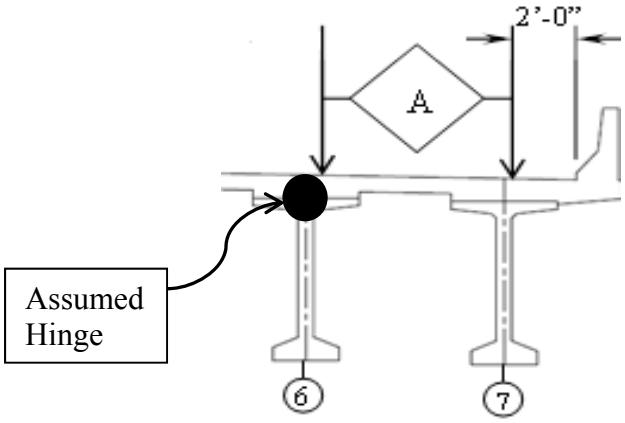

Figure 2.5. *Assumed hinge at the most exterior, interior support.*

Note: The lever rule does not include multiple-presence effects; therefore the resulting distribution factor must be multiplied by the appropriate MPF for comparison to the following methods.

Two Design or More Design Lanes Loaded:

$$g_{exterior} = e g_{interior} \qquad (2-5)$$

in which:

$$e = 0.77 + \frac{d_e}{9.1} \qquad (2-6)$$

where:

$g_{exterior}$= the distribution factor for the exterior girder

$g_{interior}$= the distribution factor for interior girders as found above

d_e= horizontal distance from the centerline of the exterior web of the exterior beam at deck level to the interior edge of curb or traffic barrier (ft) (must be between -1.0 and 5.5)

2.3.3.4 Alternate Exterior Girder Method

In section 4.6.2.2d, AASHTO LRFD Bridge Design Specifications 2012 details that when a beam-slab bridge contains diaphragms or cross-frames, the distribution factor for the exterior beam shall not be taken less than that which would be obtained by assuming the cross-section deflects and rotates as a rigid cross-section. The equation for this instance is given in the commentary of section 4.6.2.2d as:

$$g = \frac{N_L}{N_b} + \frac{X_{ext}\sum^{N_L} e}{\sum^{N_b} x^2} \qquad (2-7)$$

where:

g= reaction on exterior beams in terms of lanes

N_L= number of loaded lanes under consideration

N_b= number of beams in the cross section

e= eccentricity of a design truck or a design lane load from the center of gravity of the pattern of girders (ft)

x= horizontal distance from the center of gravity of the pattern of girders to each girder (ft)

X_{ext}= horizontal distance from the center of gravity of the pattern of girders to the exterior girder (ft)

Note: Equation 2-7 does not include multiple-presence effects; therefore the resulting distribution factor must be multiplied by the appropriate MPF for comparison to the previously-discussed methods.

2.4 Finite-Element Modeling

In bridge design, it sometimes becomes necessary for a designer to utilized finite-element modeling to determine load distribution factors. This need arises when bridge geometries fall

outside of the parameter requirements discussed in section 2.3.2 or when cost savings are desired due to the conservatism of the AASHTO LRFD distribution factor equations in certain situations.

2.4.1 AASHTO LRFD Bridge Design Specifications 2012 Requirements for Finite-Element Modeling

Section 4.6.3 of the AASHTO LRFD Bridge Design Specifications (2012) outlines the requirements for refined methods of analysis. The first item addressed in this section is the aspect ratio of the elements employed in the analysis. For beam-slab bridges, section 4.6.3.3 states that the aspect ratio of finite-elements and grid panels should not exceed 5.0. Abrupt changes in size or shape of finite-elements and grid panels should be avoided. A minimum of five, and preferably nine, nodes per beam span should be used. Live load effects in diaphragms should be calculated by the grid or finite-element analysis (AASHTO 2012).

Flexural and torsional deformation shall be considered in analysis of the deck, but vertical shear deformation may be neglected. For finite-element analysis, the slab shall be assumed to be effective for stiffness in both positive and negative flexure. Bridge decks that are solid, have uniform or close to uniform depth, and whose stiffness is close to equal in every in-plane direction shall be considered isotropic. Lastly, wheel loads shall be modeled as patch loads distributed over an approximated wheel contact area taken at the contact surface (AASHTO 2012).

Though usually neglected, continuous railings barriers or medians, determined to certainly be acting compositely with the supporting components, may be considered to be structurally active for service and fatigue limit states only (AASHTO 2012).

2.4.2. CSiBridge Bridge Modeling Software

CSiBridge is a bridge modeling software program that can be utilized for applying refined analysis to bridges. It implements a parametric object-based modeling approach when developing analytical bridge systems. This approach is achieved through the use of the program's "bridge wizard." The wizard allows users to construct the bridge as an assembly of objects. Once the objects are in place they can easily be modified using techniques similar to those used in SAP2000 to conform to the requirements of the user. The analysis engine then automatically transfers the object-based model into a finite-element model by meshing the material domain and assigning material properties. The finite-element model can then be analyzed through elastic material behavior. Frame, shell, solid, or link responses are all options for output generation (Computers and Structures 2013).

Chapter 3 Bridge Description and Instrumentation

3.1 Introduction

The girders used in the superstructure of the bridge over Hillabee Creek on Alabama Highway 22 in Tallapoosa County, Alabama were constructed at Hanson Pipe and Precast in Pelham, Alabama during the fall of 2010. The bridge extends 470 ft between abutments and is shown in Figure 1.1. The first and last spans contain PCI BT-54 girders (Figure 3.1) that span 100 ft while the second and third spans are PCI BT-72 girders (Figure 3.2) and span 135 ft each. Spans 1 and 2 contain girders made of SCC while spans 3 and 4 contain girders constructed with VC. A description of the girders, deck, webwalls, and diaphragms of each span follows.

Figure 3.1. Exterior, VC BT-54 girder in span 4.

Figure 3.2. SCC BT-72 girders.

3.2 Bridge Description

Each span contains seven precast, prestressed concrete girders spaced at 6 ft 6 in. on center. SCC girders support the first and second spans, while VC girders support the third and fourth spans, as displayed in Figure 3.3. Typical girder cross-sections are shown in Figures 3.4 and 3.5 respectively. The girders rest on neoprene bearing pads which are supported by reinforced cast-in-place, VC bents and columns between spans and reinforced cast-in-place, VC abutments at each end of the bridge. The roadway has a transverse width of 44 ft between ALDOT standard drawing number I-131 traffic barriers with a 7 in. thick, VC deck Figure 3.6. The bridge has a 15 degree skew. Figure 3.3 indicates that the girder numbering for the following research documentation is reversed from the SCC spans to the VC spans. This was implemented so that SCC and VC girders with the same number represent a pair that were loaded and supported in a congruent manner.

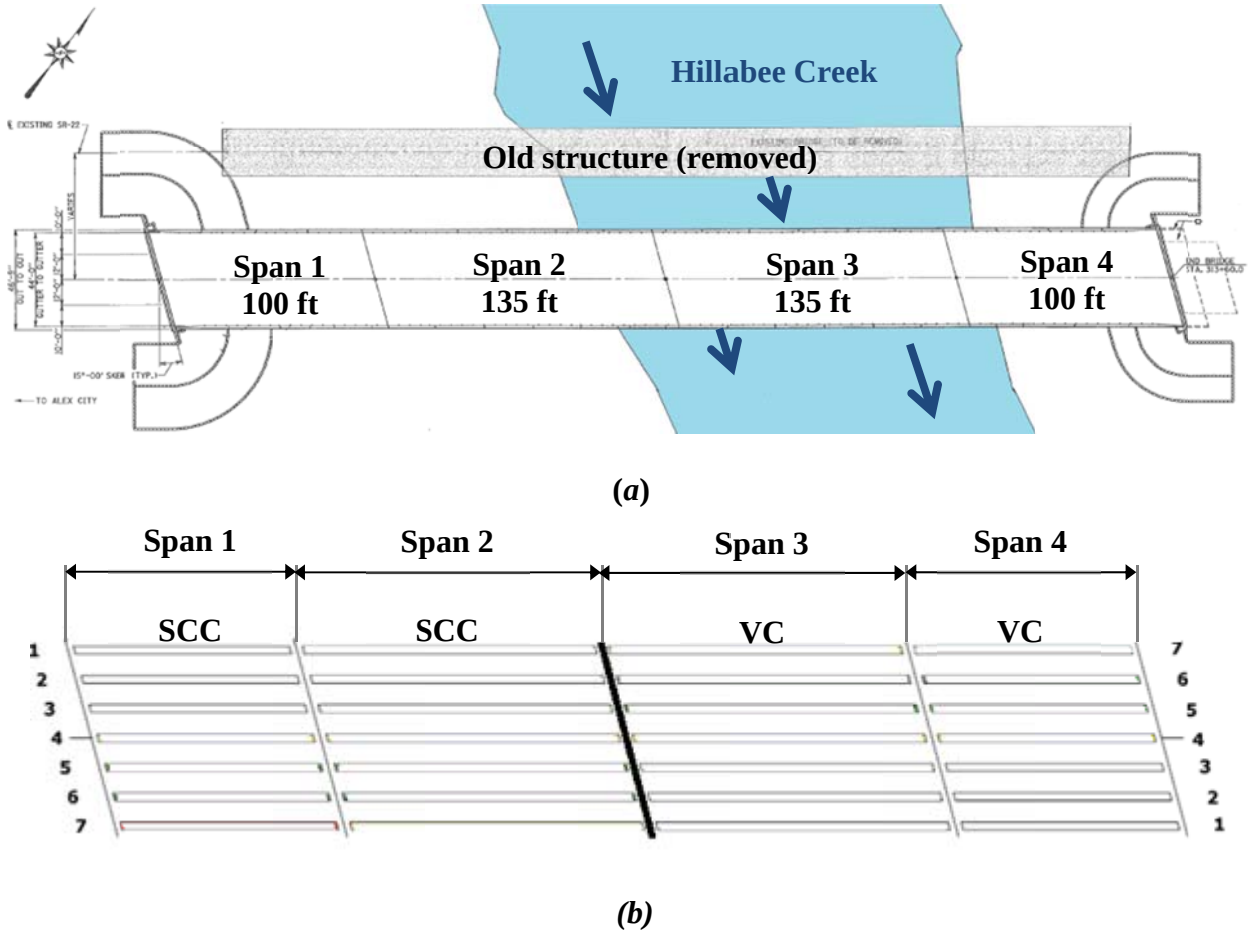

Figure 3.3. *Plan views of bridge with (a) respect to Hillabee Creek and (b) girder framing and numbering.*

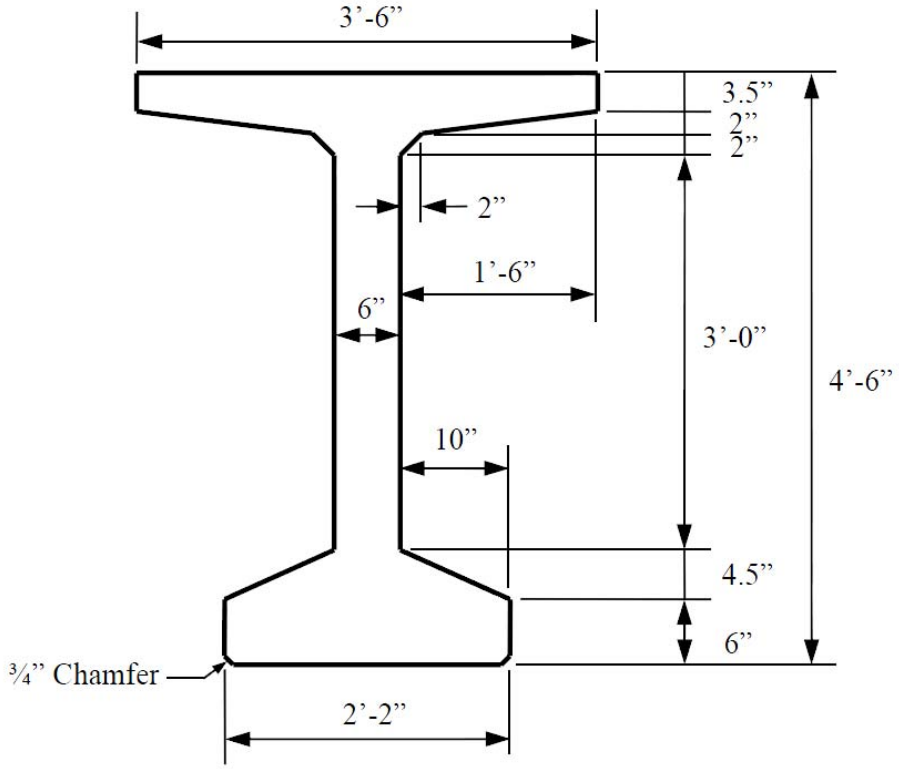

Figure 3.4. *BT-54 girder cross section dimensions.*

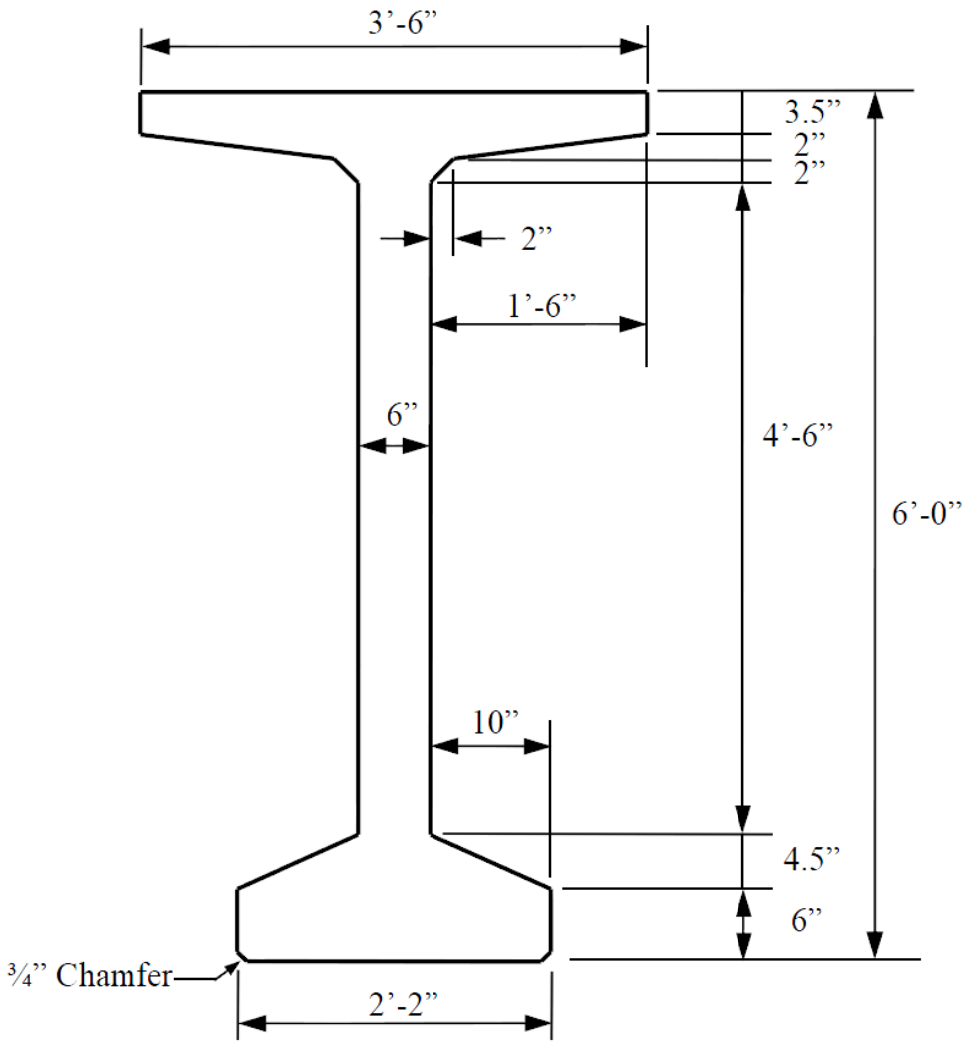

Figure 3.5. *BT-72 cross section dimensions.*

Figure 3.6. Bridge deck and barriers in place.

The girders were cast over a thirty-eight day period between September 21 and October 28, 2010. The girders were erected on four days between May 5 and May 10, 2011 (Figure 3.7). Cast-in-place, vibrated-concrete diaphragms were then gradually added, connecting to the girders using reinforcing bars, between June 6 and June 21, 2011. Diaphragms are located at the ends of each girder, at the midspan points of the girders in spans 1 and 4, and at the quarterspan and midspan points of the girders in spans 2 and 3. The bridge deck was cast on four separate days between August 3 and August 16, 2011. The deck was cast to achieve composite action with the girders and diaphragms using vibrated concrete. Lastly, traffic barriers were slip-form cast over reinforcement protruding from the deck on November 1, 2011. There is no structural continuity between any of the four spans due to the open deck joint at the end of each.

Figure 3.7. A span 3 (VC) girder lowered into position.

3.3 Girder Identification

The girder identification system is shown in Figure 12. The "S" in the label denotes "Span" while the first number in the label denotes which span the girder belongs to. The "G" denotes "Girder" while the second number denotes the girder's position within the span as shown in Figure 3.8. Johnson (2012) details the project's original girder identification system as well as the girder casting groups.

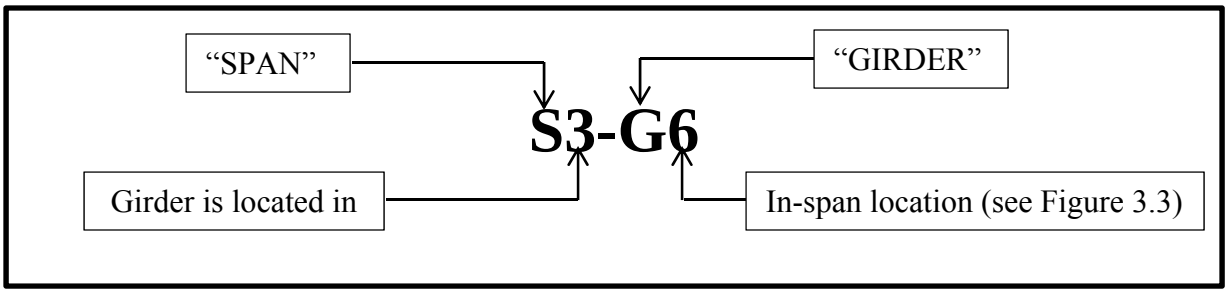

Figure 3.8. *Girder identification scheme.*

3.4 Girders

Two sizes of PCI Bulb-Tee girders were used in the bridge project. Spans 1 and 4 each contained seven BT-54s whose cross section dimensions are shown in Figure 3.4. Each BT-54 was 97'-10" in length with a bearing length of 96'-4". Seven PCI Bulb-Tee 72s were used in spans 2 and 3; cross section dimensions are shown in Figure 3.5. Each BT-72 is 134'-2" in length with a length of 132'-8" between bearing pad centers. All girders were placed on a 15 degree skew to provide proper alignment for the approaches to the bridge.

3.4.1 Girder Strand Arrangement

The BT-54 girders utilized both bonded and unbonded, seven-wire, Grade 270, low-relaxation, 0.5 in. diameter strands as profiled in Figure 3.9. The BT-72 girders also utilized both bonded and unbonded, seven-wire, Grade 270, low-relaxation strands but were 0.5 in. "special" diameter as profiled in Figure 3.10. The specified jacking stress (f_{pj}) was 202.5 ksi for

the bottom and draped strands and 32.7 ksi for the lightly tensioned top strands in each girder. A two-point draping configuration was utilized in all girders, displayed in Figures 3.9 and 3.10.

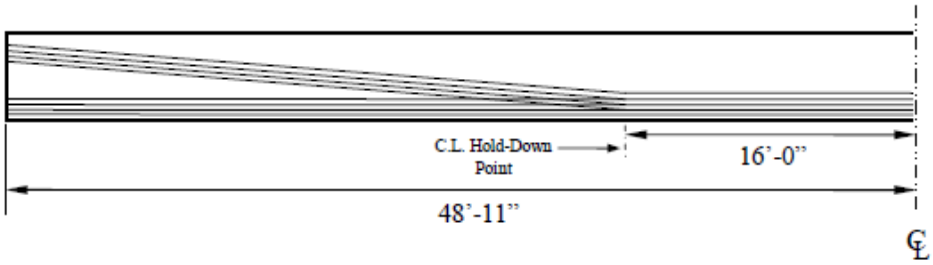

Figure 3.9. Profile of draped strands in a BT-54 girder.

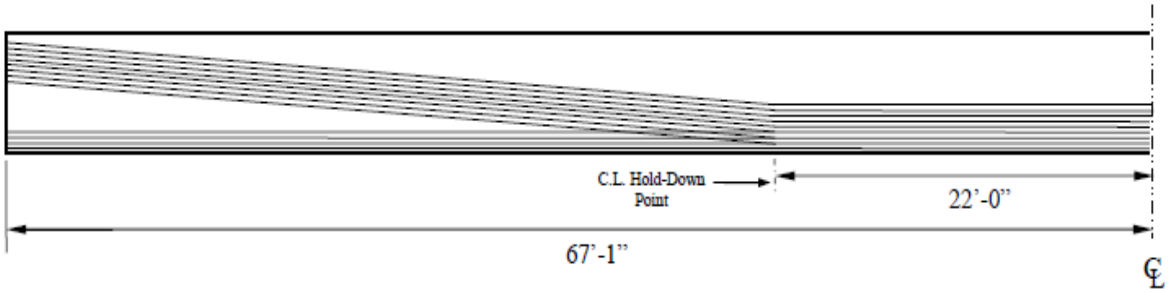

Figure 3.10. *Profile of draped strands in a BT-72 girder.*

Figure 3.11 details the strand location and mild, nonprestressed steel arrangement at midspan for each BT-54. Each girder contains forty strands including twenty-eight, ½-inch diameter strands located in the bottom flange (or "bulb"), eight strands are draped the length of the member as outlined in Figure 3.9, and four strands are lightly tensioned in the top of the girder. The bottom and draped strands were initially tensioned to 30,980 pounds each, while the top strands were tensioned to 5,000 pounds each. The locations of the strands at the ends of each BT-54 are displayed in Figure 3.12.

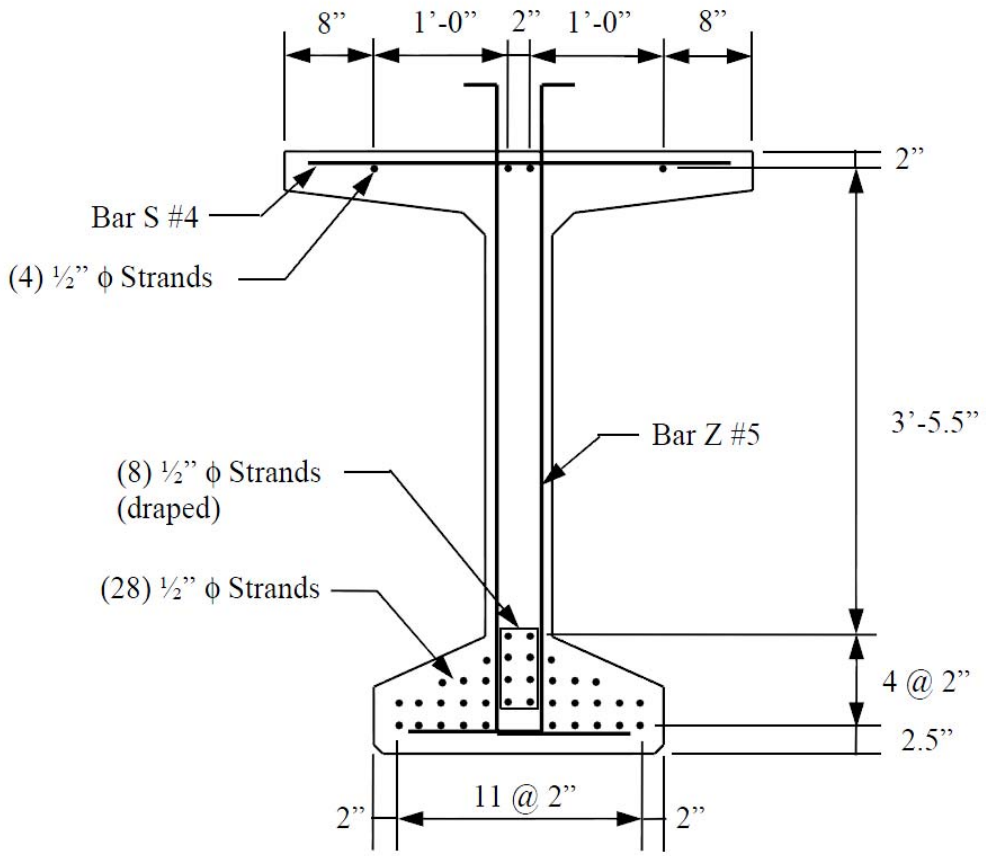

Figure 3.11. *Mild steel and strand arrangement for a BT-54 girder at midspan.*

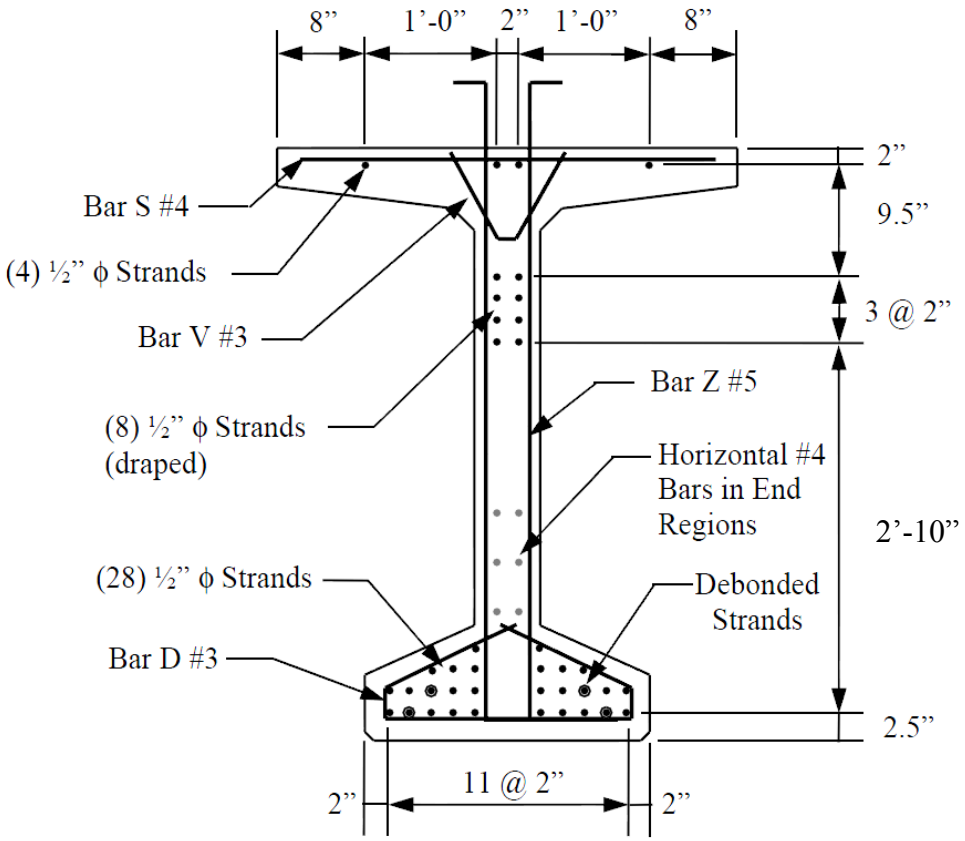

Figure 3.12. *Mild steel and strand arrangement at the ends of each BT-54 girder.*

Figure 3.13 details the strand location and mild steel arrangement at midspan for each BT-72. Each girder contains 50 strands, including 28, 0.5 in. "special" diameter strands located in the bottom bulb, eighteen strands draped along the member, and four lightly tensioned strands in the top of the girder. The bottom and draped strands were tensioned to 33,800 pounds each while the top strands were tensioned to 5,000 pounds each. The end strand locations are detailed in Figure 3.14.

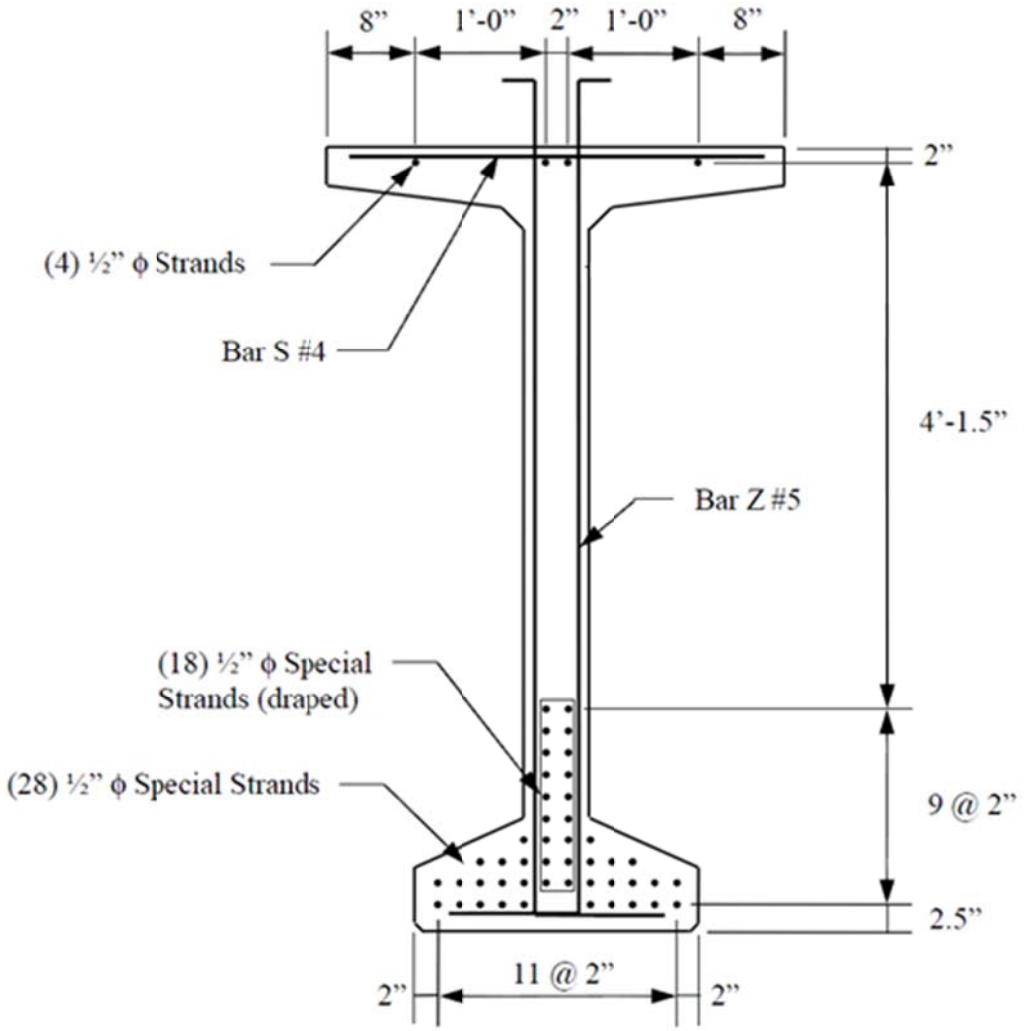

Figure 3.13. *Mild steel and strand arrangement for a BT-72 girder at midspan.*

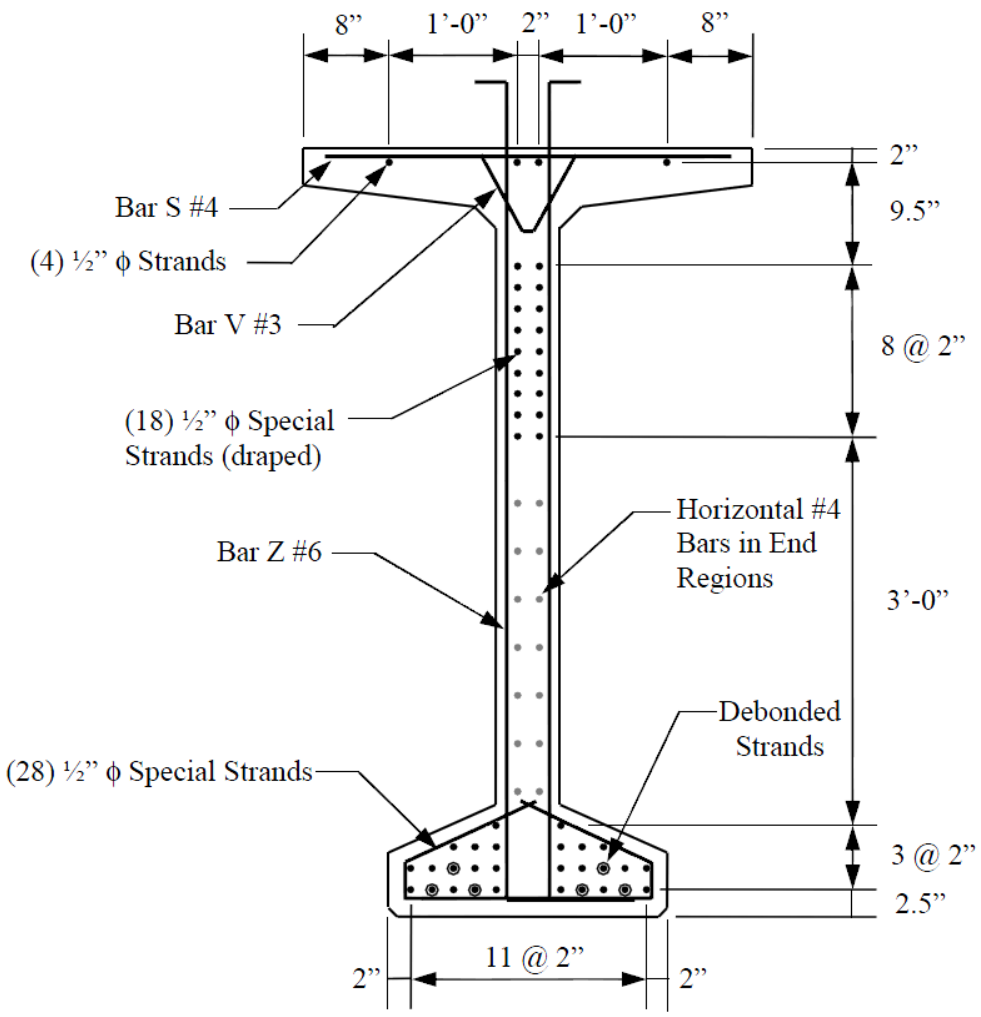

Figure 3.14. *Mild steel and strand arrangement at the ends of each BT-72 girder.*

Figures 3.12 and 3.14 indicate the presence and location of debonded strands in the girder ends of the BT-54s and BT-72s. The debonding of strands was achieved by encasing the strands in plastic tubing and sealing it with tape. This was employed for four strands in the BT-54s and six strands in the BT-72s for 10 ft from each girder end. Further fabrication details have been reported by Johnson (2012).

3.4.2 Nonprestressed Reinforcement

The nonprestressed reinforcement was required to resist shear forces throughout the length of the girder as well as anchorage zone forces at the ends of the girders. The shear resisting mild steel configuration is depicted in Figures 3.11 through 3.14. Z-bars, D-bars (bottom-flange confinement bars), S-bars (straight bars), and V-bars were used in both the BT-54s and BT-72s. Bar spacing for the BT-54s and BT-72s are illustrated in Figures 3.15 and 3.16 respectively.

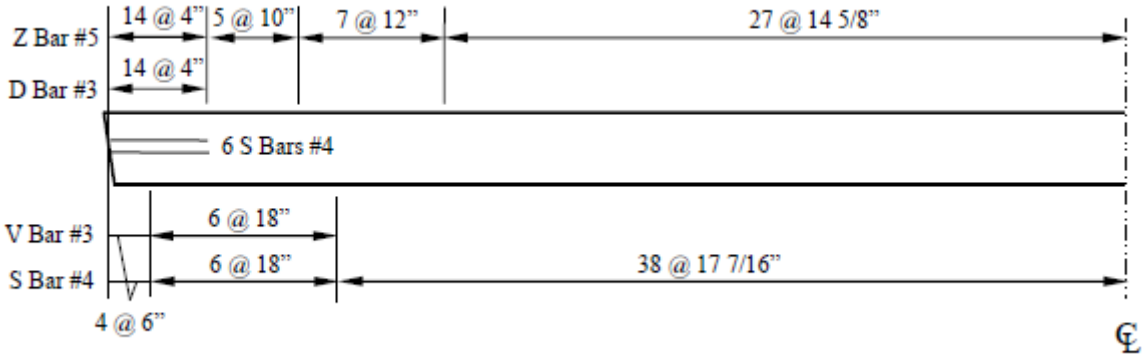

Figure 3.15. *Mild steel spacing in BT-54 girder.*

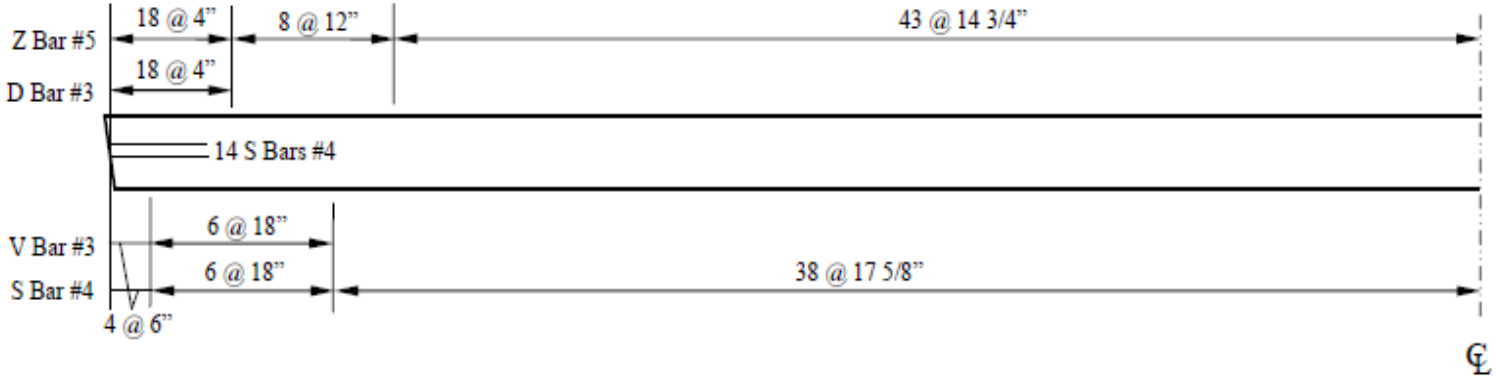

Figure 3.16. *Mild steel reinforcement in BT-72 girder.*

At the ends of all girders, additional S-bar, horizontal reinforcement was required. The cross sectional location of these bars is shown in Figures 3.12 and 3.14 and their location along the span is depicted in Figures 3.15 and 3.16. Non-prestressed reinforcement was congested at the ends of all girders. The D-bars and V-bars were only located at girder ends.

3.5 Webwalls, Deck, and Barriers

Each span in the bridge over Hillabee Creek has webwalls Figure 3.17 at each end connecting all seven girders shown in Figure 3.18. A cross section depiction of the webwall at the bearings is shown in Figure 3.19. The webwalls are 0'-8" thick and span between girders along the skew, achieving composite action with the girders through rebar inserts into the girders. The webwalls achieve composite action with the deck through #5 stirrups and have a bottom face located 0'-10 ½" from the bottom face of the adjacent girders. Spans 1 and 4 contain midspan web walls in addition to end web walls. Spans 2 and 3 contain midspan and quarterspan web walls in addition to end web walls. The midspan and quarterspan webwalls shown in Figure 3.20 have similar characteristics as the end webwalls described above except they do not follow the skew of the bridge. Each of these webwalls is oriented perpendicular to the adjacent girders.

Figure 3.17. A view from above the rebar and form of a webwall between two VC BT-54s.

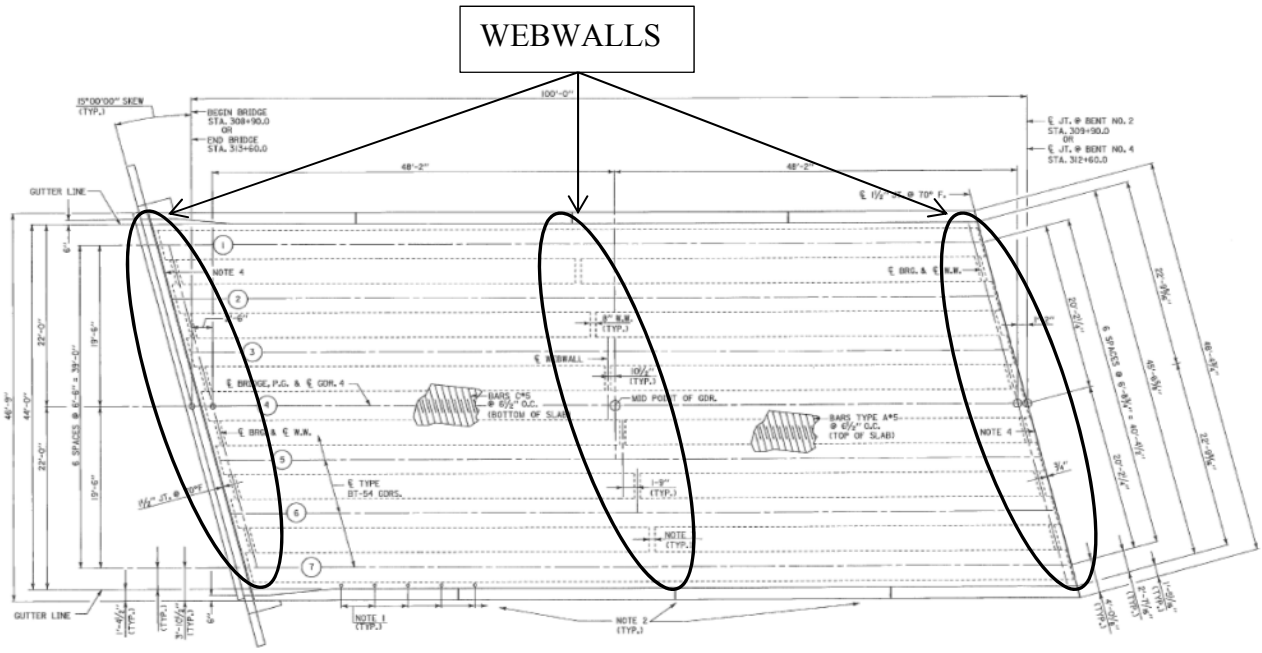

(a)

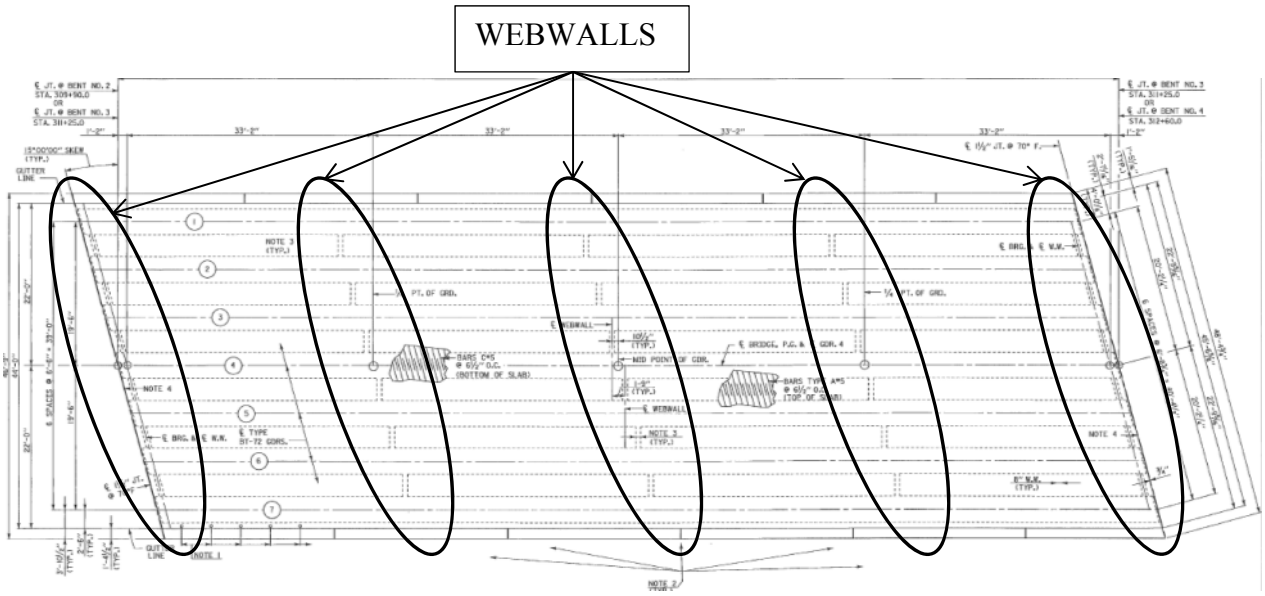

(b)

Figure 3.18. *Webwall locations in (a) spans 1 and 4 and (b) spans 2 and 3.*

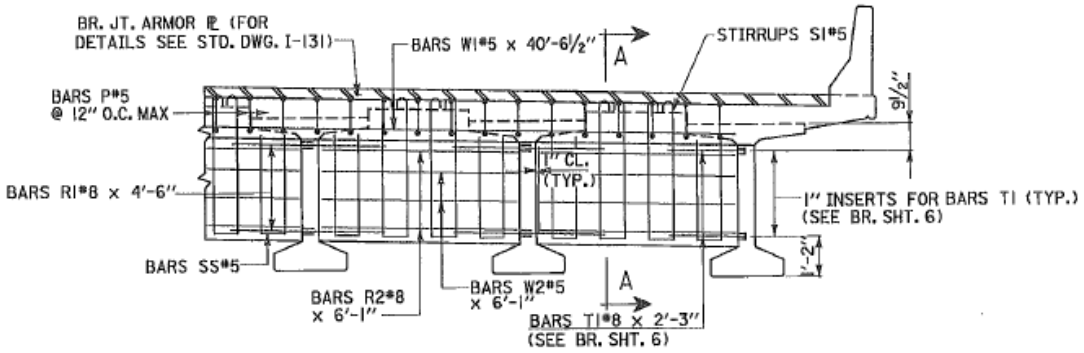

Figure 3.19. *Cross section view of web walls at the ends of each span*

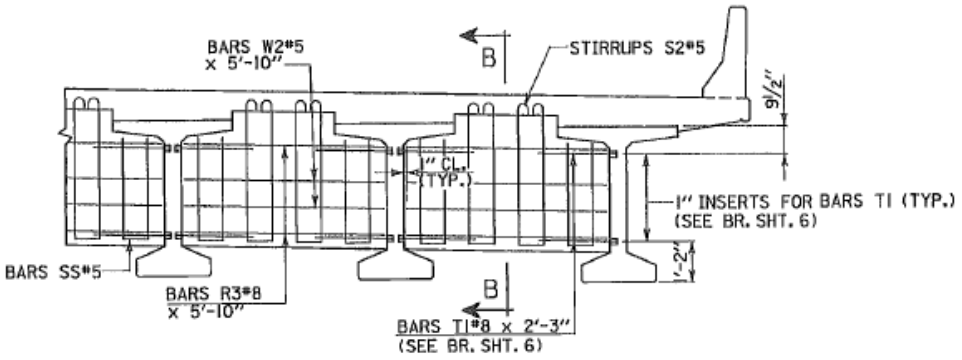

Figure 3.20. *Cross section view of midspan and quarterspan webwalls.*

The bridge over Hillabee Creek has a 46'-9" wide deck with a 44'-0" wide roadway surface between the barriers. The 7" slab, whose cross section is shown in Figure 3.21 contains two layers of longitudinal, nonprestressed steel. The top layer contains #4 bars throughout while the bottom layer contains #5 bars. The deck also contains two transverse layers of nonprestressed steel. The top layer rests upon the top longitudinal layer of steel, has 2" of clear cover, and consists of #5 bars spaced at 0'-6 ½" on center. The bottom layer of steel, located immediately below the bottom layer of longitudinal steel, has 1" of clear cover, and contains #5 bars spaced at 0'-6 ½" O.C. The deck is not continuous between spans.

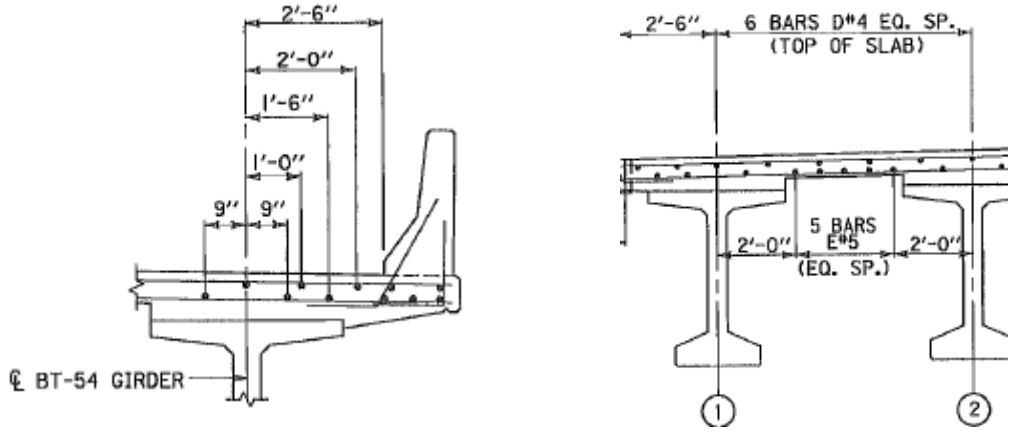

(a) ***(b)***

Figure 3.21. *Nonprestressed reinforcement in the deck at (a) near the barriers and (b) between the interior girders of the bridge.*

There is a continuous, composite barrier on both the upstream and downstream sides of the bridge over Hillabee Creek. Composite action was achieved by slip-form barrier placement over #4 and #5 bars previously cast into the deck. The barrier contains ¾" wide joint openings spaced at 25 ft for spans 1 and 4 and 22.5 ft for spans 2 and 3 (Alabama Department of Transportation 2012).

3.6 Material Properties

The primary materials used to construct the bridge superstructure included VC, SCC, prestressing strand, and nonprestressed reinforcement. The properties for these materials are discussed in this section.

3.6.1 Concrete

Both the VC and SCC mixtures contained Type III portland cement and slag cement. It was necessary to add chemical admixtures to both mixtures to obtain desired fresh concrete properties. Chemical admixtures employed in both mixes included an air-entraining admixture

(Darex AEA EH), a high-range, water-reducing (HRWR) admixture (ADVA Cast 575), and a hydration stabilizing mixture (Recover). The SCC mixes also contained a viscosity modifying admixture (V-Mar 3). All admixtures were supplied by W.R. Grace.

There were three main differences between the VC and SCC for the girders. The first was the amount and type of chemical admixtures varied to bring about the desired properties for each mixture. The second was that the SCC mixture used #78 limestone as coarse aggregate whereas the VC mixture used # 67 limestone as its coarse aggregate. The third main difference between the two mixtures was that the sand-to-total aggregate ratio for SCC was much greater than that of the VC mixture. These differences are typical to allow the SCC to have its unique properties in the fresh state. The constituents of each mixture are summarized in Table 3.1. The fresh properties of each casting group can be found in Table 3.2.

Table 3.1 *Summary of girder mixture proportions.*

Item	BT-54		BT-72	
	SCC	**VC**	**SCC**	**VC**
Water Content (pcy)	266	238	265	234
Cement Content (pcy)	758	696	760	708
GGBF Slag Content (pcy)	134	124	135	125
w/cm	0.30	0.29	0.30	0.28
SSD Coarse Agg. #78 (pcy)	1528	0	1550	0
SSD Coarse Agg. #67 (pcy)	0	1923	0	1950
SSD Fine Agg. (pcy)	1384	1163	1370	1179
s/agg (by weight)	0.48	0.38	0.47	0.38
Air-Entraining Admixture (oz/cwt)	0.3	0.3	0.2	0.2
HRWR Admixture (oz/cwt)	11	8	11	7
Viscosity-Modifying Admixture (oz/cwt)	2	0	4	0
Hydration-Stabilizing Admixture (oz/cwt)	2	1	2	1
Total Air Content (%)	4.1	4.2	4	3.2

Table 3.2. *Fresh property ranges per span*.

Span	Unit Weight (lb/ft^3)	Slump (in.)	Slump Flow (in.)	Air (%)	T50 (sec.)	VSI
1	149.1	-	26.0-27.5	2.6-5.5	6-8	1.0-1.5
2	148.1-150.1	-	23.0-28.0	3.3-4.8	5-15	1.0-1.5
3	153.3-153.4	8.25-9.25	-	2.2-4.3	-	-
4	152.3-153.2	8.50-10.00	-	3.9-4.5	-	-

The webwalls, deck, and barriers were all cast-in-place and all utilized the same ALDOT AF-1c mixture proportions. The mixtures contained Type I/II portland cement, Class C fly ash, #100 sand fine aggregate, and #67 limestone coarse aggregate. Chemical admixtures were also added including air-entraining admixture (MB AE 90), a water reducing admixture (Pozzolith 322N), and a midrange water reducing admixture (Polyheed 1025), all provided by BASF, Cleveland, Ohio. The mixture proportion summary can be found in Table 3.3.

Table 3.3. *Summary of mixture proportions used for deck, webwalls, and barriers.*

ITEM (One cubic yard)	**AF-1c**
CEMENT (lb)	496
CLASS C FLY ASH (lb)	124
AIR ENTRAINING ADMIXTURE (oz)	1.2
MAXIMUM WATER (gallons)	33.1
FINE AGGREGATE (lb)	1,200
COARSE AGGREGATE (lb)	1,870
TOTAL AIR (%)	2.5%-6.0%
ALLOWABLE SLUMP (in)	3.5
WATER REDUCER (oz)	18.6
MID RANGE WATER REDUCER (oz)	31.0

In addition to fresh properties, Auburn University researchers produced concrete cylinders to determine hardened properties of each girder, span of deck, and barrier. The 6" x 12" girder concrete cylinders were steam cured along with the girders under the curing tarps, while the deck and barrier cylinders were field cured on the Hillabee Creek bridge construction site. The cylinders were then tested at various ages including 28 days for compressive strength (f'_c) and modulus of elasticity (E_c). All cylinders were strength tested in accordance with ASTM C39 (2005). Modulus of elasticity testing was performed in accordance with ASTM C469 (2002). The averaged results for both strength and modulus of elasticity testing of all girders as well as the deck and barriers are summarized in Table 3.4.

Table 3.4 Material P*roperties of girders, deck, and barriers determined from cylinder testing.*

Components			28-Day Material Properties	
			f_c (psi)	E_c (ksi)
BT-54	SCC Span 1	G1	10,800	6,600
		G2, G5, G6	10,240	6,400
		G3, G4	10,800	6,600
		G7	10,910	6,300
	VC Span 4	G1	10,360	6,900
		G2,G5, G6	10,590	7,400
		G3, G4	9,670	6,900
		G7	9,670	6,800
BT-72	SCC Span 2	G1	10,490	6,300
		G2, G5	10,550	6,400
		G3, G4	10,770	6,400
		G6	10,070	6,000
		G7	10,490	6,300
	VC Span 3	G1	10,770	7,000
		G2, G5	10,850	7,300
		G3, G4	11,050	7,700
		G6	10,510	6,900
		G7	10,770	7,000
Decks		Span 1	6,030	6,300
		Span 2	6,510	6,400
		Span 3	6,060	6,100
		Span 4	5,910	6,400
Barriers		All	5,860	6,000

3.6.2 Prestressing Strand

The prestressing strand utilized in this project is low-relaxation, Grade 270, seven-wire strand. The strand utilized in the BT-54 girders was 0.5 in. diameter strand from Strand-Tech Martin, Inc, located in Summerville, South Carolina. The BT-72 sections contained 0.5 in. "special" strand provided by American Spring Wire, Houston, Texas. Prior to casting, all strand was stored in accordance with standard ALDOT procedure. Figure 3.22 shows the strand underwent some minor weathering, though standard storage procedure was followed.

Figure 3.22. *Prestressing wire surface condition (Johnson 2012).*

Prior to girder fabrication, strand pull-out tests were performed on September 14, 2010 onsite at Hanson Pipe and Precast. The bond quality of both the strand used in the BT-54 girders and BT-72 girders was found to be adequate (Dunham 2011).

3.6.3 Nonprestressed Steel Reinforcement

Nonprestressed steel reinforcement was used in all girders to reinforce against shear and anchorage zone forces. All nonprestressed steel reinforcement was ASTM A615 Grade 60. Figures 3.11 through 3.14 depict the location and shape of the nonprestressed reinforcement. Figures 3.15 and 3.16 detail reinforcement spacing and location along the length of girder.

3.7 Strain Gauges and Installation Procedures

3.7.1 Surface Strain Gauges

The primary strain measurement sensor used for all in-place load tests was a surface-mounted, Texas Instruments MFLA-60 350-1L, a 2.4 in. quarter-bridge, electrical-resistance strain gauge (ERSG) with a resistance of 350 Ω. A 2.4 in gauge length was necessary due to the fact that concrete is non-homogenous. The longer gauge length provides an averaging effect that includes the aggregate and hardened cement in the effective measured strain. These gauges were intended for two rounds of load testings one year apart, making weatherproofing necessary.

The first step in installing a MFLA-60 350-1L strain gauge was to measure out to midspan on the bottom face of the girder and mark with a "+" as seen in Figure 3.23. Due to concrete's inherent porous nature, a 100% solid Loctite Heavy Duty epoxy layer was applied to the concrete to seal the gauge from water. After the epoxy layer was allowed to dry, it was lightly sanded to provide an abrasive bonding surface for the gauge. The sanded surface was then cleaned with M-Prep Conditioner A and neutralized with M-Prep Neutralizer 5A (see Figure 3.23). The gauges were then removed from their protective case and taped to a small clean glass plate. The gauge and cellophane tape were then carefully removed from the plate together as one unit and placed on the location, peeled back exposing the bottom of the strain gauge as seen in Figure 3.24. A thin layer of epoxy was then used to apply the gauge to the prepped surface. The gauge was then applied to the epoxied surface and held firmly in place until properly attached. The tape was removed from the strain gauge once the epoxy had dried. Another layer of epoxy was placed over the gauge for waterproofing purposes as shown in Figure 3.25. Lastly, mastic tape was placed over the gauge for mechanical protection (Figure 3.26).

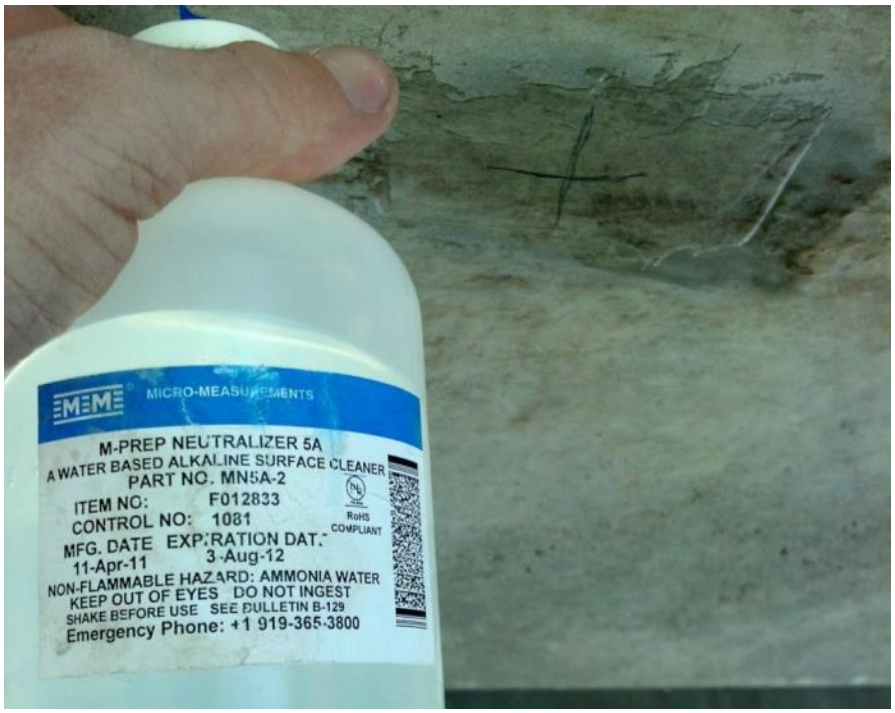

Figure 3.23. *M-prep neutralizer 5A.*

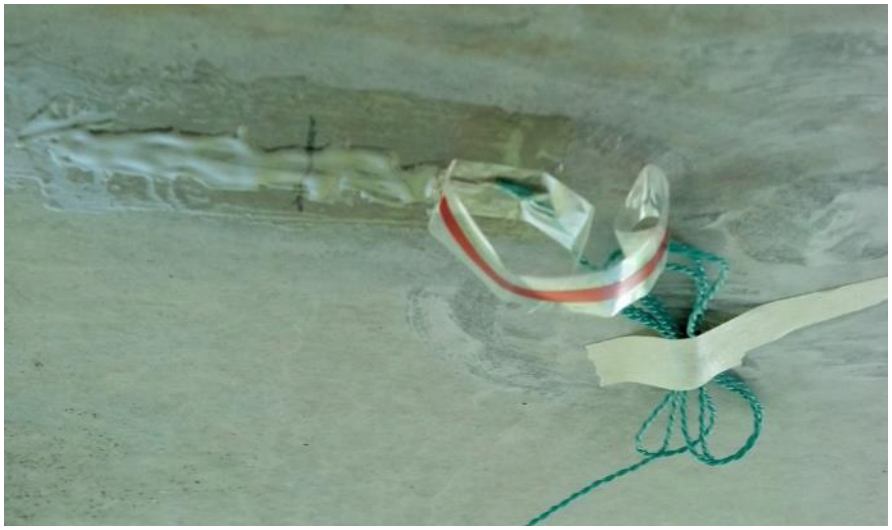

Figure 3.24. *A gauge temporarily peeled back to allow for a thin layer of epoxy.*

Figure 3.25. *Thin layer of epoxy placed over the strain gauge for waterproofing.*

Figure 3.26. *Mastic tape applied over the strain gauge for mechanical protection.*

Prepare Concrete
1. Mark area for gage.
2. Spray gaging area with degreaser (if necessary).
3. Brush area with wire brush.
4. Smooth area with grinder if needed to remove irregular ities or epoxy.
5. Blow loose dust from surface.
6. Generously apply Conditioner.
7. Scrub with wire brush.
8. Blot area with gauze sponges.
9. Rinse area thoroughly with clean water.
10. Scrub surface with Surface Neutralizer.
11. Blot area with gauze sponges.
12. Rinse with water.
13. Dry surface thoroughly (warming surface with heat gun may help).

Apply 100% solids epoxy adhesive
14. Apply adhesive to gauging area, work into voids, and smooth with putty knife.
15. Allow epoxy to cure.
16. Sand smooth with 320 grit sandpaper.
17. Using a Ball Point Pen draw layout lines.
18. Scrub with Conditioner.
19. Apply Neutralizer.
20. Dry as before.

Mounting Gage
21. Carefully mount strain gauge to glass plate with Cellophane Tape.
22. Tape gauge into correct location on concrete.
23. Peel tape and gauge back to expose back of gauge.
24. Mix 5-minute epoxy.
25. Place 5-minute epoxy on gauge and concrete.
26. Gently place gauge on concrete.
27. Hold pressure for 2 minutes.
28. After 1 hour or longer, remove tape.
29. Apply RTV silicone rubber (moisture sealer), and let dry.
30. Apply Mastic Tape.
31. Attach wire ends to mounted terminal strips.

Figure 3.27. *Step-by-step strain gauge installation procedure (Adapted from Fason 2009)*

3.7.2 Vibrating-Wire Strain Gauges

The gauges placed in the girders during girder fabrication were Geokon Inc. VCE-4200 vibrating-wire strain gauges (VWSGs). These gauges are ideally suited for long-term strain

measurements per the Geokon Inc manual (Geokon 2010). The VWSGs were installed for related research focused on time-dependent strains in the girders, but were used as a backup to the aforementioned surface-mounted ERSGs during the first load test. The VWSGs measure strain by reading the vibration frequency of a steel wire inside each gauge. Once a gauge is embedded in the concrete, it exhibits composite behavior with the concrete, expanding and contracting as the concrete does. Electromagnets pluck the wire in the gauge and measure its natural frequency of vibration. When a change in the natural frequency occurs, the tension in the wire has changed, meaning that a change in strain in the concrete at the gauge location has occurred. Figure 3.28 shows a VWSG and its components.

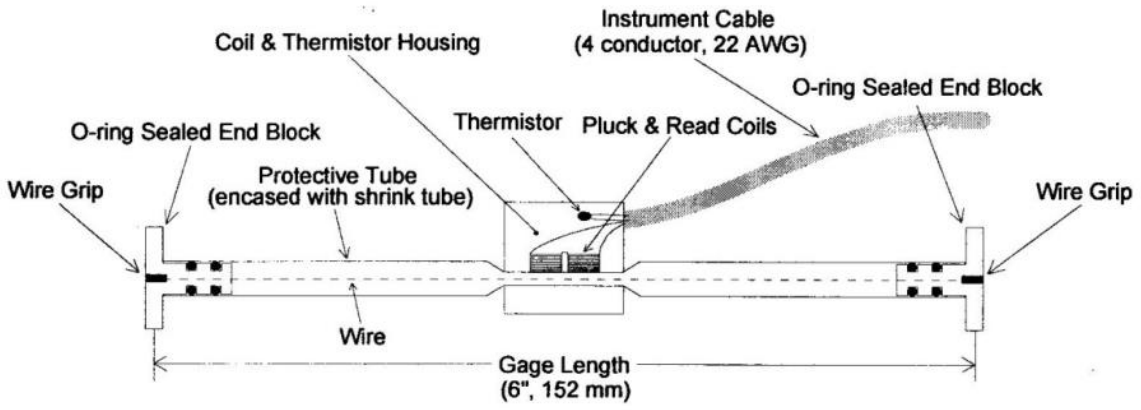

Figure 3.28. *VCE-4200 Vibrating-Wire Strain Gauge schematic (Geokon 2010)*

3.8 Deflectometers

Deflectometers were used to monitor bottom-fiber deflection for each girder during the first load test and for spans 1, 2, and 4 for the second load test. High Hillabee Creek water levels made it impractical to employ deflectometers for span 3 during the second round of load testing. The deflectometers for spans 1, 2, and 4 were positioned under the bridge on ground level and connected to each girders using an “S” hook, turnbuckle, stainless steel wire, and a hook glued to

the bottom face of the girder at midspan (Figure 3.29). For span 3, the deflectometer was attached to the girder as seen in Figure 3.30.

Figure 3.29. *A deflectometer positioned at ground level.*

Figure 3.30. *A deflectometer attached to a girder over span 3.*

Each deflectometer contained a quarter-bridge, surface mounted strain gauge on the underside of the aluminum bar to measure flexural strain. A downward deflection of the girder results in a straightening of the pretensioned, cantilevered bar, and this straightening results in a change in the flexural strain at the strain-gauge location. As long as the attachment wire remains in tension and the bar is not bent beyond its proportional limit prior to girder movement, the relationship between the strain and deflection remains linear. The strain-to-deflection conversion factors were calibrated for each deflectometer before the first load test and rechecked before the second load test.

A majority of the deflectometers used during both load tests were constructed in 2005 and detailed by Fason (2009). For spans 1, 2, and 4, hooks were epoxied onto the girders at midspan. A metal wire was then fastened to those hooks and extended down to the ground level where the girders were located. Turnbuckles were then fastened onto the wire and have metal

"S" hooks attached to the opposite end. Those "S" hooks were then slipped through an eye hook on the end of the aluminum bar of the deflectometer. The turnbuckles were then adjusted to the proper tension resulting in the bottom of the bar being approximately 5 inches from the base of the deflectometer (see Figure 3.29). Bags of soil were used to stabilize the ground level deflectometers to minimize movement of the instrument.

Span 3, which is located over Hillabee Creek, required some special provisions in order to gather girder deflection data. As previously mentioned the deflectometers were attached to the girders for the first load test and not employed at all for the second load test due to high water levels in Hillabee Creek. As shown in Figure 3.30, once the deflectometer was attached to the girder, an "S" was put through the eye hook on the end of the deflectometer bar. A turnbuckle was then connected to the "S" hook. The turnbuckle was fastened to a stainless steel wire that was lowered down to near the water surface of the creek and attached to an anchor pole. The anchor pole, pictured in Figure 3.31, consisted of a 10 ft long piece of 2 in. steel tubing that was placed in a five-gallon bucket that was filled with concrete. The anchor devices were lowered off of the platform shown in Figure 3.32 and placed by the crew in a canoe displayed in Figure 3.33. The same turnbuckle tension process used for the surface deflectometers was reused for the span 3 deflectometers before load testing.

Figure 3.31. *Deflectometer anchoring pole for span 3 over Hillabee Creek.*

Figure 3.32. *Deflectometer-wire anchoring device being lowered into Hillabee Creek.*

Figure 3.33. *Placing deflectometer-wire anchors.*

Each deflectometer was attached to the data acquisition system through conductor cables. Each deflectometer was paired with the same cable from the calibration process as well as each load test.

3.9 Sensor Location and Notation

3.9.1 Surface Strain Gauge and Deflectometer Location

Each deflectometer was either attached or anchored at the midspan of every girder during the first load test and all girders in the first, second, and fourth spans during the second load test. Surface strain gauges were also located at midspan of each girder for both load tests.

3.9.2 VWSG Location

Vibrating-wire strain gauges were placed in the girders in 2010 during casting for long-term, time-dependent measurements not discussed in this thesis. However, due to the fact that traffic was not on the bridge and the load trucks could sit in position for an extended period of time during the first load test, they were employed as backup strain gauges in the event that one of the surface gauges should fail.

Each girder contained at least two VWSGs at midspan with some containing a full vertical profile of gauges. Figure 3.34 summarizes which girders contain full VWSG profiles and which contain only two. Full-depth gauge profiles were not implemented in all girders due to data acquisition system capacity limits. As shown in Figure 38(GG), spans 3 and 4 have the reverse girder numbering of spans 1 and 2. This was implemented so that each girder pair would be loaded congruently (e.g. eastbound truck on S1-G5 and a westbound truck on S4-G5). Figures 3.35 through 3.38 report the location of the VWSGs in each of the girder size and VWSG configuration combinations. VWSG installation details can be found in Johnson (2012).

S1-G1	S2-G1	S3-G7	S4-G7
S1-G2	S2-G2	S3-G6	S4-G6
S1-G3	S2-G3	S3-G5	S4-G5
S1-G4	S2-G4	S3-G4	S4-G4
S1-G5	S2-G5	S3-G3	S4-G3
S1-G6	S2-G6	S3-G2	S4-G2
S1-G7	S2-G7	S3-G1	S4-G1

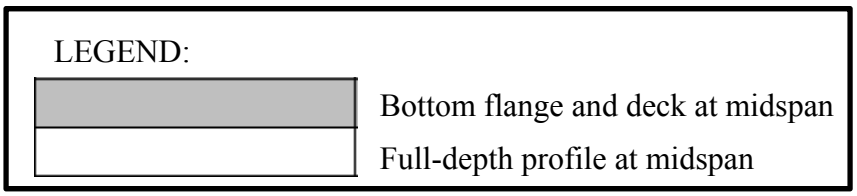

Figure 3.34. *VWSG location summary at midspan.*

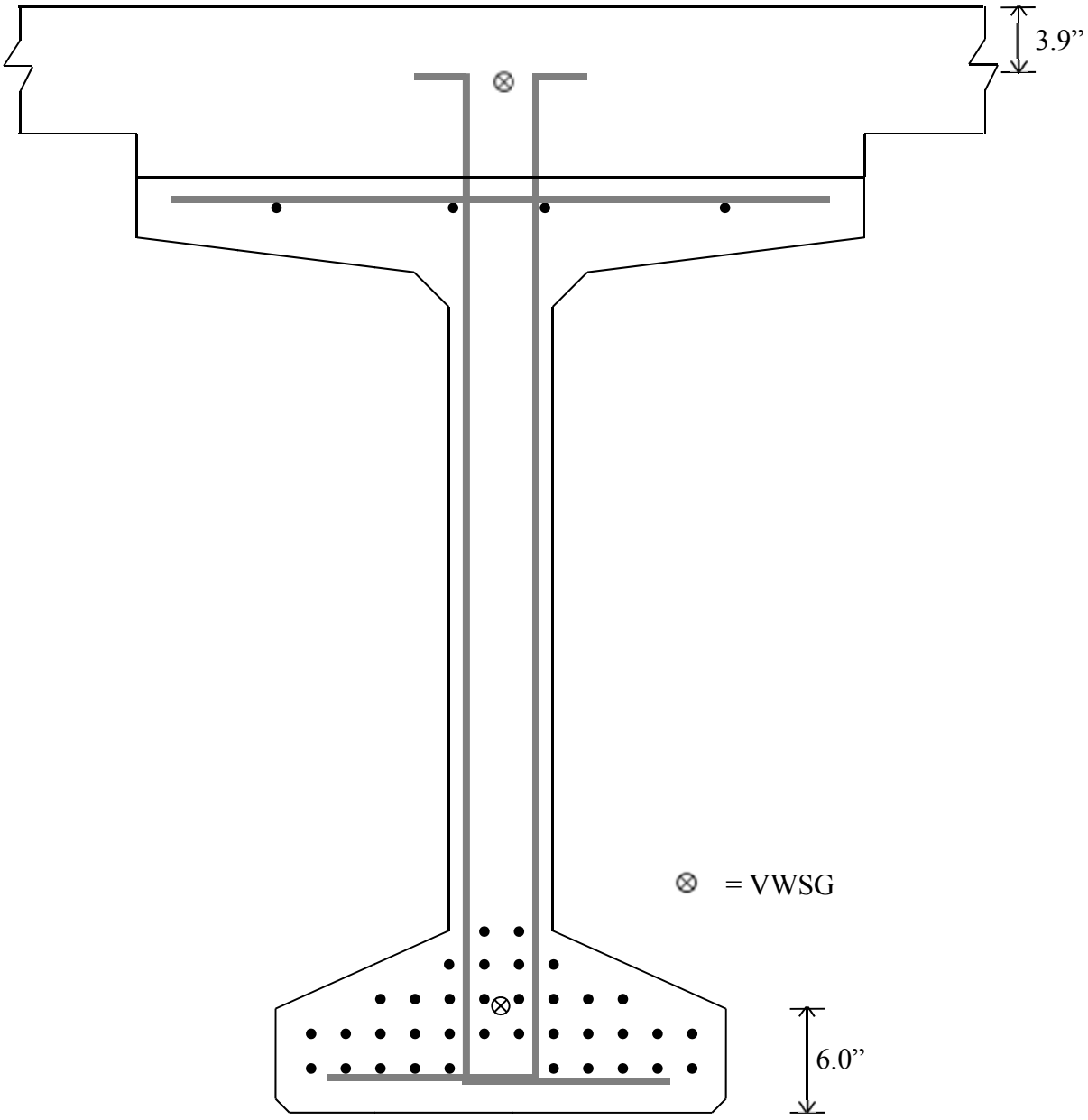

Figure 3.35. *BT-54 midspan cross section with a bottom-bulb and deck VWSGs.*

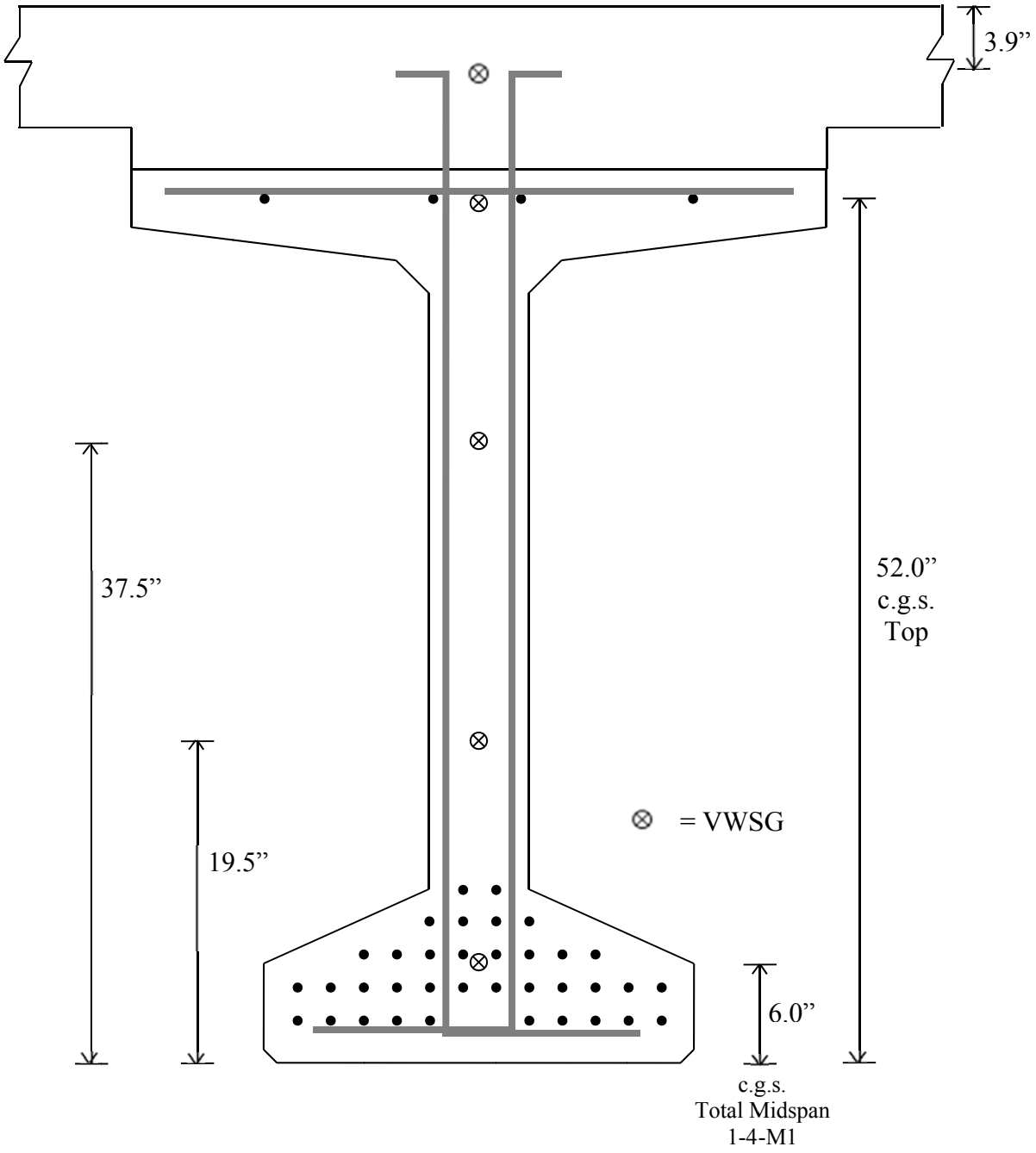

Figure 3.36. *BT-54 midspan full profile VWSG setup.*

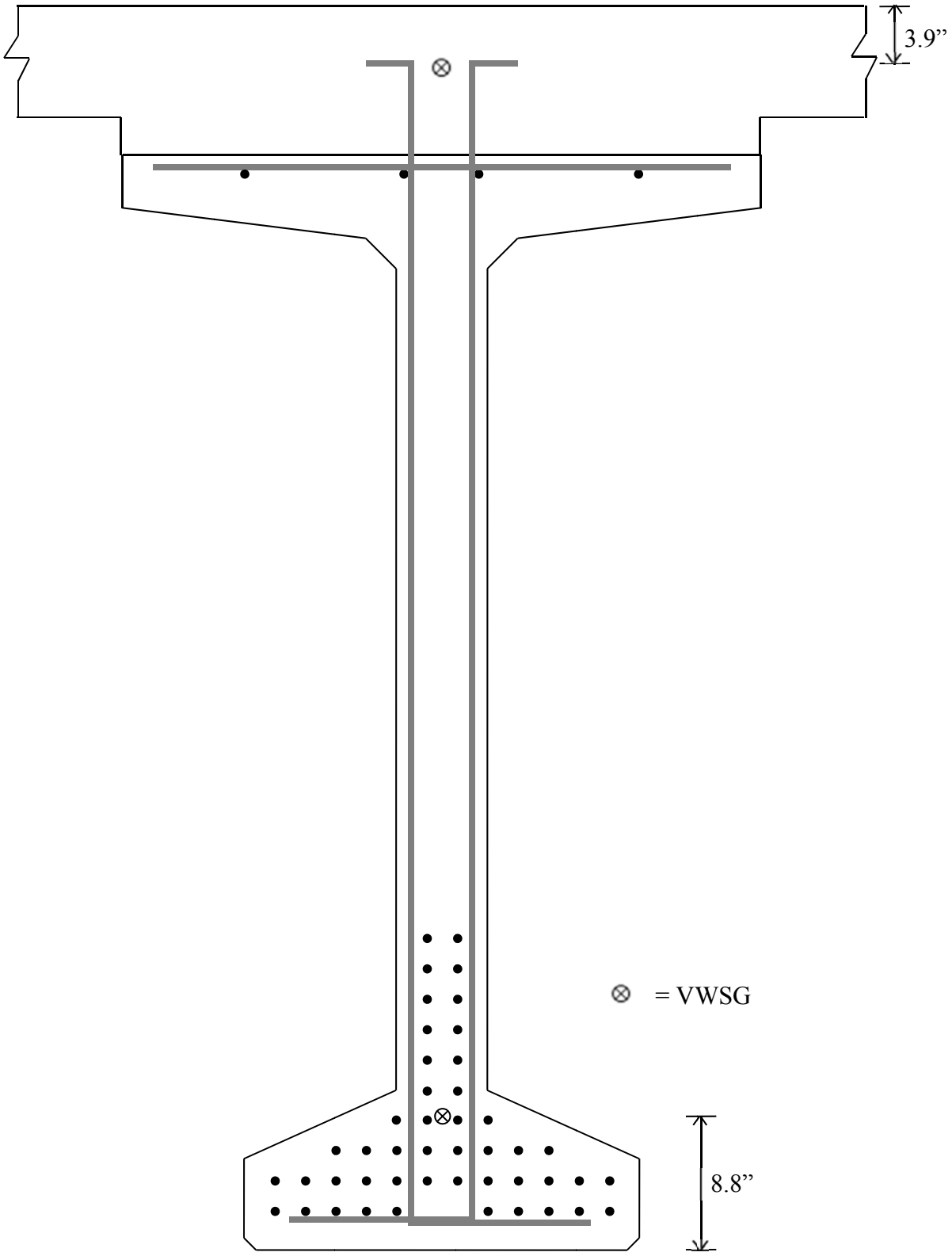

Figure 3.37. *BT-72 midspan cross section with bottom-bulb and deck VWSGs.*

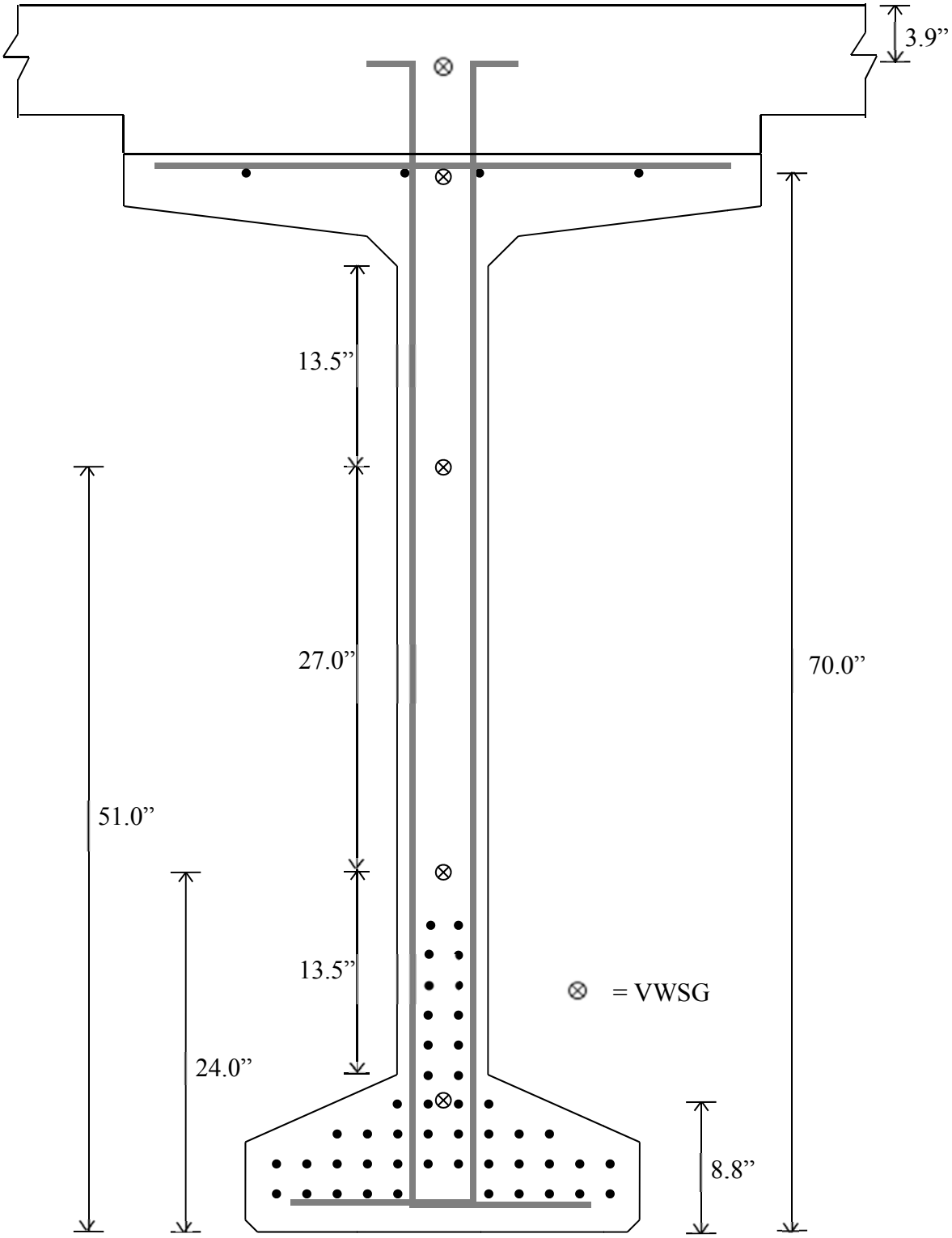

Figure 3.38. *BT-72 midspan full profile VWSG setup.*

3.10 Data Acquisition Systems

3.10.1 Surface Strain Gauges and Deflectometers

A total of 56 sensors for the first load test and 49 sensors for the second load test were attached to an Optim Megadac® data acquisition system. During each load test, each sensor was assigned a channel on the channel board as seen in Figure 3.39 below. The channel board was connected to the data acquisition system which recorded the data from the sensors at a rate of 4 scans per second for approximately 240 seconds during each load placement for the first load test while the second load test utilized a rate of 50 scans per second for approximately 10 seconds for each load placement.

Figure 3.39. *Optim Megadac® data acquisition system and sensor input channel.*

3.10.2 Vibrating Wire Strain Gauges

Two data acquisition systems (DAS) were utilized during the first load test to record data provided by the VWSGs. The VWSG DAS was not used during the second load test due to the time constraint imposed from the presence of traffic. Both systems utilized the same design consisting of a Campbell CR1000 data logger, two multiplexers, and a battery system as shown in Figure 3.40. The design configuration was the same that was used in research in Johnson (2012) which was based on a setup by Gross (2000).

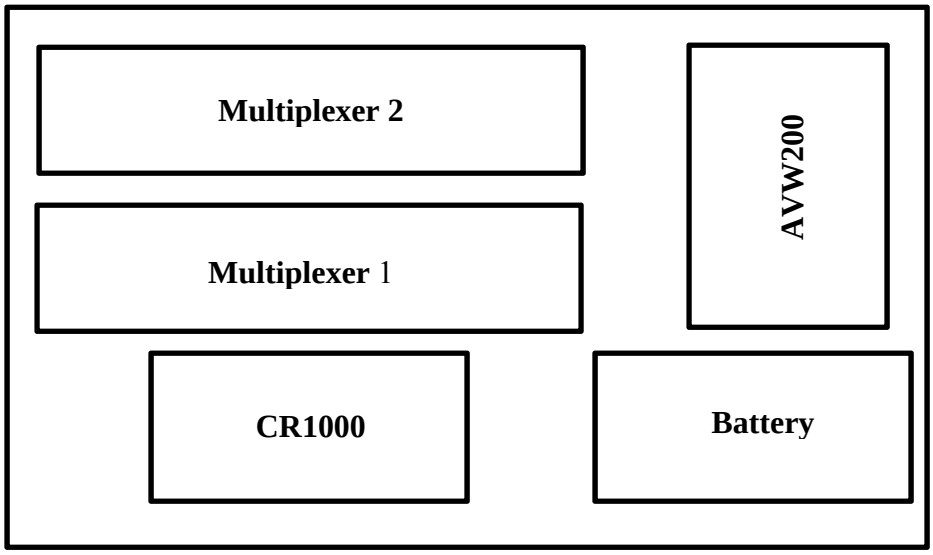

Figure 3.40. *VWSG Data Acquisition System (Johnson 2012).*

The CR1000 datalogger was programmed to activate each VWSG every 130 seconds during load testing. The datalogger recorded the resonant frequency of vibration and thermistor resistance of each VWSG. The recording process can be found in Appendix B of the Geokon Instructional Manual (Geokon 2010). Each multiplexer had a 16 VWSG capacity, allowing for 32 VWSG to be recorded simultaneously per DAS.

Chapter 4 Bridge Testing Procedures

4.1 Introduction

The bridge over Hillabee Creek was load tested two weeks prior to the start of its service life and after a year of service. Below, each load test is described including weather conditions, traffic control (if any), load truck placement on the bridge, and load truck placement procedures. The load trucks, their block weight configurations, and the weight per axle are also detailed.

4.2 Load Testing Truck

Each load test utilized load trucks like the one shown in Figure 4.1. Due to limited availability, only one truck was used during the first load test in 2012 while two trucks were available for the second load test in 2013. All trucks conformed to the ALDOT load configuration LC-5 depicted in Figure 4.2 and utilized twenty-four load blocks.

Figure 4.1. *ALDOT Load Truck with LC-5 weight configuration. (Note: Only the rear two axles of the tri-axle rear end of the vehicle are in contact with the deck.)*

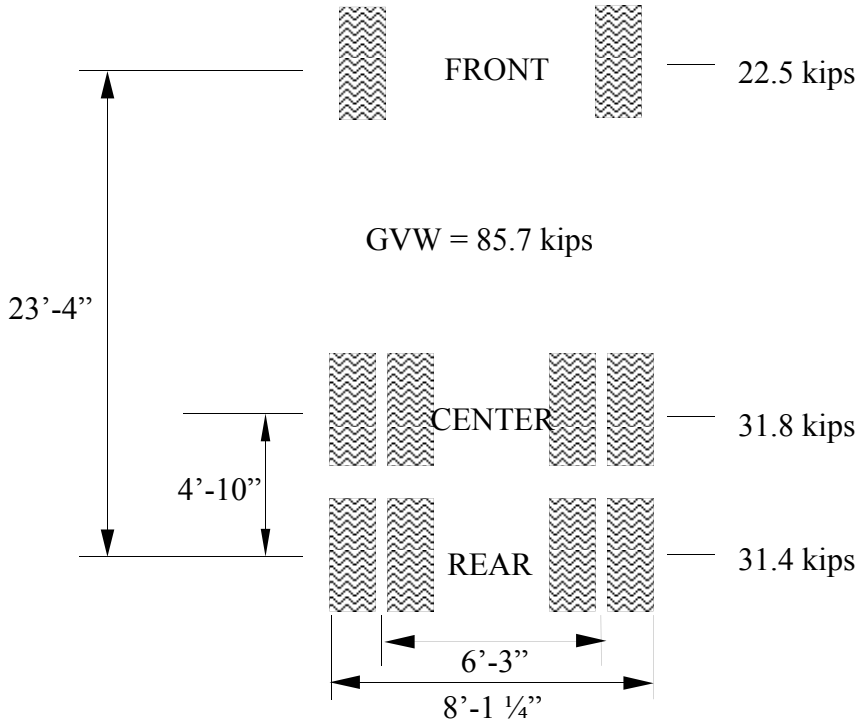

Figure 4.2. *Configuration of load test truck*

4.3 Load Test 1

The first load test on the bridge over Hillabee Creek was performed on May 14th and 15th, 2012, two weeks prior to the bridge being placed in service. The first and second spans were tested on May 14th in cloudy, windy conditions with an ambient temperature around 80 degrees Fahrenheit while the third and fourth spans were tested on May 15th in sunny conditions with a temperature of approximately 85 degrees Fahrenheit.

4.3.1 Static Test Locations on Bridge

Throughout the first day of testing, the single load truck was positioned in the eight transverse positions shown in Figures 4.5 through 4.7 in each span of spans 1 and 2 (SCC girder spans). In each position, the truck was oriented in the eastbound direction (Figure 4.3) with the midpoint of its "center" axle (Figure 4.2) positioned along the 15 degree skewed midspan of each span. This resulted in a total of sixteen truck positions being measured on the first day.

On the second day of testing, the team moved to the east side of the bridge in order to load test spans 3 and 4 (VC girder spans). The truck was positioned in the same eight positions for each span as spans 1 and 2 (Figures 4.5 through 4.7), except that the truck was facing westbound (Figure 4.4). Note: Spans 3 and 4 utilize a reverse numbering scheme from spans 1 and 2 (Figure 4.4). This scheme results in a load truck in load position A on spans 1 or 2 being located a clear distance of 2 ft from the *downstream* barrier while a load truck placed in load position A on spans 3 or 4 having a clear distance of 2 ft from the *upstream* barrier.

Recall from section 3.2 that Figure 3.3 indicates the girder numbering for the research documentation is reversed from the SCC spans to the VC spans. This was implemented so that SCC and VC girders with the same number represent a pair that were loaded and supported in a congruent manner.

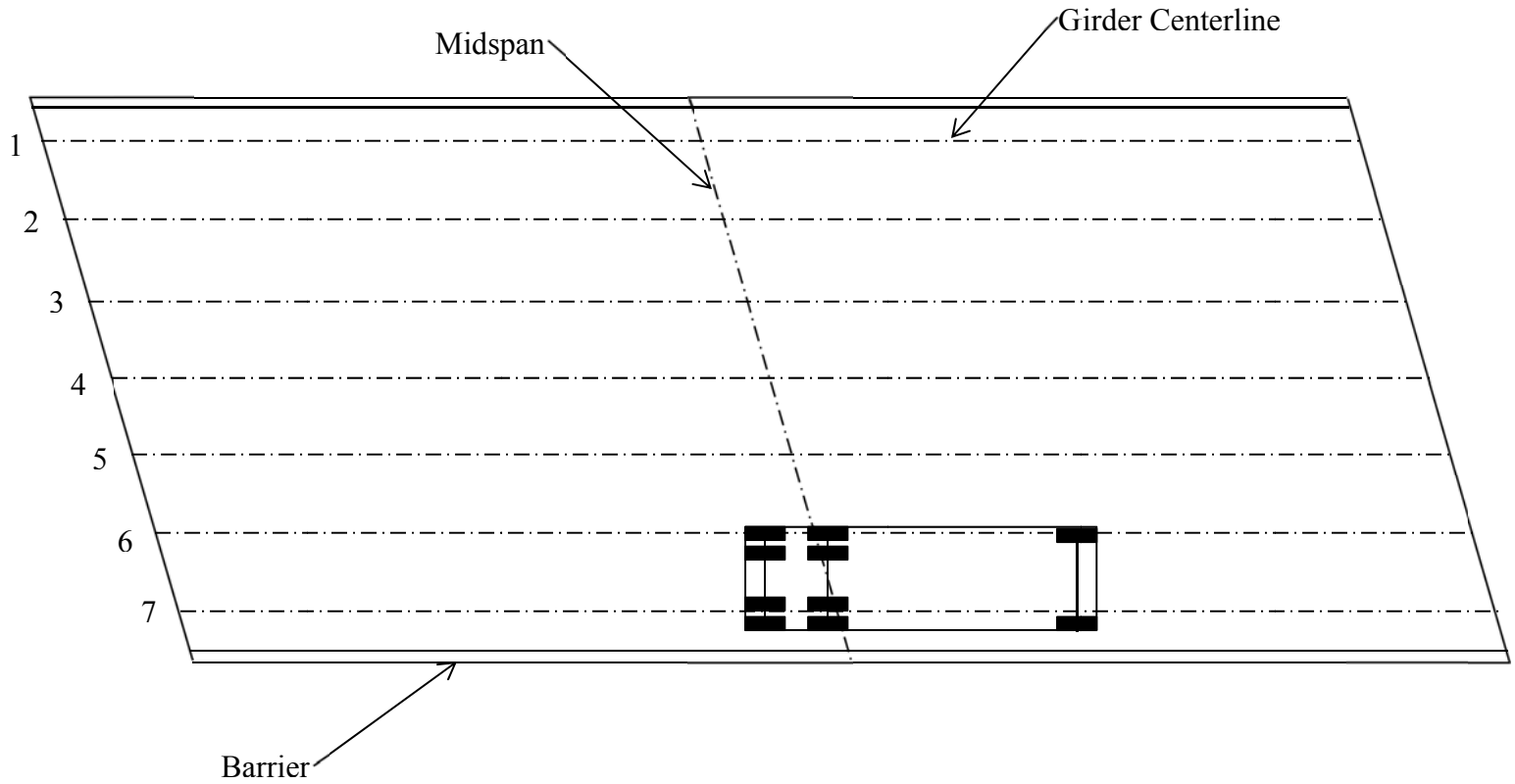

Figure 4.3. *Eastbound load truck placement for position A on spans 1 and 2.*

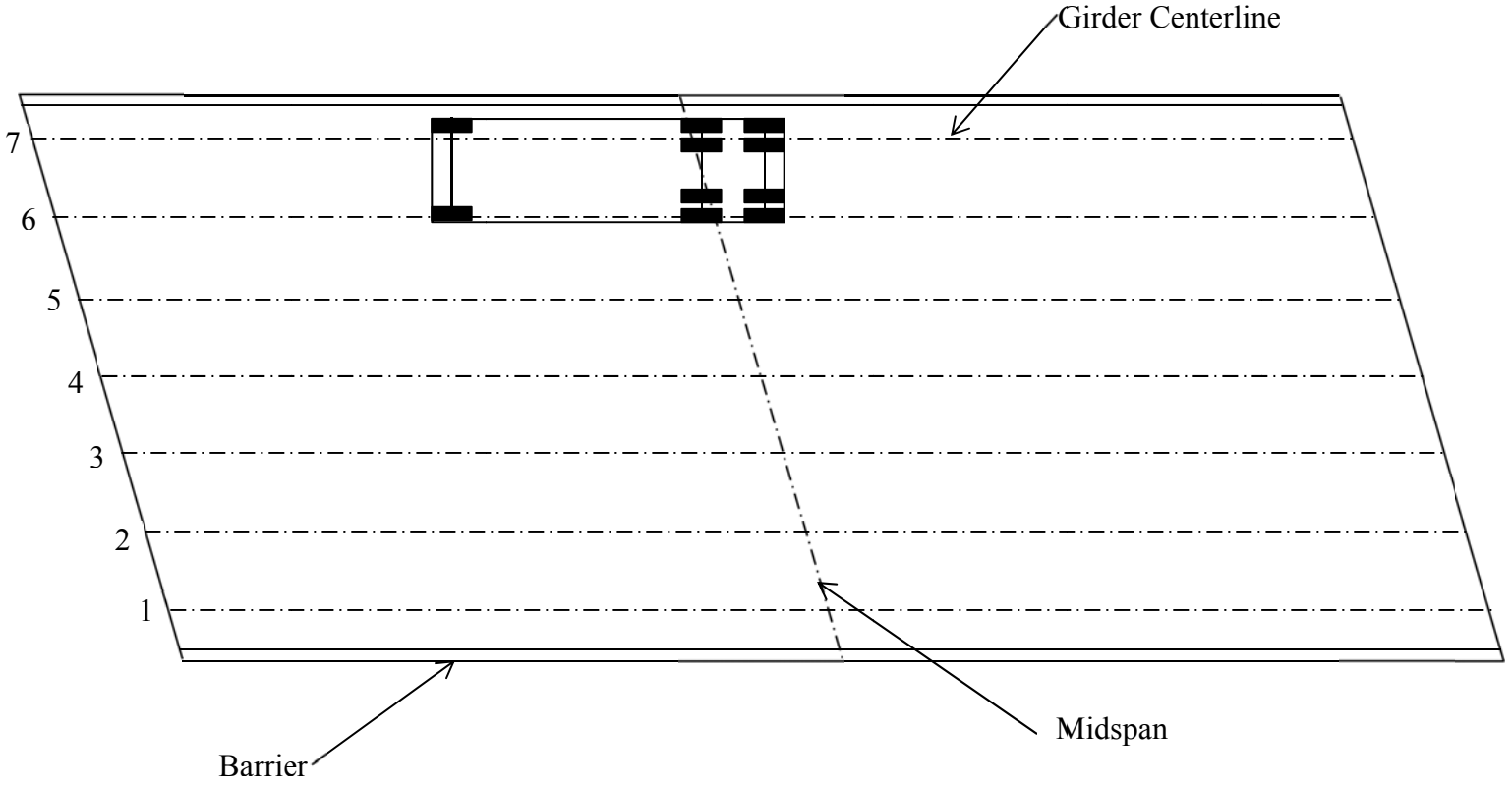

Figure 4.4. *Westbound load truck placement for position A on spans 3 and 4.*

In order for the testing team to accurately place the truck into the correct positions, the bridge deck was marked the morning of the load test with blue masking tape (Figure 4.8) and 4.9). Each tape mark was placed so that it would line up with the outermost edge of the outer tire tread on the "Center" axle of the truck.

Load truck positions were chosen to determine the worst-case scenario truck combinations for an exterior and interior girder within each span. Truck positions A, E, and H were utilized to impart the worst case load scenario on girder 7. Positions B, E, and H were utilized to impart the worst case load scenario for girder 6. The combination of positions C, F, and H and the combination of D and G were utilized to determine the worst case load scenario for girder 4.

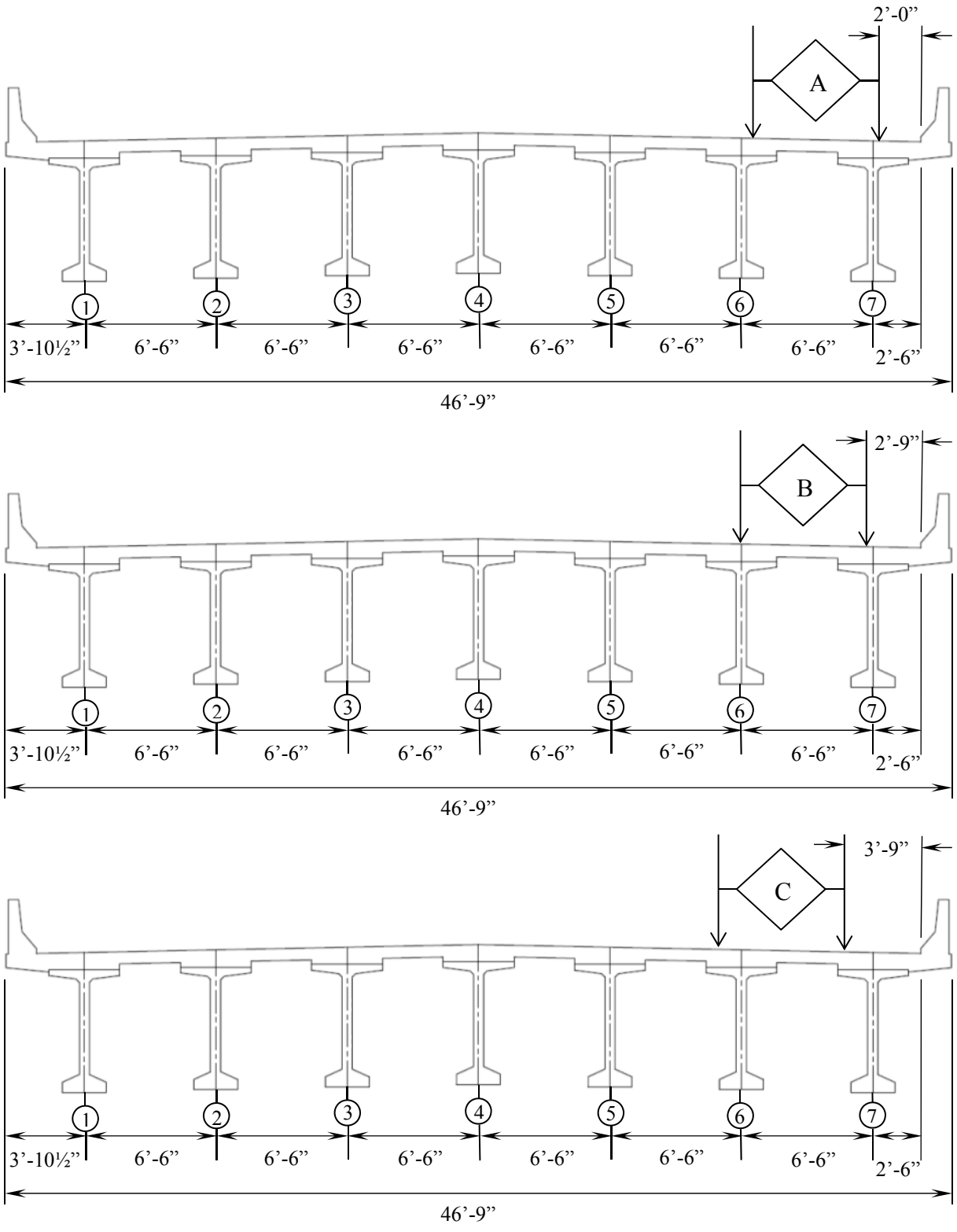

Figure 4.5. *Transverse load-truck positions A, B, and C from first load test.*

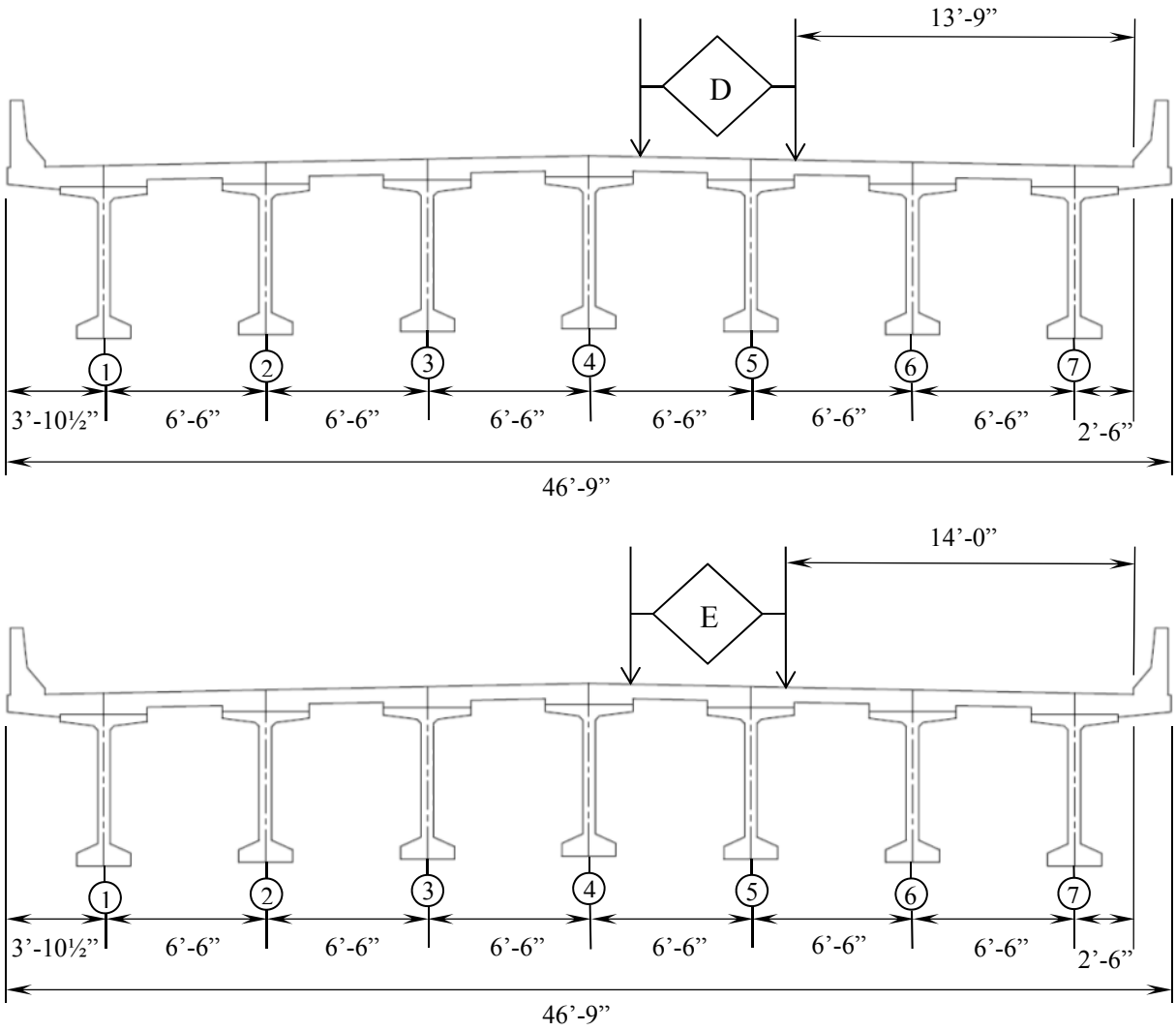

Figure 4.6. *Transverse load-truck positions D and E from first load test.*

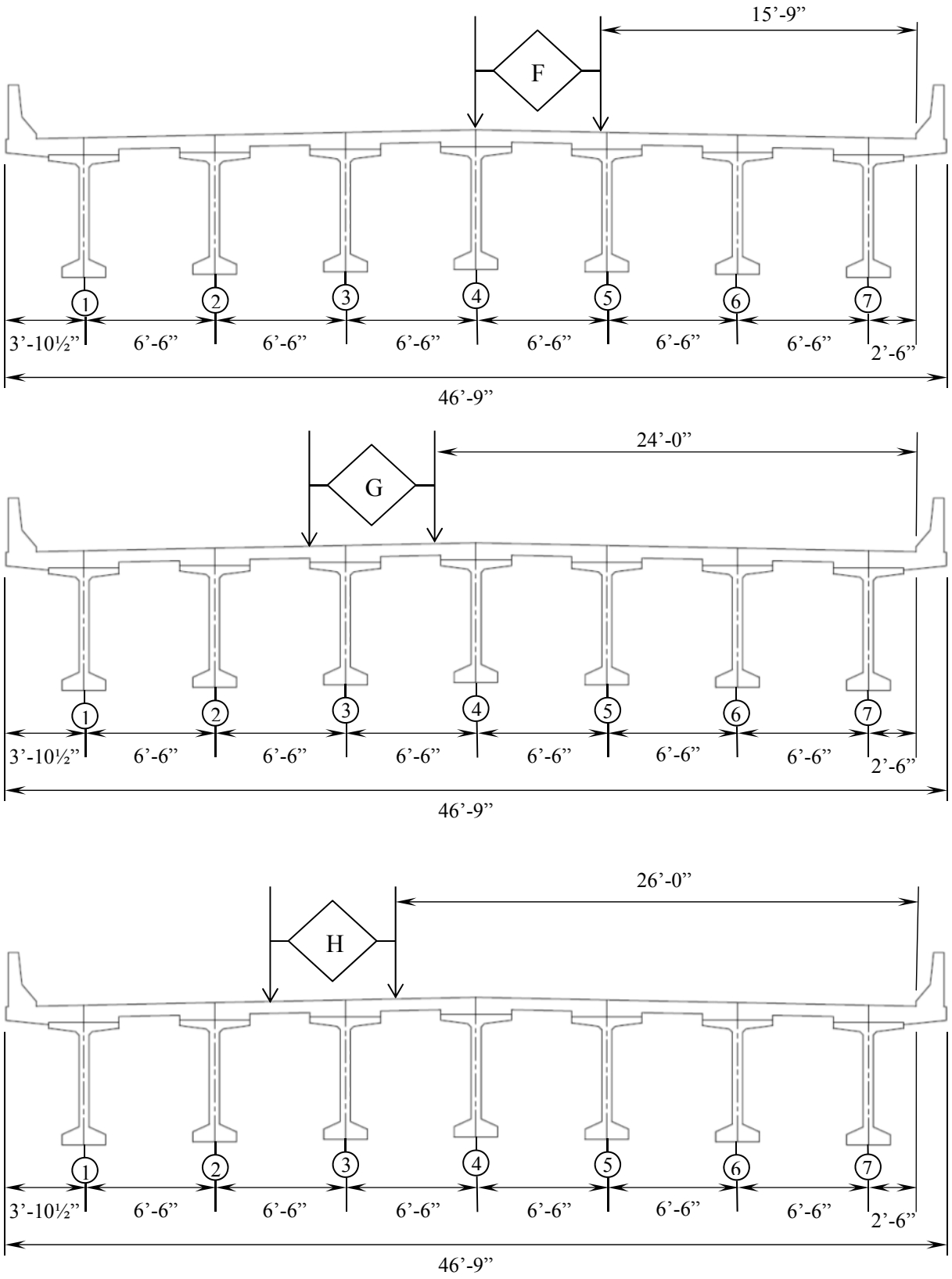

Figure 4.7. *Transverse load-truck positions F, G, and H from first load test.*

Figure 4.8. *Tire positioning marks on the bridge deck.*

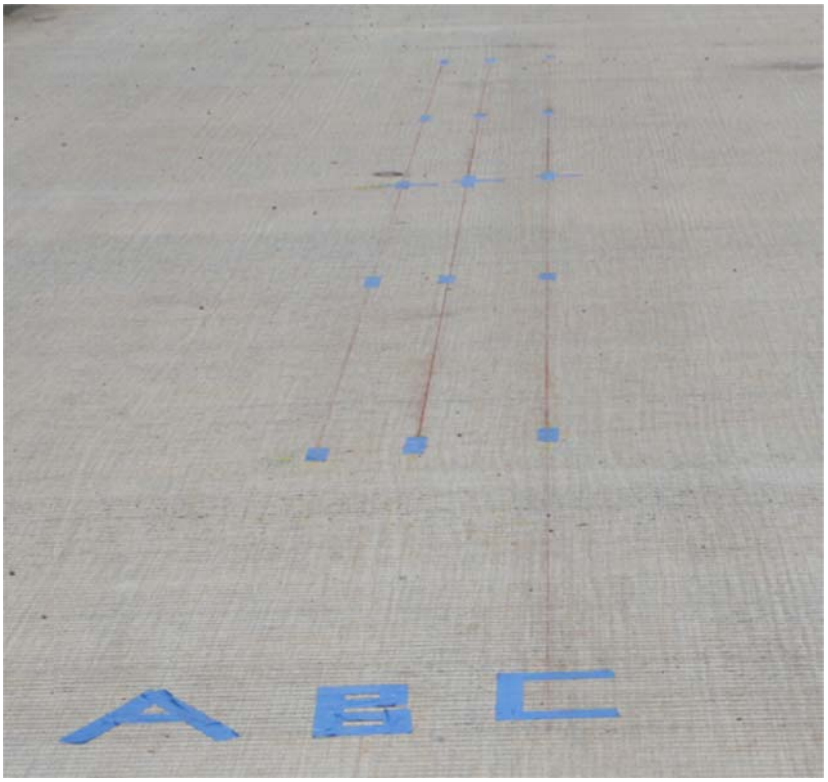

Figure 4.9. Load-truck placement markings on the bridge deck.

4.3.2 Truck Placement Procedure

Only one load-truck was used for Load Test 1 due to limited ALDOT load-truck availability. To begin the first day of testing, the truck was faced in the eastbound direction (Figure 4.3); in line with the transverse load position A but just off of span 1of the bridge. An initial baseline sensor reading set was then taken for about twenty seconds for the data acquisition system. The load truck was then pulled onto span 1 and put into position A for approximately four and one half minutes. The truck was then pulled directly forward to span 2, position A and left in position for approximately four and one half minutes. While the truck was on span 2, this allowed for a second baseline reading to occur for the span 1 sensors while the span was unloaded. Likewise, an initial baseline reading was taken for the span 2 sensors while the load truck was on span 1. After the span 2 readings were taken, the truck was removed from span 2 to allow for the last span 2 baseline readings to be taken. The truck was then moved to just off of span 1 again, but this time along the transverse position B line. The process was then repeated for each of the seven remaining position lines. Once every load position on spans 1 and 2 had been tested, transverse position lines A, B, C, D, and F were loaded an additional time for both spans. Time limitations did not allow for every transverse position line to be run an additional time at midspan for each span.

To begin the second day of testing, the truck was oriented westbound and place in line with transverse load position A, but located just off of span 4 of the bridge. A "baseline" reading was then taken for the data acquisition system, lasting approximately four and one half minutes. The truck then pulled onto span 4 and rested at midspan in transverse load position A for four and a half minutes. The truck was then moved from span 4 to span 3 along the transverse load position A line and allowed to rest at midspan while the DAS recorded sensor data. The truck

was then removed from span 3 and another baseline reading was taken. The same process was then repeated for the remaining seven transverse position lines on spans 3 and 4. Once each load position had been tested, transverse position lines A, B, and F were retested for both spans 3 and 4. Time limitations once again did not allow for every transverse position line to be tested an additional time at midspan for each span.

4.4 Load Test 2

The second load test on the bridge over Hillabee Creek was performed on May 21st and 22nd, 2013. The first and second spans were tested on May 21st under sunny skies with temperatures in the upper 80s degrees Fahrenheit while the third and fourth spans were tested on May 22nd under mostly cloudy skies with temperatures in the middle 80s degrees Fahrenheit.

4.4.1 Static Test Locations on Bridge

Load Test 2 utilized two ALDOT LC-5 configured load trucks shown in Figure 4.2. The test utilized transverse singe-truck load positions A, E, and H shown in Figures 4.5, 4.6, and 4.7. Load positions B, C, D, F, and G were not utilized for the second load test. The results from the first load test indicated that positions A, E, and H provided the critical load combinations for both girder 6 and girder 7. Girder 4 was determined not to be a critical girder for design of the bridge. In order to test superposition, the two trucks were positioned simultaneously as shown in Figure 4.10. Thus, the second load test utilized a total of five static truck positions (A, E, H, A&E and E&H) per span. Like the first load test, the middle of the "Center" axle of each truck was place over the midspan of the bridge for each transverse load position.

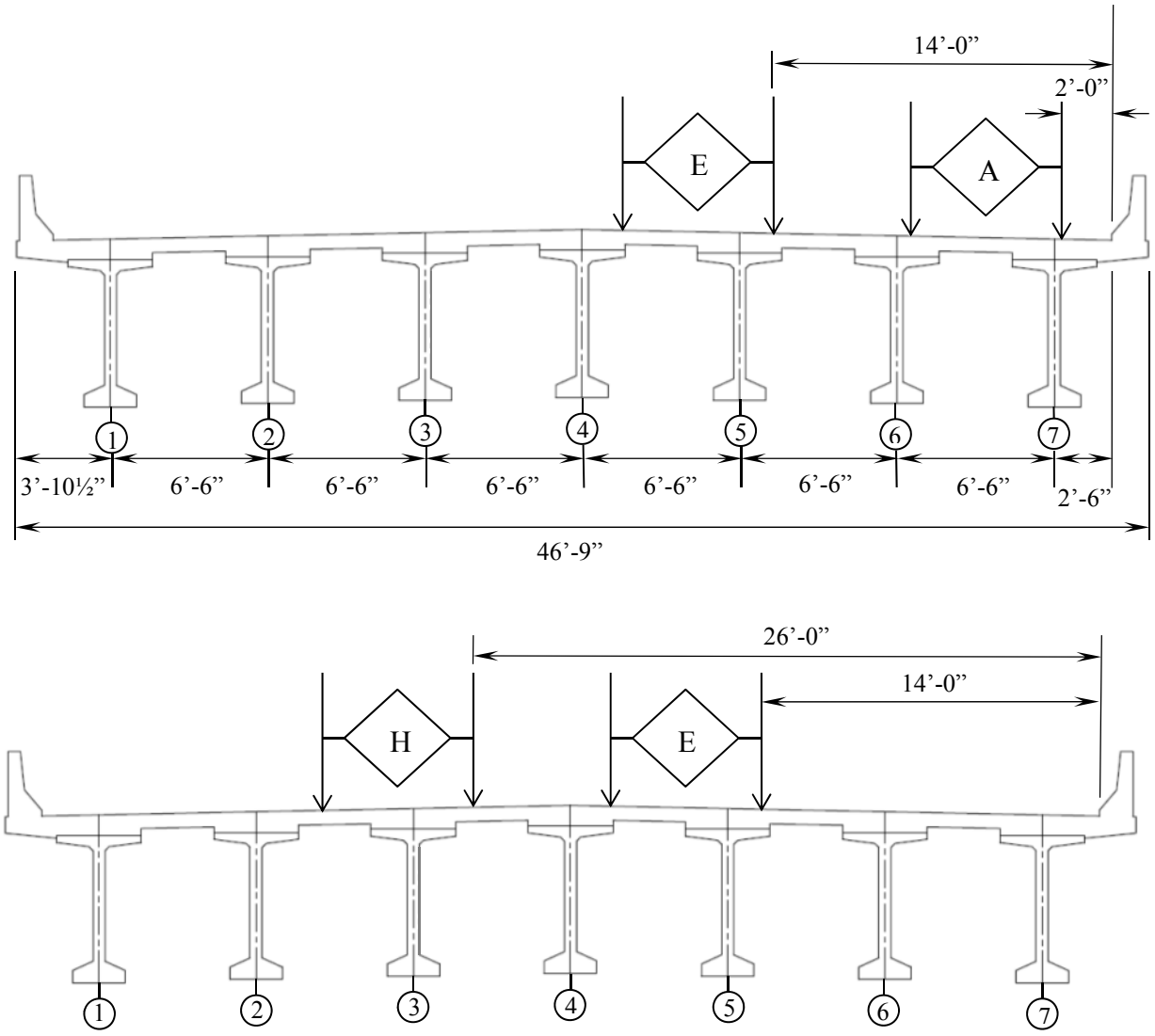

Figure 4.10. *Two-truck load cases, A&E and E&H, from the second load test.*

4.4.2 Truck Placement Procedure

Similar to load test 1, the load trucks began the test in line with a transverse load position but off of the east side of the bridge. Load truck 1 (LT1) was aligned with position A while LT2 was aligned with position E. The bridge was then cleared of all traffic and a six second baseline reading was taken by the DAS. LT1 was then pulled onto span 4 at midspan of transverse position A and allowed to sit for ten seconds. Next LT2 was pulled onto span 4 at midspan of

transverse position E while LT1 was left in place. Ten seconds was again allowed to pass and LT1 was pulled forward to transverse position A at the midspan of span 3 where it remained static for ten seconds while the DAS logged sensor data. LT2 was then pulled forward to midspan of span 3 where another ten second reading occurred. LT1 was then moved off of span 3 while LT2 remained for another ten second reading. Finally, both trucks were removed from the bridge to allow for another baseline reading. This same process was then repeated to allow for duplicate readings to be taken for each load position in case of a DAS malfunction.

The preceding procedure was then repeated with the exception of transverse truck placement. LT2 was still aligned with transverse position E while LT1 was aligned with transverse position H. The previous procedure was then followed and repeated to protect against DAS malfunctions or inconsistencies.

Day two included tests of spans 1 and 2 of the bridge. The load trucks began the test in line with a transverse load position off of the west side of the bridge. Load Truck 1 (LT1) was aligned with position A while LT2 was aligned with position E. The bridge was then cleared of all traffic and a six second baseline reading was taken by the DAS. LT1 was then pulled onto span 1 at midspan of transverse position A and allowed to sit for ten seconds. Next LT2 was pulled onto span 1 at midspan of transverse position E while LT1 was left in place. Ten seconds was again allowed to pass and LT1 was pulled forward to transverse position A at the midspan of span 2 where it remained static for ten seconds while the DAS logged sensor data. LT2 was then pulled forward to midspan of span 2 where another ten second reading occurred. LT1 was then moved off of span 2 while LT2 remained for another ten second reading. Finally, both trucks were removed from the bridge to allow for another baseline reading. This same process was then

repeated to allow for duplicate readings to be taken for each load position in case of a DAS malfunction.

The preceding procedure was then repeated with the exception of transverse truck placement. LT2 was still aligned with transverse position E while LT1 was aligned with transverse position H. The same loading process from above was then followed and repeated to protect against DAS malfunctions or inconsistencies.

Due to having more time remaining in the workday than the previous load testing session, the team decided to make another run down transverse positions E and H as well as positions A and E. The preceding procedure was then repeated with LT2 aligned with position E while LT1 was aligned with position H. Next, LT1 was moved to transverse position A while LT2 remained on position E and the procedure was repeated again. This extra testing resulted in ten additional data recordings for the DAS.

4.5 Data Processing

A single number result was desired for each sensor for each recorded event during load testing of the bridge. Even though data collection occurred during static conditions, every sensor experienced some level of noise throughout all of the load tests. The noise variance seemed to be due to electrical noise. Although all lanes of the bridge were closed to traffic during the load test, some residual bridge movement could have been present due to the movement of the load trucks prior to data collection. Due to the sensor noise, the effective precision of the measurement systems was determined to be +/- 1 microstrain for the bottom surface strain gauges and +/- 0.005 in. of girder deflection.

During collection, separate raw data files were created for each load truck position interval. Each file was then extracted and plotted with respect to time. The plots were then

analyzed, deleting all extreme outliers. The analyzed sensor data were then averaged to produce a single measurement value per sensor per load truck position interval. Single measurements determined from when the bridge was unloaded immediately before the load truck was put into position were then subtracted from the single measurements determined when a load truck was in place. This data analyzing technique was employed to filter out thermal effects on the concrete throughout the course of the load test. Each resulting measurement value represents a change of strain or deflection due to the placement of a load truck in a load position.

Chapter 5 Finite-Element Bridge Model

5.1 Introduction

The bridge over Hillabee Creek was modeled in CSiBridge analysis software (Figure 5.1) to determine the effects of barriers and changes in the webwall orientation on bridge performance. It was also desired to compare analysis results of a full model of the in-situ bridge to the field load test results. CSiBridge is an object-based interface that converts bridge objects to a finite-element model to be analyzed using SAP2000 structural analysis techniques. Three separate models of the bridge were created. The first solely utilized the built-in "model-building wizard" in CSiBridge. The second utilized a modified form of the first, manually changing the intermediate webwalls from a 15 degree skew to the in-situ bridge condition of perpendicular to the girders. The last model utilized the second modified model but added barriers to the model. The software was utilized to implement loads equivalent to the live loads applied to the bridge over Hillabee Creek and allowed for strains and bridge model deflections to be calculated for all three model forms and compared to the live-load test results. Models one and two and models two and three were also compared to determine the effects of the adjusted intermediate diaphragms and traffic barriers on bridge behavior.

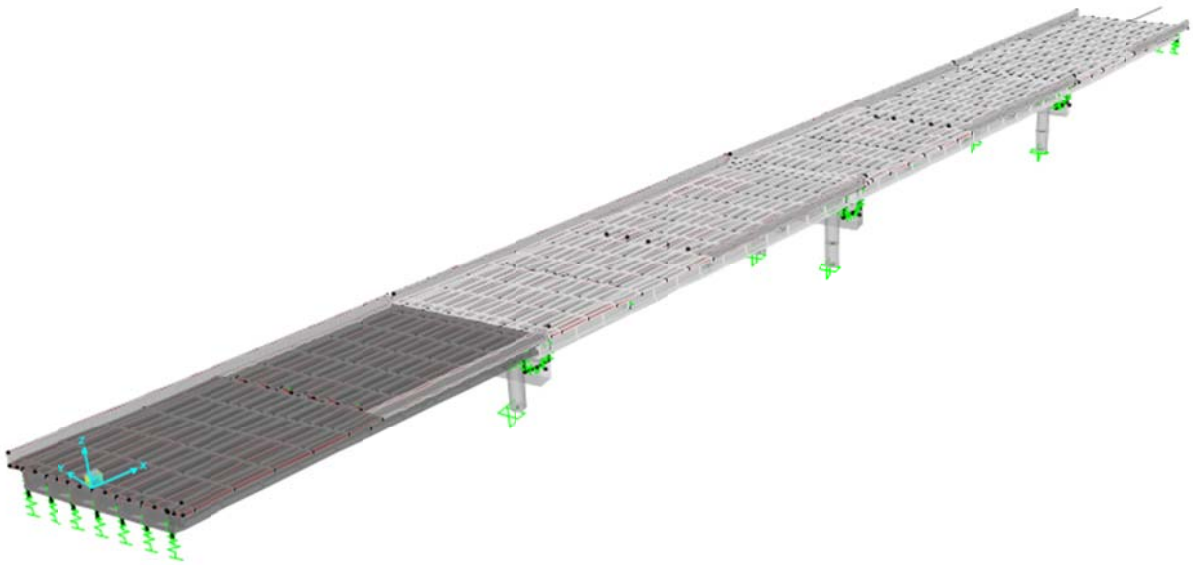

Figure 5.1. An extruded view of the full bridge model with barriers and staggered webwalls.

5.2 Bridge Model with Barriers and Simplified Webwalls

To create the first model, CSiBridge was opened and the *model-building wizard* was engaged. The first step involved creating a layout line. This line served as the reference line for the rest of the model construction. To create the line, the *define/show layout lines* button was utilized. The *add new line* button was then used to create a layout line for the model. The appropriate line bearing (bearing of the bridge), initial and end line stations (the same as the start and end stations of the bridge) were then input into the appropriate fields.

5.2.1 Define Material Properties

The next required step in the model was to identify the basic material properties of the model components. The *materials* field in the wizard was highlighted and the *define/show material properties* button depressed. Material properties (from Table 3) were then added for each bridge component (deck span, barriers, webwalls, and girders). The *add new material* button was utilized to add material properties for each bridge component. In the window, the

material name, display color, material type, modulus of elasticity, and concrete compressive strength were specified for each component. Though concrete modulus of elasticity and compressive strength test values were available for concrete from each girder in this bridge, CSiBridge only allows users to input a single set of girder property values per span. Therefore, girder properties were averaged on a per span basis and entered into the program accordingly. Substructure and diaphragm concrete, which was not collected and tested for the project, was assumed to be 4000 psi in compressive strength with a modulus of elasticity of 3600 ksi for all models. Reinforcement properties were not input due to the assumption that the bridge superstructure behaved completely within its uncracked, linear-elastic range during all testing and modeling.

5.2.2 Define Frame Sections

Following material properties, frame cross sections for columns, bents, and girders were defined for the model. The *Frame Sections* label was highlighted in the bridge modeler wizard and the *Define/Show Frame Sections* button selected. Frame section properties were then defined for each column, bent, and girder span. First the bents were created by clicking *Add New Property*. The *Frame Section Property Type* was set to *Other* and *Section Designer* was selected due to the desired bent section not being included in the default frame shapes. The section was then appropriately named and the appropriate *Base Material* was selected from the list of previously created material properties. The model was only sought for analyzing bridge behavior and not for design; therefore *No Check/Design* was selected under *Design Type*. The *Section Designer* button was then selected under *Define/Edit/Show Section*. The *Designer* then allowed the cross section of the bent to be drawn, as shown in Figure 5.2. The bent creating process was repeated twice to accommodate bents 3 and 4. Next, the column cross section was

created. The *Frame Section Property Type* was set to *Concrete* and *Circular* was selected. The section was the appropriately named and the appropriate *Material* was selected from the list of previously created material properties. The diameter of the column was specified under the *dimensions* section. All columns in the project utilized the same cross section. No reinforcement was detailed for the column due to the limited substructure scope of the model. Lastly, the girder section from each span was created. Girders were defined as straight frame elements. The *Frame Section Property Type* was set to *concrete* and the *Precast I* button was selected. The proper span-girder material group was selected from the previously created material properties. Lastly, the proper AASHTO PCI bulb tee section was then selected from the *Set Section Dimensions Based on a Standard Section* tab. This selection activated the auto-fill function for all dimensions for the girder cross section.

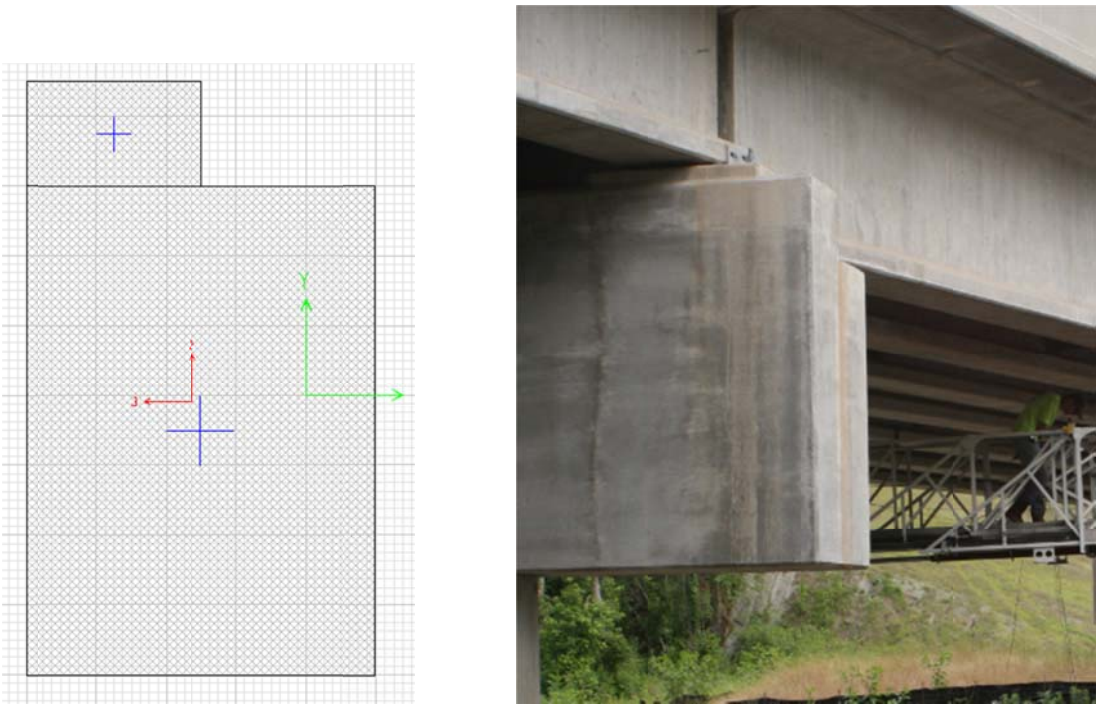

Figure 5.2. *Cross section of Bent 2 drawn in CSiBridge Modeler Section Designer and a picture of the in-situ bent.*

5.2.3 Define Bridge Component Properties

The Bridge Component Properties were addressed next. The first required label highlighted was *Deck Sections*. The *Define/Show Deck Sections* button was utilized for the deck on Span 1 and a new section was added. The *Precast I Girder* was selected under *Other Concrete Sections*. In the resulting window, the deck section was properly named. The corresponding *Slab Material Property* was then selected from the previously defined *basic material properties*. Element type was set to thin shell element. The *Number of Interior Girders* was set to 5 and the *Total Width* of the bridge was input. The *Girder Longitudinal Layout* was set to *Along Layout Line* so that the bridge girders parallel the previously defined model layout line. *Constant Girder Spacing*, *Constant Girder Haunch Thickness* and *Constant Girder Frame Section* were all set to *Yes* as seen in Figure 5.3. The appropriate *Top Slab Thickness* from the plans was then inserted. The *Concrete Haunch Thickness*, averaged over the length of the bridge span (Table 5), was then input into the appropriate field. Next, the *Girder Section* for Span 1 was selected from the previously defined *Frame Sections*. The *Fillet Horizontal Dimension Data*, *Left Overhang Data* and *Right Overhang Data* fields were completed utilizing information from the bridge plans. The *Live Load Curb Locations* and *Insertion Point Location* were left at *0* due to the manual insertion of live loads into the model. This *Deck Sections* procedure was then repeated three times for spans 2, 3, and 4.

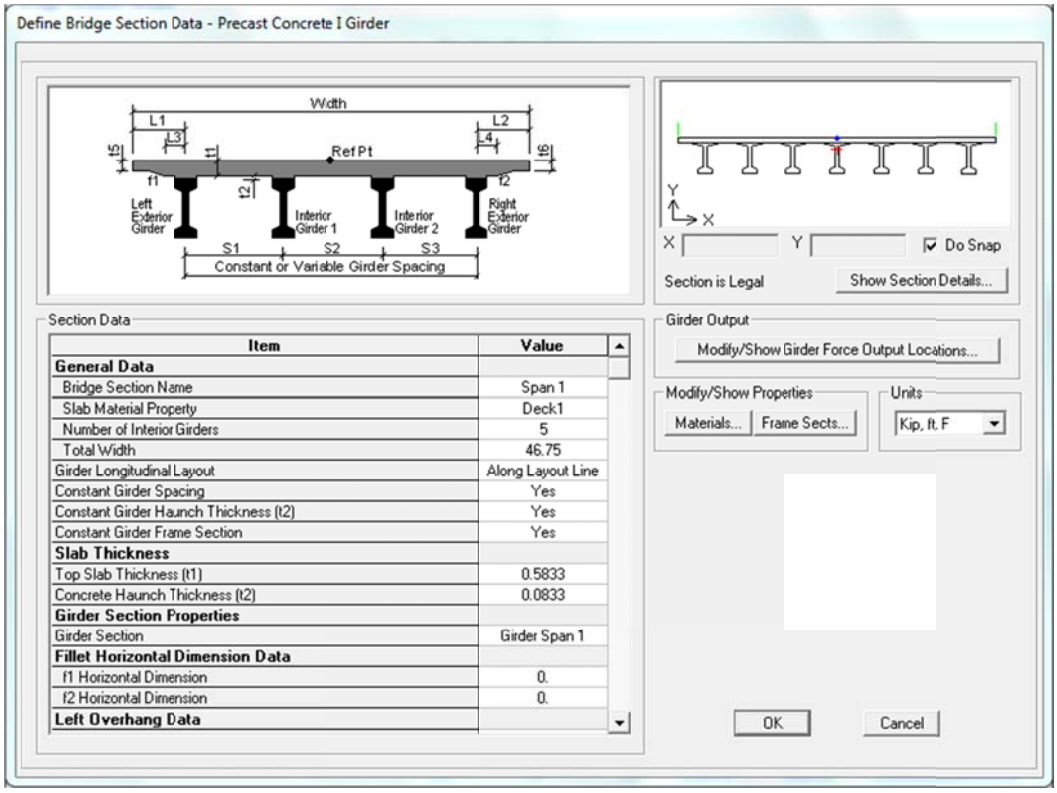

Figure 5.3. *Define Bridge Section Data Window*.

Diaphragms were then added to the model. The *Diaphragms* field was highlighted and *Define/Show Diaphragms* was clicked. *Add New Diaphragm* was selected in the resulting window. In the *Add New Diaphragm* window, the diaphragm was named and set as a *Solid* diaphragm type. The *Diaphragm Thickness* was defined. The diaphragms were defined as thin shell elements.

5.2.4 Define Bridge Bearings

The next section that required addressing was *Bearings*. *Bearings* was selected and "Define/Show Bearings" clicked. A new bearing was added by clicking *Add New Bridge Bearing*. The bearing was appropriately named as *Fixed End* and then set to *User Definition* under the *Bridge Bearing is Defined By* section. The *User Bearing Properties* were defined as follows: Translation Vertical (U1)-Fixed, Translation Normal to Layout Line (U2)-Fixed,

Translation Along Layout Line (U3)-Fixed, Rotation About Vertical (R1)-Free, Rotation About Normal to Layout Line (R2)- Free, Rotation About Layout Line (R3)-Free. The window was then closed and another bearing condition, named *Free End* was created. The *Free End* bearing utilized the same setup as the *Fixed End* bearing with the exception of *Translation Along Layout Line*. It was set to *Free* instead of *Fixed*.

The next required step was to define *Foundation Springs*. The *Define/Show Foundation Springs* button was employed to bring up the editing window. In the editing window, the foundation spring was appropriately named, and *User Definition* was selected under *Foundation Spring is Defined By*. The *Property is Defined for This Length in a Line Spring* was input as the length of the abutments in the bridge. The *Property is Defined for This Area in an Area Spring* defined as the area of the columns in the bridge. All degree of freedom *Release Types* were set to *Fixed*.

Abutments were then defined. The *Define/Show Abutments* button was utilized to bring up the editing window. *Add New Bridge Abutment* was clicked and the abutment was named *Abutment1* in the window. The *Girder Support Condition* was set to *Connect to Girder Bottom Only* and *Substructure Type* was set to *Foundation Spring*. The appropriate *Foundation Spring Property* was selected from the drop-down list of previously defined foundation springs. The abutment procedure was then repeated and named *Abutment5* for the abutment at the far end of the bridge.

Next, the three bents were defined. *Bents* was highlighted in the wizard and *Define/Show Bents* was selected. *Add New Bridge Bent* was utilized to bring up the edit window and define *Bent2*. The *Cap Beam Length* and *Number of Column* fields were completed. The appropriate *Cap Beam Section*, as defined in *Frame Sections*, was selected. The *Bent Type* was set as

Double Bearing Line. The *Girder Support Condition Before Bent* was changed from *Integral* to *Connect to Girder Bottom Only*. Under *Location of Bearing Line Before Bent* the *Distance from Bent to Bearing Line* was input as the distance from the center of mass of the bent to the bottom fiber of the girders from span 1. *Girder Support Condition After Bent* was also changed from *Integral* to *Connect to Girder Bottom Only*. The *Location of Bearing Line After Bent,* a vertical distance, was changed to reflect the location on the span 2 side of *Bent 2*. The preceding bent-definition process was repeated two times to define *Bent 3* and *Bent 4*.

5.2.5 Assign Bridge Objects

The next step required the bridge objects to be defined. Under *bridge object definitions* all superstructure objects orientations are defined along with how the superstructure objects related to one another. *Bridge Object Definitions* was highlighted and *Define/Show Bridge Objects* was selected. *Add New Bridge Object* was then selected in the resulting window yielding a bridge object editing window Figure 5.4. The bridge object was properly named and the previously defined layout line was selected from the pull-down menu under *Layout Line Name*. Under *Define Bridge Object Reference Line*, *Span 1* was entered into the *Span Label* box along with the appropriate span 1 *ending* station. *Add* was then selected. The action was repeated for spans 2 and 3 as well. The program-created *Span to End Abutment* was then modified by entering the appropriate station and selecting *Modify*. Under the *Modify/Show Assignments*, *Abutments* was highlighted and *Modify/Show* was selected. *Start Abutment* was then highlighted and under *Superstructure Assignment*. *Abutment Direction* was changed to read *Default+15* to properly skew the abutment and superstructure attached to it. *Diaphragm Property* was assigned *None*. All diaphragms, intermediate and end, were added later under *In-Span Cross Diaphragms* to ensure proper diaphragm location. *Substructure Assignment* was

changed to *Abutment Property* and the proper previously defined *Abutment Property* was selected from the drop-down menu. Under *Substructure Location*, "*Elevation*" was set to the proper global *Z* distance from the *Layout Line* (Note: This distance was a negative number to denote a decrease in elevation). Under *Bearing Assignment*, the *Bearing Property* was set to the proper previously defined *Bearing* (either *Fixed* or *Free*). The *Restrainer Property at Bearing* was set to *None* and the *Elevation at Layout Line* was set as the same as it was under *Substructure Location*. These steps were repeated for the *End Abutment* tab.

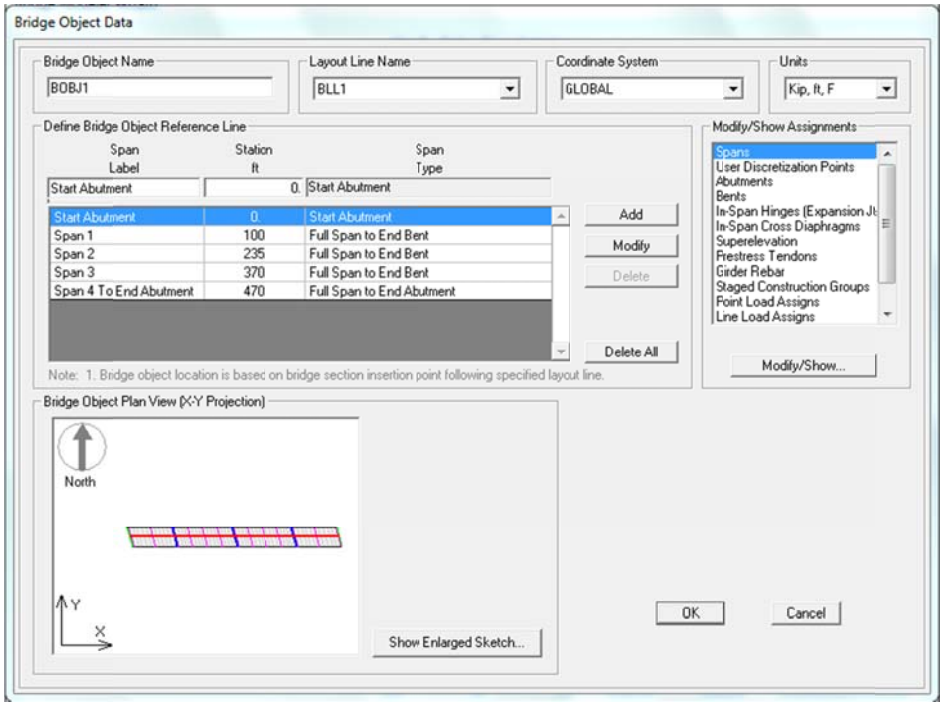

Figure 5.4. *Bridge Object editing window in CSiBridge software.*

Under the *Modify/Show Assignments*, *Bents* was highlighted and *Modify/Show* was selected. Under *Specify Bent Considered*, *Bent is at the End of this Span* was set to *Span 1* in order to change the properties of Bent 2. Under *Superstructure Assignment*, *Mesh Superstructure to Match Bent Bearing* was set to *Yes*. *Diaphragm Property Before Bent*, *Diaphragm Property After Bent*, and *Restrainer Property* remained marked *None*. Under *Bent*

Assignment, *Bent Property* was labeled *Bent2* from the previously defined *Bents*. The *Bent Direction* was once again defined as *Default+15* to accommodate the 15-degree skew of the bridge's substructure and superstructure. Under *Bent Location*, the proper *Elevation* was input with respect to previously defined *Layout Line* with *0 Horizontal Offset*. The *Bearing Assignment Before Bent* and *Bearing Assignment After Bent* sections were completed the same as they were in the *Abutments* section. These steps were twice repeated to assign objects to Bents 3 and 4 by changing the *Bent Considered Section* to the end of the span at which the desired bent is located.

Under the *Modify/Show Assignments*, *In-Span Cross Diaphragms* was highlighted and *Modify/Show* was selected. In the resulting diaphragm assignment window, the appropriate previously defined span was selected from the drop-down menu in the *Span* column, the appropriate predefined diaphragm was selected from the drop-down menu in the *Diaphragm Property* column, the appropriate distance from the beginning of the span to the center of the diaphragm was entered into the *Distance* column. *Default+15* was entered into the *Bearing* column to accommodate the proper skew of the bridge, and the *Location* column remained labeled as *All Spaces*. The *Add* button was then selected to create a line of diaphragms in the span. These steps were repeated for all of the lines of diaphragms, including end diaphragms, in all spans in the bridge.

5.2.6 Create Load Definitions

The *Define Bridge Objects* window was then temporarily exited to allow for point-load definitions to be created. Due to limited experience with CSiBridge, the project utilized manually inputted point loads for load-truck wheel loads. The program is capable of utilizing model-constructed load trucks assigned to traffic lanes on the bridge model; but it was not

practical for the scope of this project since exact replication of actual live-load truck positions was required for comparison with test results. Item 4.8, *Point Load Definitions* was highlighted in the Bridge Wizard window and *Define/Show Point Loads* was selected. *Add New Point Load* was selected to add a point representative of one wheel/wheel group of the load truck. The appropriate *Load Name* was input ("VC D back driver" indicated the driver's side, back axle wheel group of a load truck over VC girders, in load-truck position D). Under *Load Direction*, *Load Type* was set to *Force*, *Coordinate System* was set to *GLOBAL*, and *Direction* was set to *Gravity*. Under *Load Value*, *Value* was input with the appropriate force for the wheel group. *Load Transverse Location* was set to *Left Edge of Deck*, implying that the *Load Distance from Reference Location* would be measured normal to the leftmost edge of the deck to the wheel group's location. The process was repeated until all truck wheel groups that were necessary for every load truck position were input into the model.

5.2.7 Define Load Patterns

Once the point loads were defined, in the Bridge Wizard, *Point Loads* was highlighted under the *Bridge Object Assignments* step and *Assign/Show Point Loads* was selected. The *Load Patterns* button on the right side of the pop-up window was then selected. Load patterns were then defined. Load patterns served as *load cases* from the live-load test on the bridge. Each load-truck position (A, B, C, D…etc.) for each span was a load pattern in the model (Span 1F, Span 2F, Span 3F…etc.). The appropriate *Load Pattern Name* was then entered into the field, *Type* was set to *VEHICLE LIVE*, and *Self Weight Multiplier* was set to *0*. *Add New Load Pattern* was then selected to create the new load pattern. This step was repeated until every load truck position for each span had been accounted for. The *Define Load Patterns* window was then closed and returned to the *Point Load Assignments* window. The *Add New* button was selected

and *Load Pattern* was changed from the drop-down menu to the appropriate previously defined pattern, the appropriate, previously defined *Load Distribution* was selected. The appropriate *Start Station* was selected. The *Start Station* refers to the location of the static point load for the model and is referenced in the *X* direction from the onscreen coordinate system. The coordinate system is usually originated from beginning station of the first span, and was in this model. The *Spacing* field was left in its original condition due to only one, static point load being utilized. *Number* was set to *1*. This process was repeated until all appropriate combinations of *Load Patterns* and *Load Distributions* had been accounted for.

5.2.8 Bridge Model Analysis

Once the *Point Loads* had been assigned the proper magnitude and location, the loads were applied to the model, finite-element analysis performed and the results documented. The Bridge Wizard was closed and returned to the 3-D view of the model (Figure 5.5). The *Home* tab was chosen and *Update Model* selected. In the resulting window, the proper *Bridge Object* was selected and *Update Linked Model* was selected under *Action*. Under *Structural Model Options*, *Update as Area Object Model* was selected and the *Maximum Submesh Size* defined as 4 ft^2. The appropriate maximum submesh size was determined through model iterations, gradually decreasing the maximum submesh size until the results approached a constant value. Under *Discretization Information, Maximum Segment Length for Deck Spans* was defined as 10 feet in order to comply with AASHTO LRFD Bridge Specifications section 4.6.3.3.1 which states that a minimum of five, and preferably nine, nodes shall be utilized per span. With a maximum segment length of 10 feet, spans 1 and 4 were assured to be assigned at least nine nodes each. These settings also ensured that the maximum aspect ratio for finite element models of 5.0 was not surpassed within the decks.

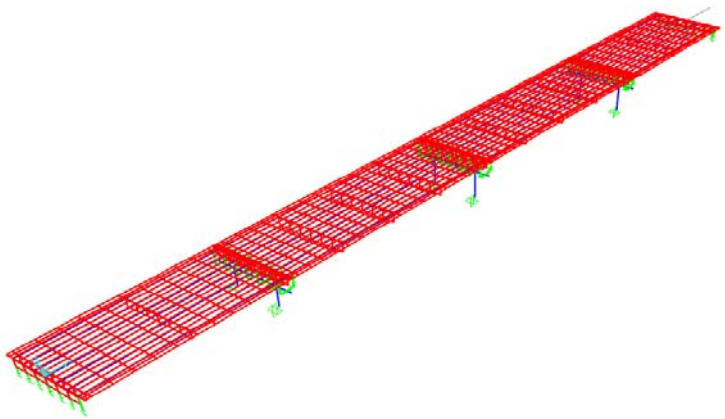

Figure 5.5. *Three-dimensional view of the unextruded bridge model.*

The *Analysis* tab was then chosen and *Run Analysis* selected. In the resulting *Set Load Cases to Run* window, the appropriate *Case Name* was highlighted and *Run/Do Not Run Case* was selected. The selection caused the *Action* column to change from *Do Not Run* to *Run* for the selected *Case Name*. The *Run Now* button was then selected and the program was allowed to apply the selected load case to the bridge model. After the model completed the linear, static analysis, a three-dimensional, deformed bridge model was displayed (Figure 5.6). When the cursor was hovered over the bridge at any point, the displacements and rotations for all degrees of freedom were displayed. This method was utilized for extracting midspan deflected values from the model. In order to extract model strains, the *Home* tab was selected and *Show Bridge Superstructure Forces/Stresses* chosen. The resulting window, *Bridge Object Response Display*, allowed the user to extract stresses at a variety of locations in the superstructure. Under *Select Display Component*, the *Show Results for* field was set to the desired girder (i.e. "Left Exterior Girder"), and the *Force* field was deselected while the *Stress* field was selected. The last dropdown menu was changed to *Longitudinal Stress – Bottom Center (S11)* to reflect the longitudinal stress along the bottom of the desired girder. In order to obtain the midspan longitudinal stress along the bottom of the girder, under the *Mouse Pointer Location* section, the

midspan distance was input into the *Distance from Start of Bridge Object* field. The *Response Quantity At Current Location* then displayed the longitudinal stress at the bottom fiber at midspan of the girder. That stress was then divided by the previously input girder- modulus of elasticity to obtain the corresponding longitudinal strain value. That strain was then recorded.

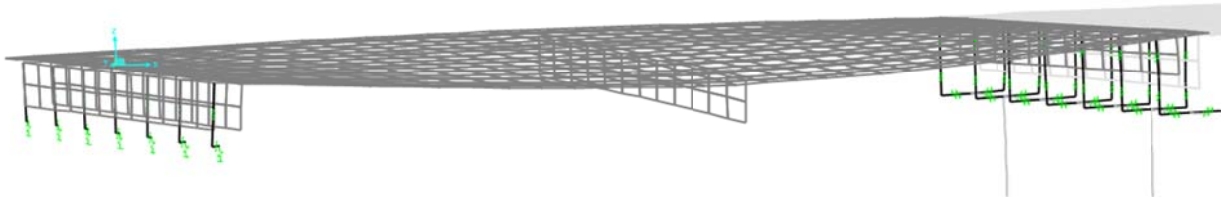

Figure 5.6. *Deformed shape of span 1 after analysis of truck position A.*

In order to run the model for the next test or make any changes or adjustments to the model, the *Analysis* tab was selected and *Model Lock* was chosen to unlock the model. This resulted in all data from the previous run being deleted by CSiBridge. Great care was taken to ensure that the data had already been logged in a separate spreadsheet. Once the model was unlocked and changed if necessary, the next load case was set to run and the process was repeated as many times as necessary to document all load cases and load combinations necessary for comparison to the actual bridge load test.

5.3 Bridge Model with Staggered Webwalls but without Barriers

This model was created in order to analyze the effect of intermediate diaphragms and barriers on the performance of a bridge modeled utilizing the CSiBridge interface.

The CSiBridge Modeler Wizard could only be utilized to insert “straight-line” web walls transversely across the bridge as shown in Figure 5.7. The bridge over Hillabee Creek, however, utilized discrete webwalls that, though they were located along the skew of the bridge, were oriented normal to each girder, also seen in Figure 5.7. In order to obtain a more accurate model

of the in-situ bridge, the model was edited to include webwalls similar to those in the bridge over Hillabee Creek.

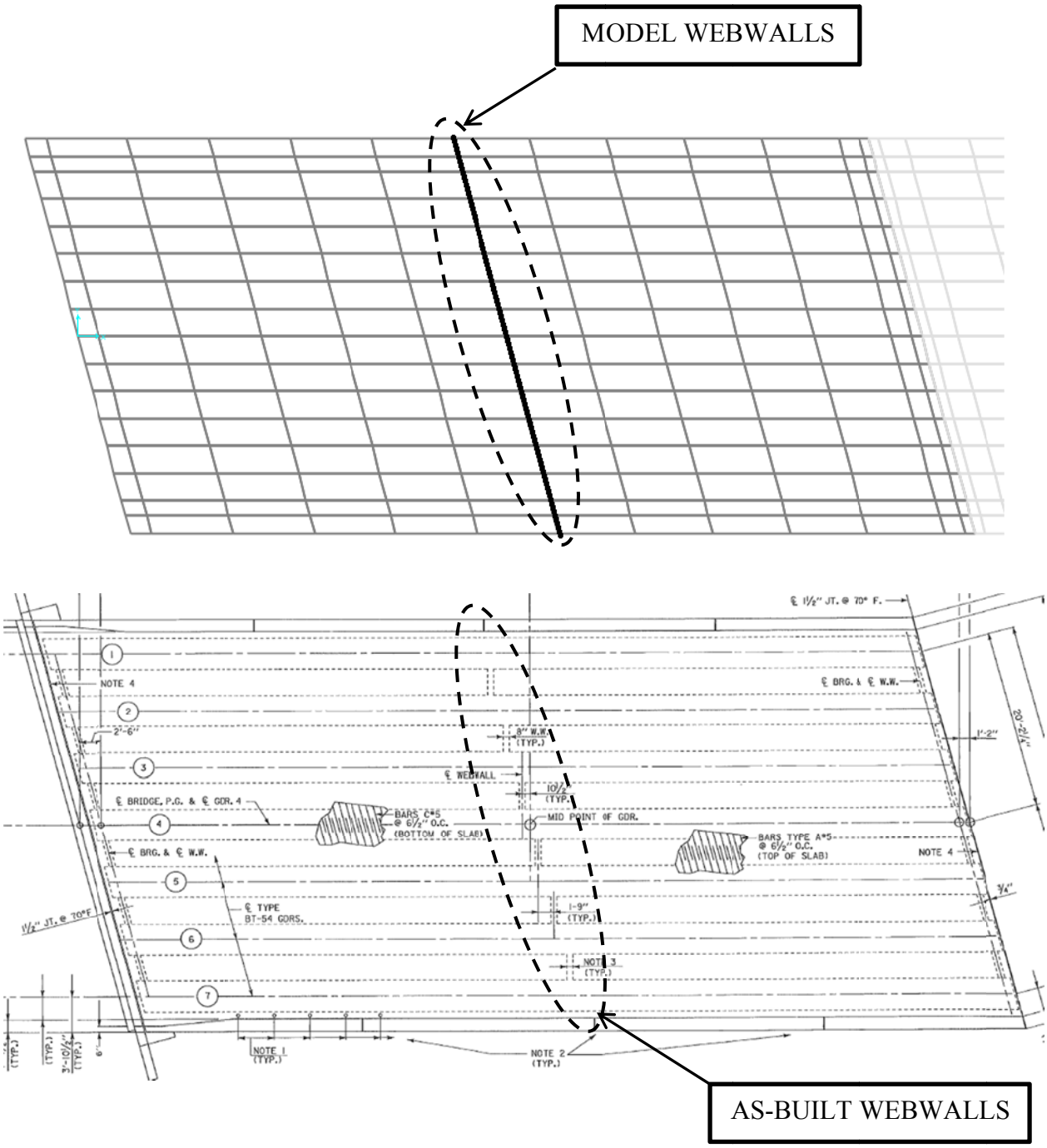

Figure 5.7. *CSiBridge Wizard-defined webwalls and as-built webwalls for span 1 of the bridge.*

5.3.1 Webwall Adjustment

The web walls were adjusted utilizing the *Advanced* tab in CSiBridge modeler. Prior to the utilization of the editing techniques available in the *Advanced* tab, the bridge model was completed to the most accurate condition possible utilizing the Bridge Wizard. The *Bridge* tab was then selected, and *Auto Update* was deselected. The *Update* option was then chosen. Under *Select a Bridge Object and Action* in the resulting window, the proper bridge object was selected and the *Action* was set to *Convert to Unlinked Model*. This step converted the model from a model that utilized the Bridge Wizard only, to one that allowed the *Advanced* tab to be used to customize the model. It is important to note that the model was completed to the most accurate extent possible utilizing the Bridge Wizard. After the model was unlinked, it could only be edited manually under the *Advanced* tab, eliminating the Bridge Wizard's editing advantage.

Once the model was unlinked and the *Advanced* tab selected, the bridge model was prepared to be edited. The tools under the *Advanced* tab are similar to those in SAP2000. The model was then edited utilizing SAP2000 editing techniques. The first editing step necessary was to delete all intermediate, Bridge-Wizard-created webwalls. Each webwall was individually selected and deleted. The next necessary step was to define the webwall section material properties and thickness. *Define -> Section Properties -> Area Sections* was selected. In the resulting window, the *Select Section Type to Add* section was defined as *Shell*. *Add New Section* was then chosen and the section appropriately named. Under *Type*, *Shell-Thin* was selected. *Material Name* was set to the appropriate predefined material property for the webwalls. Both *Membrane* and *Bending* thickness under the *Thickness* section were set to 0.66 ft. The thickness of the webwalls was measured normal to the later-defined, user-drawn area object. The next step required was to define nodes to help graphically create the diaphragms. In the *Draw* section of

the *Advanced* tab *Draw Special Joint* was selected. The resulting window allowed the input of global coordinates for the desired joint. A joint was created for all four corners of each rectangular diaphragm. The top two joints for each diaphragm were defined at mid-height of the deck. Joints were then defined for the remaining six diaphragms in the span. When all of the span's joints had been defined, the *Draw Poly Area* tool was selected from the *Draw* area of the *Advanced* tab. In the resulting window, the *Section* field was set to the appropriate previously-defined, webwall shell section. *Drawing Control Type* was set to *None <space bar>*. The model was then engaged, selecting one set of previously-defined joints that served as the corners for one webwall. When all seven in-span diaphragms were drawn, all were selected. Under the *Advanced* tab, *Assign -> Areas -> Generate Edge Constraints* was utilized. *Generate Edge Constraints* simulated the in situ connectivity between the webwall and the deck/*top* of the adjacent girders.

5.3.2 Connecting Staggered Webwalls to Girders

In order to simulate the connectivity between the bottom of the adjacent girders and the web walls, rigid links were employed between the bottom of the webwalls and the adjacent girders. In order to employ a rigid link between the two elements, joints are required on both elements at the same longitudinal (parallel to traffic lanes) point. The girders created from the Bridge Wizard did not contain a joint at the longitudinal diaphragm location. To create a joint in the girders at the proper location, one of the adjacent girders was selected. In the "Advanced" tab, under *Edit*, *Lines -> Divide Frames* was selected. In the resulting window, *Divide at Specified Distance from I-end of Frame* was chosen, *Distance Type* set to *Absolute*, and the appropriate absolute distance was entered. The same process was repeated for the other adjacent girder, creating a joint in each adjacent girder at the longitudinal diaphragm location. The *Draw*

Two-Joint Link was then selected under *Draw*. In the resulting window, *Property* was set to the previously-defined bearing *Fixed*. *Fixed* ensured the link did not rotate or displace in any direction. *XY Plane Offset Normal* was set to "0" and *Drawing Control Type* set to *None <space bar>*. On the model, a bottom joint of a diaphragm was selected. The corresponding joint in the girder located directly adjacent to the selected bottom diaphragm joint was then selected. This created a rigid link between the bottom corner of the diaphragm and the girder in the model, recreating the in-situ conditions for the model. Links were then inserted in this manner for the rest of the six diaphragms remaining in the span. The preceding webwall definition process was then repeated for the remaining three spans in the bridge. Afterwards, the *Bridge* tab was chosen, and *Update* was utilized. In the resulting window, *Action* was set to *Update Linked Model*. The *Analysis* tab was then selected and the model was analyzed in the same manner as previously described in section two of this chapter. Deflection and strain results were also obtained and recorded using the same procedure.

5.4 Bridge Model with Barriers and Staggered Webwalls

An additional model containing bridge deck barrier walls was also desired for the project to determine the effect of barriers acting compositely with the deck under service loads and to compare model analysis results to measured load-test values.

In order to ensure composite action between the deck and the barriers in the model, the barriers were inserted as rectangular area objects that were extruded *normal* to the traffic lanes (Figure 5.8). The actual bridge barriers were not rectangular in shape, but a rectangular model section was required because they were extruded through the width of the barrier (rather than along the length of the barrier). Therefore, an extruded thickness was desired to yield an equivalent moment of inertia to the in-situ bridge barrier while the height of the model barriers

was equivalent to the height of the bridge barriers. To obtain the desired equivalent moment of inertia, the model barrier thickness was found by first calculating the moment of inertia of the bridge barrier, I_{bridge}. The desired model barrier width was then obtained utilizing Equation 5-1.

$$I_{bridge} = \frac{1}{12} t_{model} h^3 \qquad (5-1)$$

Where:

I_{bridge} = *moment of inertia of a bridge barrier (in.^{4})*

t_{model} = *thickness of model barrier measured normal to traffic lanes (in.)*

h = *height of both the bridge and model barriers (in.)*

Equation 5-1 was then modified to solve for t_{model}.

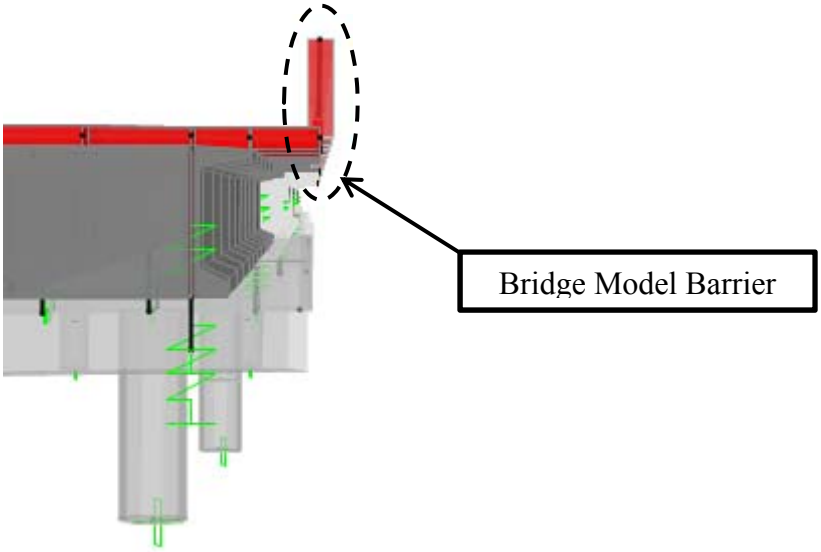

Figure 5.8. *Transverse section cut of downstream side of bridge model displaying inserted barriers.*

With the thickness obtained from Equation 5-1, the barrier area section was then defined in the model utilizing the *Advanced* tab, *Define -> Section Properties -> Area Sections*. *Add New Section* was selected after the *Select Section Type to Add* was set to *Shell*. The section was then appropriately named and *Type* was set as *Shell-Thin*. *Material Name* was defined as the

appropriate previously defined material property and *Material Angle* remained at zero. *Membrane* and *Bending* thickness was input as the value determined from Equation 5-1, t_{model}.

After the barrier area section was defined, the joints necessary to insert the barriers were defined through the process described in section three of Chapter 5. Joints were added at the ends of each span and on both sides of the bridge model, as seen in Figure 5.9. The *Draw Poly Area* tool was then selected, and *Section* set as the barrier area section defined above. The barriers were then drawn on the model as seen in Figure 5.9. It is important to note that every joint on the outside edge of the deck was selected while drawing each barrier to ensure composite action occurs between the deck and the barrier for the *Generate Edge Constraints* command. After all barriers were completed, all were selected and the *Generate Edge Constraints* command utilized to complete the composite action between the deck and barriers.

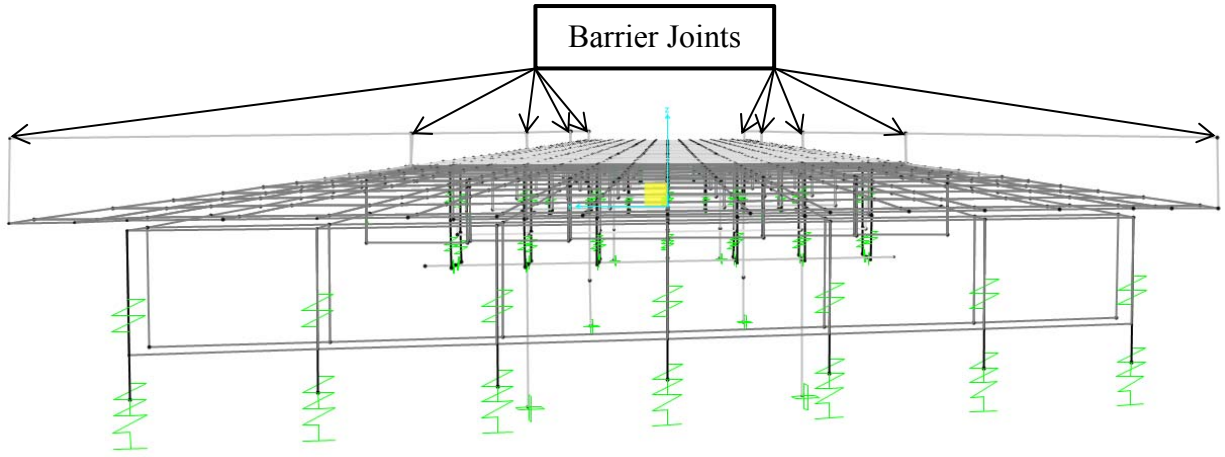

Figure 5.9. *Non-extruded view of barrier joint locations on bridge model.*

When all barriers were fully constrained, the model-load-testing procedure described in sections two and three of this chapter was repeated, outputting strain and deflection results at midspan.

Chapter 6 Results and Discussion

6.1 Introduction

Two live-load tests, one performed immediately before the bridge was put into service and the other after one year of service, were performed on the bridge over Hillabee Creek on Alabama State Highway 22. The load-test data were utilized to compare the performance of SCC girders to VC girders of the same geometry, to investigate any performance changes over a year of service of the SCC girders, to assess the accuracy of refined analysis techniques, and to assess the effects of cast-in-place web walls and barriers on the distribution of service-level truck loads to individual bridge girders.

6.2 Linear-Elastic Response to Service Loads

6.2.1 Superposition of Service Loads

If the bridge response to service loads is linear and elastic, then the principle of superposition should be valid for the test results. The use of two load trucks during the second load test allowed evaluation of linear-elastic response via comparison of measured two-truck response to superposition of measured single-truck responses. A representative example of these comparisons is illustrated for bottom-surface girder strains in the BT-54 spans in Figures 6.1 through 6.4 and the BT-72 spans Figures 6.5 through 6.8. Truck positions are graphically indicated on the horizontal axis. Each comparison is based on single-truck measurements and two-truck measurements recorded on the same strain gauge on the same day. In Figures 6.6 and 6.8 the missing markers over Girder 2 are a result of a malfunctioning strain gauge during load testing.

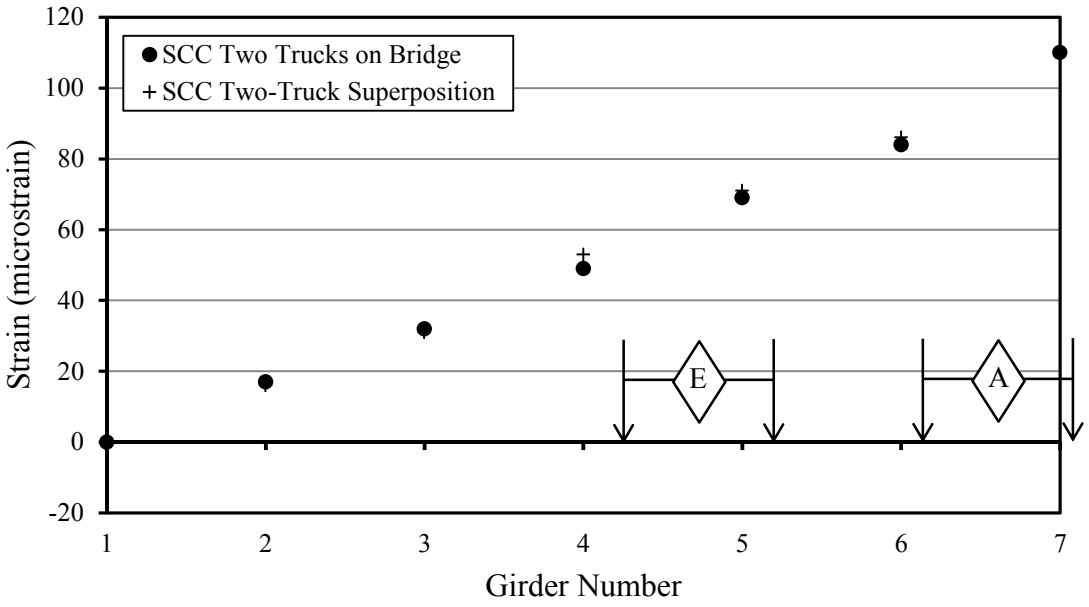

Figure 6.1. *Bottom-surface strains from two trucks on bridge (A & E) and load positions A + E superimposed on span 1 (SCC).*

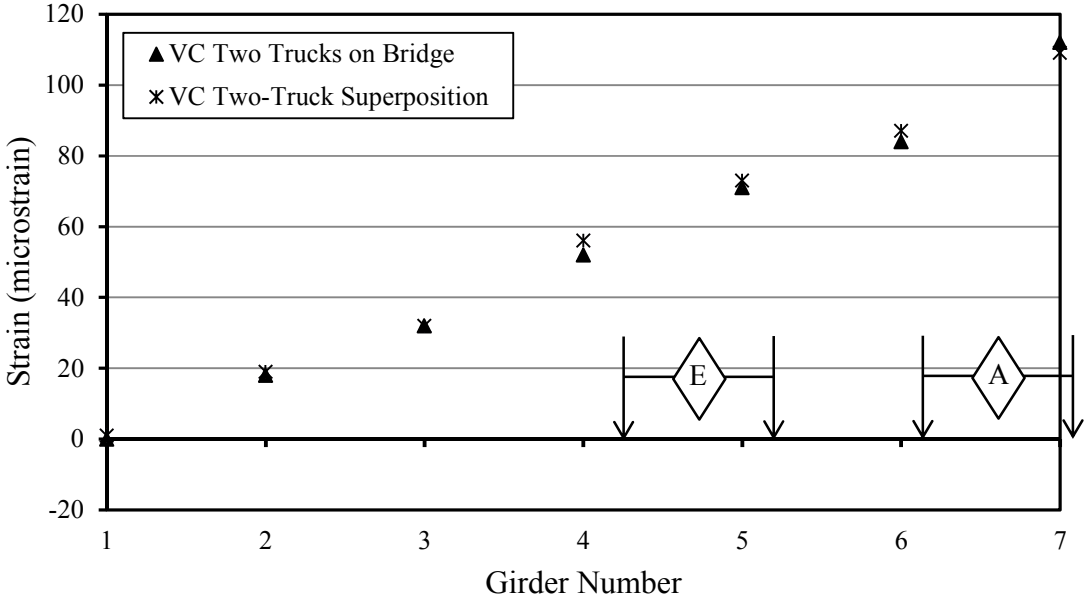

Figure 6.2. *Bottom-surface strains from two trucks on bridge (A & E) and load positions A + E superimposed on span 4 (VC).*

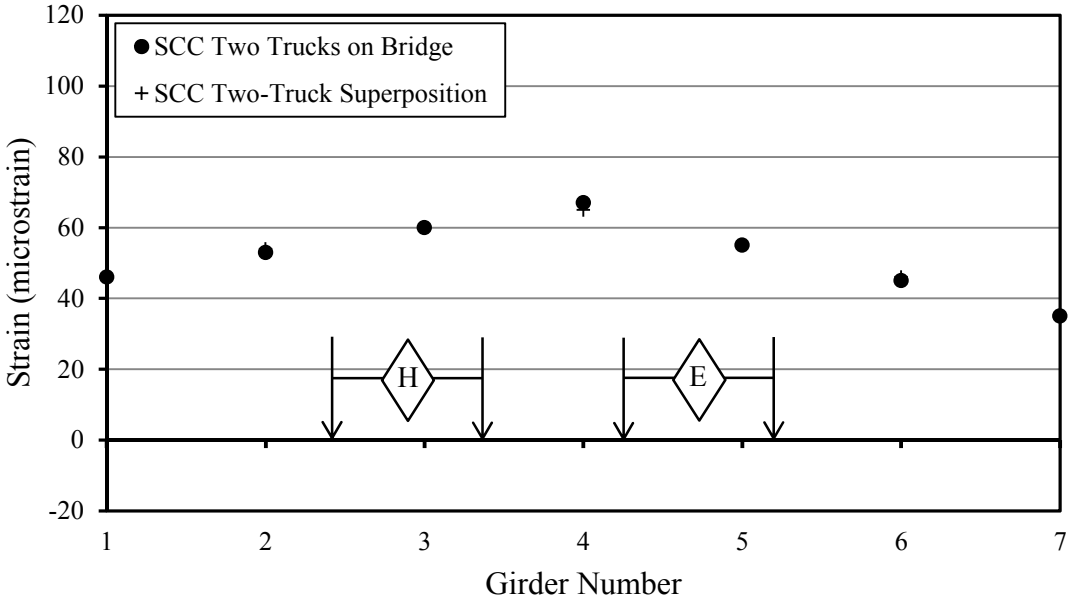

Figure 6.3. *Bottom-surface strains from two trucks on bridge (E & H) and load positions E + H superimposed on span 1 (SCC).*

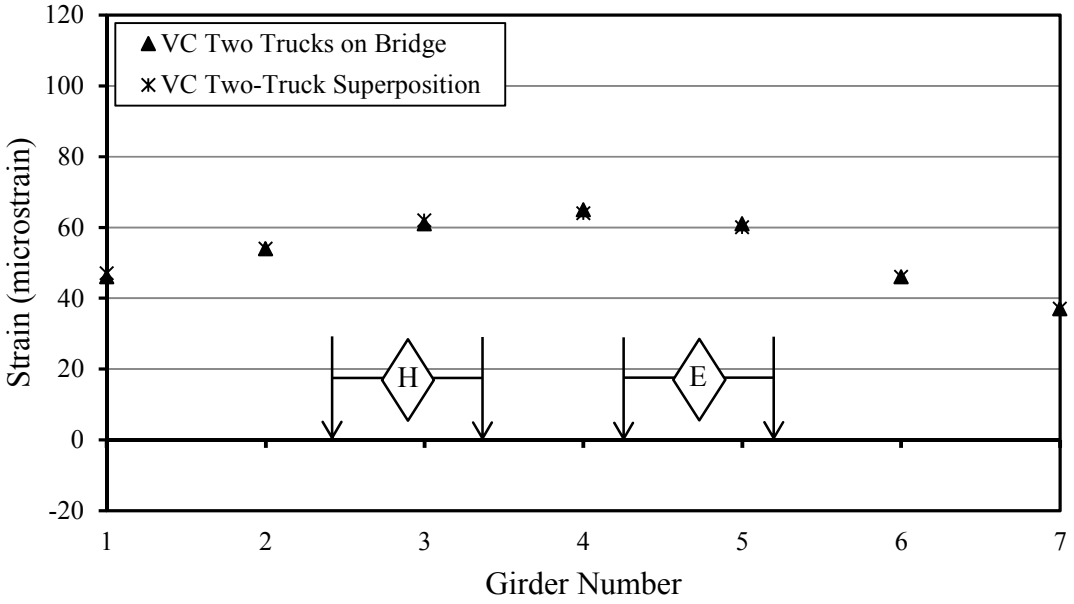

Figure 6.4. *Bottom-surface strains from two trucks on bridge (E & H) and load positions E + H superimposed on span 4 (VC).*

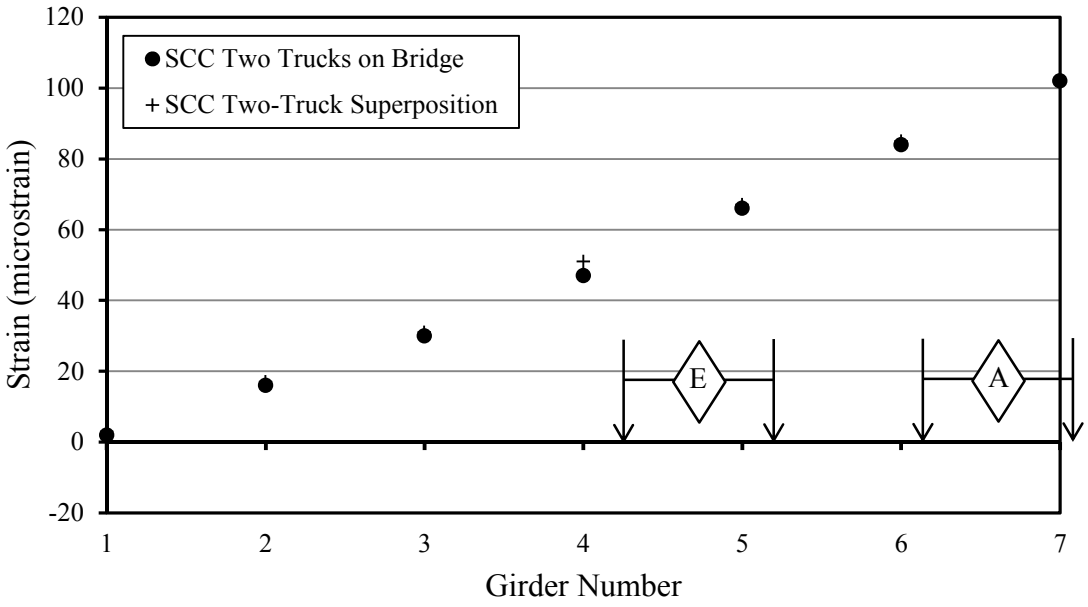

Figure 6.5. *Bottom-surface strains from two trucks on bridge (A & E) and load positions A + E superimposed on span 2 (SCC).*

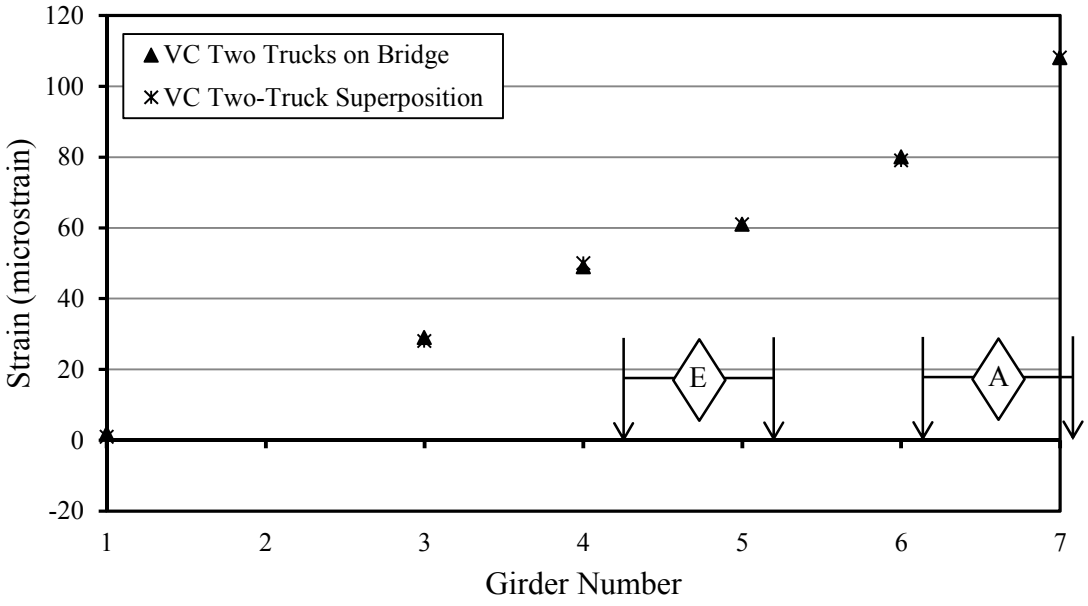

Figure 6.6. *Bottom-surface strains from two trucks on bridge (A & E) and load positions A + E superimposed on span 3 (VC).*

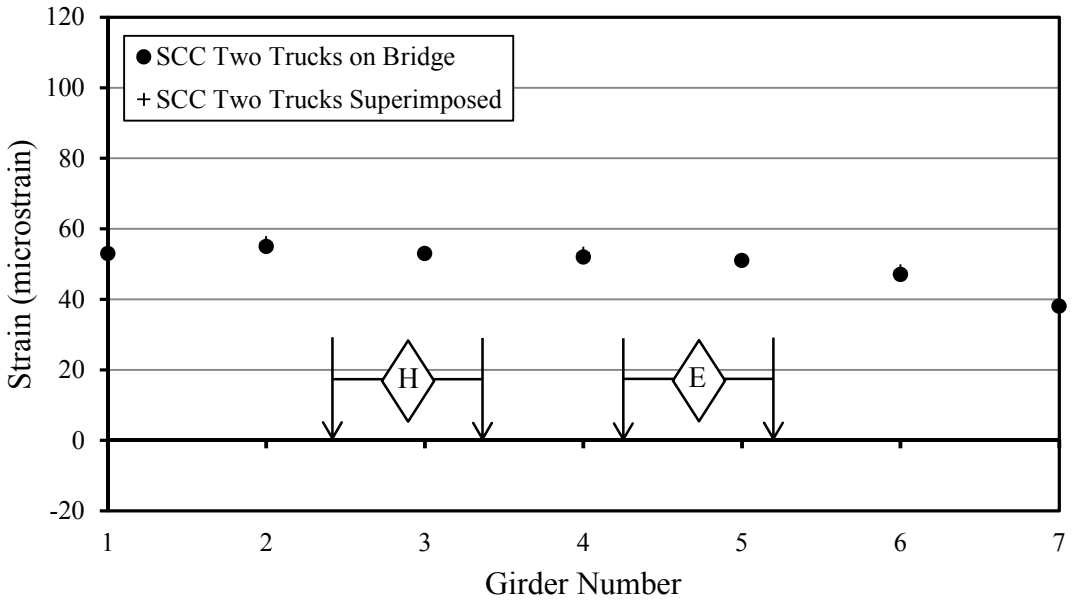

Figure 6.7. *Bottom-surface strains from two trucks on bridge (E & H) and load positions E + H superimposed on span 2 (SCC).*

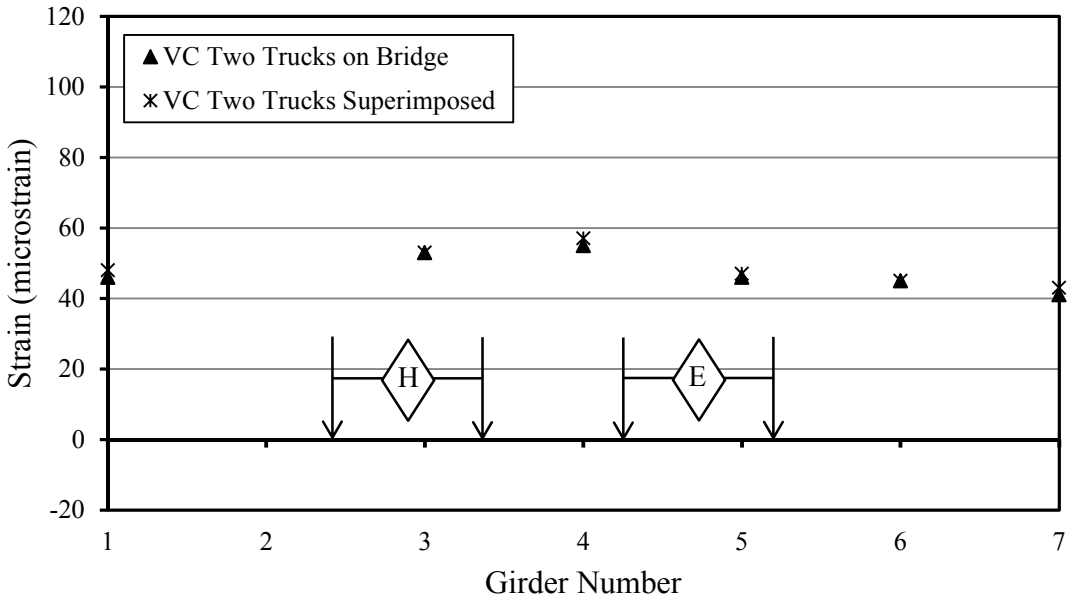

Figure 6.8. *Bottom-surface strains from two trucks on bridge (E & H) and load positions E + H superimposed on span 3 (VC).*

In the figures, asterisk and plus markers are barely distinguishable from solid black circle and triangle markers because the measured two-truck responses are essentially identical to the corresponding, summed single-truck responses. This is true for the SCC girders and the VC girders. Superimposed single-truck and actual two-truck responses never differed by more than 2 microstrain, which roughly corresponds to the practical precision of the testing and measurement techniques. Therefore, the bridge is responding to these service loads in a linear-elastic manner, thereby supporting the usual service limit state design practice based on uncracked behavior of all concrete and full participation of the deck. Service limit state design allows for the continuous barriers to be considered for exterior girders. Superposition may be used to estimate the response of the bridge to a three-truck load configuration.

6.2.2 Plane Sections Remain Plane

In addition to linear-elastic material response, another fundamental assumption for flexural girder design is that plane sections remain plane during bending This assumption is the basis for the assertion that strain is proportional to the distance from the neutral axis. The test results were used to evaluate the validity of this assumption. As discussed in chapter 3, select girders throughout the bridge had a full profile VWSGs installed throughout their depth. Figures 6.9 and 6.10 show full-profile girder strains from spans 2 and 3 when loaded with a truck. The y axis represents the location of the strain gauge from the *bottom* surface of the girder while the x axis contains the change in strain due to the load truck being put in place. The two figures clearly show that plane sections in the girder remained plane during load testing.

During load test 1, some ERSGs located on the bottom surface of the girders malfunctioned. In order to obtain an approximate bottom-surface strain in those girders, linear strain profiles from the VWSGs, such as those shown in Figures 6.9 and 6.10, were utilized. The

linear profiles were extended to the bottom surface of the girders utilizing a best-fit line. All strain gauges in the girders in the figures functioned properly during load testing. The measured strain for each ERSG is shown on the x axis to display that the linear projection of VWSG strains was an appropriate method for estimating bottom-surface strain for a girder without a functioning ERSG.

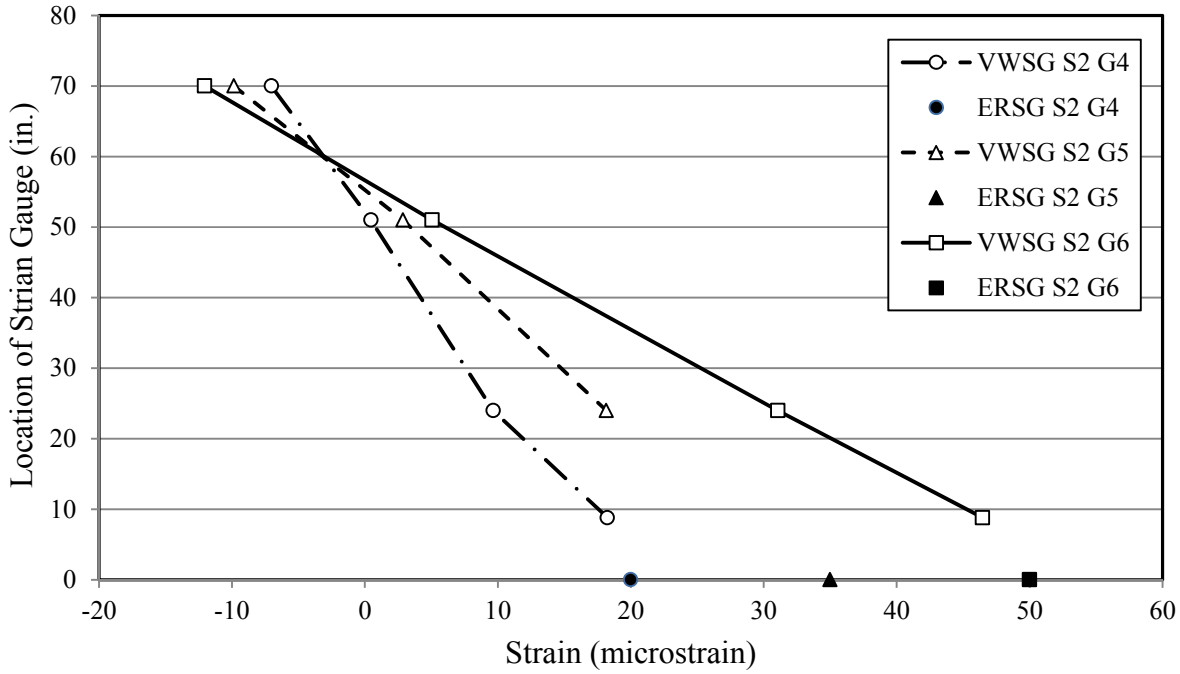

Figure 6.9. *Full profile strains of girders in span 2 under load truck position A (SCC BT-72).*

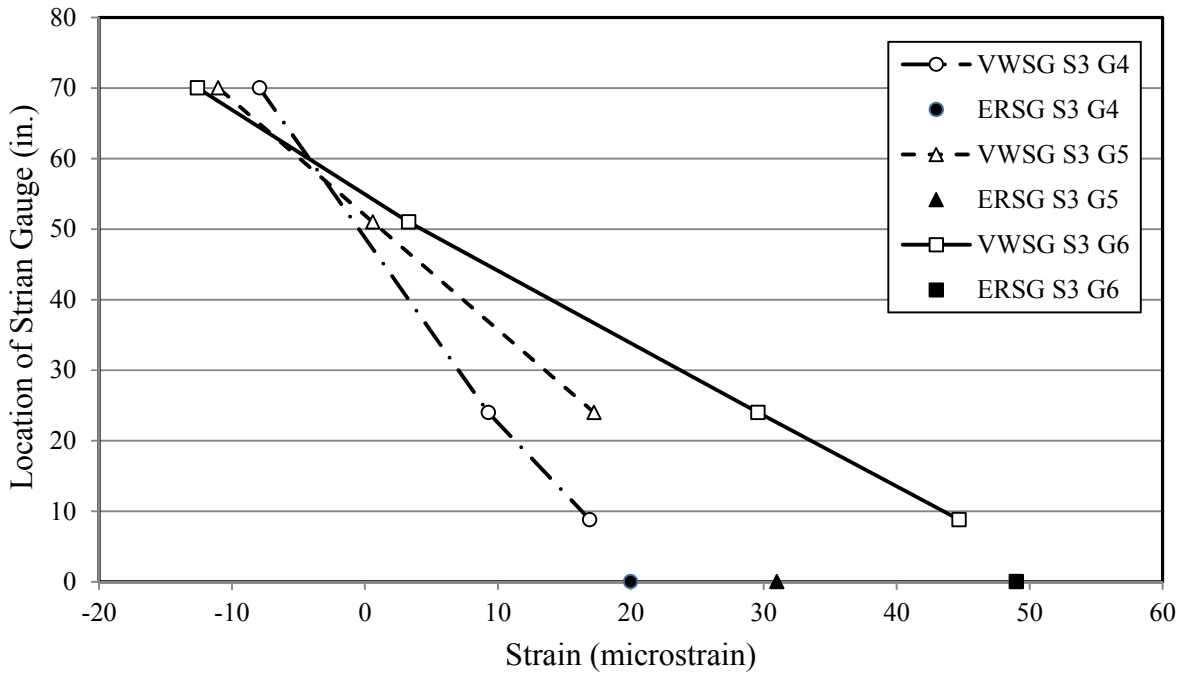

Figure 6.10. *Full profile strains of girders in span 3 under load truck position A (VC BT-72).*

6.3 Service-Load Response of SCC Girders

6.3.1 Strain Comparison Methodology

When assessing the live-load response of a bridge to service loads, it is important to understand *how* results should be compared to meet the objectives of the test. Bridges designed for the same load capacity but constructed of different materials deform differently under the same service load due to their different geometries and material properties. When evaluating a new material, it is important to establish whether its in-service performance is as reliable as that of a conventional material after accounting for reasonable differences in geometry and material properties. The Hillabee Creek bridge is configured so that the span pairs (1 versus 4 and 2 versus 3) are each geometrically equivalent (within normal construction tolerances). Thus, equitable comparisons between the deformation responses of an SCC girder and its companion VC girder can be made, but only after consideration of the different stiffnesses of the girder

materials. The material stiffness in the linear-elastic, service-load response range is quantified by the modulus of elasticity of the concrete, E_c.

Recall that the same 28-day compressive strength was specified for VC and SCC of each girder size. As may be seen in Table 3.4, the f_c of SCC and VC girders were similar, but the average measured E_c of VC was 10% higher than in equivalent SCC BT-54s and 15% higher than in equivalent SCC BT-72s. Although they differ, the SCC and VC E_c values are in line with previous research and guidelines for the use of SCC, as well as standard ACI and AASHTO predictive relationships (Schindler et al. 2007; ACI 237 2010; Johnson 2012). This difference is expected, due mainly to the lower coarse aggregate volume and increased paste content typical of SCC. Nonetheless, it should be accounted for when comparing the SCC girder strains to the companion VC girder strains.

For simply supported bridge girders with a composite, cast-in-place concrete deck, bottom-flange strains near midspan are the most sensitive indicators of individual girder response to service-level live loads. The reference (expected) response for SCC versus VC comparisons in this study was taken to be that of the VC girders. To equitably determine if the SCC girders responded as should be expected, the measured strain response of each VC girder was transformed to the value that would be expected if the measured value of E_c equaled that of its companion SCC girder.

In order to accurately transform the VC girder strains to the expected strains if the girder had companion SCC girder properties, transformed section analysis was required using the properties displayed in Table 6.1. An effective slab width, b_e (Figure 6.11), of 78 in. (the clear distance from center-to- center of each girder) was used for all transformed section calculations for interior girders according to 4.6.2.6 of AASHTO LRFD Bridge Design Specifications (2012).

As-built haunch thickness, h, was determined by utilizing surveying equipment to measure the vertical height of a point on the top of the deck at midspan and the vertical height of a point at midspan on the bottom face of the girder. The vertical height of the point on the bottom face of the girder, the thickness of the deck (7 in.) and the depth of the girder were then subtracted from the vertical height of the point on top of the deck, yielding the thickness of the buildup (haunch). Deck plus haunch thickness is shown averaged over each span in Table 6.1. On the interior side of the exterior girders, the deck width for calculating transformed properties was extended to half way between the centers of the exterior girder and the first interior girder. The exterior portion of the deck was extended all the way to the edge of the bridge (Figure 3.21) yielding a b_e of 85.5 in. In order to accurately describe the full flexural stiffness under service loads, the barriers were included for transformed-section property calculations for exterior girders.

Table 6.1. Section and Transformed Section Properties of the bridge girders.

Components			Thickness	Transformed-Section Properties	
			Deck+Haunch (in.)	y_{tr} (in.)	I_{tr} ($\times 10^3$ in^4)
BT-54	SCC Span 1	G1	*	14.4	890
		G2, G5, G6	*	20.6	605
		G3, G4	*	20.8	598
		G7	*	13.9	912
	VC Span 4	G1	*	14.5	858
		G2,G5, G6	*	21.5	564
		G3, G4	*	21.0	578
		G7	*	14.3	863
BT-72	SCC Span 2	G1	*	20.0	1967
		G2, G5	*	26.9	1143
		G3, G4	*	26.9	1143
		G6	*	26.3	1168
		G7	*	20.0	1958
	VC Span 3	G1	*	20.0	1902
		G2, G5	*	28.5	1077
		G3, G4	*	29.0	1056
		G6	*	28.0	1098
		G7	*	20.0	1899
Decks	All	*	8.7	—	—
		*	8.5	—	—
		*	8.5	—	—
		*	8.1	—	—
Barriers	All	*	*	—	—

Note: — = data integrated into composite-girder transformed-section properties.
**= Not applicable*

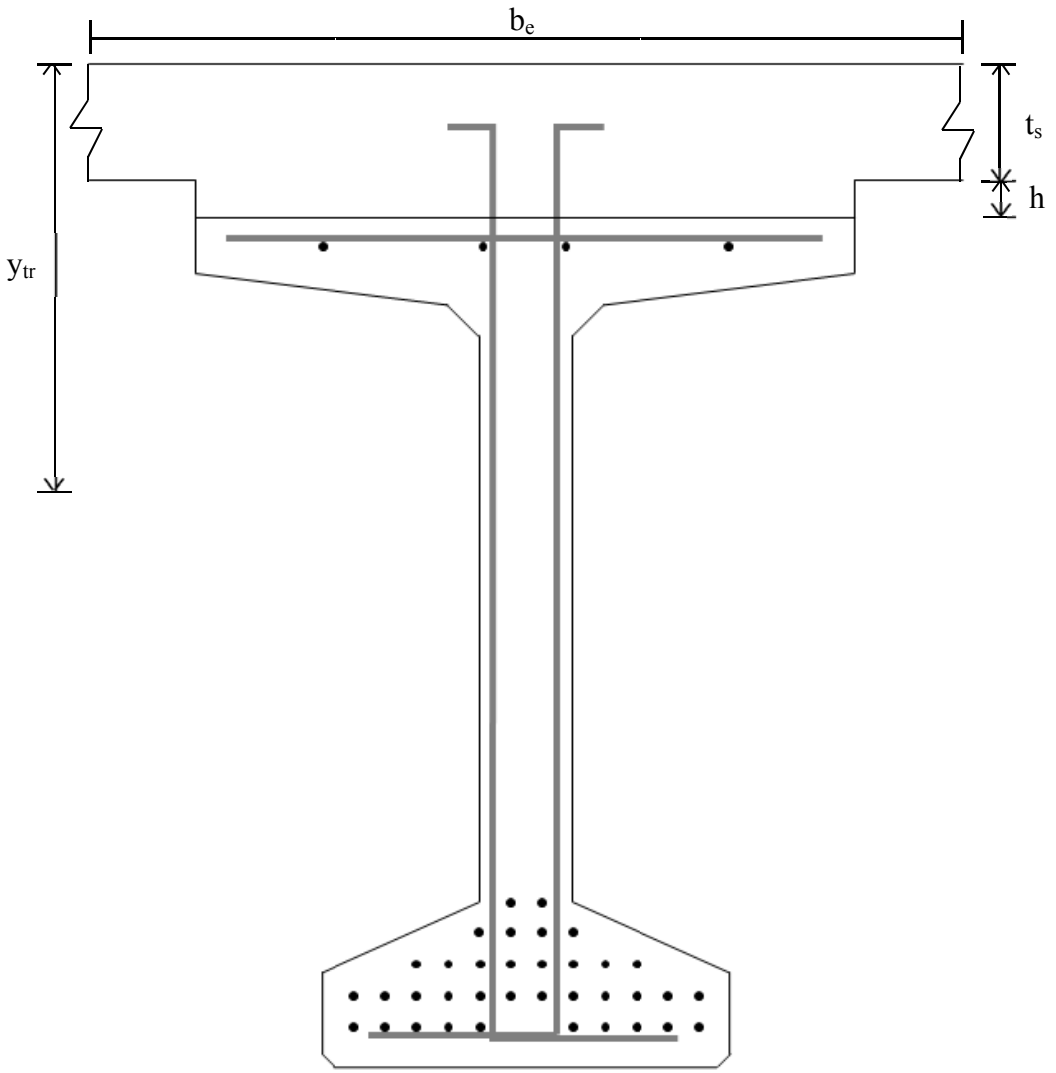

Figure 6.11. Effective width, deck thickness, and haunch (buildup) of cross section.

Transforming measured VC girder strain responses to the expected value if each VC girder had the same measured E_c value as its companion SCC girder was accomplished by first assuming that the midspan bending moments for each SCC and VC girder pair under the same truck load are equivalent:

$$M_{SCC} = M_{VC} \tag{6 - 1}$$

where

M_{SCC} = midspan bending moment in an SCC girder due to the applied live load

M_{VC} = midspan bending moment in companion VC girder due to same applied live load

The prestressed girders in this study were designed to exhibit linear-elastic material behavior under service-level bending moments. Because the composite girder cross section comprises both precast and cast-in-place concrete, transformed-section analysis is warranted. For these computations all materials are transformed to an equivalent area of the precast concrete. Assuming linear-elastic behavior and that plane sections remain plane during bending, the expected *change* in longitudinal bottom-fiber strain resulting from the live load can be computed as shown in Equation 6-2.

$$\varepsilon_{gauge} = \frac{My_{gauge}}{E_c I_{tr}} \qquad (6-2)$$

where

ε_{gauge} = change in longitudinal strain at a gauge location (in./in.)

M = bending moment due to the applied live load (kip-in.)

y_{gauge}= vertical distance from the transformed-section centroid to the gauge (in.)

E_c = measured precast concrete modulus of elasticity (ksi)

I_{tr} = transformed-section area moment of inertia of the composite girder cross section (in.^{4})

Equation 6-2 can then be rewritten as follows:

$$M = \frac{\varepsilon_{gauge} E_c I_{tr}}{y_{gauge}} \qquad (6-3)$$

Equation 6-3 can then be substituted into Equation 6-1 for equally loaded VC and SCC girders:

$$\left[\frac{\varepsilon_{gauge} E_c I_{tr}}{y_{gauge}}\right]_{SCC} = \left[\frac{\varepsilon_{gauge} E_c I_{tr}}{y_{gauge}}\right]_{VC} \qquad (6-4)$$

Equation 6-4 can be solved to produce the expected strain change in an SCC girder in terms of the strain change measured in the companion VC girder when subjected to the same load:

$$\varepsilon_{gauge,SCC} = \varepsilon_{gauge,VC} \frac{\left[\frac{E_c I_{tr}}{y_{gauge}}\right]_{VC}}{\left[\frac{E_c I_{tr}}{y_{gauge}}\right]_{SCC}} \qquad (6-5)$$

where

$\varepsilon_{gauge,SCC}$ = expected change in SCC strain due to the applied live load (in./in.)

$\varepsilon_{gauge,VC}$ = measured change in VC strain due to the applied live load (in./in.)

For the strain comparisons between SCC and VC girders reported in this thesis, Equation 6-5 is used to transform each strain measured in a VC girder to an expected strain for the companion SCC girder. This makes it possible to evaluate whether the SCC girder responds to service loads as would a VC girder with the same material stiffness. It also compensates for slight differences in the deck concrete stiffness between comparison girders. The measured f_c and E_c of each bridge component are reported in Table 3.4. The transformed-section properties necessary for conversion according to Equation 6-5 are reported in Table 6.1, because they depend on the measured E_c of the associated girder, deck segment, and (where applicable) barrier. All reported bottom-surface strain VC data for direct comparisons between SCC and VC girders (girders with differing modulus of elasticity values) were subjected to Equation 6-5 to make equitable comparisons between objects with different material stiffness.

6.3.2 SCC Girder Response Compared to VC Girder Response

Bottom-surface strains of all girders in response to the superpositioning of load truck placements A+E+H are illustrated in Figures 6.12 through 6.15 and Appendices A and B. The load truck placement combination A+E+H is used because the load combination created the critical load effects near midspan for girders 6 and 7, which exhibited the largest interior and exterior girder strains achieved, respectively. VC girder strains have been transformed using Equation 6-5 for this comparison. Instances in which surface strain measurements were unavailable during the second test are omitted.

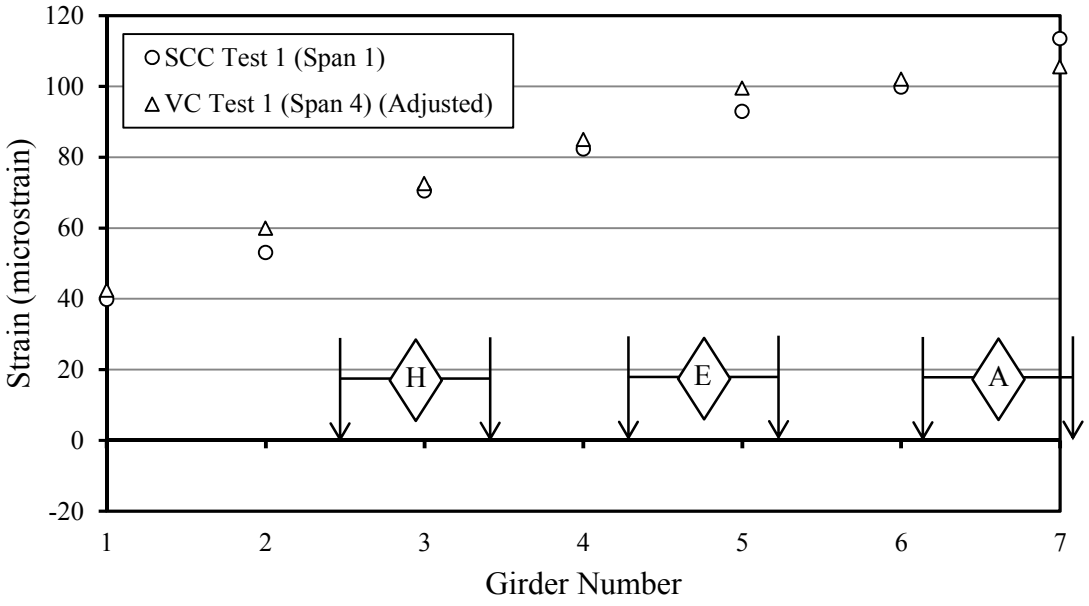

Figure 6.12. *Bottom-surface strains from the superposition of three trucks (A+E+H) on BT-54 spans from the first load test.*

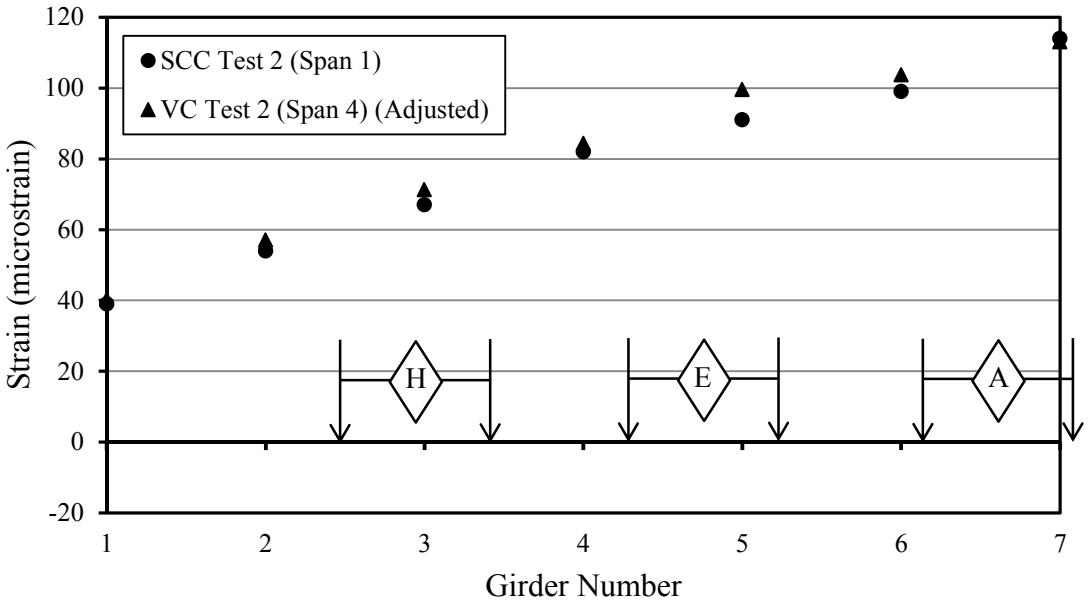

Figure 6.13. *Bottom-surface strains from the superposition of three trucks (A+E+H) on BT-54 spans from the second load test.*

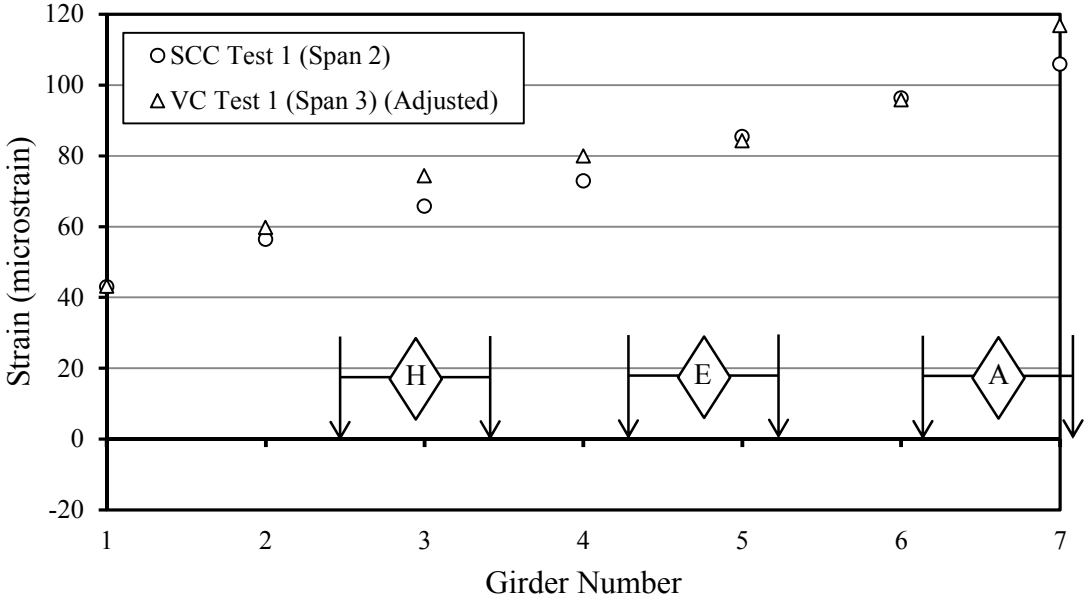

Figure 6.14. *Bottom-surface strains from the superposition of three trucks (A+E+H) on BT-72 spans from the first load test.*

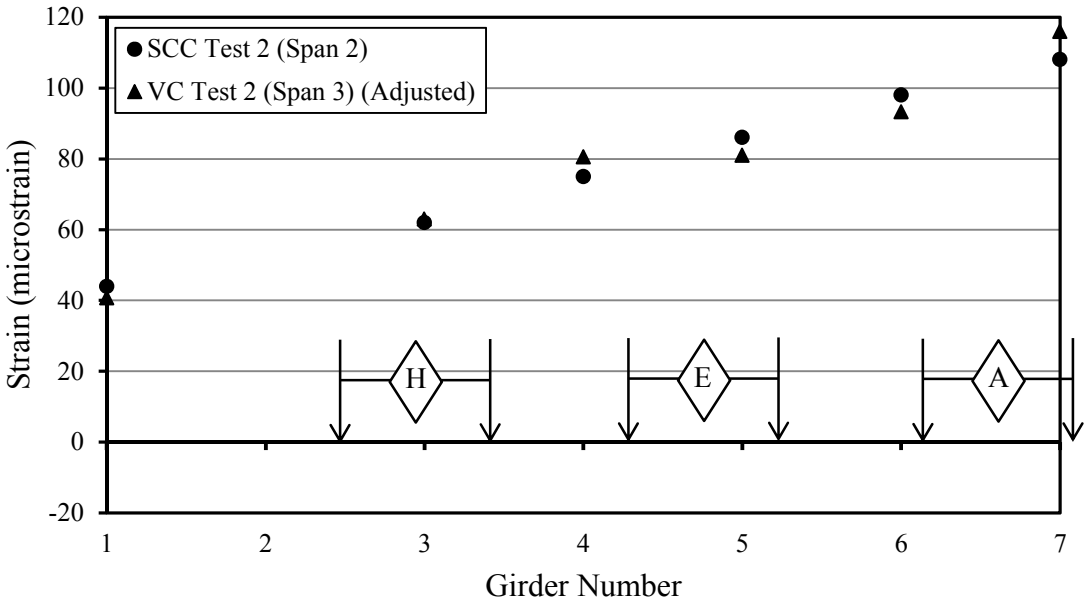

Figure 6.15. *Bottom-surface strains from the superposition of three trucks (A+E+H) on BT-72 spans from the second load test.*

SCC girder bottom-flange strains were practically no different than companion VC strains. The SCC strains were, for both tests, on average 2 microstrain less than the VC strains for the same loading (after compensation for the measured concrete stiffness). Considering the precision of these field measurements, these values indicate that each SCC girder strain is acceptably similar to its companion VC girder strain.

6.3.3 Change in Response of Girders after One Year of Service

The similarity between the two test responses after one year of service apparent in the figures is also confirmed numerically. Only two of the differences between an SCC girder strain and its companion VC strain changed by more than 4 microstrain within the year (BT-54 Girder 7 and BT-72 Girder 3). Furthermore, in both of these cases, the VC girder strain changed significantly between the two tests, while the SCC girder strain remained virtually the same over the year of service as shown in Figures 6.16 through 6.19. Figures 6.16 and 6.18 show that SCC girders never differed by more than 4 microstrain between the first and second load tests, with

many strain values remaining relatively unchanged, while VC girders varied by up to 10 microstrain. This confirms that the ability of SCC girders to resist degradation over time is acceptable—and no worse than the ability of VC girders.

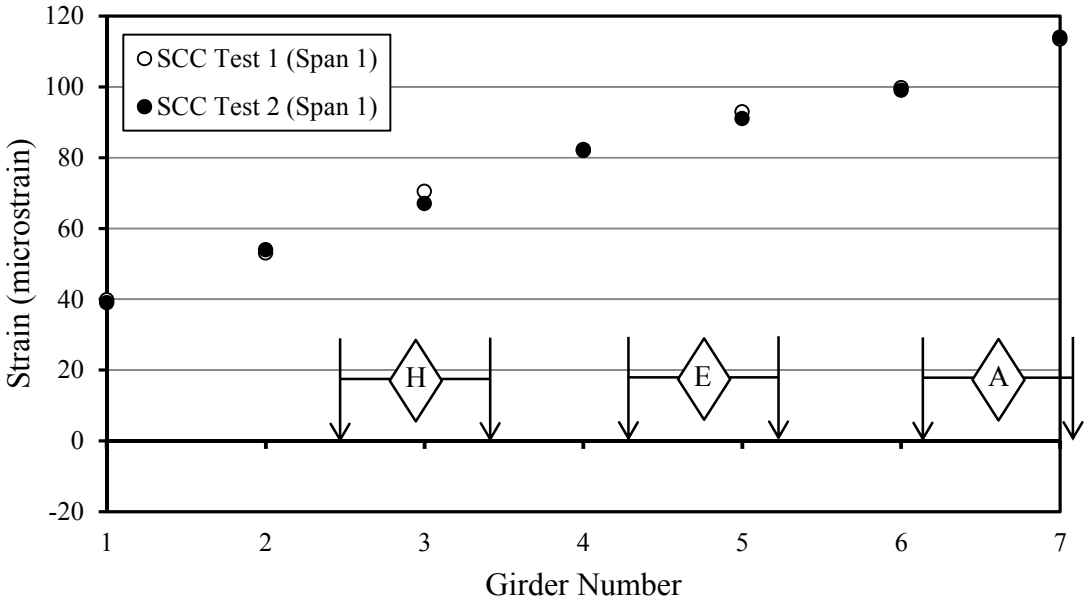

Figure 6.16. *Bottom-surface strains from the superposition of three trucks (A+E+H) on span 1 of the bridge from both the first and second load tests.*

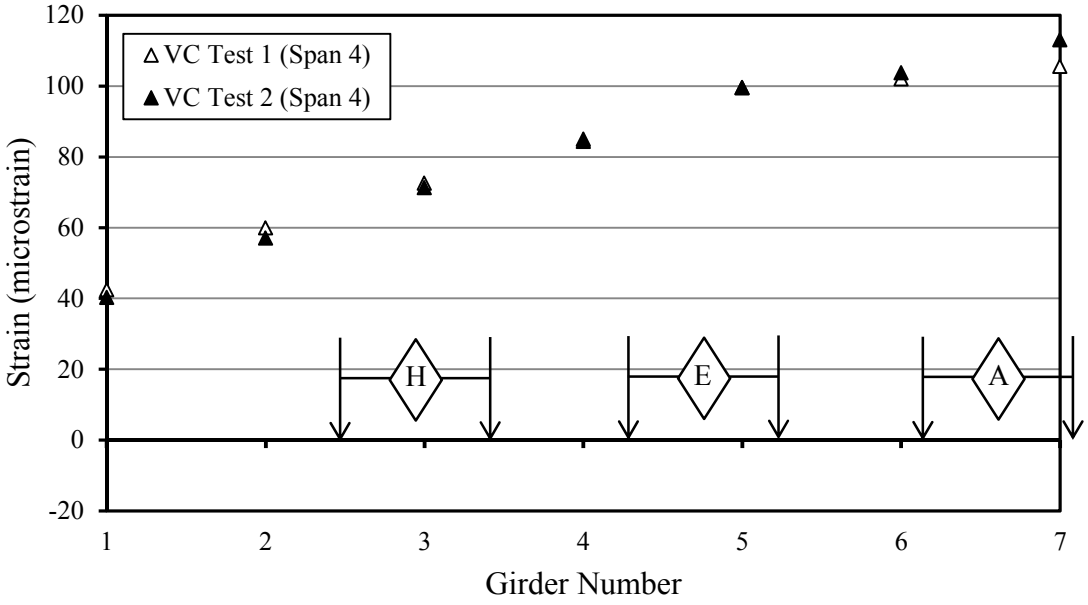

Figure 6.17. *Bottom-surface strains from the superposition of three trucks (A+E+H) on span 4 of the bridge from both the first and second load tests.*

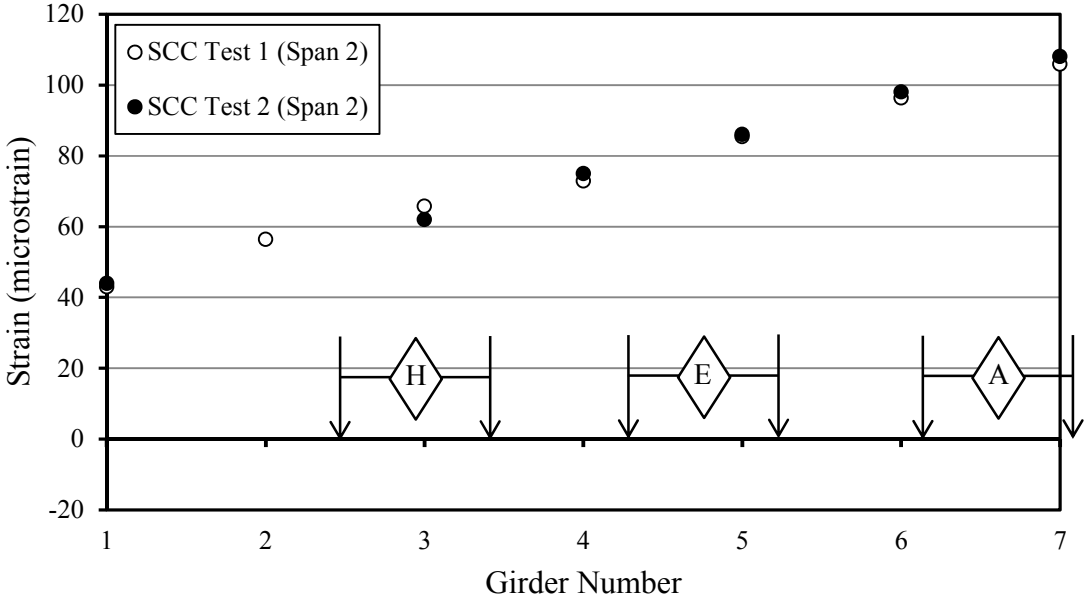

Figure 6.18. *Bottom-surface strains from the superposition of three trucks (A+E+H) on span 2 of the bridge from both the first and second load tests.*

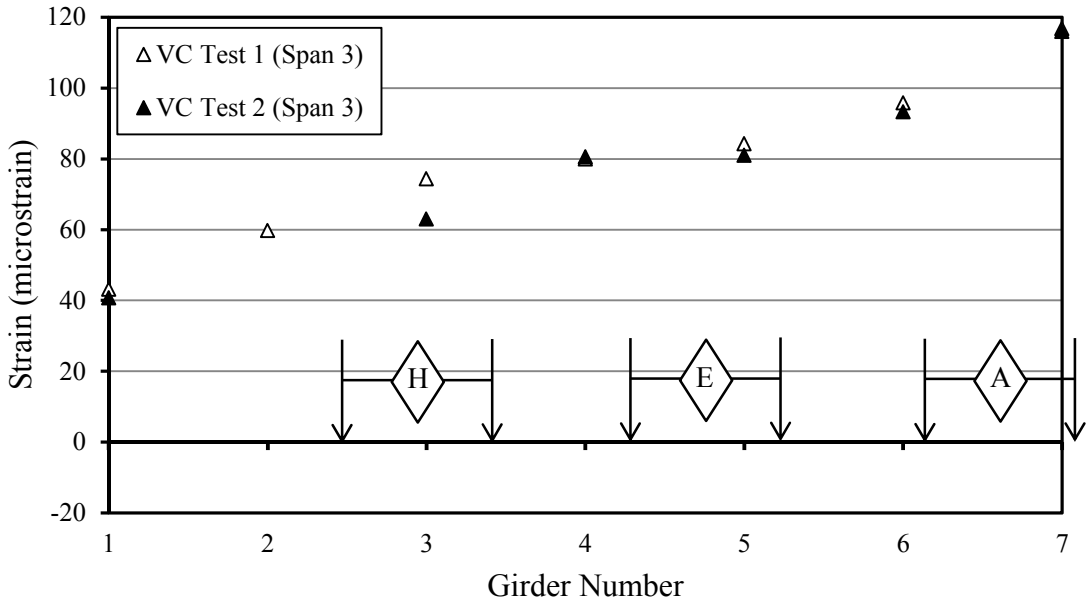

Figure 6.19. *Bottom-surface strains from the superposition of three trucks (A+E+H) on span 3 of the bridge from both the first and second load tests.*

6.4 Accuracy of AASHTO LRFD Distribution Factors for Prediction of Service-Load Response

6.4.1 Computation of AASHTO LRFD Predicted Response

In order to compare the AASHTO LRFD 4.6.2.2.2 live-load distribution approximation to the live-load test results as well as results gathered from the CSiBridge refined analysis of the bridge over Hillabee Creek, the LRFD approximations were converted from a "distribution factor" (*g* from Chapter 2) to an equivalent expected bottom surface strain of a girder utilizing the following equation:

$$\varepsilon_g = \frac{gM_{bending}y_{gauge}}{E_c I_{tr}} \qquad 6-6$$

where

ε_g= *expected bottom-surface strain computed using girder distribution factor (in./in.)*

g = distribution factor as determined from AASHTO LRFD in Chapter 2 of this paper

$M_{bending}$ = the total predicted bending moment for a lane loaded with one truck placed at midspan of the bridge (kip-in.)

y_{gauge} = distance from the extreme bottom fiber of the girder to the neutral axis of the girder cross section (in.)

E_c = modulus of elasticity of girder (ksi)

I_{tr} = transformed area moment of inertia for the selected composite cross section ($in.^4$)

This computed bottom-surface strain represents maximum expected strain if the bridge distributes truck weight to each girder in accordance with AASHTO LRFD distribution factors. As noted in Chapter 2 of this paper, some calculated AASHTO LRFD distribution factors already incorporate truck multipresence effects, while others require application of a multiple presence factor (MPF). MPFs for this project were taken as 1.2 for a single lane load, 1.0 for two lanes loaded, and 0.85 for three lanes loaded in accordance with AASHTO LRFD 3.6.1.1.2. For this exercise, those distribution factors that require multiplication by a MPF (lever rule and C4.6.2.2.2d for exterior girders) as well as *all* measured strains were multiplied by the appropriate MPF to provide an equitable comparison.

6.4.2 Predicted Transverse Bridge Response Compared to Measured Response

As discussed in Chapter 2, not all AASHTO LRFD distribution factors contain truck multiple presence considerations. Equations 2-3 and 2-4 for interior girders incorporate multiple presence effects, as does equation 2-5 for exterior girders with multiple lanes loaded. However, calculated factors for exterior girders with only one lane loaded and for all load cases of the

exterior-girder alternate method to account for intermediate diaphragms (equation 2-7) do not account for truck multiple presence. Therefore, these factors and all measured girder strains were multiplied by the proper MPF to facilitate equitable comparison to the aforementioned distribution factors (Table 6) that do incorporate multiple truck presence in Figures 6.20 through 6.27.

Table 5.2. *Distribution factors calculated from AASHTO LRFD 4.6.2.2.2.*

	BT-54 Spans				BT-72 Spans			
	SCC (S1)		VC (S4)		SCC (S2)		VC(S3)	
	Int.	Ext.	Int.	Ext.	Int.	Ext.	Int.	Ext.
One lane Loaded (LRFD 4.6.2.2.2):	0.40	**0.71**	0.41	**0.71**	0.38	**0.71**	0.39	**0.71**
Two or more lanes loaded (LRFD 4.6.2.2.2):	**0.56**	0.58	**0.57**	0.59	**0.55**	0.57	**0.56**	0.58
One lane Loaded (LRFD C4.6.2.2.2d) (due to webwalls):		0.51		0.51		0.51		0.51
Two lanes Loaded (LRFD C4.6.2.2.2d) (due to webwalls):		0.64		0.64		0.64		0.64
Three lanes Loaded (LRFD C4.6.2.2.2d) (due to webwalls):		0.57		0.57		0.57		0.57

Note: Bold indicates girder-design controlling factors.

In order to obtain the AASHTO LRFD expected strain values, ε_g, in Figures 6.20 through 6.27 a predicted bending moment from one lane loaded with a truck at midspan of the simply-supported span was calculated. A bending moment, $M_{bending}$, of 21,360 kip-in was calculated for spans 1 and 4 while a moment of 30,740 kip-in was calculated for spans 2 and 3. The moments were then utilized in Equation 6-6 to determine the expected strain values (Table 6.3). It is important to note that when computing the values in Table 6.3, all exterior girder values were determined utilizing transformed-section properties accounting for composite action of the barrier and the deck. For comparison purposes, a design truck (HL-93) according to AASHTO LRFD was predicted to cause a midspan bending moment of 17,450 kip-in. with a predicted

bending moment from the lane-load (0.64 kips/lf) of 8,910 kip-in for spans 1 and 4. A bending moment due to the AASHTO LRFD design truck of 25,320 kip-in. was calculated for spans 2 and 3 while a lane-load induced bending moment was calculated to be 16,900 kip-in.

Table 6.3. *AASHTO LRFD expected strain values as calculated from Equation 6-6.*

	BT-54 Spans				BT-72 Spans			
	SCC (S1)		VC (S4)		SCC (S2)		VC(S3)	
	Int. με	Ext. με	Int. με	Ext. με	Int. με	Ext. με	Int. με	Ext. με
One lane Loaded (LRFD 4.6.2.2.2):	92	132	85	124	91	108	83	100
Two or more lanes loaded (LRFD 4.6.2.2.2):	128	108	118	102	130	87	119	82
One lane Loaded (LRFD C4.6.2.2.2d) (due to webwalls):		93		88		76		71
Two lanes Loaded (LRFD C4.6.2.2.2d) (due to webwalls):		119		112		97		90
Three lanes Loaded (LRFD C4.6.2.2.2d) (due to webwalls):		105		99		86		80

Figures 6.20 through 6.23 compare the calculated expected strains derived from AASHTO LRFD distribution factors to the experimental results for interior girders. All values in the figures take into account multiple presence considerations. Girder 6 was chosen as the highest loaded (critical) interior girder from analyzing the results of load tests 1 and 2. The *LRFD Load Distribution (Interior Girder)* column represents the expected bottom-surface strain in the girder computed from the calculated distribution factors in Table 6.2. The *Experimental One or Two Lanes Loaded* column represents the bottom-surface strain of girder 6 from load test 1 for one design lane loaded above the *One Lane Loaded* axis label or two design lanes loaded above the *Multiple Lanes Loaded* axis label. The *Experimental Three Lanes Loaded* column

represents the bottom-surface strain of girder 6 when the load test data were superimposed to project three load trucks on the bridge.

In Figures 6.20 through 6.23, the expected strain values calculated from AASHTO LRFD for interior girders exceed the observed worst case load scenario experimental strain by an average of 43% for one lane loaded (truck position A), 46% for two lanes loaded (truck positions A & E), and 50% for three lanes loaded (truck positions A + E + H).

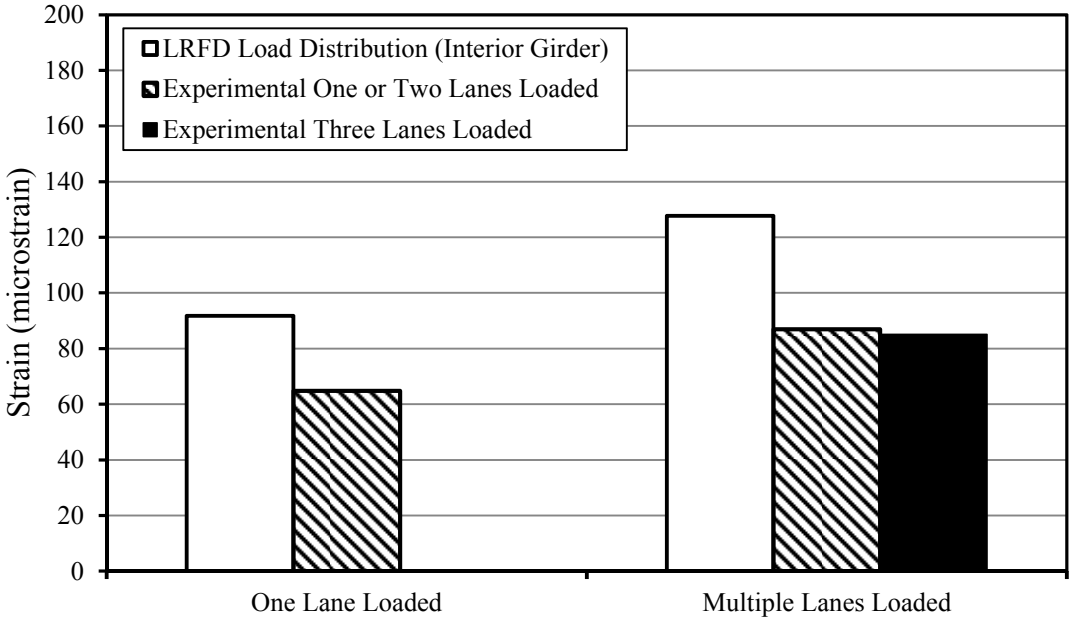

Figure 6.20. *Interior-girder, bottom-surface strains—BT-54 SCC span.*

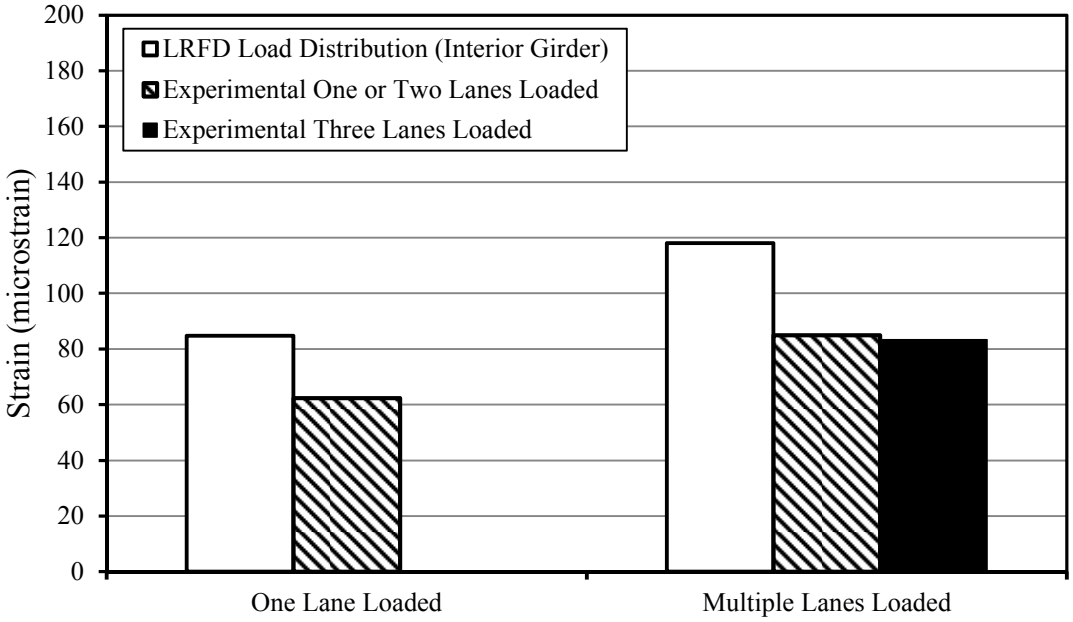

Figure 6.21. *Interior-girder, bottom-surface strains—BT-54 VC span.*

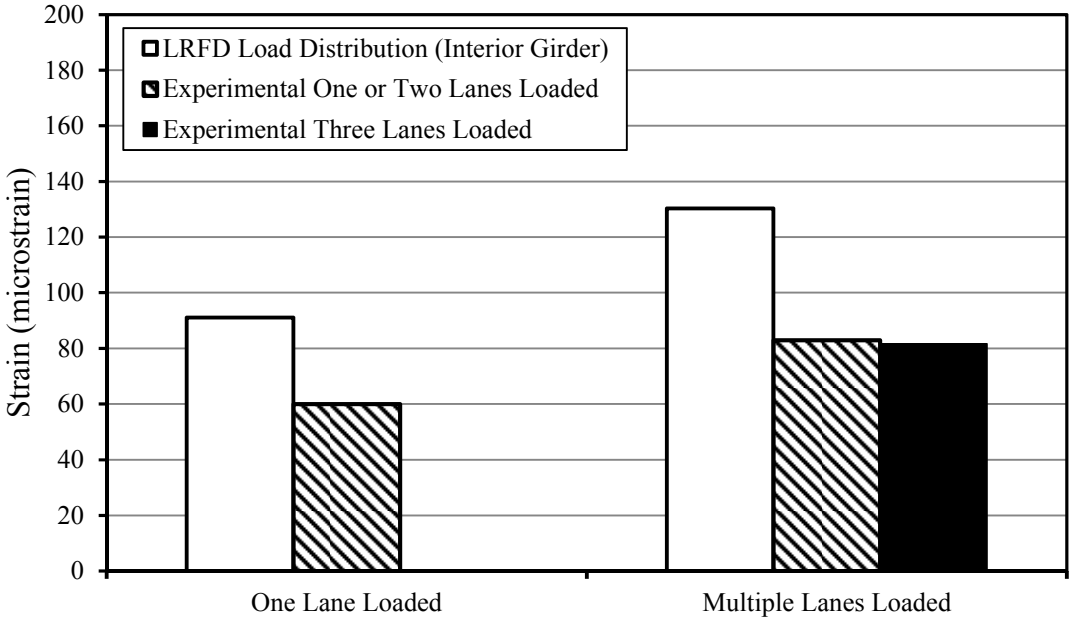

Figure 6.22. *Interior-girder, bottom-surface strains—BT-72 SCC span..*

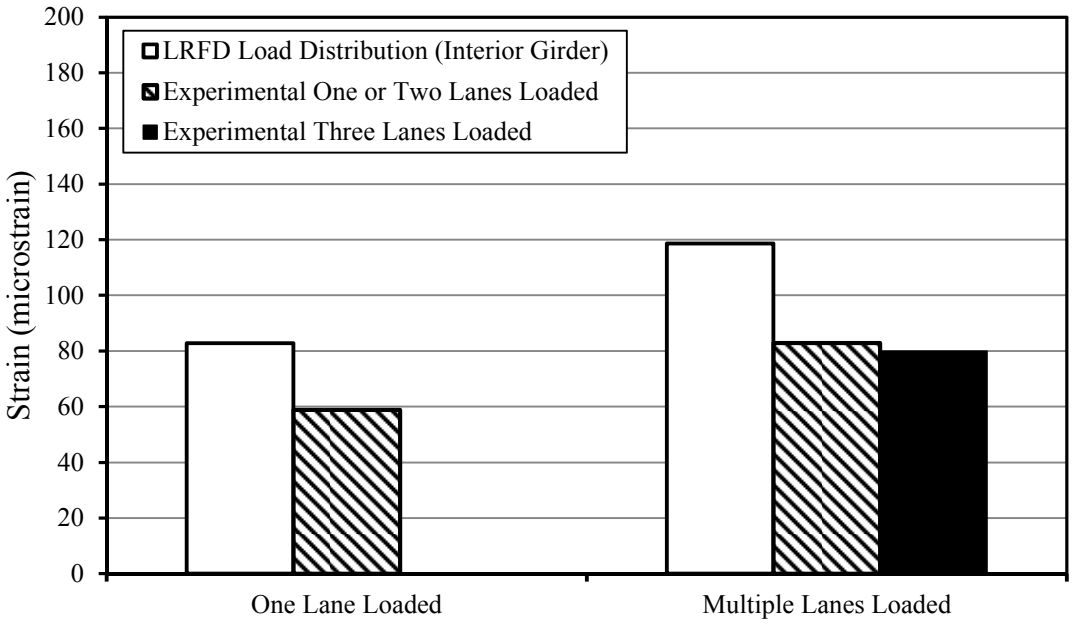

Figure 6.23. *Interior-girder, bottom-surface strains—BT-72 VC span.*

Figures 6.24 through 6.27 compare the calculated expected strains derived from AASHTO LRFD distribution factors to the experimental results for exterior girders. All values in the figures take into account multiple presence considerations. The *LRFD Load Distribution* column represents the expected bottom-surface strain in the girder computed from the calculated distribution factors in Table 6.2 utilizing the lever rule when one lane was loaded and equation 6-6 when two or three lanes were loaded. The *LRFD Load Distribution (Intermediate Diaphragms)* column represents the bottom-surface strain of girder 7 for the special distribution factor provision required by AASHTO LRFD 4.6.2.2.2d. This provision, for bridges with webwalls, assumes the bridge deflects and rotates as a rigid body, forcing the exterior girders to resist the largest portion of the eccentric truck load. The worst case scenario (largest strain) between the *LRFD Load Distribution* and *LRFD Load Distribution (Intermediate Diaphragms)* controls the exterior girder design. The *Measured Field Results* column represents the bottom-

surface strain of the exterior girder (G7) of the bridge loaded with one (A) or two (A&E) trucks, while superposition was utilized to simulate a three truck load (A+E+H).

In Figures 6.24 through 6.27 the expected values for *LRFD Load Distribution* for exterior girders were greater than the observed experimental strain by an average over all four spans of 32% for one lane loaded (truck position A), were less than the experimental values by an average of 8% for two lanes loaded (truck positions A & E), and greater than the experimental values by an average of 3% for three lanes loaded (truck positions A + E + H). The expected values for *LRFD Load Distribution (Intermediate Diaphragms)* for exterior girders were less than the experimental values by 7% when one lane was loaded, greater than the experimental values by an average of 1% when two lanes were loaded and greater than the experimental values by an average of 1% when three lanes were loaded. However, when looking at only the longer (BT-72) spans, the LRFD Load Distribution (Intermediate Diaphragms) method (the most accurate of the two LRFD methods) expected values for exterior girders with two and three lanes loaded for spans 2 and 3 were generally *unconservative* by an average of 7%.

Recall that the expected LRFD Load Distribution values are to be taken as the worst case scenario of the *LRFD Load Distribution* and *LRFD Load Distribution (Intermediate Diaphragms)*. The *LRFD Load Distribution (lever rule)* values for one lane of loading would control design for all four spans and were conservative by an average of 12%, even though the maximum measured strain for design purposes was experienced with two lanes loaded.

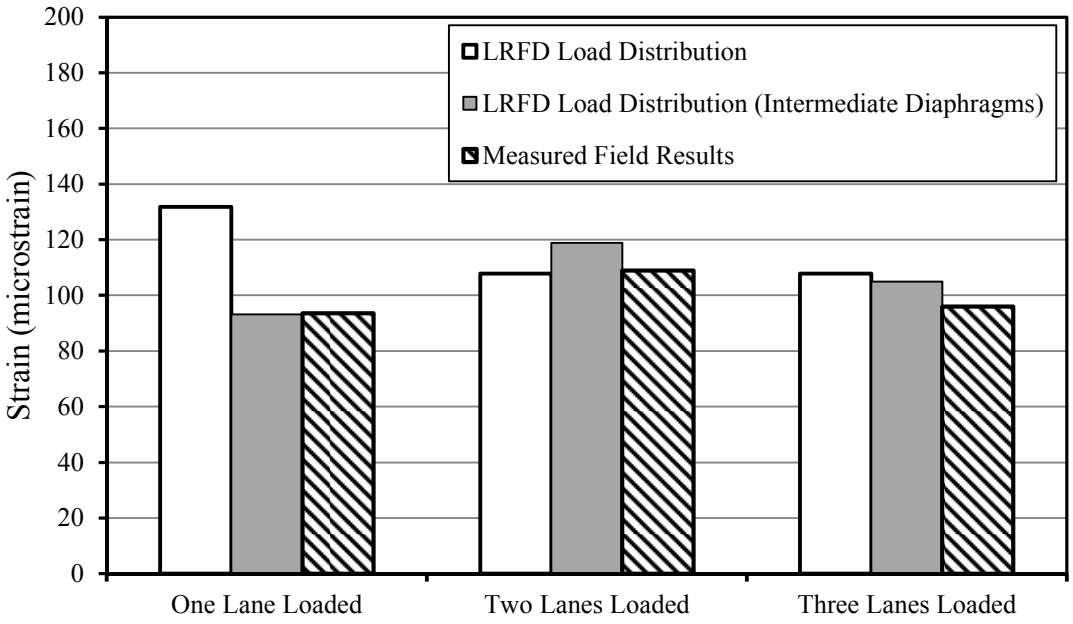

Figure 6.24. *Exterior-girder, bottom-surface strains—BT-54 SCC span.*

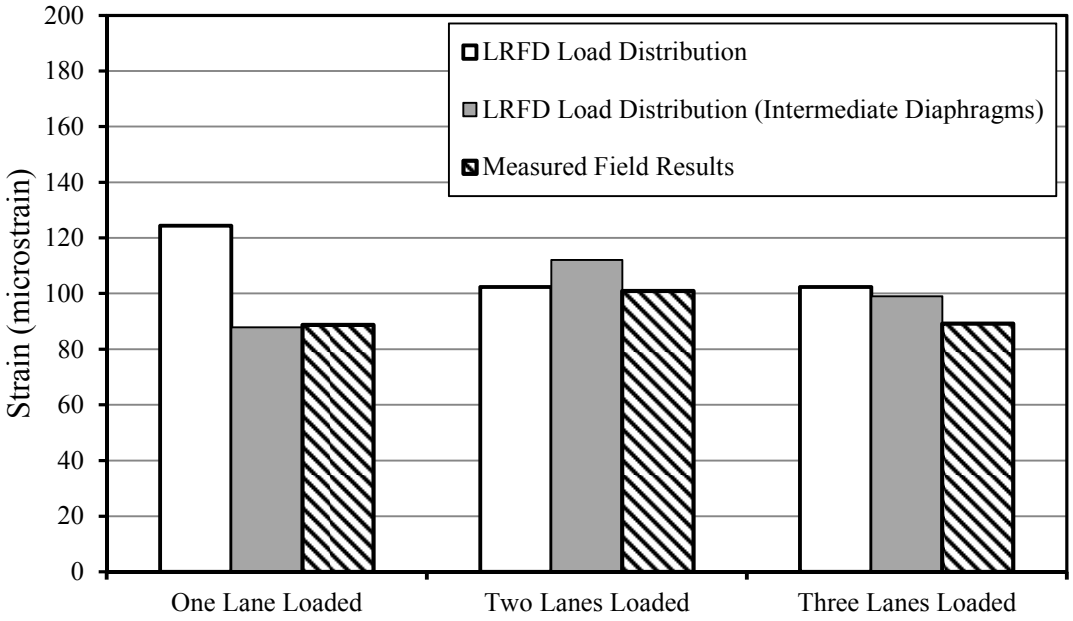

Figure 6.25. *Exterior-girder, bottom-surface strains—BT-54 VC span.*

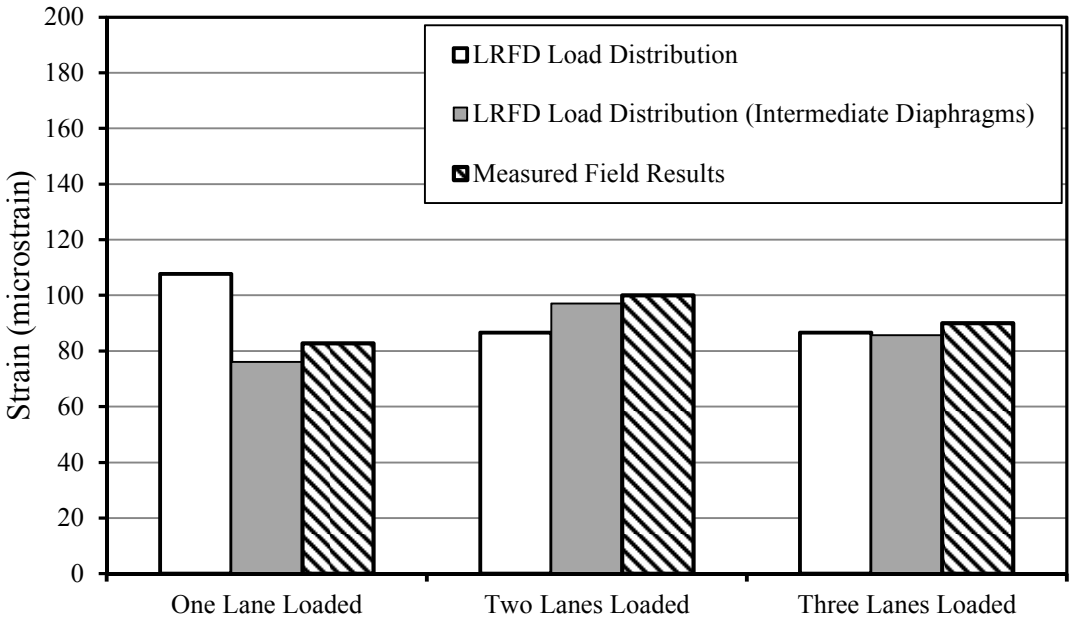

Figure 6.26. *Exterior-girder, bottom-surface strains—BT-72 SCC span.*

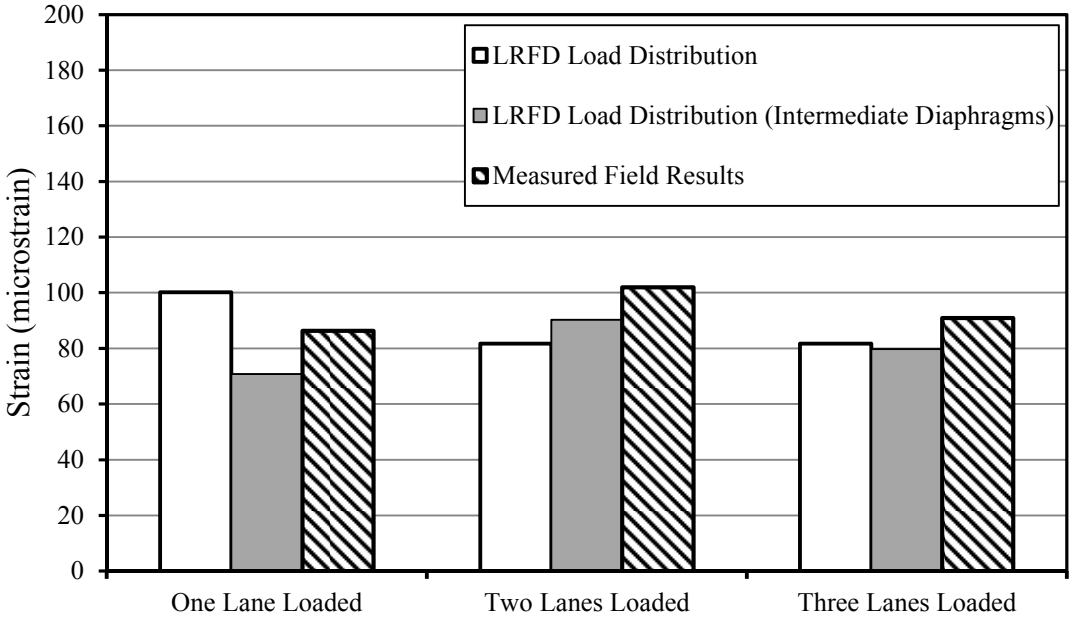

Figure 6.27. *Exterior-girder, bottom-surface strains—BT-72 VC span.*

In general, the LRFD expected values for interior girders were conservative, by an average of 46%. The LRFD worst case scenario expected values for exterior girders for the

shorter (BT-54) spans were also generally conservative by an average of 21%. LRFD worst case scenario expected values for exterior girders with one lane loaded (lever rule) for longer (BT-72) spans were generally conservative by an average of 23%. However, LRFD worst case scenario expected values for exterior girders with two and three lanes loaded for the longer spans were generally unconservative by an average of 7%. These findings generally agree with Barr, Eberhard, and Stanton (2001) findings that AASHTO LRFD load distribution factors are generally conservative. The findings also generally agree with Barnes, Stallings, and Porter (2003) findings—with the exception of the "special" (alternate) exterior girder procedure from AASHTO LRFD. They reported the "special" exterior girder procedure to be overly conservative, while this project's findings indicate that the "special" exterior girder procedure when two and three lanes were loaded was slightly *unconservative*. Note that barriers *were* considered in the calculations for the expected strains for exterior girders in this study, however, they were neglected by Barnes, Stallings, and Porter (2003).

Overall, the exterior-girder AASHTO distribution factor for both the standard and intermediate diaphragm method predicted load distribution well for this project when multiple lanes were loaded. However, for a single lane loaded, the standard AASHTO LRFD method (lever rule) was conservative while the intermediate diaphragm method was slightly unconservative. Critical AASHTO LRFD interior girder distribution factors for all spans were conservative by at least 39%.

6.5 Accuracy of CSiBridge Model Refined Analysis for Prediction of Service-Load Response

The bridge model analysis replicating the in-situ bridge (with barriers and staggered diaphragms) constructed as discussed in Chapter 5 of this thesis is compared to the experimental strain and deflection values from the first load test on the bridge over Hillabee Creek in Figures

6.28 through 6.31. Detailed results are presented in Appendix C. In order to focus on design-critical response, only strains and deflections of at least 20 με and 0.10 in., respectively are used for making numerical comparisons. Truck position A causes the greatest bottom-surface strain on both the critical interior girder (G6) and exterior girder (G7) and was therefore used for these comparisons. CSiBridge model strains were an average of 24% greater than the measured field strains for span 1 (SCC) and an average of 16% greater than measured field strains for span 4 (VC). CSiBridge model deflections were 17% greater than the measured field strains for span 1 and 1% greater than measured field strains in span 4 (VC). Model strains were an average of 24% greater than measured field strains for span 2 (SCC) and 2% greater for span 3 (VC). Model deflections were on average 5% greater than field results for span 2 compared with on average 12% less than measured field results for span 3. The bridge model seemed to generally accurately predict the SCC and VC deflection behavior and VC strain values while consistently over-predicting strain values in the SCC spans. The over-prediction of SCC strain values could potentially be attributed to possible growth of the modulus of elasticity for the SCC from the time of 28-day cylinder testing until the day of load testing more than a year later.

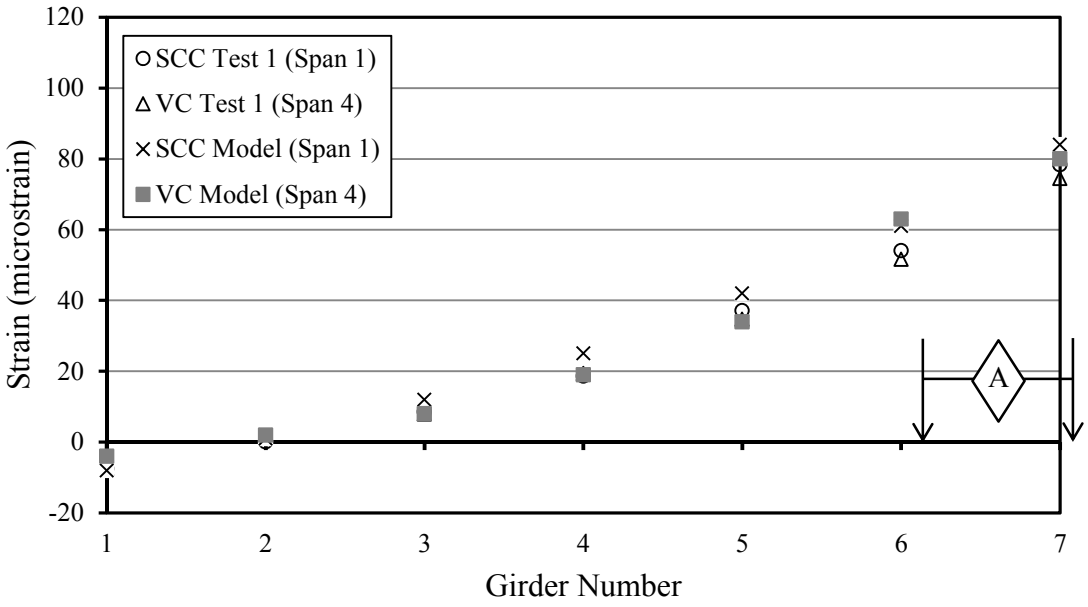

Figure 6.28. Measured live-load test and CSiBridge model strain results for spans 1 and 4.

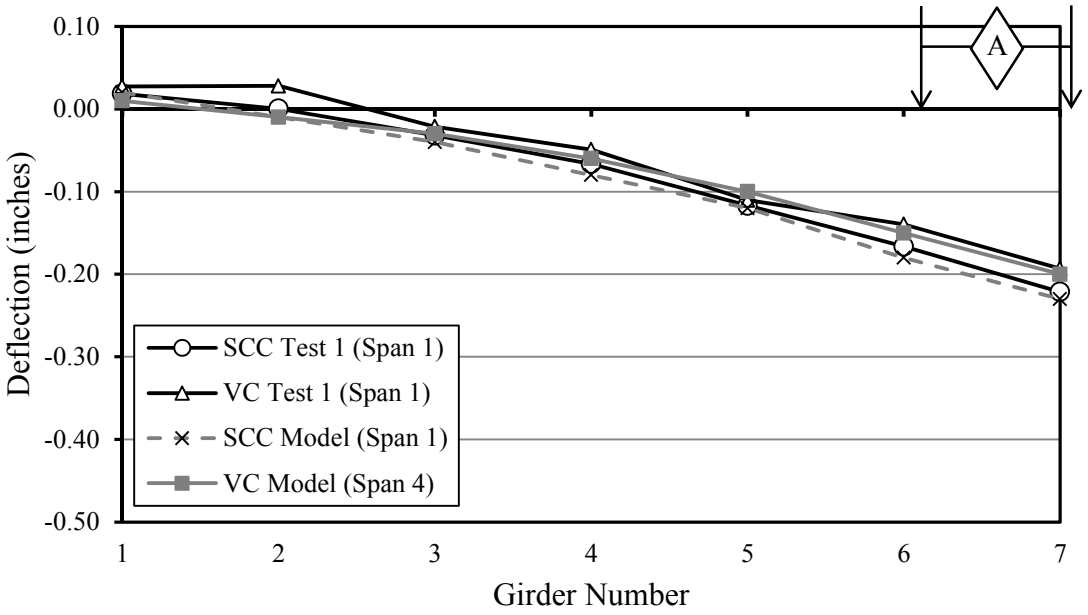

Figure 6.29. Measured live-load test and CSiBridge model deflection results for spans 1 and 4.

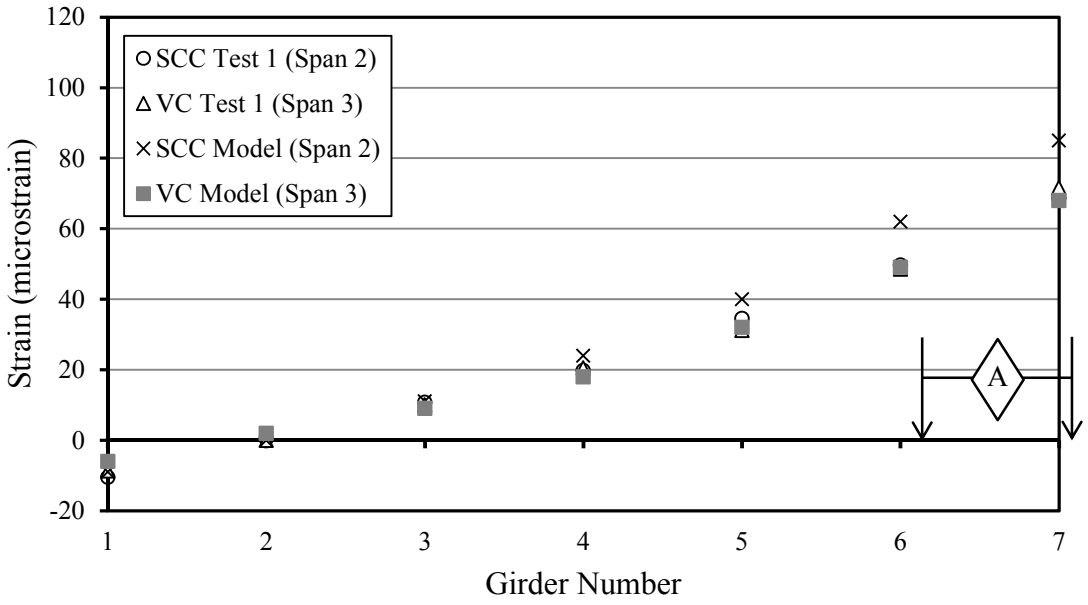

Figure 6.30. Measured live-load test and CSiBridge model strain results for spans 2 and 3.

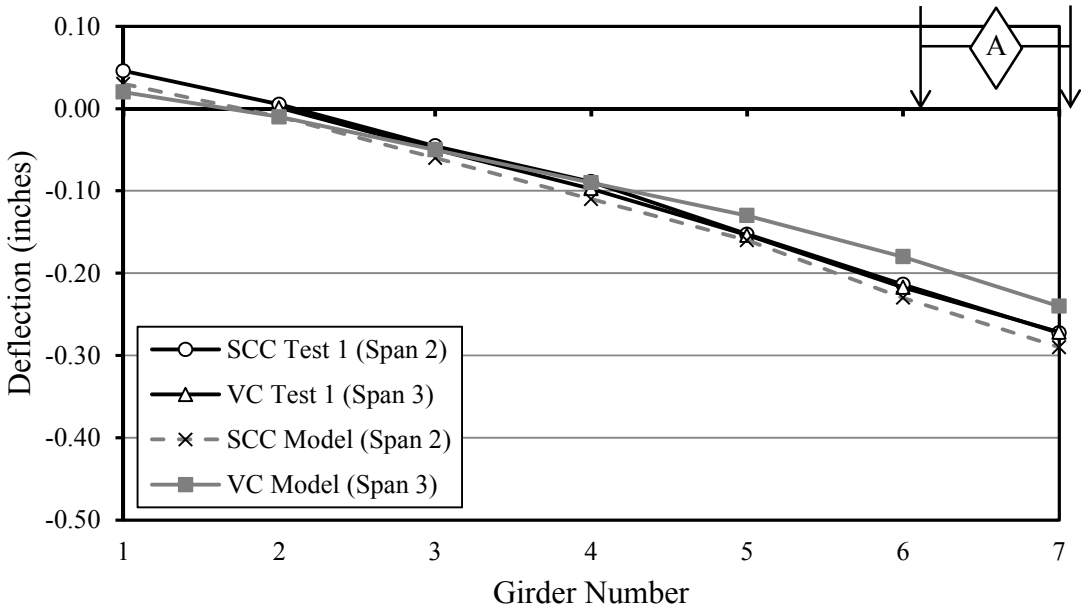

Figure 6.31. Measured live-load test and CSiBridge model deflection results for spans 2 and 3.

Some factors that may have contributed to the differences between the measured results and the model results are the necessary girder property averaging across each span in the model,

haunch thicknesses being averaged for each span in the model, barriers modeled as rectangular cross section members (as discussed in section 4 of Chapter 5), as well as model webwall restraints not exactly replicating the in-situ bridge.

When constructing the model utilizing the CSiBridge wizard as described in Chapter 5 of this paper, the wizard only allowed for a uniform set of girder properties per span. Therefore, all modulus of elasticity and strength properties for each girder were averaged on a per span basis. Modulus of elasticity values varied 300 ksi (4%) in girders across span 1, 400 ksi (6%) in girders across span 2, 800 ksi (10%) in span 3, and 600 ksi (8%) in span 4. The program wizard also required a uniform haunch measurement across all spans. Haunch thicknesses of the in-situ bridge, measured utilizing surveying equipment, ranged anywhere from 0 to 2 inches. A uniform haunch thickness of 1 in. was applied to all spans in the model. In order to achieve proper connectivity to recreate the composite action between the barrier and the deck, the barrier was modeled as a rectangular cross section as described in Chapter 5. Though the rectangular barrier represented an equivalent area moment of inertia to that of the in-situ barrier, discrepancies between barrier widths may have contributed to end girder average strains being greater than field measured strains. Field-cut joints within the barriers were not modeled and may have contributed to discrepancies between the model and experimental results. The webwalls were modeled as described in section 3 of Chapter 5. Webwalls were attached to girders utilizing rigid links in the model. This only allowed for the webwalls to connect to each girder at two discrete points rather than along the full depth of the webwall.

6.6 CSiBridge Model versus CSiBridge Model without Traffic Barriers

The full CSiBridge model of the bridge over Hillabee Creek (Appendix C) is compared to a model of the bridge without traffic barriers (detailed in Appendix D) in Figures 6.32 through

6.39. In order to focus on design-critical response, only strains and deflections of at least 20 με and 0.10 in., respectively are used for making comparisons.

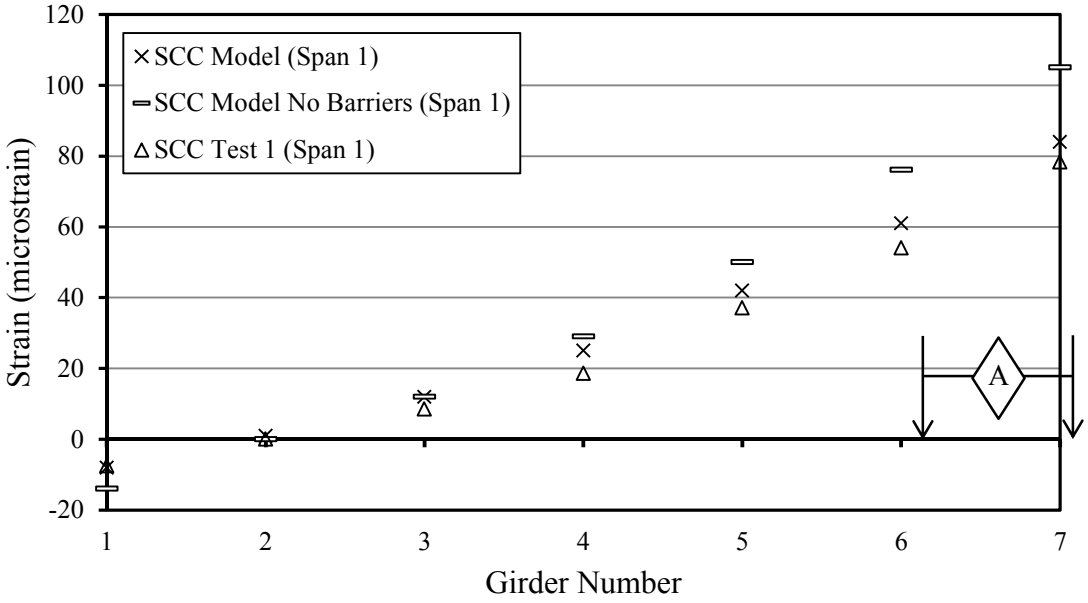

Figure 6.32. *CSiBridge model and experimental bottom-surface strains compared to a CSiBridge model without traffic barriers for span 1.*

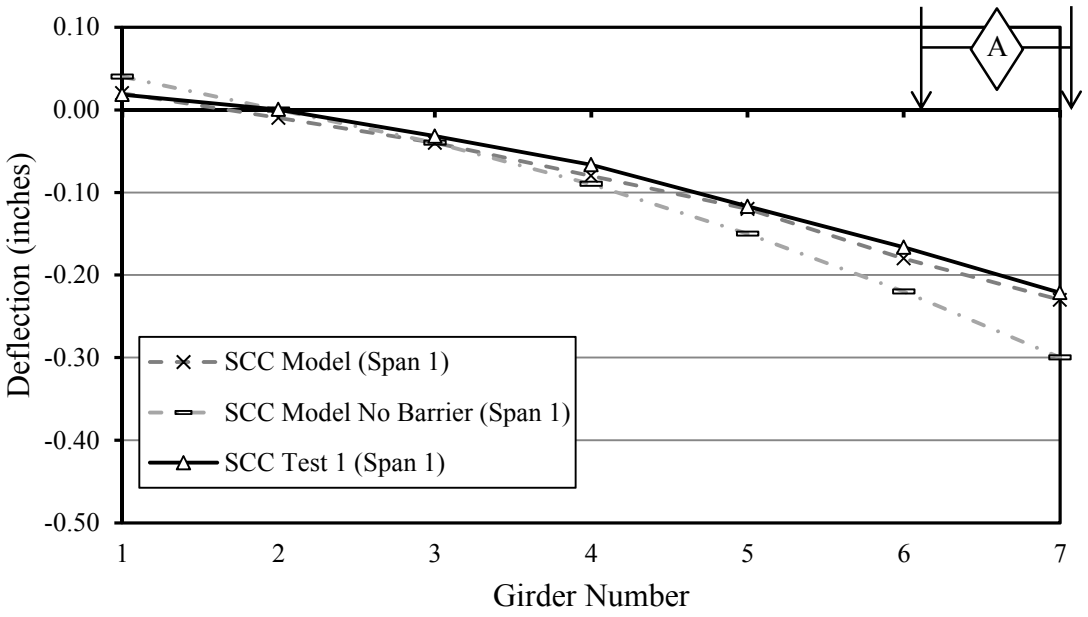

Figure 6.33. *CSiBridge model and experimental girder deflections compared to a CSiBridge model without traffic barriers for spans 1.*

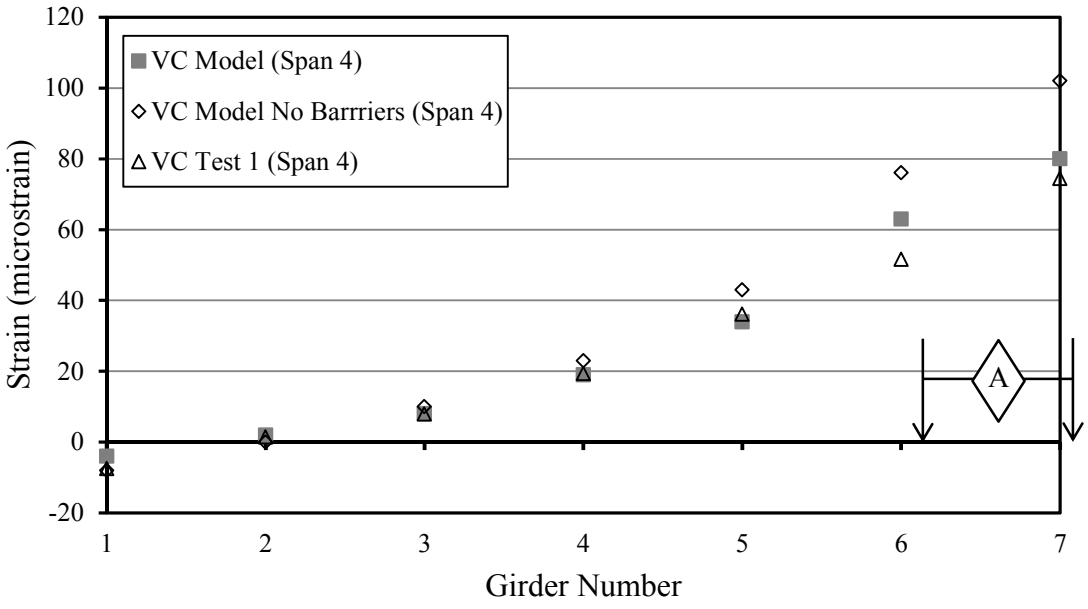

Figure 6.34. *CSiBridge model and experimental bottom-surface strains compared to a CSiBridge model without traffic barriers for span 4.*

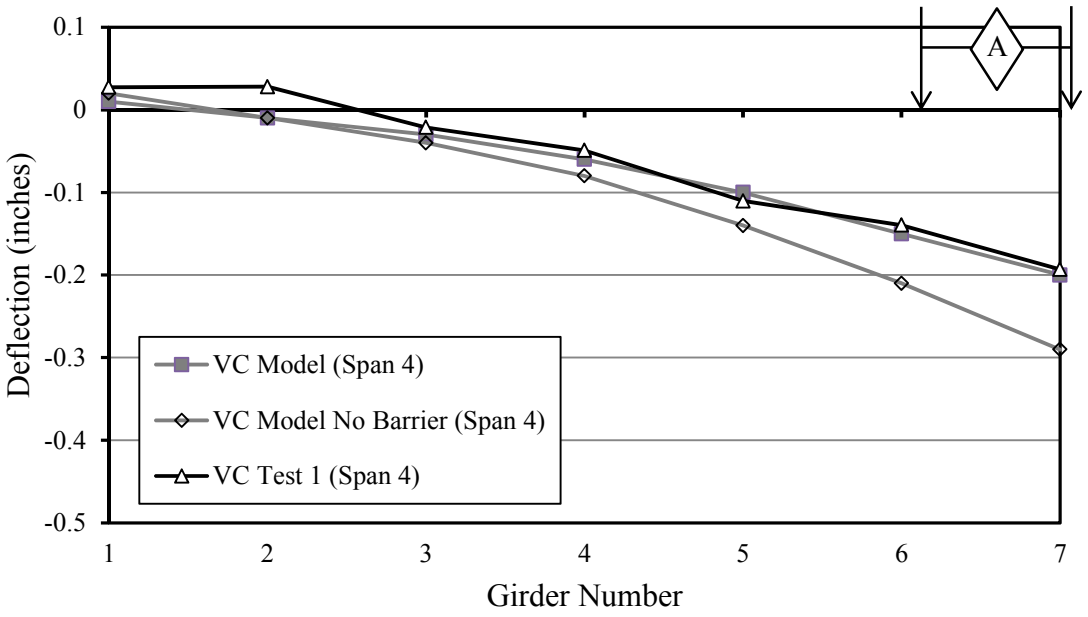

Figure 6.35. *CSiBridge model and experimental girder deflections compared to a CSiBridge model without traffic barriers for span 4.*

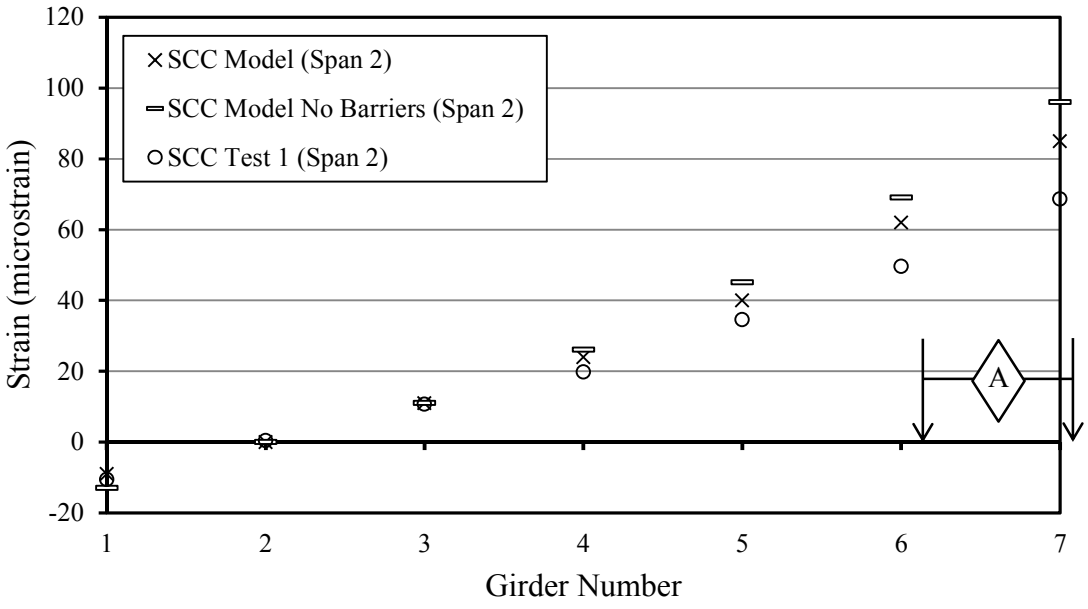

Figure 6.36. *CSiBridge model and experimental strains compared to a CSiBridge model without traffic barriers for span 2.*

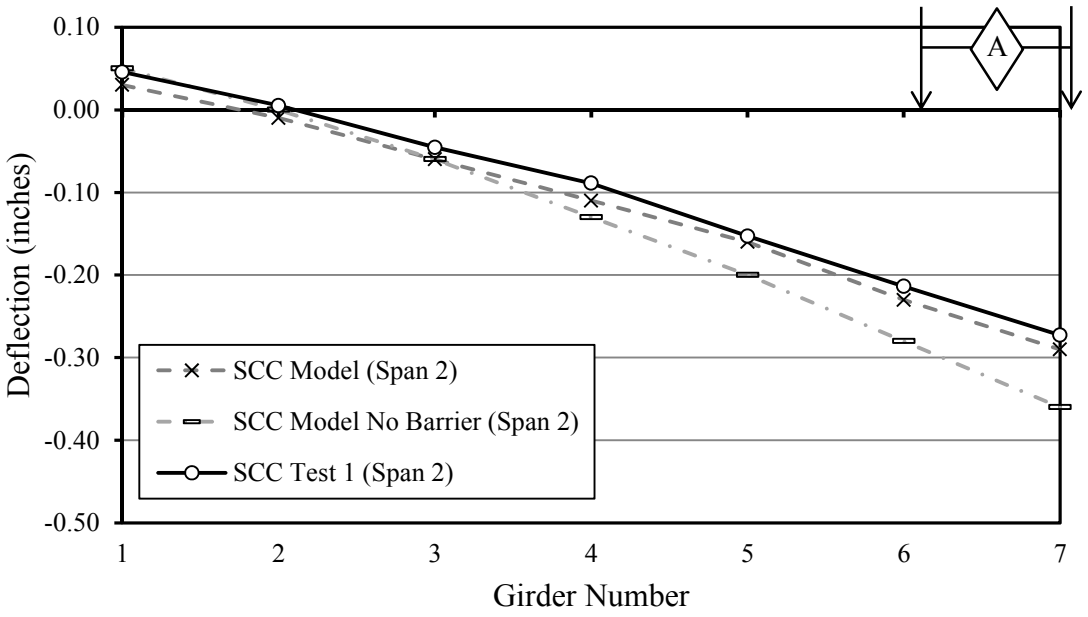

Figure 6.37. *CSiBridge model and experimental girder deflections compared to a CSiBridge model without traffic barriers for span 2.*

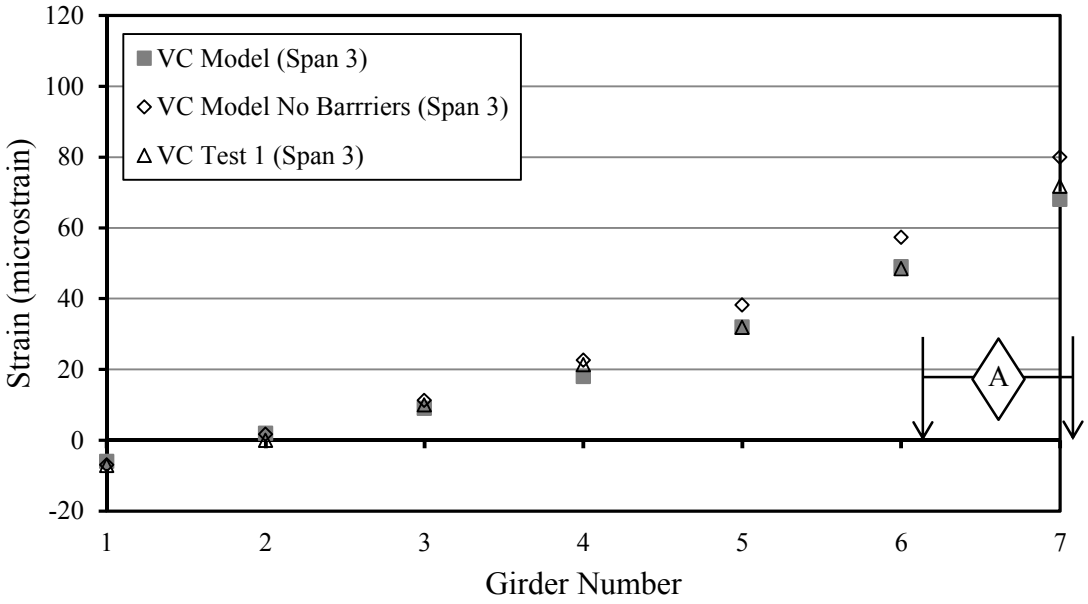

Figure 6.38. *CSiBridge model and experimental strains compared to a CSiBridge model without traffic barriers for span 3.*

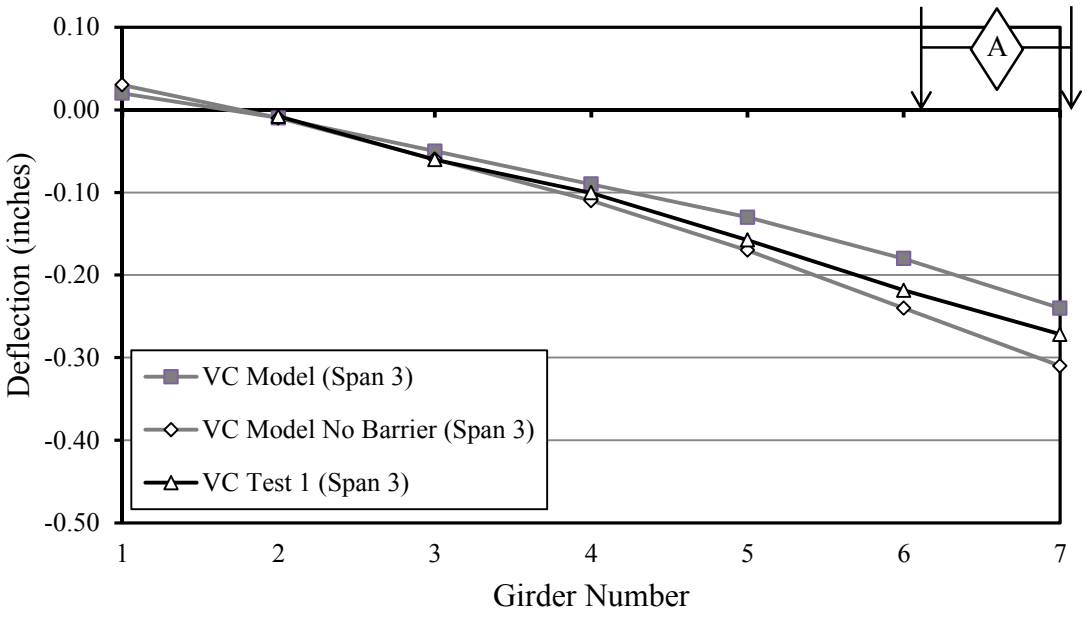

Figure 6.39. *CSiBridge model deflections compared to a CSiBridge model without traffic barriers for span 3.*

As can be seen in the figures, the model without barriers consistently had strains on average 16% greater than the full CSiBridge model with barriers for all spans. The figures also show that the largest discrepancy between models is in the exterior girder (G7). For the SCC BT-54 exterior girder, the strain and deflection values for the model without barriers exceeded the model with barriers by 21 με (26%) and 0.07 in. (35%), respectively. For the VC BT-54 exterior girder, strain and deflection values for the model without barriers exceeded the values of the model with barriers by 22 με (28%) and 0.09 in. (39%), respectively. For the SCC BT-72 exterior girder, the strain and deflection values for the model without barriers exceeded the model with barriers by 11 με (13%) and 0.07 in. (23%), respectively. For the VC BT-72 exterior girder, strain and deflection values for the model without barriers exceeded the values of the model with barriers by 12 με (17%) and 0.07 in. (28%), respectively. All elements except for the presence of barriers remained the same between the two models; therefore it can be concluded

that barriers were the sole factor that lead to the discrepancy in strain readings between the two models. It is clear from comparison with the test results that including barrier stiffness produces the most accurate bridge behavior prediction for service loads.

6.7 Effects of Using a Bridge Model with Simplified Intermediate Diaphragms

Figures 6.40 through 6.43 display the strain and deflection results from the previously discussed CSiBridge model with staggered webwalls, no traffic barriers and a model with simplified webwalls and without traffic barriers. Results for the model with staggered webwalls are detailed in Appendix D and results for the model with simplified intermediate diaphragms (no adjusted webwalls) are detailed in Appendix E. In order to focus on design-critical response, only strains and deflections of at least 20 με and 0.10 in., respectively are used for making comparisons. The two models' strain and deflection readings differed throughout the bridge by only an average of 2%. However, the model with simplified webwalls resulted in exterior girder strains and deflections that averaged 5% higher than the model with staggered webwalls and no barriers. This suggests that the model with simplified webwalls acted as a more rigid body than the model with staggered webwalls. Due to the low percentage difference between the results of the two models for the design-critical girders, the simplified CSiBridge intermediate diaphragm model is an adequate representation for design purposes of intermediate webwalls located along the skew of a bridge but staggered as to be perpendicular to girders.

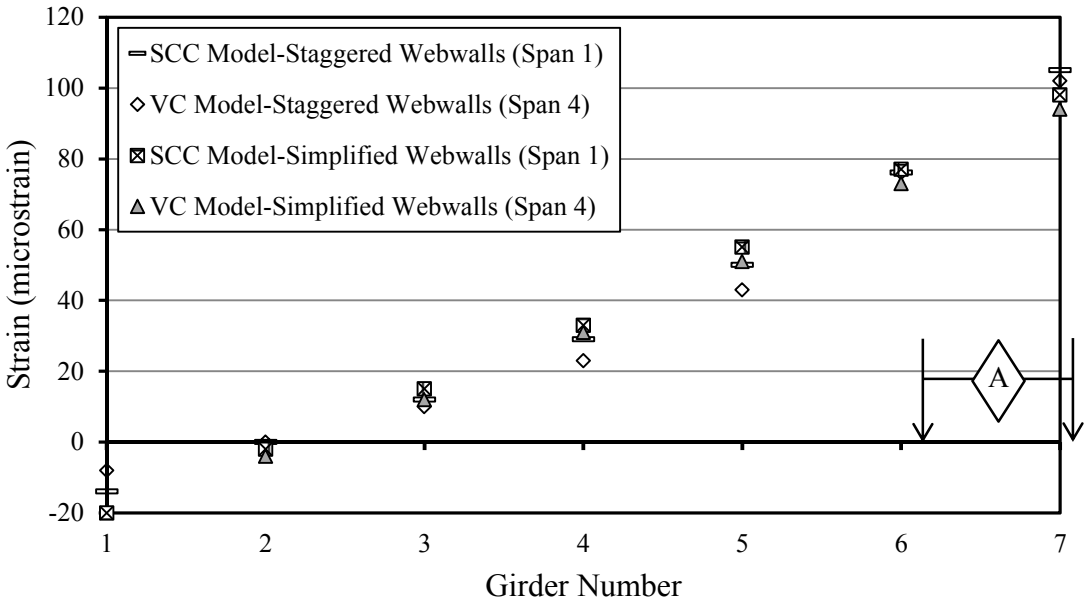

Figure 6.40. *CSiBridge model-without traffic barriers-strains compared to a CSiBridge model with simplified webwalls but without traffic barriers, for spans 1 and 4.*

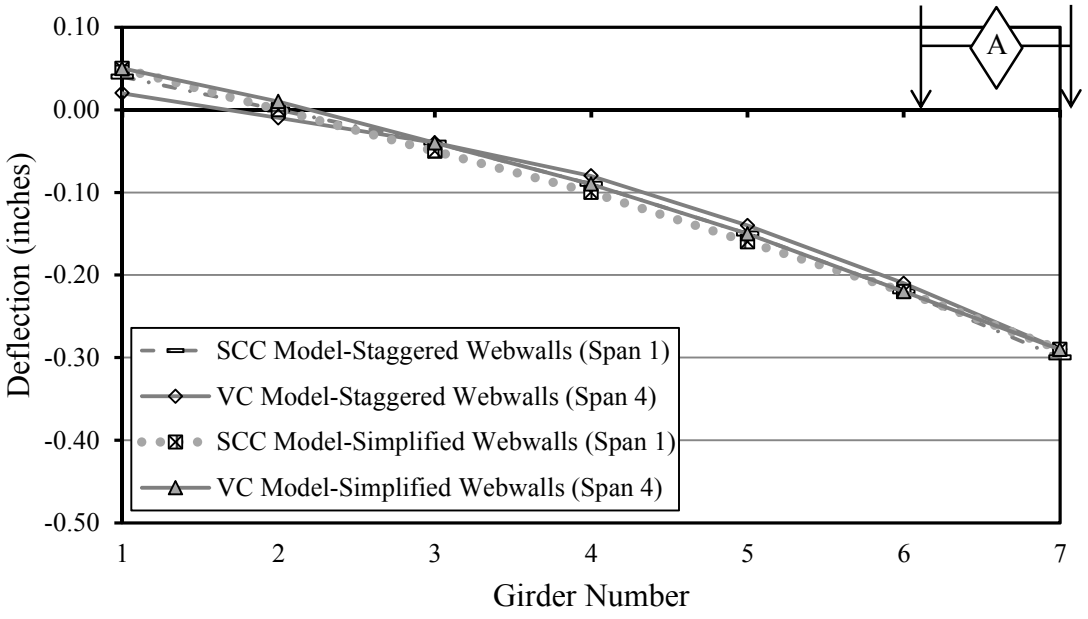

Figure 6.41. *CSiBridge model-without traffic barriers-deflections compared to a CSiBridge model with simplified webwalls but without traffic barriers, for spans 1 and 4.*

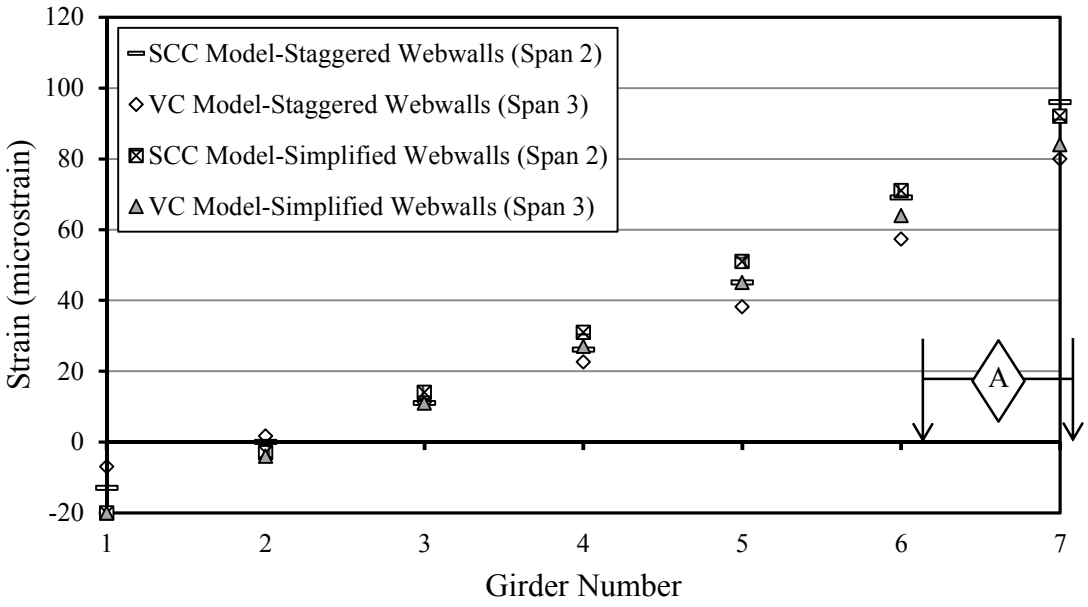

Figure 6.42. *CSiBridge model-without traffic barriers-strains compared to a CSiBridge model with simplified webwalls but without traffic barriers, for spans 2 and 3.*

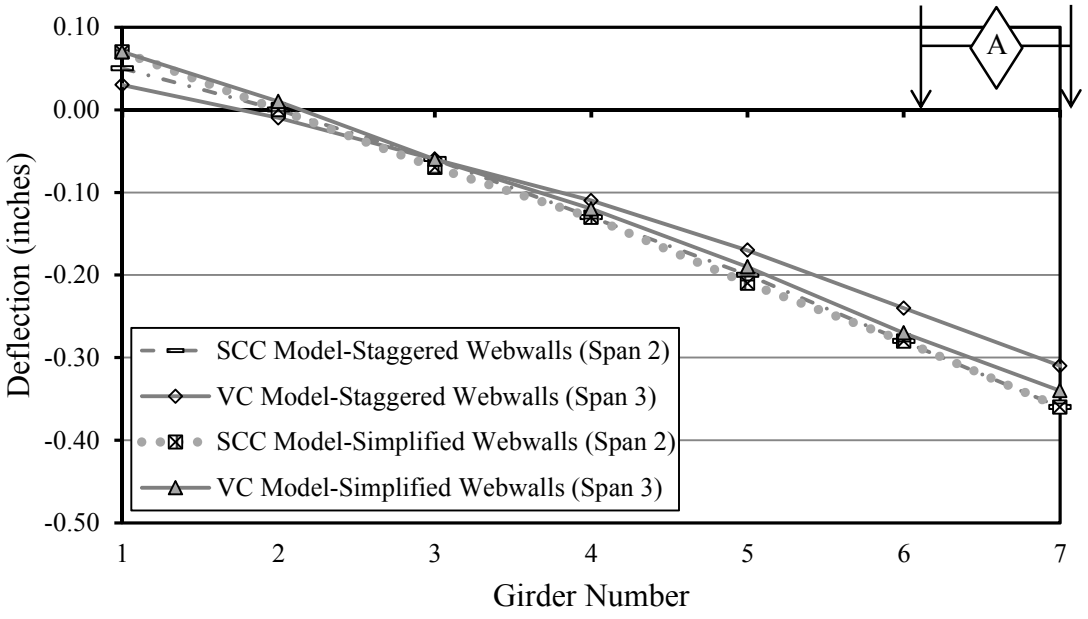

Figure 6.43. *CSiBridge model-without traffic barriers-deflections compared to a CSiBridge model with simplified webwalls but without traffic barriers, for spans 1 and 4.*

Chapter 7 Summary and Conclusions

The Hillabee Creek Bridge, the first bridge in Alabama produced with SCC precast, prestressed girders, was instrumented during and after construction. A span of BT-54 girders and a span of BT-72 girders were constructed with SCC, and identical companion spans were constructed with VC girders. Just before opening to traffic and once again after a year of service, static load tests were performed on all four spans of the bridge. After accounting for the unique, measured E_c of each girder and deck segment through the use of transformed-section analysis, SCC and VC midspan strains were compared at each time of testing and over the first year of service. SCC and VC midspan deflections were also directly compared. Several conclusions are drawn based on these results:

1. Superimposed deflection and strain responses to single-truck loads were consistently within 0.01 in. (0.3 mm) and 1 microstrain of actual responses to multiple-truck loads. Therefore, the bridge is exhibiting linear-elastic behavior in response to service loads after one year of service.
2. Measure flexural strains were found to be proportional to the distance from the neutral axis in both SCC and VC girders, as would be assumed in design.
3. Considering the precision of the measured values, there is little or no practical difference between the SCC and VC girder deflections in this bridge. Therefore, the service-level live-load deflection behavior of SCC girders is acceptably similar to that of VC girders.

4. Within each load test, bottom-flange strains in SCC girders were consistently similar to strains in equivalent VC girders. Therefore, the flexural behavior of SCC girders is acceptably similar to that of VC girders.

5. The deformation response of all girders was essentially the same during the first load test as during a second load test conducted one year later. Therefore, the bridge response to service loads has experienced no significant deterioration due to exposure to one year of service conditions.

6. Overall, the service-load flexural response of SCC girders is acceptably similar to that of VC girders. Therefore, service-load behavior should not restrict the implementation of SCC in the construction of precast, prestressed bridge girders.

7. AASHTO LRFD Bridge Design Specifications (2012) methods for determining load distribution to girders within a span were determined to be generally accurate for SCC and VC girders, but overly conservative in some instances and slightly *unconservative* in others. All interior girder AASHTO distribution factors were found to be conservative by at least 39 percent. The method for predicting distribution factors for exterior girders when one lane was loaded on the bridge (lever rule) was also found to be slightly conservative by an average of 12 percent. AASHTO methods for predicting load distribution to exterior girders for multiple lanes loaded for the longer spans (BT-72) were found to be slightly *unconservative*.

8. Overall, there was not a noticeable difference in load distribution between the SCC and VC girders.

Three finite-element models of the bridge over Hillabee Creek were constructed in CSiBridge software. A model attempting to most accurately replicate the in-situ bridge was

constructed and analyzed under the same service-load conditions as the two load tests performed on the Hillabee Creek bridge. The results from the in-situ load test and the model were analyzed. A second model of the bridge was constructed identical to the replica bridge model with the only difference being no barriers were included in the model. It was subjected to the same service-load conditions, analyzed, and compared to the replica model to determine the effect of barriers on the performance of a bridge under service-load conditions. A third and final model was constructed exactly the same as the model without barriers with the only difference being that simplified intermediate diaphragms were included in the place of the more complex staggered diaphragms in the actual bridge.. This simplified model was subjected to the same service-load conditions as the other two models, analyzed, and compared to the model with replica webwalls to determine the effect of simplified intermediate diaphragm modeling on the performance of the bridge. Several conclusions are drawn based on these results:

1. The refined analysis model replicating the in-situ bridge adequately predicted VC span behavior and SCC span behavior. SCC span behavior was predicted slightly more conservatively than VC span behavior.
2. The refined analysis model that did not include traffic barriers had an average of 32% higher exterior girder strains for short spans (BT-54s) and 20% higher exterior girder strains for long spans (BT-72s) than the model with traffic barriers. It can be concluded that the inclusion of traffic barriers in analysis tends to make a significant difference in the behavior of exterior bridge girders. The effect of the traffic barriers was less pronounced on interior girders.
3. The refined analysis model with simplified intermediate diaphragms behaved very similarly to the model that more accurately replicated the actual in-situ diaphragms.

The implementation of the simplified intermediate diaphragms described in this thesis is adequate for service-load state design.

References

ACI Committee 237. 2007. *Self-Consolidating Concrete (ACI 237R-07)*. American Concrete Institute (ACI), Farmington Hills, Michigan.

ACI Committee 318. 2008. *Building Code Requirements for Structural Concrete (ACI 318-08) and Commentary.* Farmington Hills, MI: American Concrete Institute.

Alabama Department of Transportation. "Bridge Standard Drawing I-131." *ALDOT Standard and Special Drawings for Highway Construction.* 2012.

American Association of State Highway and Transportation Officials. 2012. *AASHTO LRFD Bridge Design Specifications.* Washington, DC.

ASTM C 39. 2005. Standard Test Method for Compressive Strength of Cylindrical Concrete Specimens. ASTM International. West Conshohocken, PA.

ASTM C 469. 2002. Standard Test Method for Static Modulus of Elasticity and Poisson's Ratio of Concrete in Compression. ASTM International. West Conshohocken, PA.

Barnes, Robert W., Stallings, J. Michael, and Porter, Paul W. "Live-load Response of Alabama's High-performance Concrete Bridge." *Transportation Research Record*, 2003: No. 1845, 115-124.

Barr, Paul J., Marc. O. Eberhard, and John F. Stanton. "Live-Load Distribution Factors in Prestressed Concrete Girder Bridges." *Journal of Bridge Engineering*, 2001: Vol. 6 No. 5, 298-306.

Boehm, Kevin. *Structural Performance of Self-Consolidating Concrete in AASHTO Type I Prestressed Girders.* Thesis, Auburn: Auburn University, 2010.

Boehm, Kurtis M., Robert W. Barnes, and Anton K. Schindler. *Performance of Self-Consolidating Concrete In Prestressed Girders.* Auburn, AL: Auburn University Highway Research Center, April 2010: pp. 102-127.

Cai, C.S. "Discussion on AASHTO LRFD Load Distribution Factors for Slab-on-Girder Bridges." *Practice Periodical on Structural Design and Construction*, 2005: 171-176.

Celik Ozyildirim, Ph.D., P.E. "Bulb-T Beams with Self Consolidating Concrete on the Route 33 Bridge Over the Pamunkey River in Virginia." *Virginia Transportation Research Council*, 2008.

Computers and Structures, Inc. *CSiBridge Overview.* 2013. http://www.csiamerica.com/csibridge (accessed August 9, 2013).

Dunham, Emily. *Transfer Length in Bulb-Tee Girders Constructed with Self-Consolidating Concrete.* Thesis, Auburn, AL: Auburn University, 2011.

Erkmen, Bulent, Catherine E. Wolfgram French, and Carol K. Shield. *Self-Compacting Concrete for Prestressed Bridge Girders.* Dissertation, University of Minnesota, 2008.

Fason, William. *Static Load Testing of a Damaged, Continuous Prestressed Concrete Bridge.* Thesis, Auburn, AL: Auburn University, 2009.

Fu, Gongkang, Lang Liu, and Mark D. Bowman. "Multiple Presence Factor for Truck Load on Highway Bridges." *Journal of Bridge Engineering*, 2013: Vol. 18, No. 3, 240-249.

Geokon Instruction Manual. Model 4200/4204/4210 Vibrating Wire Strain Gauges. Rev N, 8/10.

Gross, Shawn P. and Ned H. Burns. Field Performance of Prestressed High Performance Concrete Highway Bridges in Texas. Federal Highway Administration Report No. FHWA/TX-05/9-580/589-2. February 2000.

Huo, Xiaoming Sharon, Edward P. Wasserman, and Pingsheng Zhu. "Simpified Method of Lateral Distribution of Live Load Moment." *Journal of Bridge Engineering*, 2004: 382-390.

Johnson, Brandon. *Time-Dependent Deformations in Precast, Prestressed Bridge Girders.* Thesis, Auburn, AL: Auburn University, 2012.

Kavanaugh, Bryan. *Creep Behavior of Self-Consolidating Concrete.* Thesis, Auburn, AL: Auburn University, 2008.

Keske, Samuel D., Anton K. Schindler, and Robert W. Barnes. "Assessment of Stability Test Methods for Self-Consolidating Concrete." *ACI Materials Journal*, 2013: Vol. 110, No. 4, 385-393.

Khayat, Kamal Henri, and Denis Mitchell. *NCHRP Report 628 Self-Consolidating Concrete for Precast, Prestressed Concrete Bridge Elements.* Washington, D.C.: Transportation Research Board, 2009.

Kim, Young Hoon. *Characterization of Self-Consolidating Concrete for the Design of Precast, Pretensioned Bridge Superstructure Elements.* Dissertation, College Station, Texas: Texas A&M University, 2008.

Kulicki, J., Z. Prucz, C. M. Clancy, D. R. Mertz, and A. S. Nowak. *Updating the Calibration Report for AASHTO LRFD Code.* Washington, D.C.: Final Report NCHRP 20-7/186. Transportation Research Board, 2007.

Naito, Clay, Geoffrey Brunn, Greg Parent, and Tyler Tate. *Comparative Performance of High Early Strength and Self Consolidating Concrete for Use in Precast Bridge Beam Construction.* Paper 58, ATLSS Reports, 2005.

Schindler, A.K., R.W. Barnes, J.B. Roberts, and S. Rodriguez. Properties of Self-Consolidating Concrete (SCC) for Prestressed Members. *ACI Materials Journal*, Vol. 104, No. 1, pp. 53-61, 2007.

Sotelino, Elisa D., Judy Liu, Wonseok Chung, and Kitjapat Phuvoravan. *Simplified Load Distribution Factor for Use in LRFD Design.* West Lafayette, Indiana: Joint Transportation Research Program, Indiana Department of Transportation and Purdue University, 2004.

Trejo, David, Mary Beth Hueste, Young Hoon Kim, and Hakan Atahan. *Characterization of Self-Consolidating Concrete for Design of Precast, Prestressed Bridge Girders.* College Station, Texas: Texas Transportation Institute, 2008.

Zia, Paul, Roberto A. Nunez, and Luis A. Mata. *Implementation of Self-Consolidating Concrete for Prestressed Concrete Girders.* Raleigh, NC: North Carolina Department of Transportation, 2005.

Zokaie, T., T.A. Osterkamp, and R.A. Imbsen. *Distribution of Wheel Load on Highway Bridges.* Washington, D.C.: National Cooperative Highway Research Program Report 12-26/1 Transportation Research Board, 1991.

Appendix A:

Load Test Results - Strains and Deflections – May 14-15, 2012

Table A-1. *Live-load test results for spans 1 and 4 of the bridge over Hillabee Creek.*

	S1 G1		**S1 G2**		**S1 G3**		**S1 G4**		**S1 G5**		**S1 G6**		**S1 G7**	
Load Truck Position	SCC													
	Defl.	Strain	Defl.	Strain	Defl.	Strain	Defl.	Strain	Defl.	Strain	Defl.	Strain	Defl.	Strain
	in.	με	in.	με	in.	με	in.	με	in.	με	in.	με	in.	με
A	0.02	-7	0.00	0	-0.03	9	-0.07	19	-0.12	37	-0.17	54	-0.22	78
B	0.02	-6	0.00	1	-0.03	10	-0.07	20	-0.11	38	-0.16	53	-0.21	74
C	0.02	-5	0.01	2	-0.03	11	-0.06	21	-0.11	38	-0.15	51	-0.19	70
D	-0.03	7	-0.06	16	-0.08	24	-0.11	35	-0.12	37	-0.11	33	-0.09	31
E	-0.02	8	-0.04	16	-0.07	24	-0.09	34	-0.10	35	-0.09	33	-0.09	31
F	-0.04	11	-0.06	18	-0.08	26	-0.11	37	-0.11	33	-0.09	30	-0.07	25
G	-0.09	32	-0.11	32	-0.11	38	-0.10	31	-0.07	22	-0.05	16	-0.02	7
H	-0.11	39	-0.12	37	-0.11	38	-0.09	29	-0.06	21	-0.04	13	-0.01	4
	S4 G1		**S4 G2**		**S4 G3**		**S4 G4**		**S4 G5**		**S4 G6**		**S4 G7**	
Load Truck Position	VC													
	Defl.	Strain	Defl.	Strain	Defl.	Strain	Defl.	Strain	Defl.	Strain	Defl.	Strain	Defl.	Strain
	in.	με	in.	με	in.	με	in.	με	in.	με	in.	με	in.	με
A	0.03	-8	0.03	1	-0.02	8	-0.05	19	-0.11	36	-0.14	54	-0.19	75
B	0.01	-7	0.01	2	-0.04	10	-0.07	21	-0.11	37	-0.16	53	-0.21	72
C	0.02	-6	0.00	4	-0.03	9	-0.07	21	-0.09	36	-0.11	51	-0.15	66
D	-0.03	8	--	18	-0.07	24	-0.09	34	-0.10	38	-0.12	36	-0.07	25
E	-0.03	9	--	19	-0.08	26	-0.12	37	-0.12	40	-0.11	35	-0.12	27
F	-0.05	12	--	21	-0.10	27	-0.12	38	-0.12	38	-0.11	30	-0.09	24
G	-0.09	34	--	35	-0.10	38	-0.09	30	-0.07	26	-0.03	16	-0.01	7
H	-0.12	41	--	40	-0.13	38	-0.11	29	-0.08	24	-0.06	13	-0.02	4

"--" denotes missing data due to equipment malfunction.

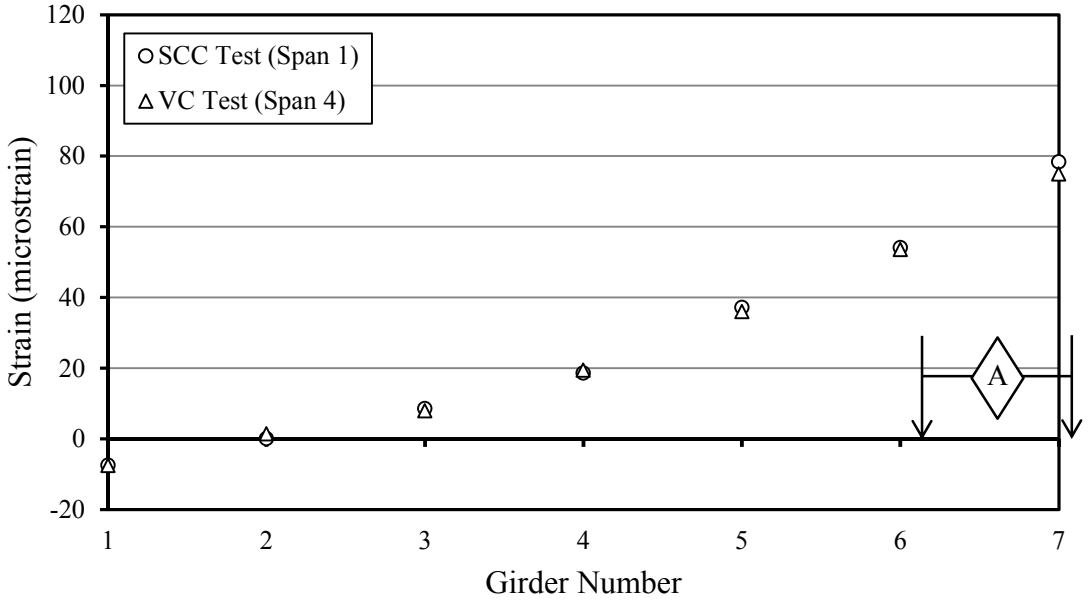

Figure A-1. *Strain results from load-truck-position A on spans with BT-54 girders.*

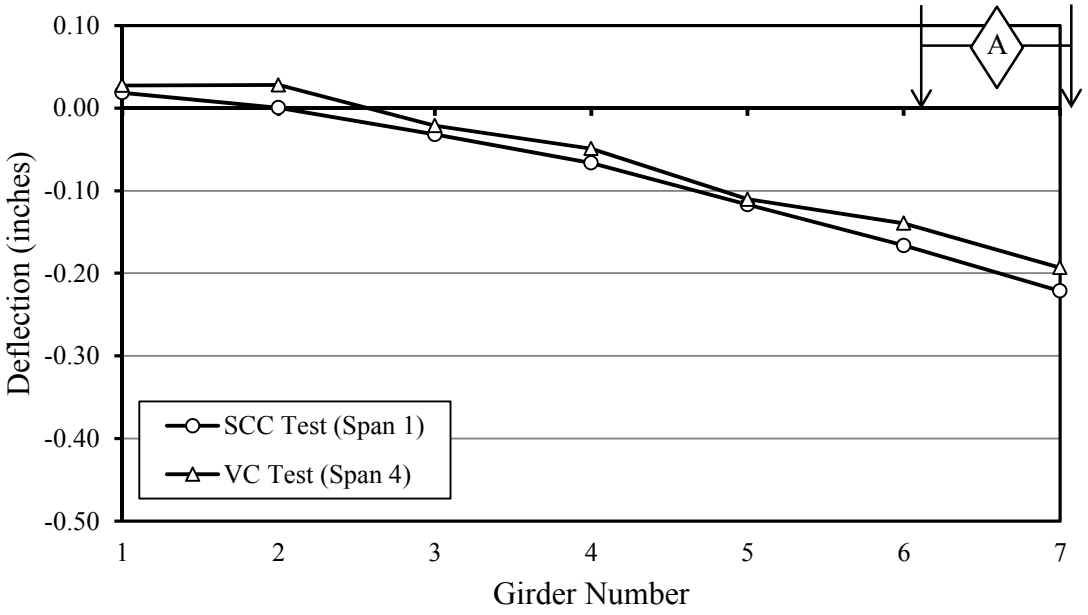

Figure A-2. *Deflection results from load-truck position A on spans with BT-54 girders.*

Figure A-3. *Strain results from load-truck-position B on spans with BT-54 girders.*

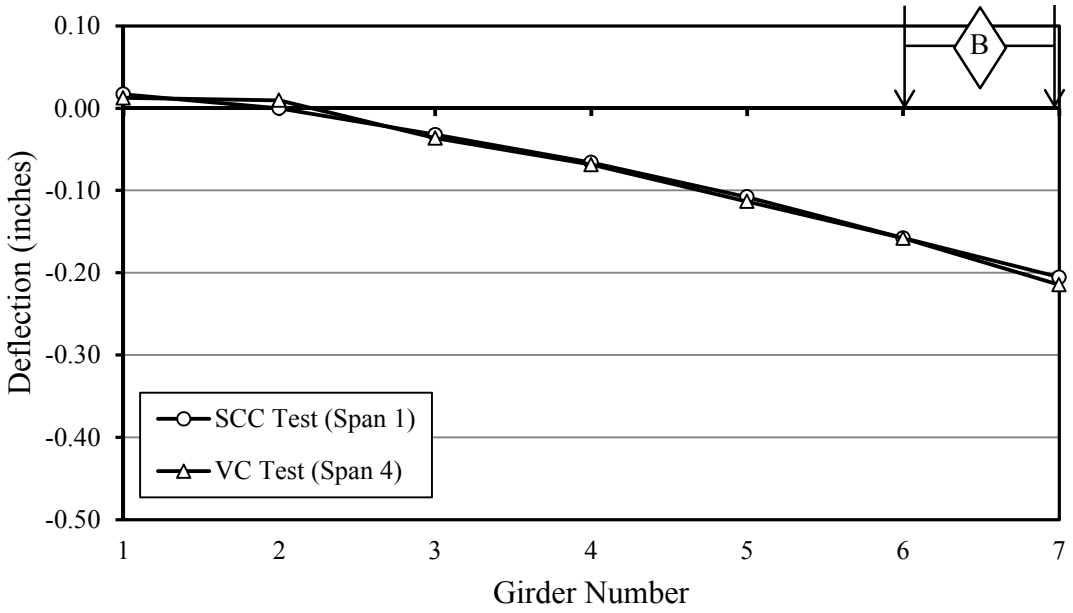

Figure A-4. *Deflection results from load-truck position B on spans with BT-54 girders.*

Figure A-5. *Strain results from load-truck-position C on spans with BT-54 girders.*

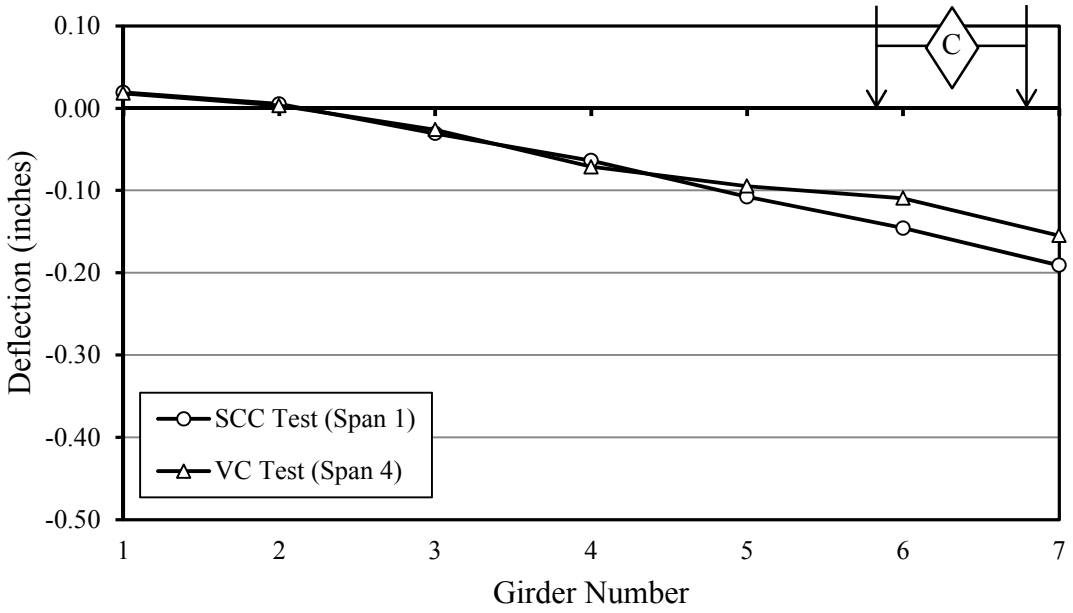

Figure A-6. *Deflection results from load-truck position C on spans with BT-54 girders.*

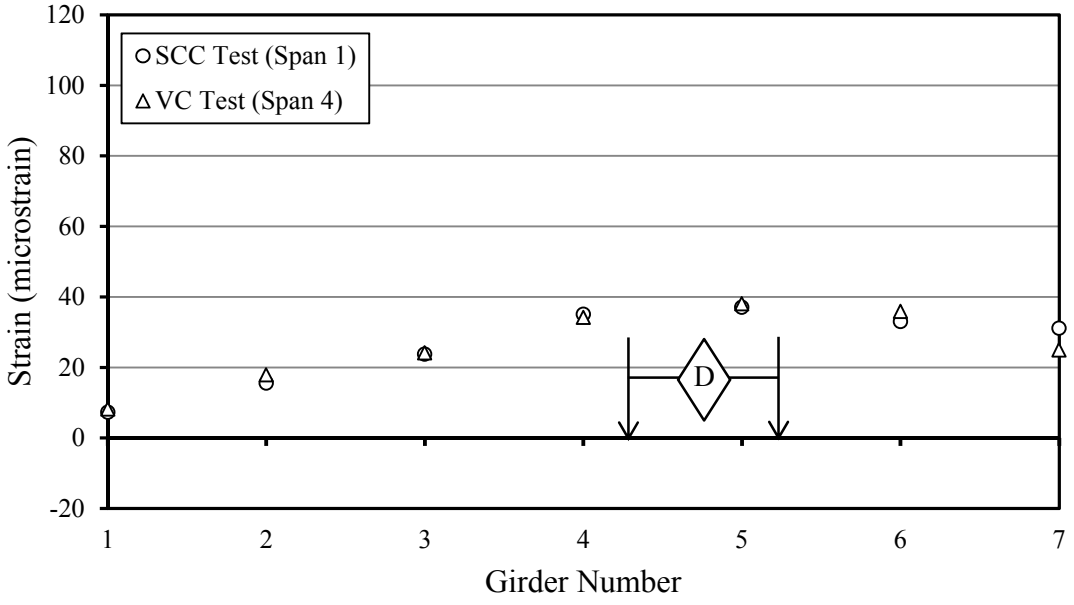

Figure A-7. *Strain results from load-truck-position D on spans with BT-54 girders.*

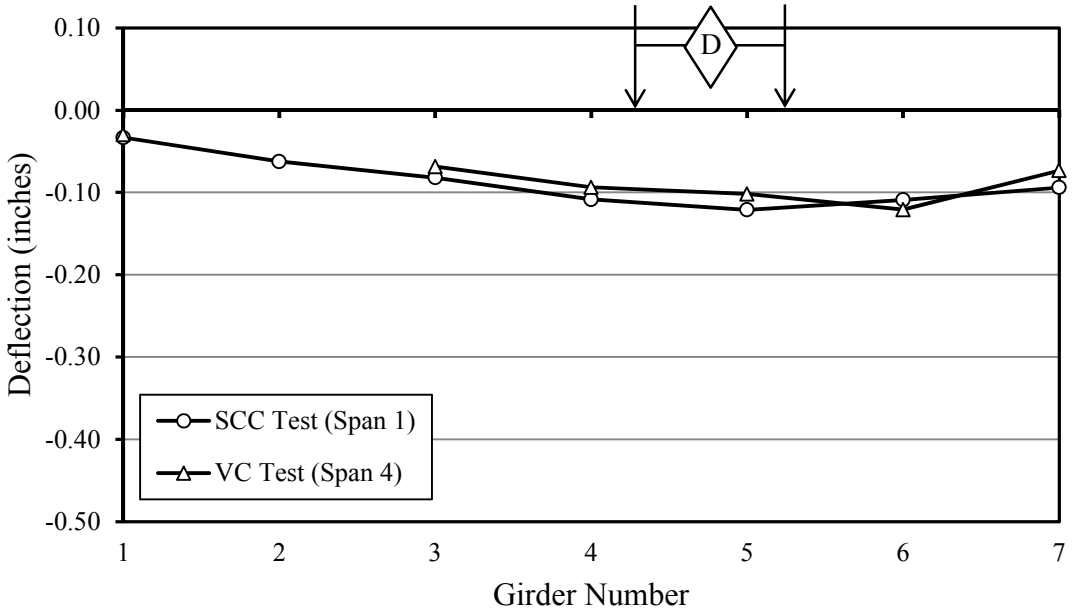

Figure A-8. *Deflection results from load-truck position D on spans with BT-54 girders.*

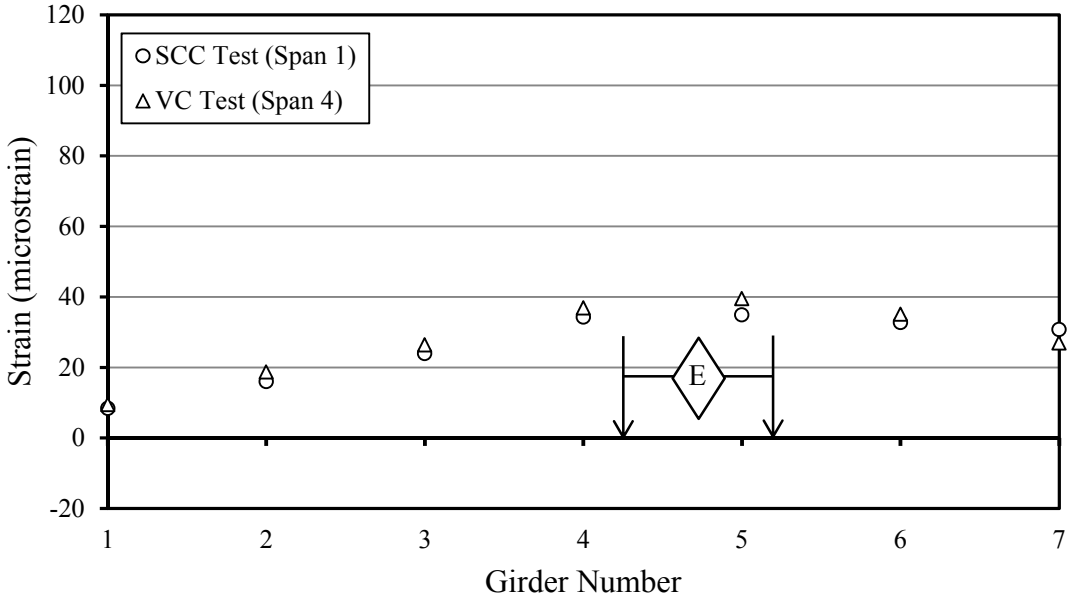

Figure A-9. *Strain results from load-truck-position E on spans with BT-54 girders.*

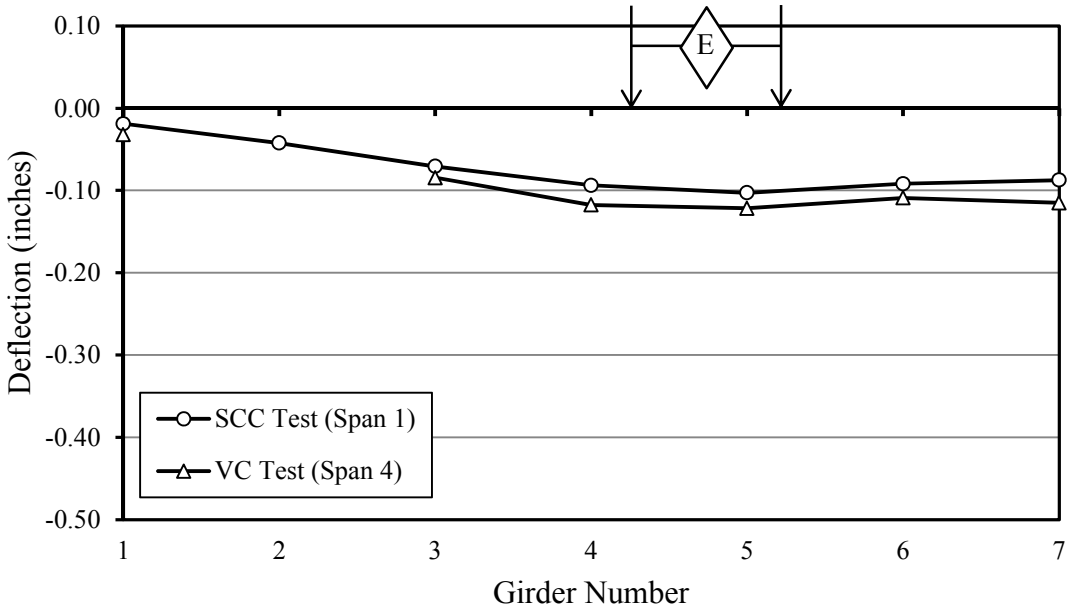

Figure A-10. *Deflection results from load-truck position E on spans with BT-54 girders.*

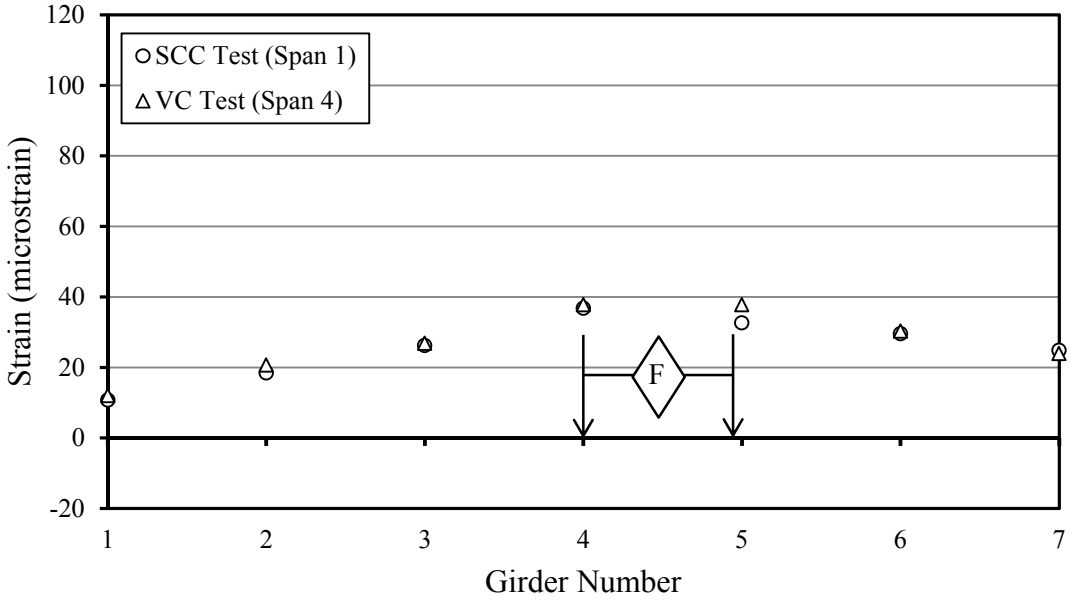

Figure A-11. *Strain results from load-truck-position F on spans with BT-54 girders.*

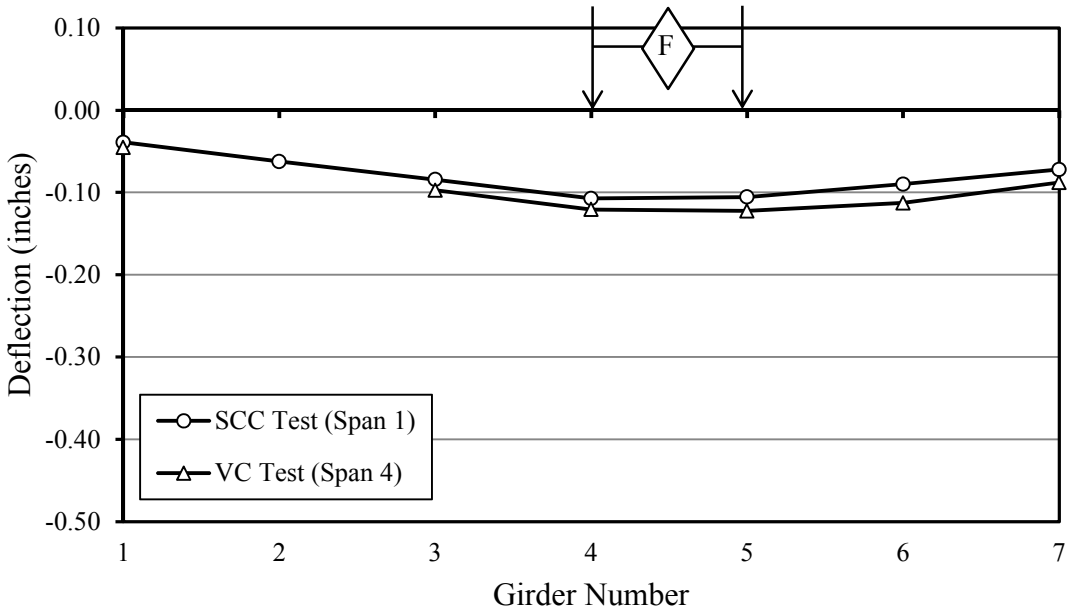

Figure A-12. *Deflection results from load-truck position F on spans with BT-54 girders.*

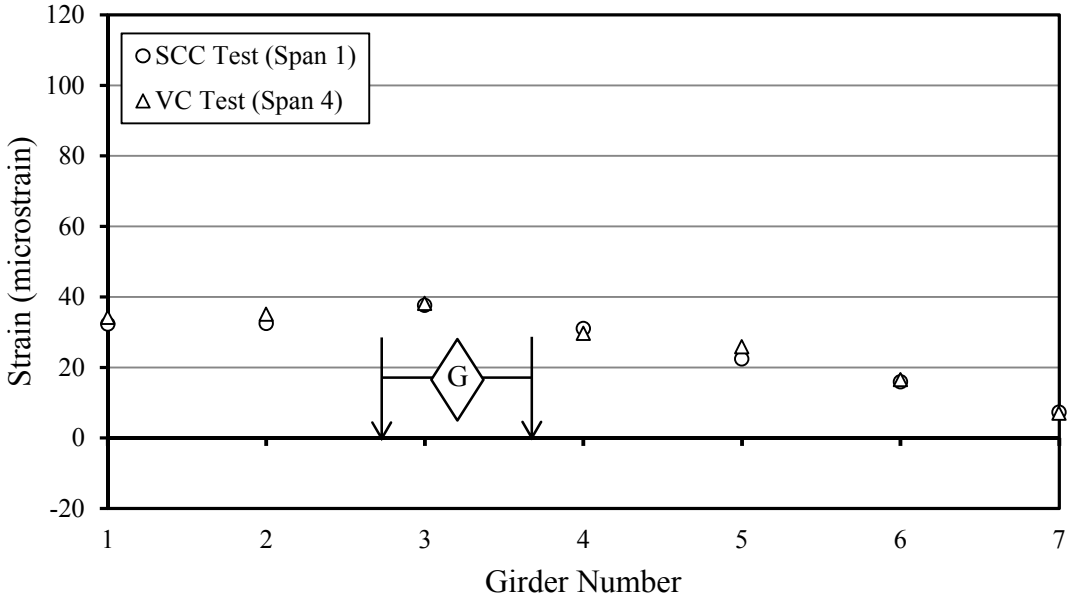

Figure A-13. *Strain results from load-truck-position G on spans with BT-54 girders.*

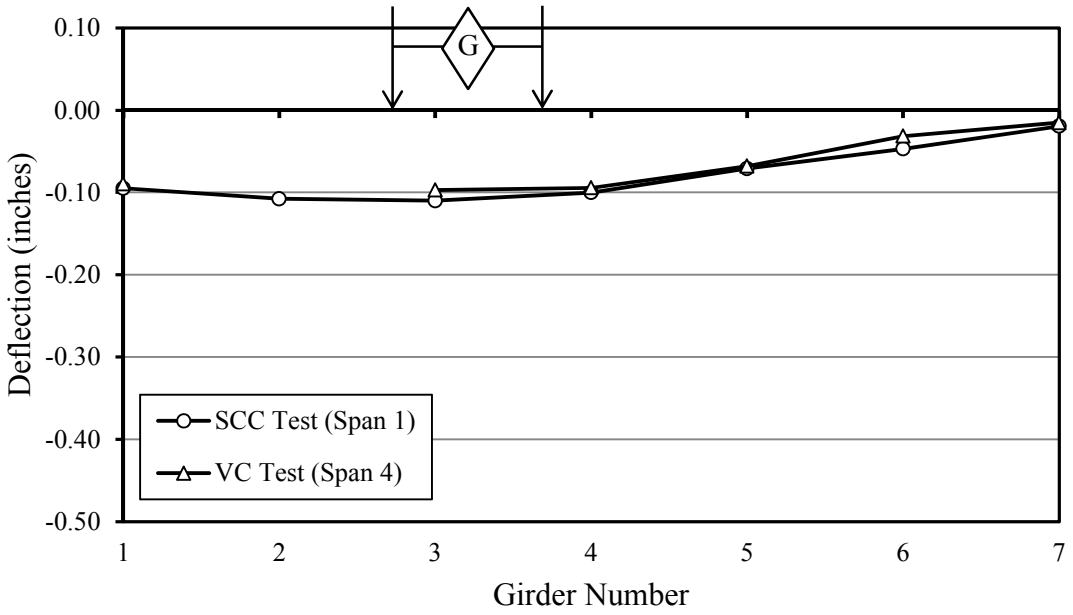

Figure A-14. *Deflection results from load-truck position G on spans with BT-54 girders.*

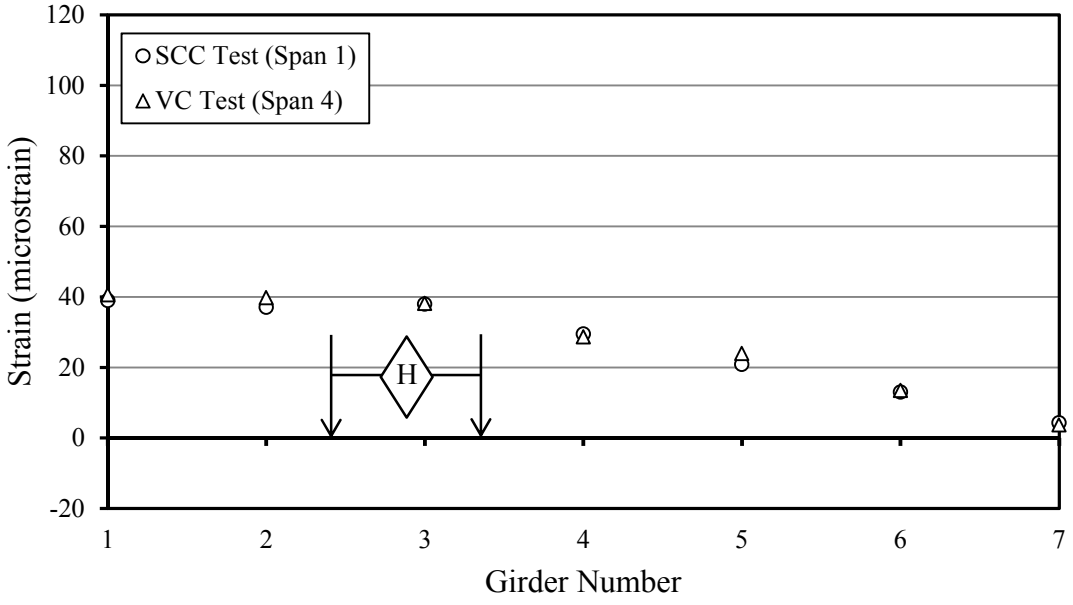

Figure A-15. *Strain results from load-truck-position H on spans with BT-54 girders.*

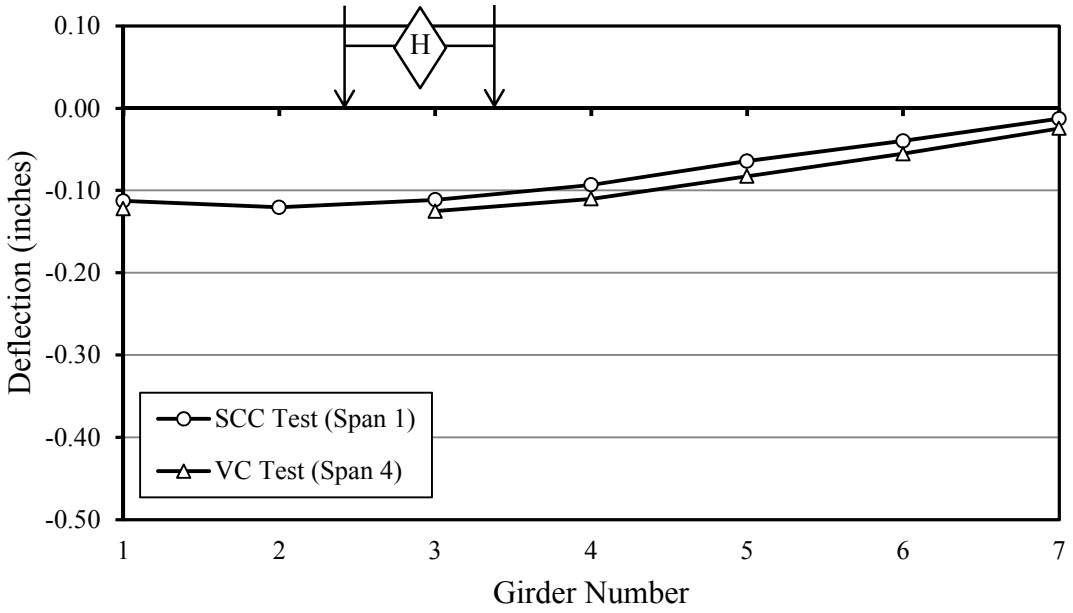

Figure A-16. *Deflection results from load-truck position H on spans with BT-54 girders.*

Table A-2. *Load-test results for spans 2 and 3 of the bridge over Hillabee Creek.*

	S2 G1		**S2 G2**		**S2 G3**		**S2 G4**		**S2 G5**		**S2 G6**		**S2 G7**	
Load Truck Position	SCC													
	Defl.	Strain	Defl.	Strain	Defl.	Strain	Defl.	Strain	Defl.	Strain	Defl.	Strain	Defl.	Strain
	in.	με	in.	με	in.	με	in.	με	in.	με	in.	με	in.	με
A	0.05	-11	0.01	0	-0.05	11	-0.09	20	-0.15	35	-0.21	50	-0.27	69
B	0.03	-8	-0.02	1	-0.06	10	-0.10	21	-0.16	34	-0.22	49	-0.27	66
C	0.02	-7	-0.03	3	-0.07	11	-0.10	21	-0.16	34	-0.21	49	-0.27	63
D	-0.05	11	-0.07	16	-0.10	22	-0.12	28	-0.14	32	-0.15	34	-0.15	31
E	-0.05	12	-0.07	18	-0.10	23	-0.12	28	-0.14	31	-0.14	34	-0.15	31
F	-0.06	15	-0.07	19	-0.11	24	-0.12	29	-0.13	30	-0.13	31	-0.13	27
G	-0.16	37	-0.15	36	-0.14	32	-0.12	25	-0.10	22	-0.07	16	-0.05	10
H	-0.18	41	-0.17	38	-0.15	32	-0.12	25	-0.09	19	-0.07	13	-0.03	6
	S3 G1		**S3 G2**		**S3 G3**		**S3 G4**		**S3 G5**		**S3 G6**		**S3 G7**	
Load Truck Position	VC													
	Defl.	Strain	Defl.	Strain	Defl.	Strain	Defl.	Strain	Defl.	Strain	Defl.	Strain	Defl.	Strain
	in.	με	in.	με	in.	με	in.	με	in.	με	in.	με	in.	με
A	--	-10	0.00	0	-0.05	10	-0.10	21	-0.15	32	-0.22	49	-0.27	78
B	--	-8	-0.01	1	-0.06	10	-0.10	21	-0.15	30	-0.21	47	-0.27	75
C	--	-5	0.00	2	-0.05	10	-0.09	21	-0.14	31	-0.20	47	-0.25	71
D	--	11	-0.07	17	-0.10	24	-0.11	32	-0.15	25	-0.14	33	-0.10	37
E	--	12	-0.08	18	-0.11	25	-0.12	31	-0.16	34	-0.15	35	-0.18	33
F	--	15	-0.09	20	-0.11	27	-0.12	29	-0.13	29	-0.13	28	-0.14	31
G	--	35	-0.15	37	-0.14	39	-0.13	28	-0.10	20	-0.08	14	-0.05	10
H	--	41	-0.17	42	-0.15	39	-0.13	28	-0.09	19	-0.06	12	-0.04	6

. *-- denotes missing data due to equipment malfunction.*

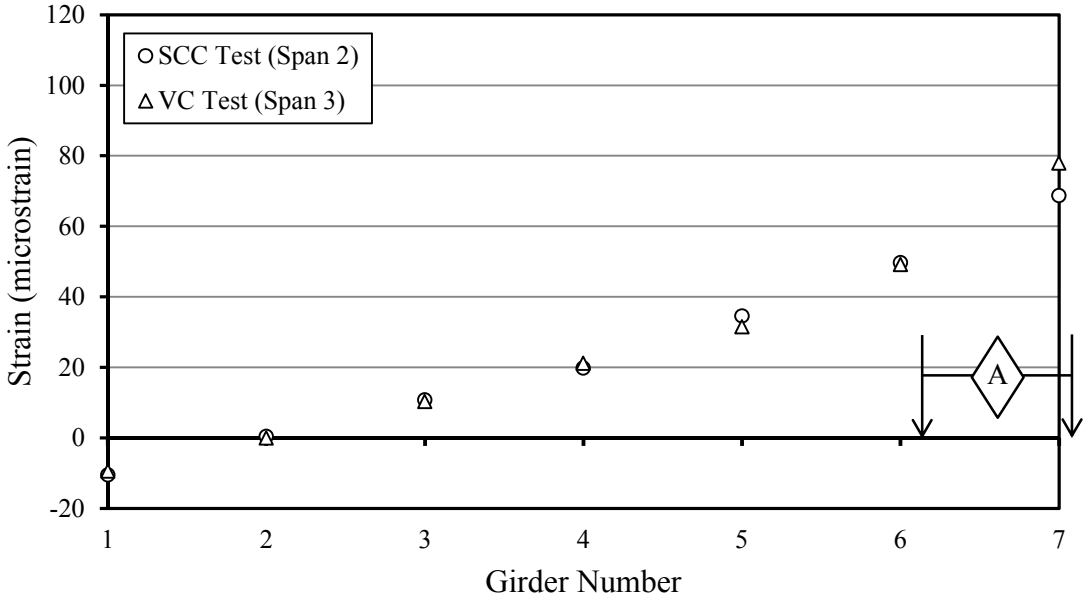

Figure A-17. *Strain results from load-truck-position A on spans with BT-72 girders.*

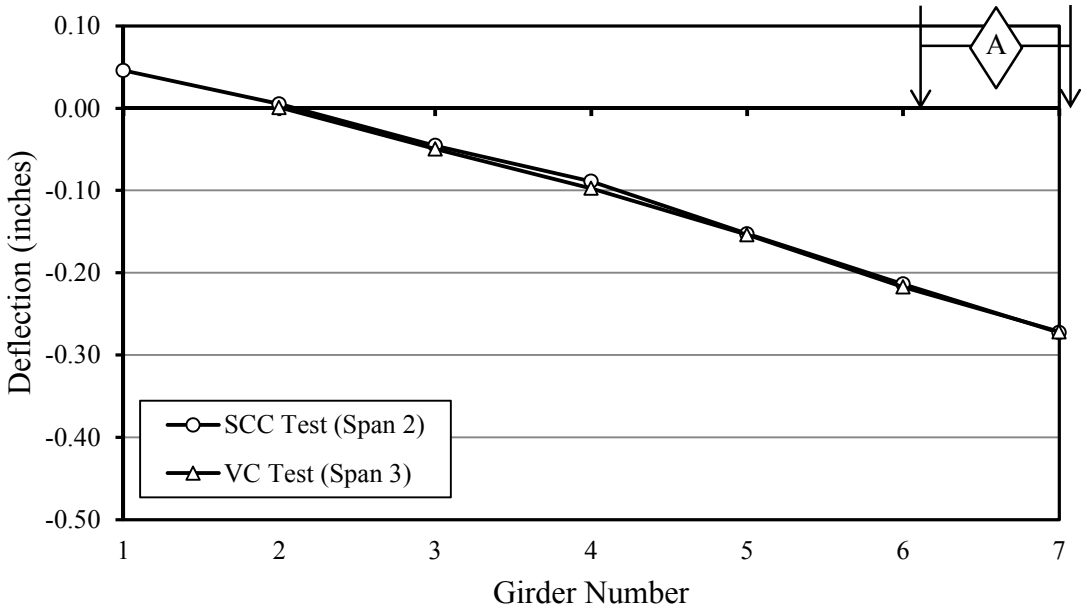

Figure A-18. *Deflection results from load-truck position A on spans with BT-72 girders.*

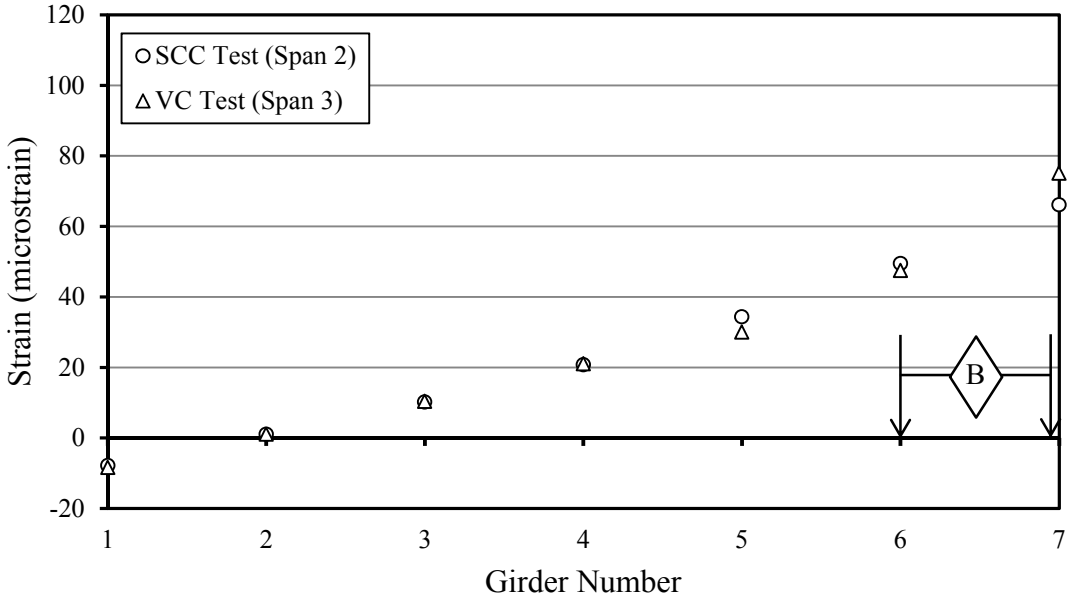

Figure A-19. *Strain results from load-truck-position B on spans with BT-72 girders.*

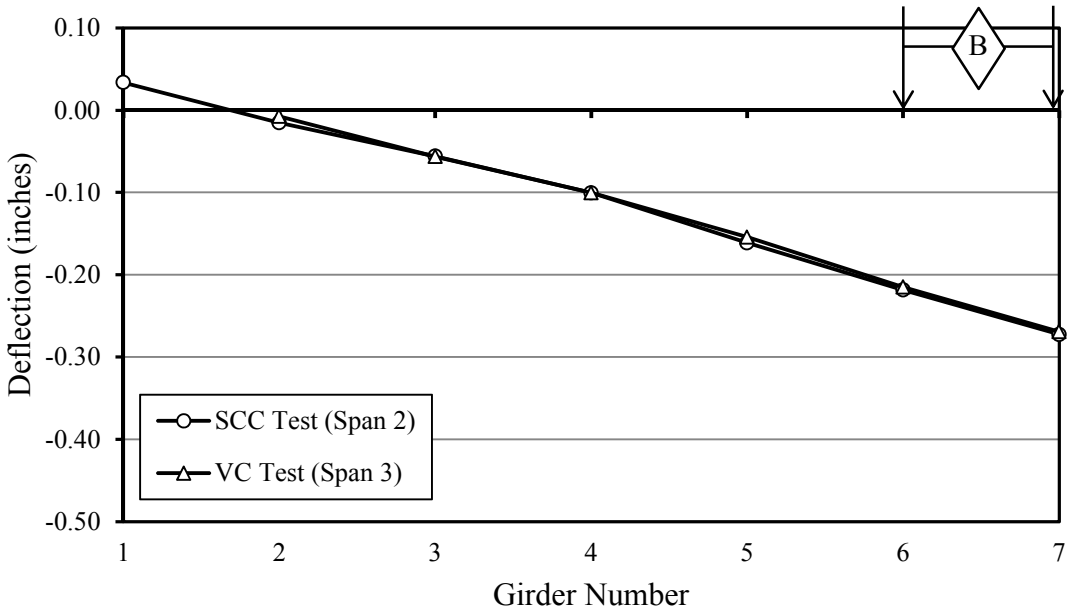

Figure A-20. *Deflection results from load-truck position B on spans with BT-72 girders.*

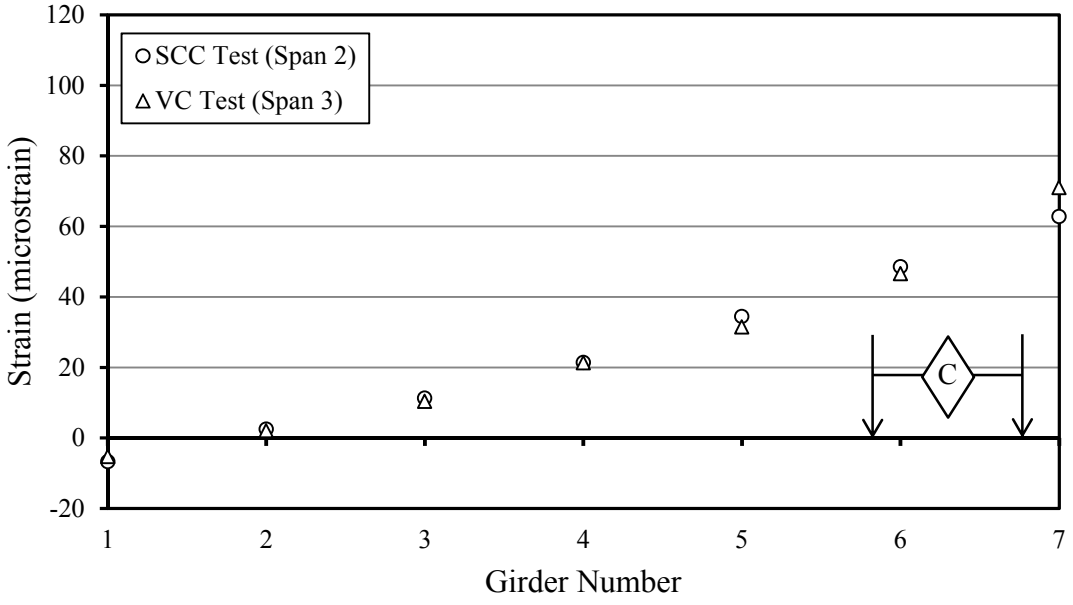

Figure A-21. *Strain results from load-truck-position C on spans with BT-72 girders.*

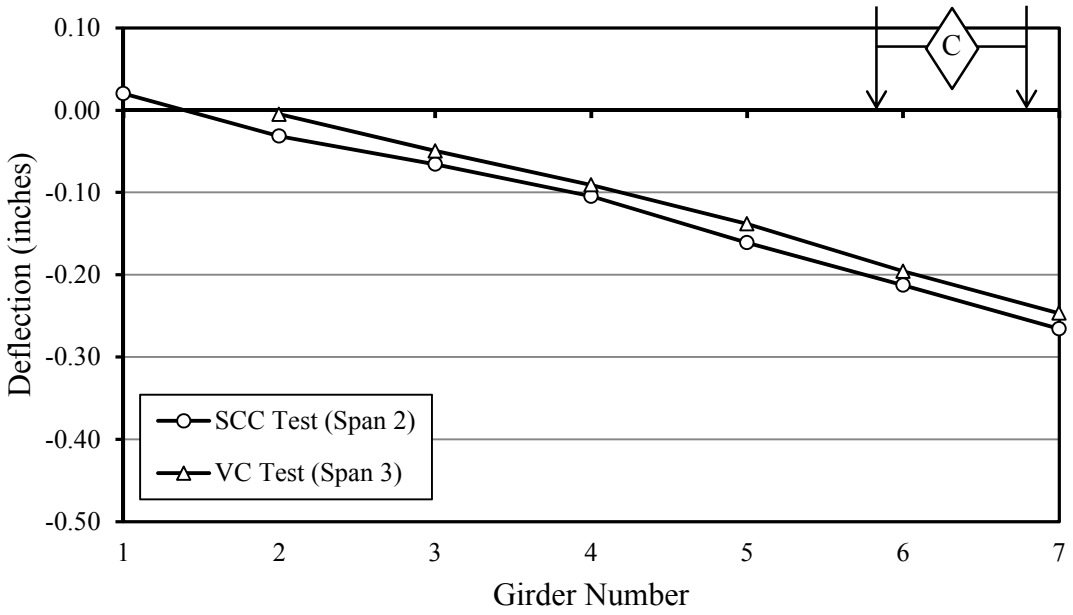

Figure A-22. *Deflection results from load-truck position C on spans with BT-72 girders.*

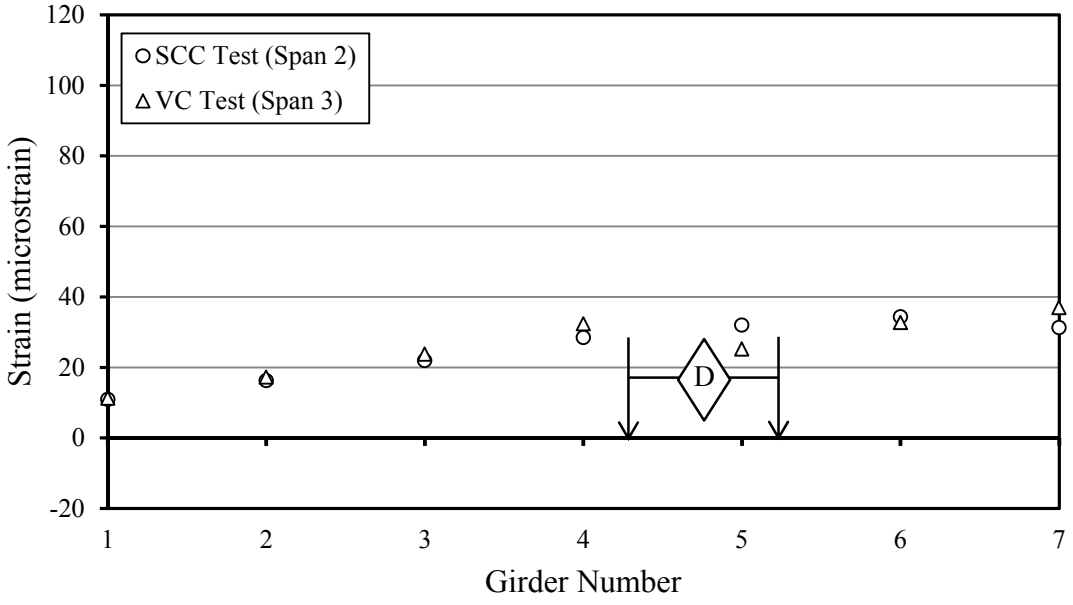

Figure A-23. *Strain results from load-truck-position D on spans with BT-72 girders.*

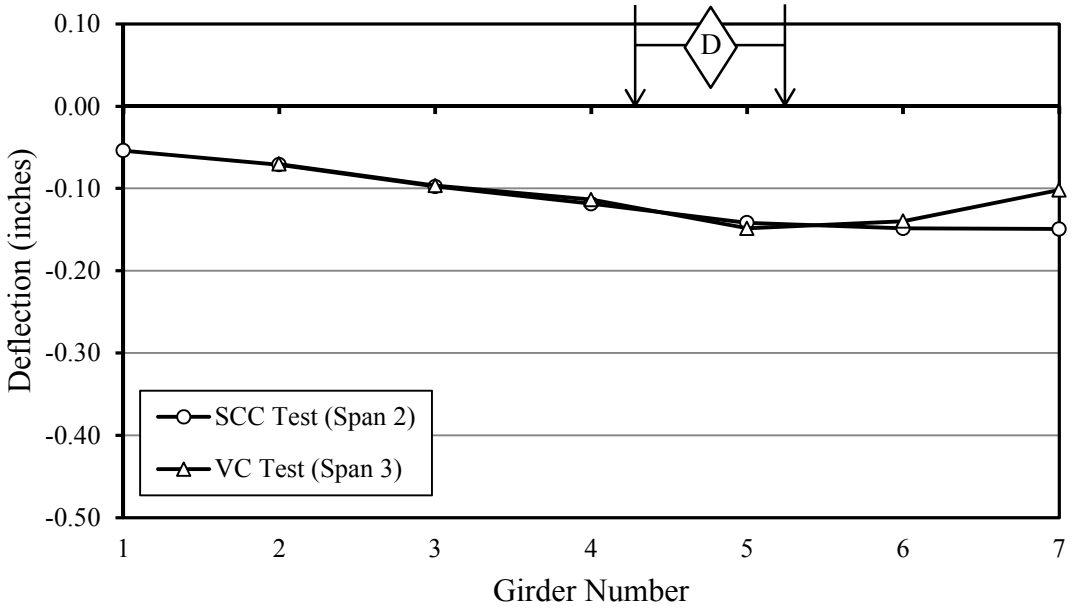

Figure A-24. *Deflection results from load-truck position D on spans with BT-72 girders.*

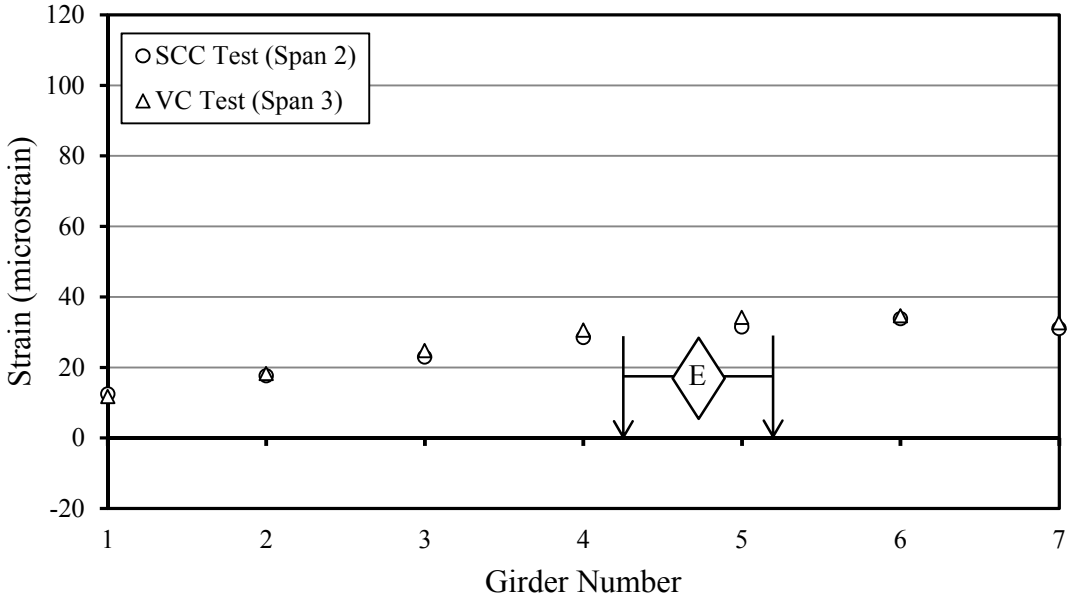

Figure A-25. *Strain results from load-truck-position E on spans with BT-72 girders.*

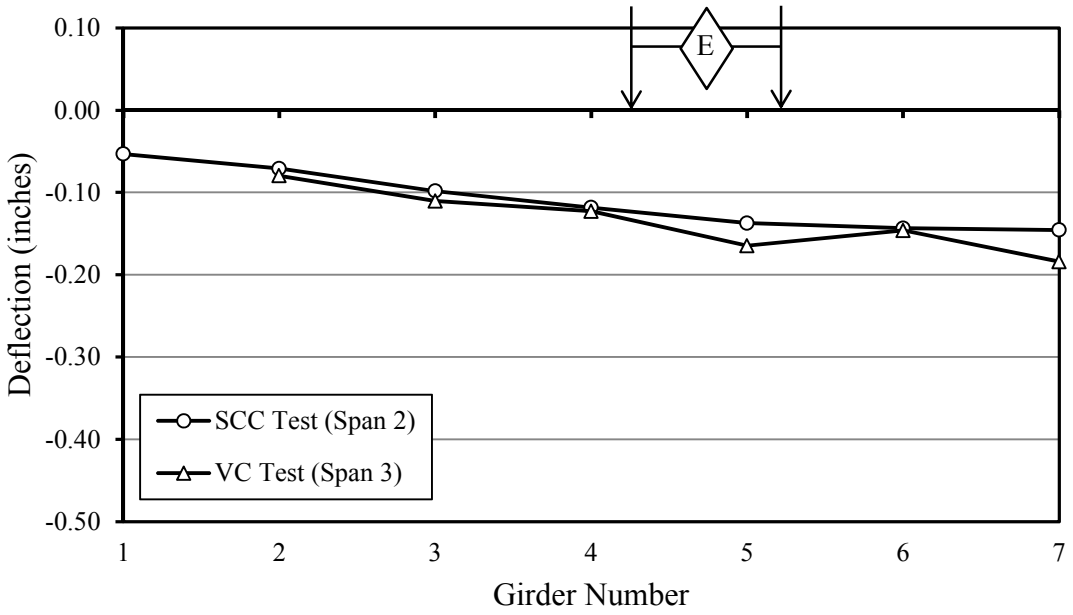

Figure A-26. *Deflection results from load-truck position E on spans with BT-72 girders.*

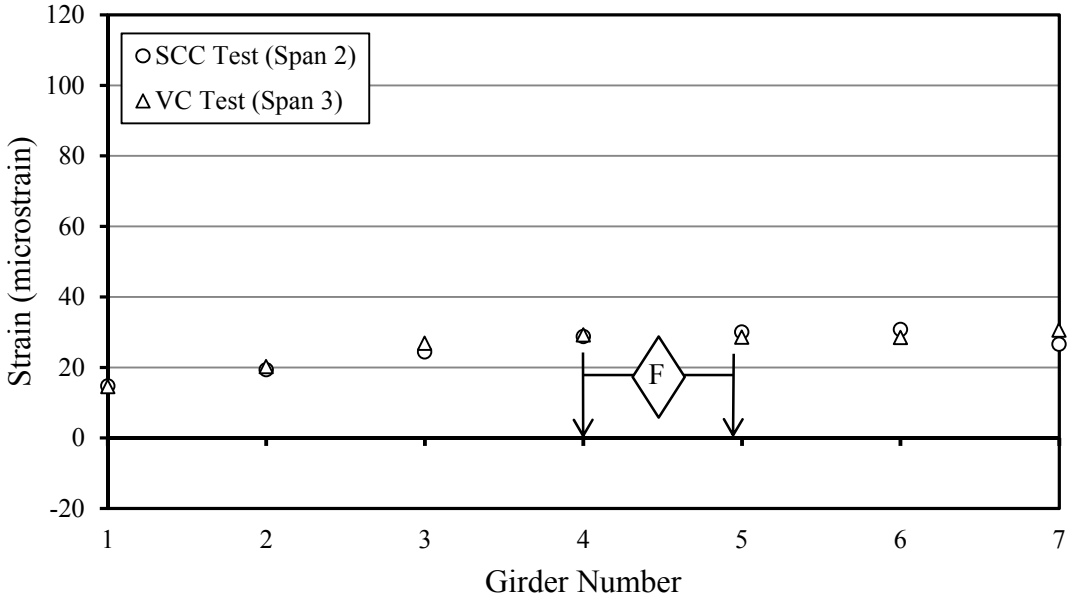

Figure A-27. *Strain results from load-truck-position F on spans with BT-72 girders.*

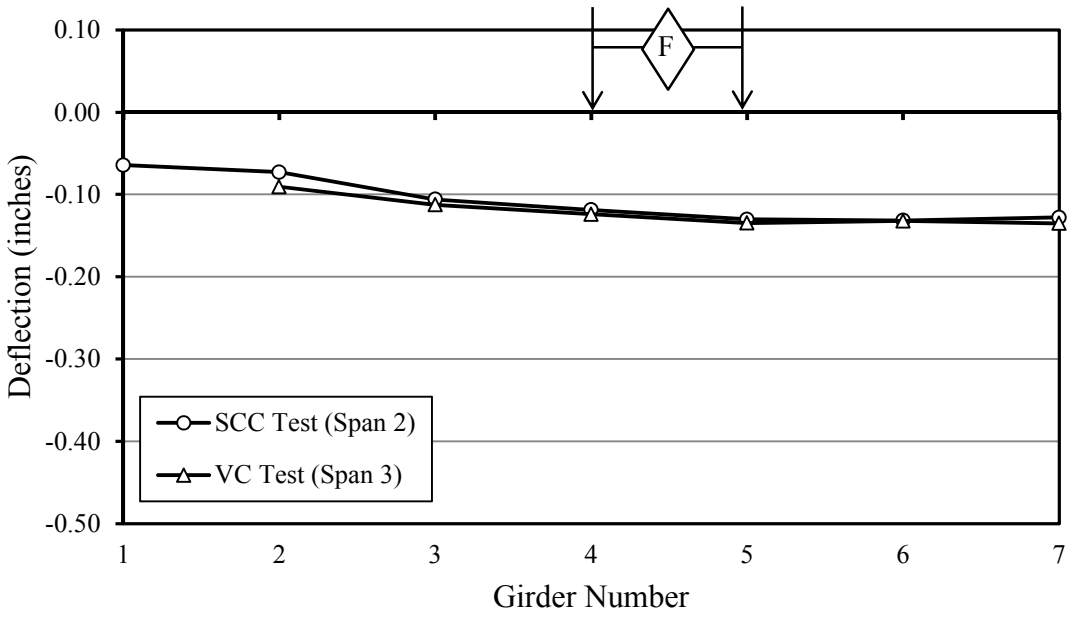

Figure A-28. *Deflection results from load-truck position F on spans with BT-72 girders.*

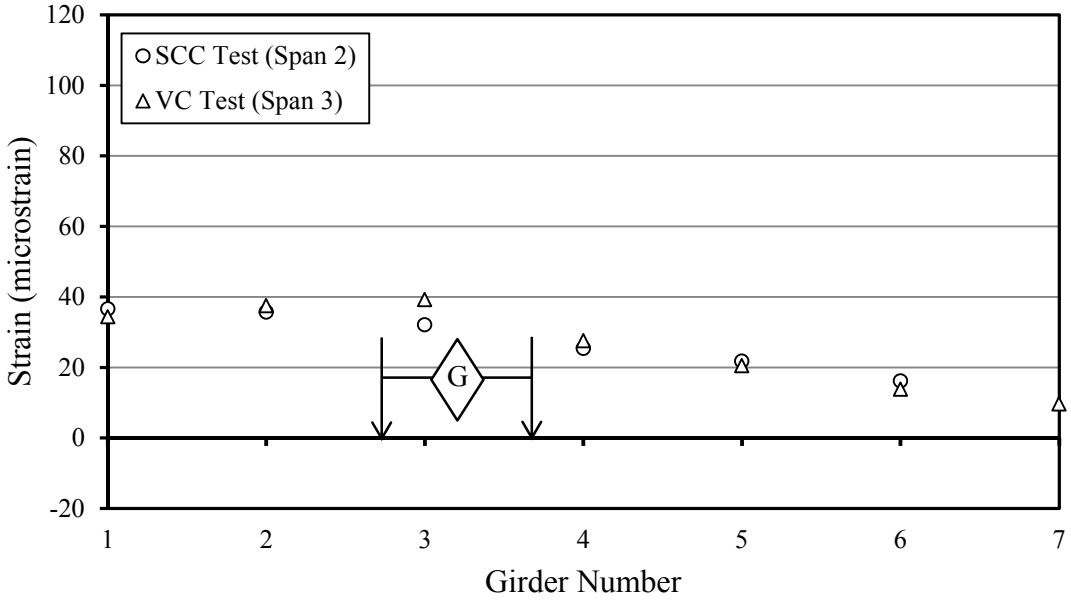

Figure A-29. *Strain results from load-truck-position G on spans with BT-72 girders.*

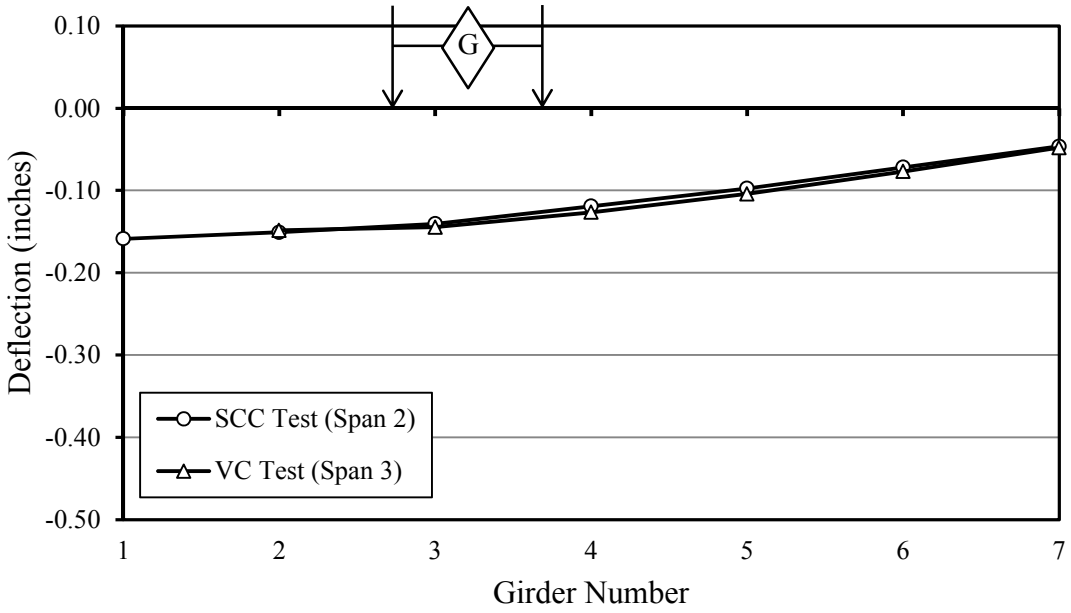

Figure A-30. *Deflection results from load-truck position G on spans with BT-72 girders.*

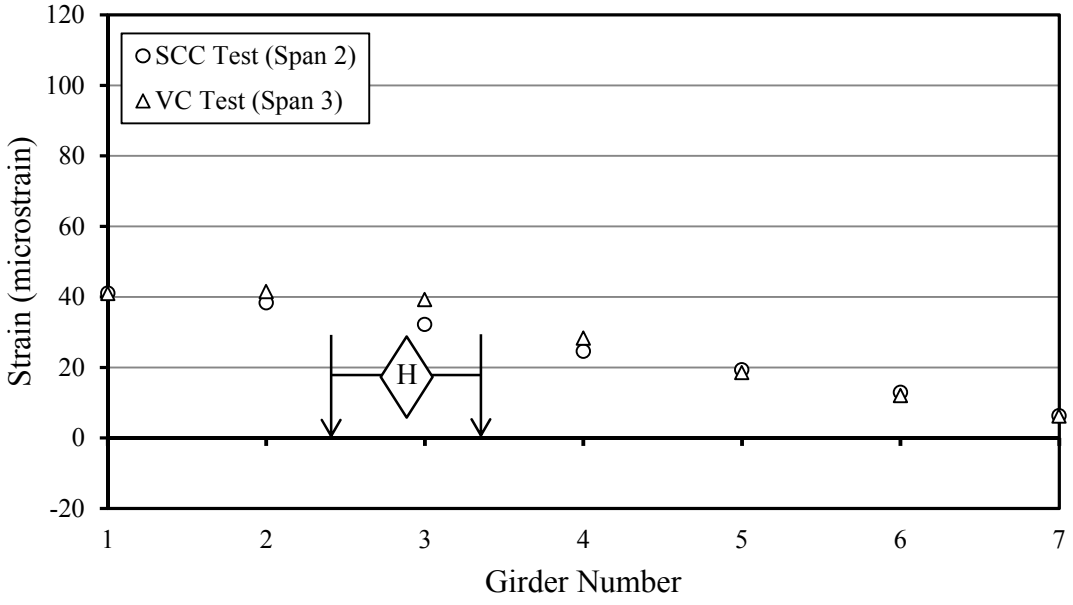

Figure A-31. *Strain results from load-truck-position H on spans with BT-72 girders.*

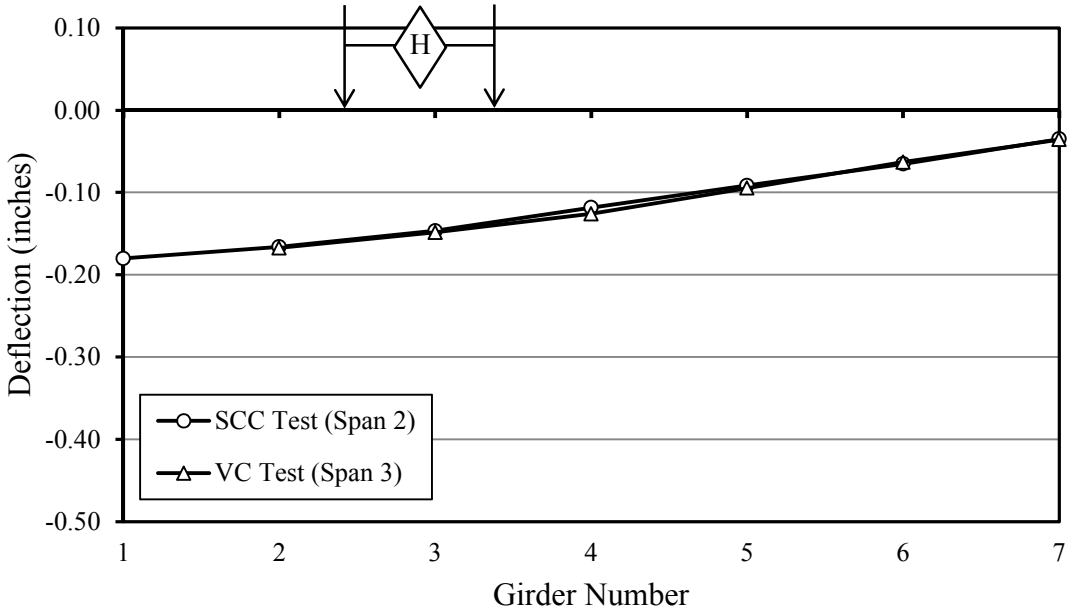

Figure A-32. *Deflection results from load-truck position H on spans with BT-72 girders.*

Appendix B:

Second Load Test Results - Strains and Deflections – May 21-22, 2013

Table B-1. *Load-test results for spans 1 and 4 of the bridge over Hillabee Creek.*

	S1 G1		**S1 G2**		**S1 G3**		**S1 G4**		**S1 G5**		**S1 G6**		**S1 G7**	
Load Truck Position	SCC													
	Defl.	Strain	Defl.	Strain	Defl.	Strain	Defl.	Strain	Defl.	Strain	Defl.	Strain	Defl.	Strain
	in.	με	in.	με	in.	με	in.	με	in.	με	in.	με	in.	με
A	0.03	-7	0.00	0	-0.02	7	-0.05	17	-0.10	36	--	53	-0.21	79
A & E	-0.01	0	-0.05	17	-0.10	32	-0.16	49	-0.21	69	--	84	-0.29	110
E	-0.03	7	-0.05	16	-0.07	24	-0.10	35	-0.10	35	--	33	-0.09	31
E & H	-0.13	46	-0.17	53	-0.17	60	-0.19	67	-0.17	55	--	45	-0.10	35
H	-0.10	39	-0.11	38	-0.10	36	-0.09	30	-0.06	20	--	13	-0.01	4
A + E	0.00	0	-0.05	16	-0.09	31	-0.15	53	-0.20	71	--	86	-0.30	110
E + H	-0.13	46	-0.16	54	-0.17	60	-0.20	64	-0.16	55	--	46	-0.10	35
	S4 G1		**S4 G2**		**S4 G3**		**S4 G4**		**S4 G5**		**S4 G6**		**S4 G7**	
Load Truck Position	VC													
	Defl.	Strain	Defl.	Strain	Defl.	Strain	Defl.	Strain	Defl.	Strain	Defl.	Strain	Defl.	Strain
	in.	με	in.	με	in.	με	in.	με	in.	με	in.	με	in.	με
A	0.02	-7	0.00	2	-0.02	9	-0.07	20	-0.10	37	--	56	-0.20	77
A & E	0.00	0	--	18	-0.10	32	-0.15	52	-0.21	71	--	84	-0.30	112
E	-0.02	8	--	17	-0.07	24	-0.10	36	-0.11	38	--	34	-0.09	33
E & H	-0.13	46	--	54	-0.19	61	-0.20	65	-0.18	61	--	46	-0.11	37
H	-0.10	39	--	38	-0.12	38	-0.10	28	-0.07	24	--	13	-0.02	4
A + E	0.00	1	--	19	-0.09	32	-0.17	56	-0.21	73	--	87	-0.29	109
E + H	-0.12	47	--	54	-0.19	62	-0.19	65	-0.18	60	--	46	-0.11	37

"--"denotes missing data due to equipment malfunction. "&"denotes two trucks on the bridge. "+"denotes superposition. Note: data for two trucks on bridge and superposition was not adjusted according to chapter six, section three.

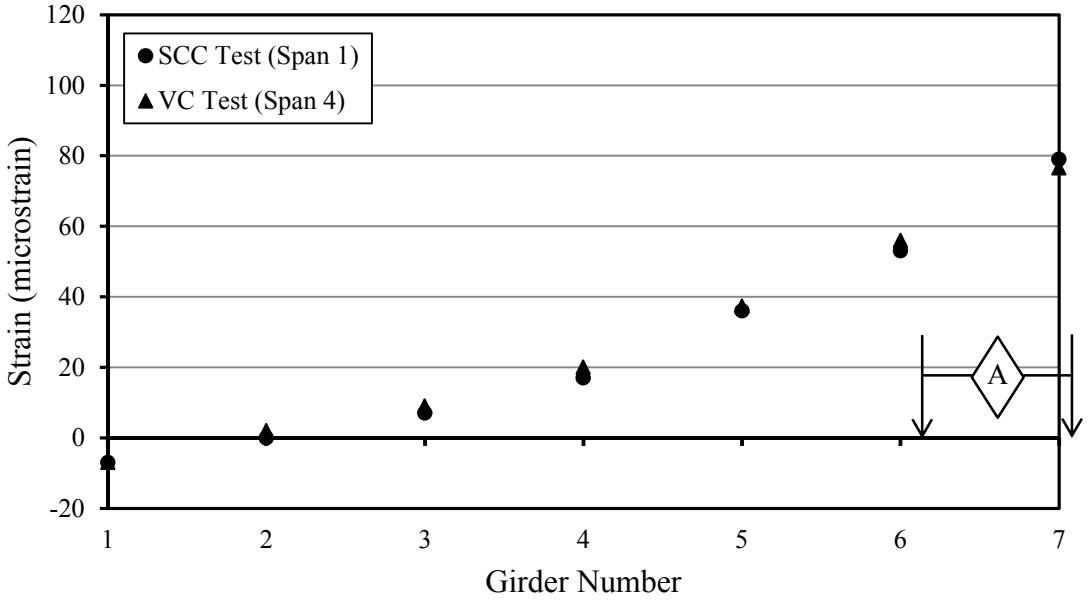

Figure B-1. *Strain results from load-truck-position A on spans with BT-54 girders.*

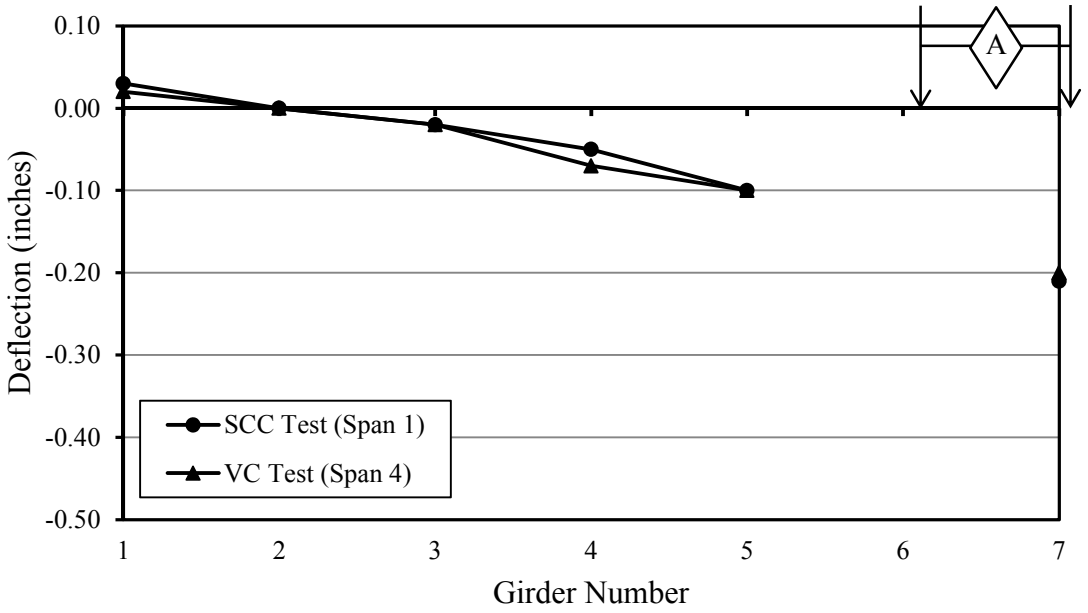

Figure B-2. *Deflection results from load-truck position A on spans with BT-54 girders.*

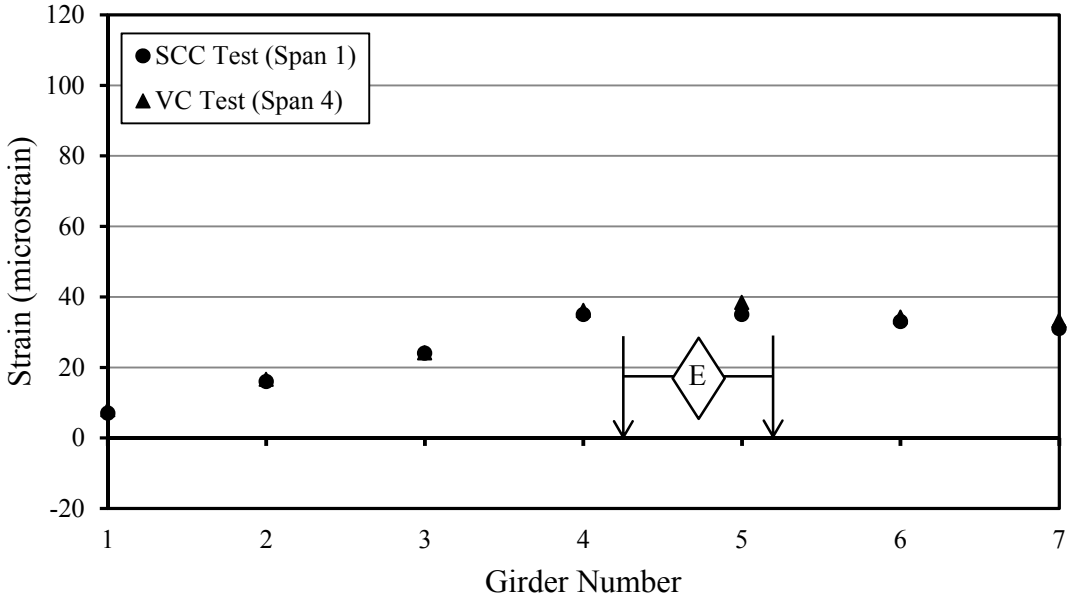

Figure B-3. *Strain results from load-truck-position E on spans with BT-54 girders.*

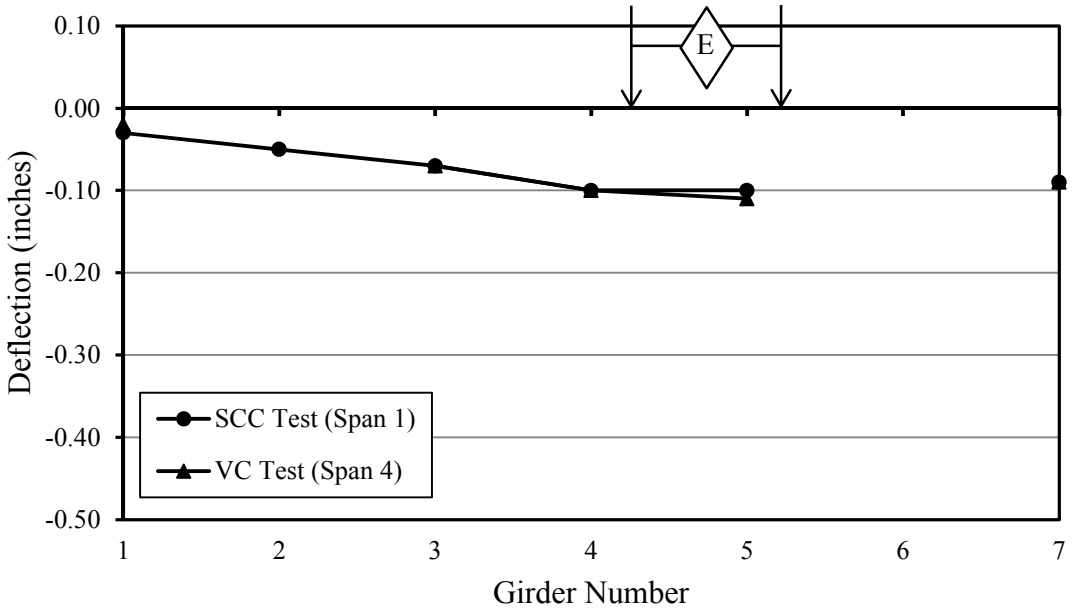

Figure B-4. *Deflection results from load-truck position E on spans with BT-54 girders.*

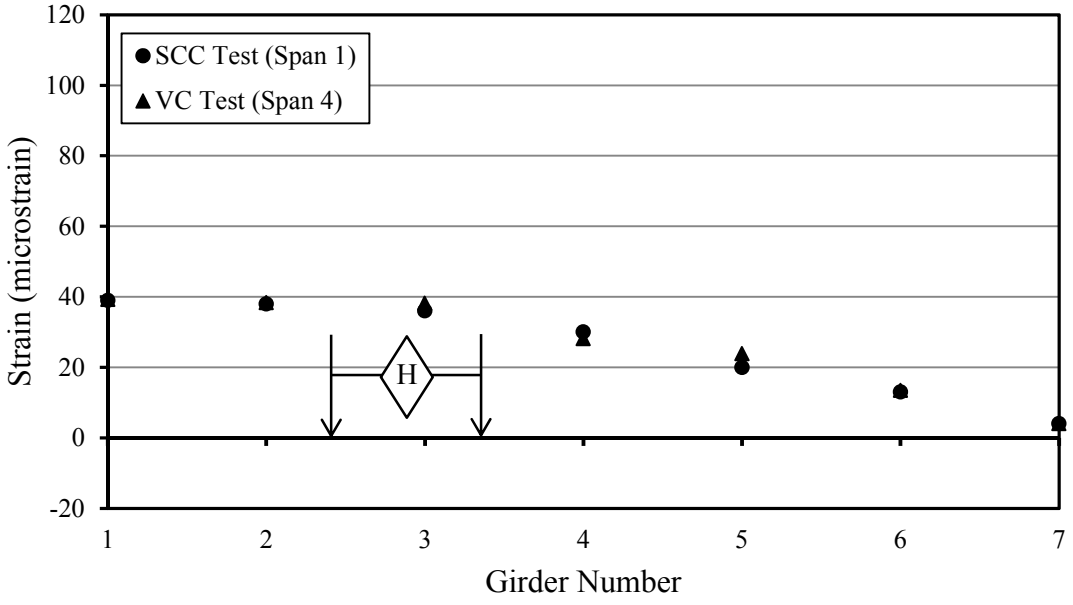

Figure B-5. *Strain results from load-truck-position H on spans with BT-54 girders.*

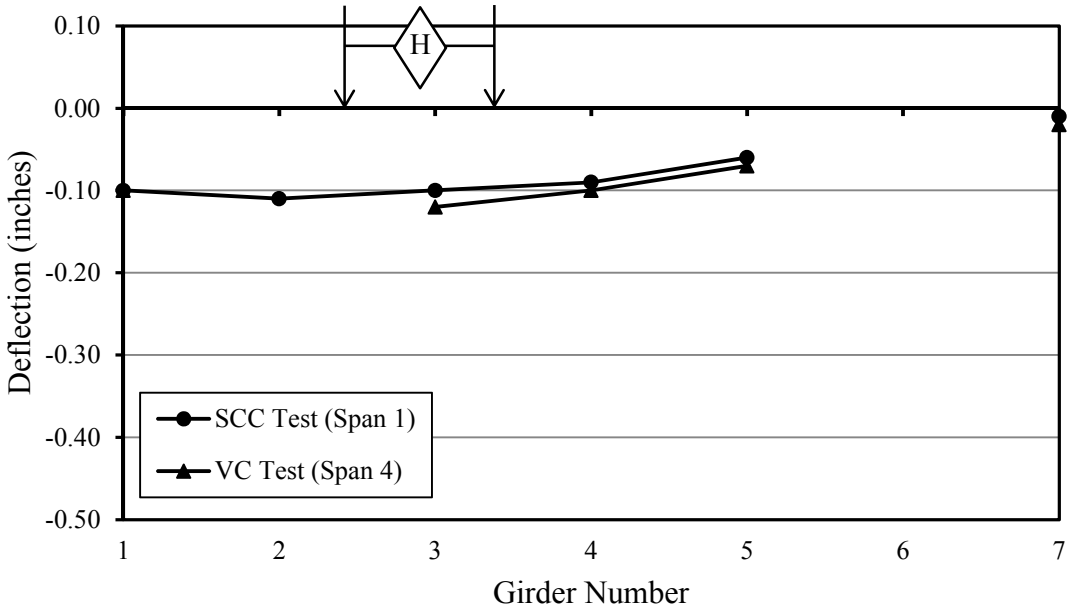

Figure B-6. *Deflection results from load-truck position H on spans with BT-54 girders.*

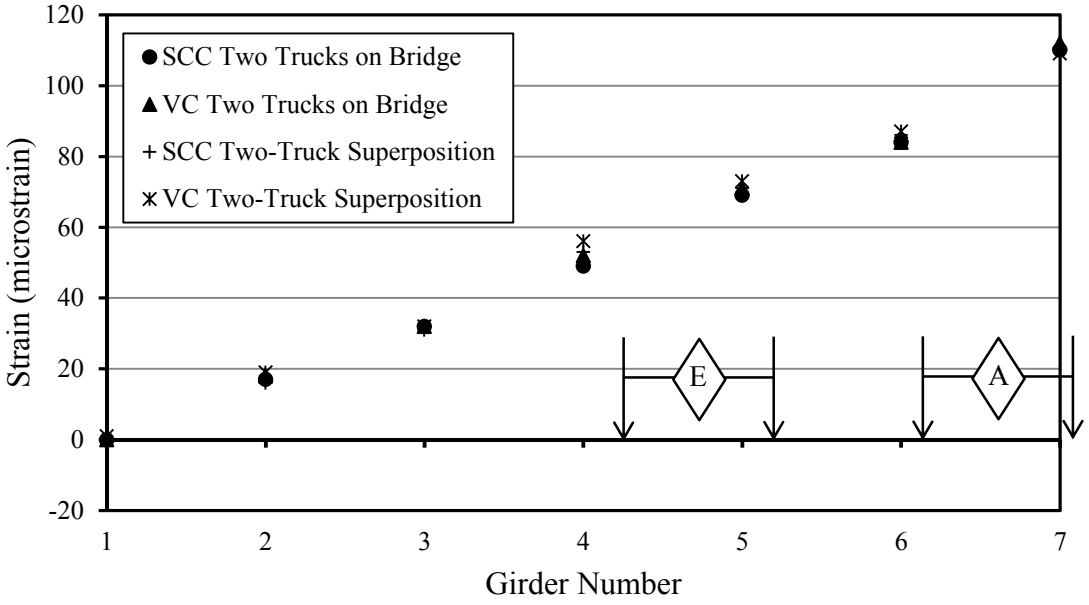

Figure B-7. *Strain results from two trucks on bridge and load positions A + E superimposed on spans 1 and 4.*

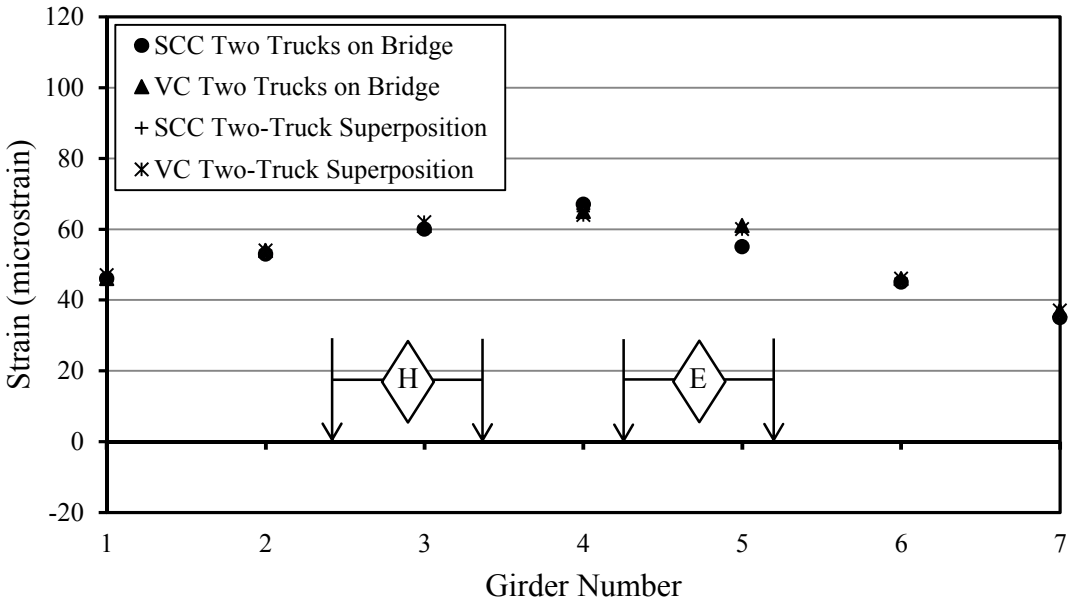

Figure B-8. *Strain results from two trucks on bridge and load positions E + H superimposed on spans 1 and 4.*

Table B-2. *Load-test results for spans 2 and 3 of the bridge over Hillabee Creek.*

	S2 G1		**S2 G2**		**S2 G3**		**S2 G4**		**S2 G5**		**S2 G6**		**S2 G7**	
Load Truck Position	SCC													
	Defl.	Strain	Defl.	Strain	Defl.	Strain	Defl.	Strain	Defl.	Strain	Defl.	Strain	Defl.	Strain
	in.	με	in.	με	in.	με	in.	με	in.	με	in.	με	in.	με
A	0.05	-9	0.00	0	-0.05	9	-0.09	22	-0.15	35	-0.20	50	-0.28	70
A & E*	-0.02	2	-0.08	16	-0.15	30	-0.21	47	-0.29	66	-0.33	84	-0.42	102
E	-0.06	12	-0.07	17	-0.10	22	-0.12	29	-0.13	32	-0.13	35	-0.14	32
E & H*	-0.25	53	-0.22	55	-0.24	53	-0.23	52	-0.22	51	-0.19	47	-0.17	38
H	-0.19	41	-0.15	39	-0.14	31	-0.11	24	-0.09	19	-0.06	13	-0.03	6
A + E*	-0.01	3	-0.07	17	-0.15	31	-0.21	51	-0.28	67	-0.33	85	-0.42	102
E + H*	-0.25	53	-0.22	56	-0.24	53	-0.23	53	-0.22	51	-0.19	48	-0.17	38
	S3 G1		**S3 G2**		**S3 G3**		**S3 G4**		**S3 G5**		**S3 G6**		**S3 G7**	
Load Truck Position	VC													
	Defl.	Strain	Defl.	Strain	Defl.	Strain	Defl.	Strain	Defl.	Strain	Defl.	Strain	Defl.	Strain
	in.	με	in.	με	in.	με	in.	με	in.	με	in.	με	in.	με
A	--	-11	--	--	--	8	--	22	--	33	--	48	--	80
A & E*	--	2	--	--	--	29	--	49	--	61	--	80	--	108
E	--	12	--	--	--	21	--	30	--	28	--	32	--	38
E & H*	--	46	--	--	--	53	--	55	--	46	--	45	--	41
H	--	40	--	--	--	34	--	29	--	19	--	13	--	9
A + E*	--	1	--	--	--	28	--	50	--	61	--	79	--	108
E + H*	--	48	--	--	--	53	--	57	--	47	--	45	--	43

*Note: "--"denotes missing data due to equipment malfunction. "&"denotes two trucks on the bridge. "+"denotes superposition. * notes that data for two trucks on bridge and superposition was not adjusted according to chapter six, section three. Deflections were not measured for span three due to high water conditions in Hillabee Creek.*

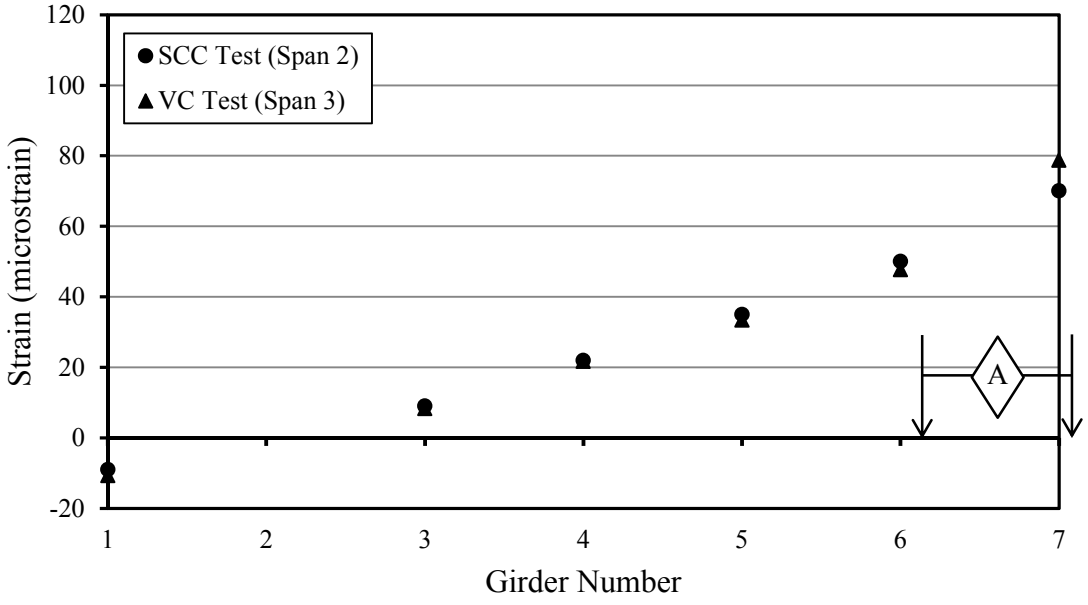

Figure B-9. *Strain results from load-truck-position A on spans with BT-72 girders.*

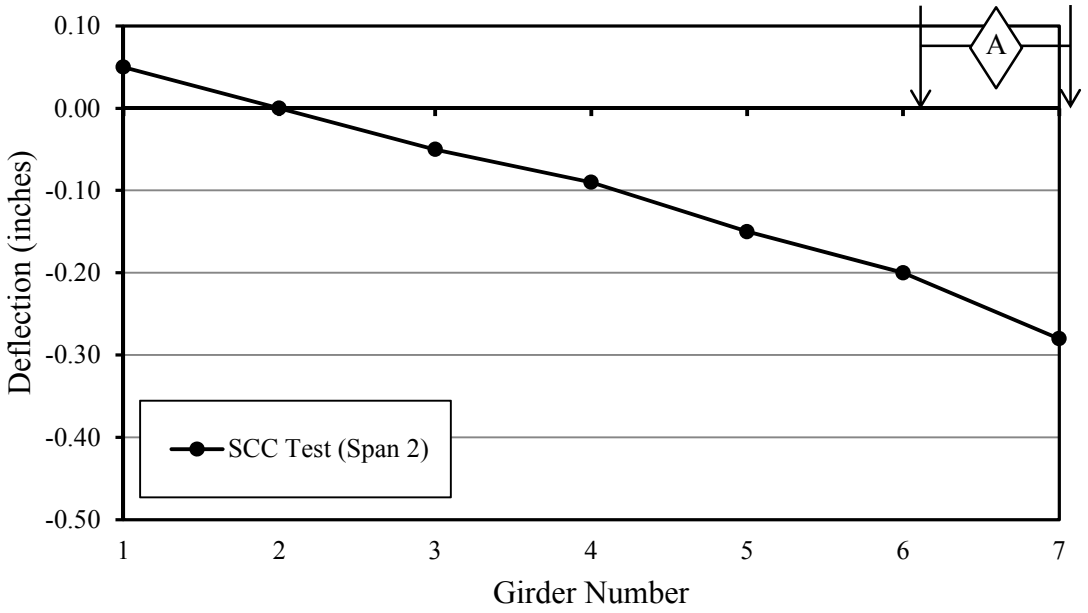

Figure B-10. *Deflection results from load-truck position A on spans with BT-72 girders. Note: VC (Span 3) deflections not measured due to high water conditions in Hillabee Creek.*

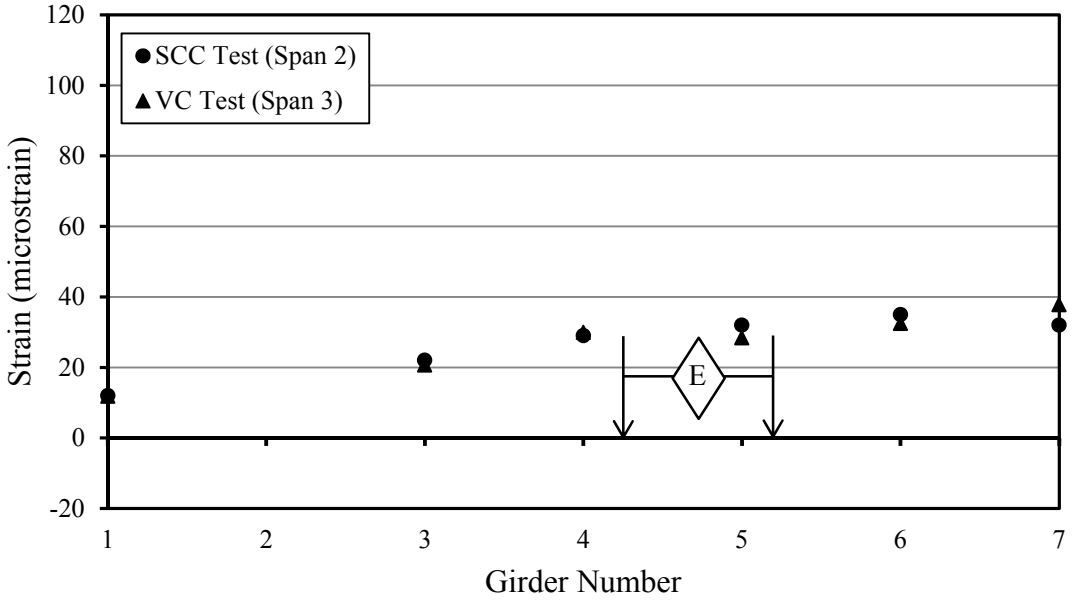

Figure B-11. *Strain results from load-truck-position E on spans with BT-72 girders.*

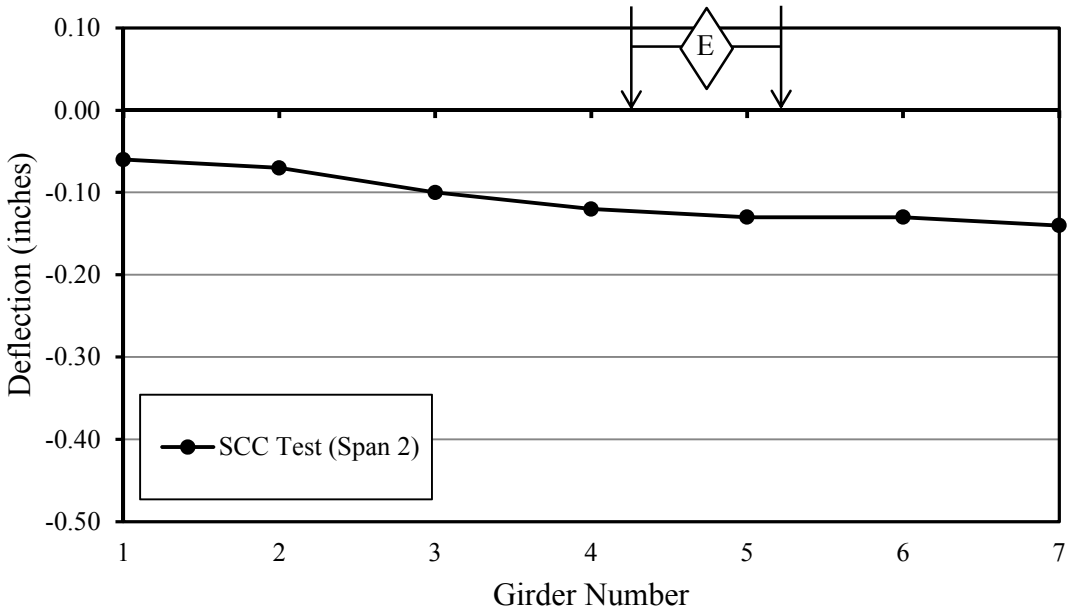

Figure B-12. *Deflection results from load-truck position E on spans with BT-72 girders. Note: VC (Span 3) deflections not measured due to high water conditions in Hillabee Creek.*

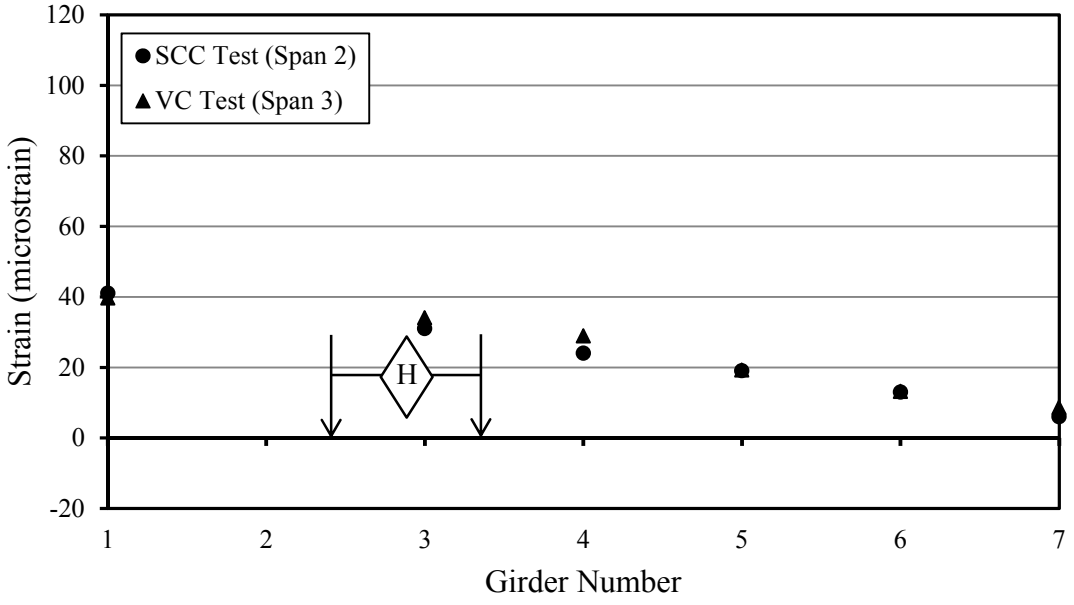

Figure B-13. *Strain results from load-truck-position H on spans with BT-72 girders.*

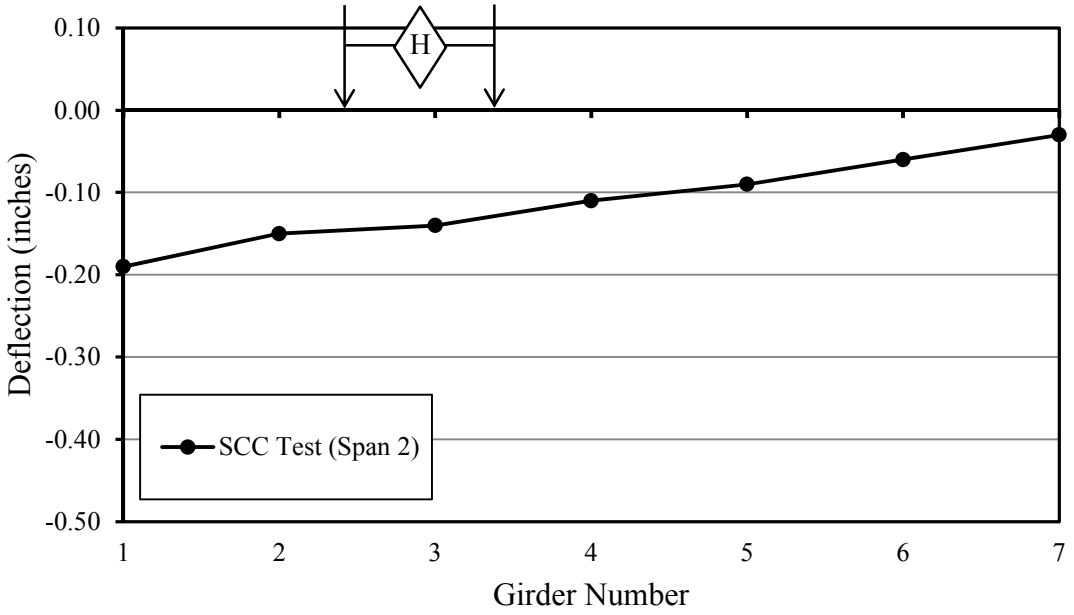

Figure B-14. *Deflection results from load-truck position H on spans with BT-72 girders. Note: VC (Span 3) deflections not measured due to high water conditions in Hillabee Creek.*

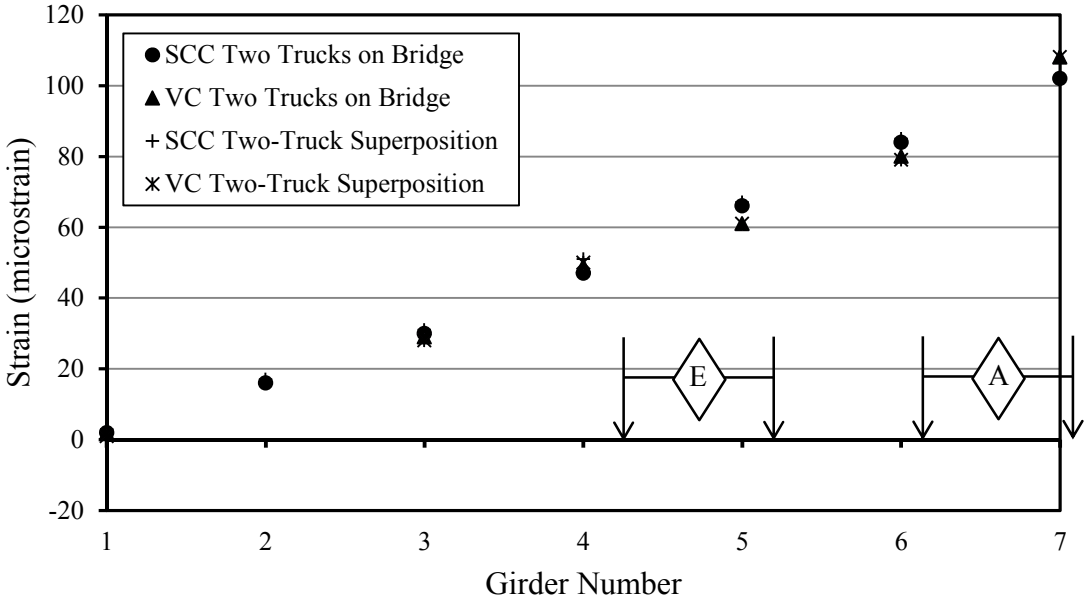

Figure B-15. *Strain results from two trucks on bridge and load positions A + E superimposed on spans 2 and 3.*

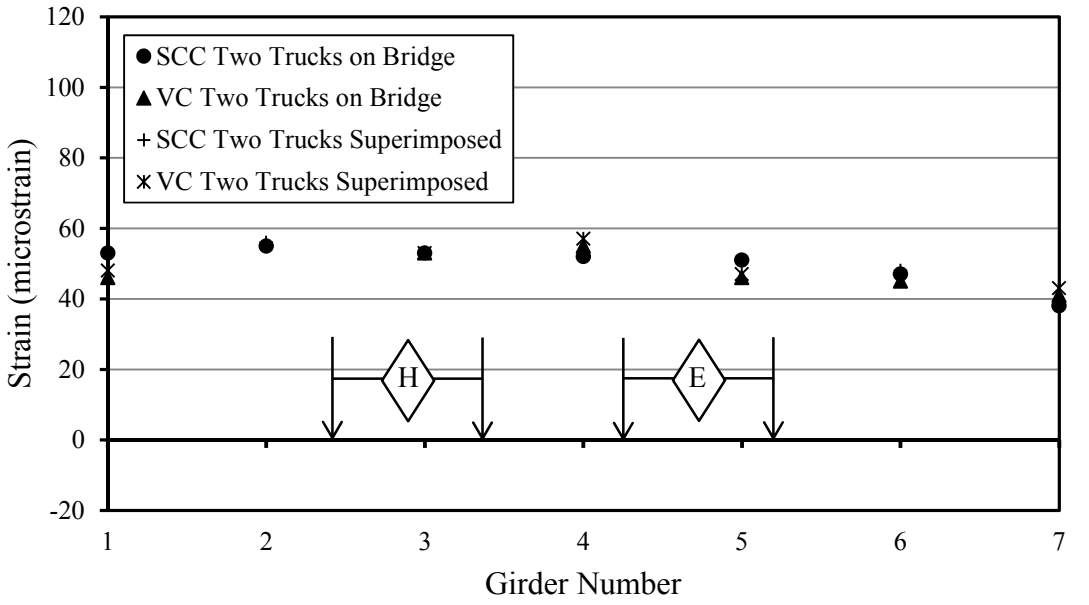

Figure B-16. *Strain results from two trucks on bridge and load positions E + H superimposed on spans 2 and 3.*

Appendix C:

CSiBridge Model with Barriers and Staggered Webwalls Results – Strains and Deflections

Table C-1. *CSiBridge modeler analysis results for spans 1 and 4 of the bridge model with barriers and adjusted web walls.*

	S1 G1		**S1 G2**		**S1 G3**		**S1 G4**		**S1 G5**		**S1 G6**		**S1 G7**	
Load Truck Position	SCC													
	Defl. (in.)	Strain (με)	Defl. (in.)	Strain (με)	Defl. (in.)	Strain (με)	Defl. (in.)	Strain (με)	Defl. (in.)	Strain (με)	Defl. (in.)	Strain (με)	Defl. (in.)	Strain (με)
A	0.02	-8	-0.01	1	-0.04	12	-0.08	25	-0.12	42	-0.18	61	-0.23	84
B	0.02	-7	0.01	2	-0.04	13	-0.08	26	-0.12	43	-0.18	60	-0.22	81
C	0.01	-6	-0.02	4	-0.05	15	-0.08	28	-0.13	43	-0.17	58	-0.21	77
D	-0.04	10	-0.06	21	-0.09	31	-0.12	38	-0.13	45	-0.12	41	-0.11	38
E	-0.04	11	-0.07	22	-0.09	32	-0.12	41	-0.13	45	-0.12	44	-0.11	40
F	-0.05	14	-0.07	25	-0.10	34	-0.12	43	-0.12	44	-0.11	40	-0.09	34
G	-0.11	38	-0.12	42	-0.13	45	-0.12	41	-0.09	33	-0.06	23	-0.04	12
H	-0.13	46	-0.13	47	-0.13	46	-0.11	40	-0.08	30	-0.05	18	-0.03	7
	S4 G1		**S4 G2**		**S4 G3**		**S4 G4**		**S4 G5**		**S4 G6**		**S4 G7**	
Load Truck Position	VC													
	Defl. (in.)	Strain (με)	Defl. (in.)	Strain (με)	Defl. (in.)	Strain (με)	Defl. (in.)	Strain (με)	Defl. (in.)	Strain (με)	Defl. (in.)	Strain (με)	Defl. (in.)	Strain (με)
A	0.01	-4	-0.01	2	-0.03	8	-0.06	19	-0.10	34	-0.15	63	-0.20	80
B	0.01	-4	-0.01	2	-0.03	9	-0.06	20	-0.11	36	-0.15	64	-0.20	77
C	0	-3	-0.02	5	-0.04	11	-0.07	22	-0.11	38	-0.15	62	-0.19	71
D	-0.03	6	-0.05	17	-0.08	28	-0.11	44	-0.12	49	-0.11	39	-0.09	30
E	-0.03	7	-0.06	17	-0.09	28	-0.11	45	-0.12	49	-0.11	38	-0.09	29
F	-0.04	9	-0.06	20	-0.09	32	-0.12	50	-0.12	47	-0.10	34	-0.07	23
G	-0.09	28	-0.11	39	-0.12	50	-0.11	43	-0.08	29	-0.06	18	-0.03	8
H	-0.1	34	-0.12	46	-0.12	50	-0.10	38	-0.07	25	-0.05	14	-0.02	4

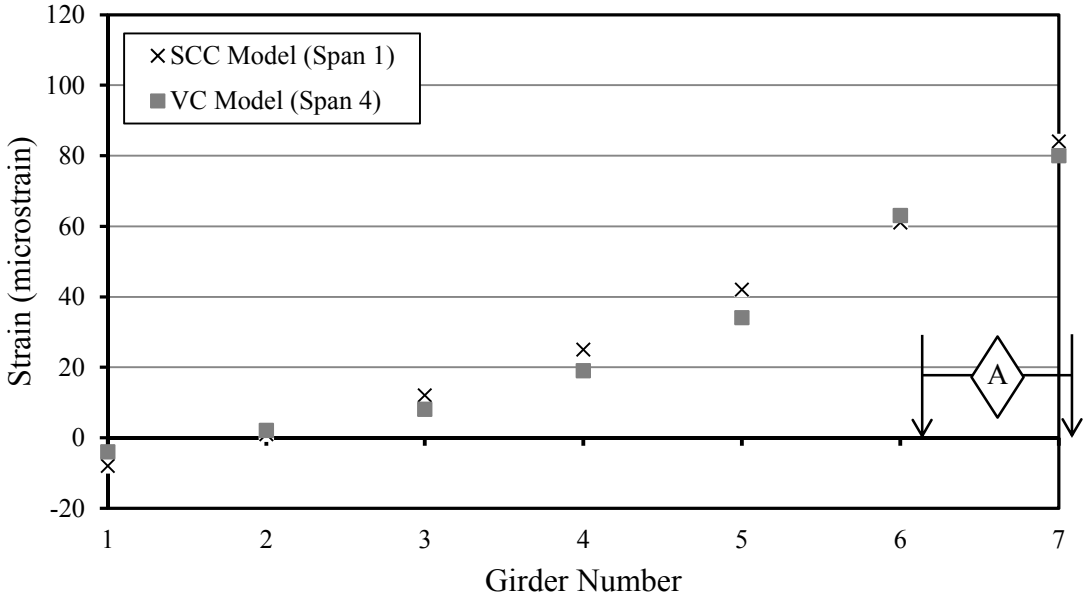

Figure C-1. *Strain results from load-truck-position A on spans with BT-54 girders.*

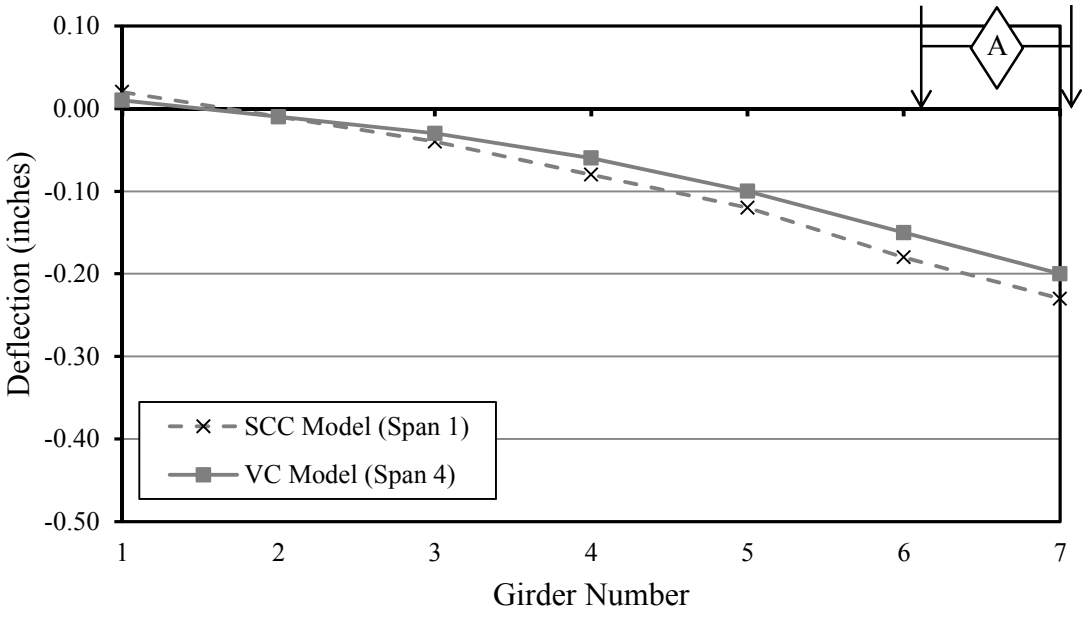

Figure C-2. *Deflection results from load-truck position A on spans with BT-54 girders.*

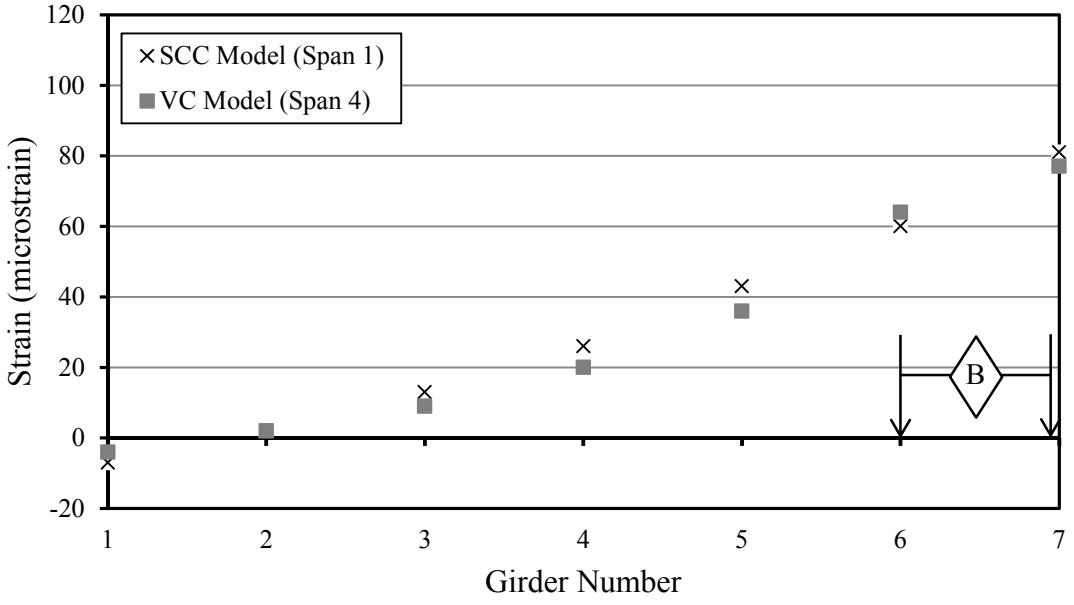

Figure C-3. *Strain results from load-truck-position B on spans with BT-54 girders.*

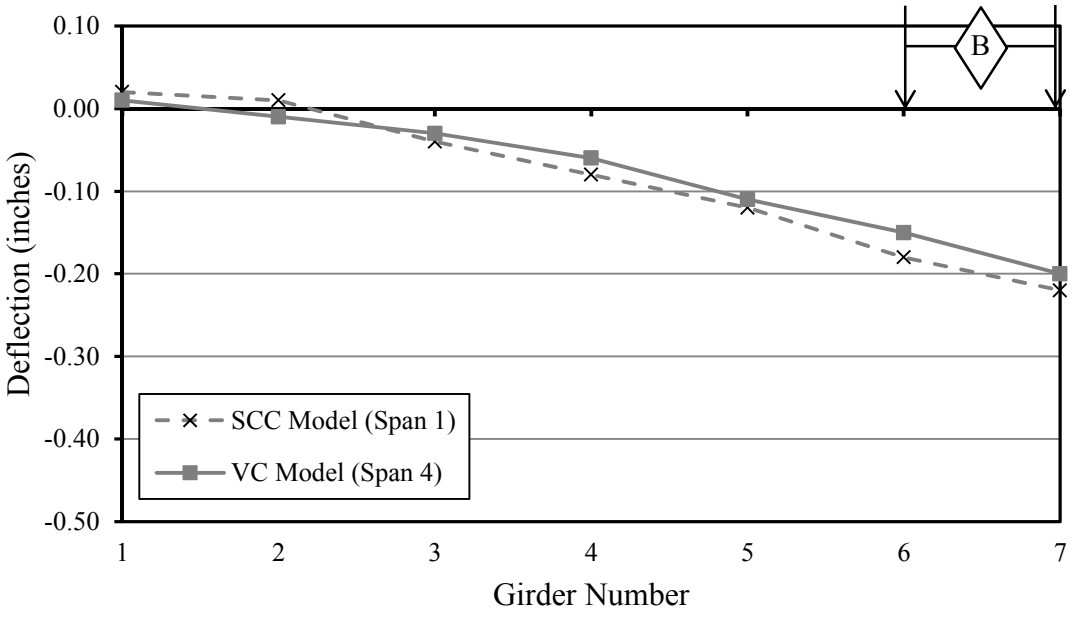

Figure C-4. *Deflection results from load-truck position B on spans with BT-54 girders.*

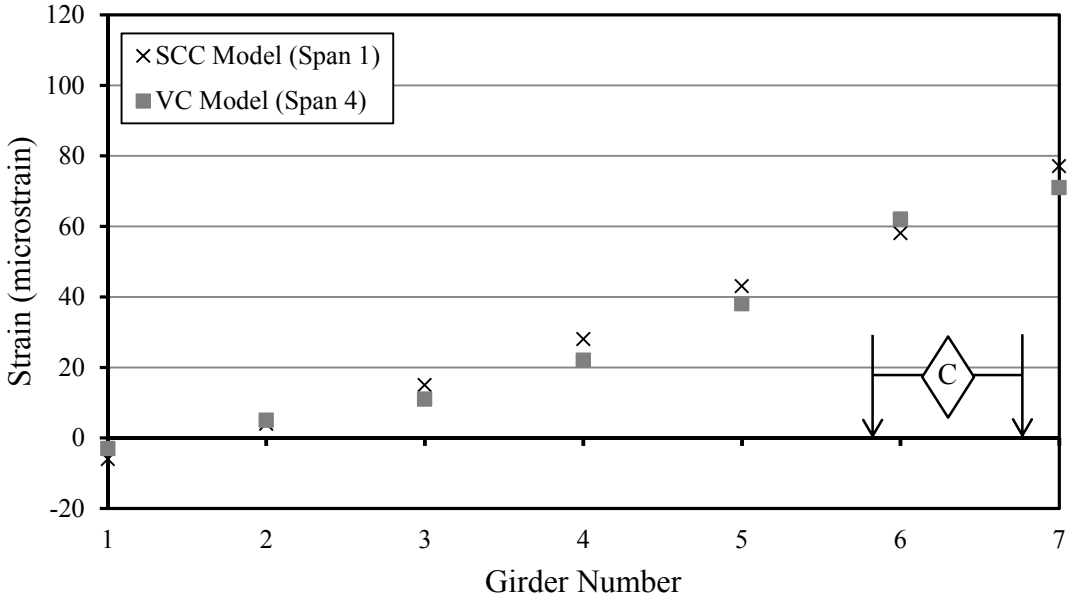

Figure C-5. *Strain results from load-truck-position C on spans with BT-54 girders.*

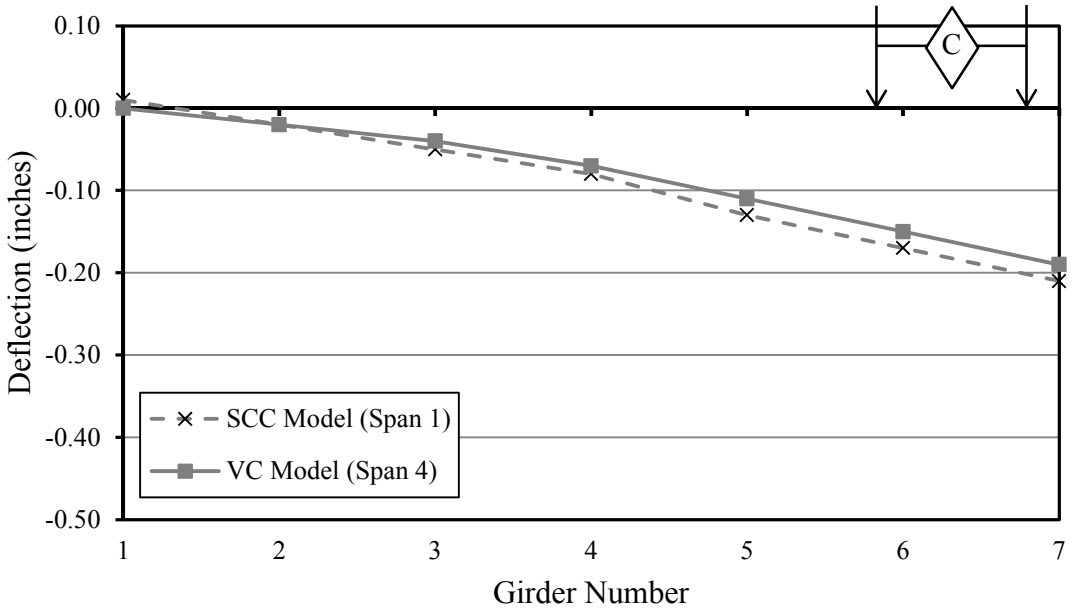

Figure C-6. *Deflection results from load-truck position C on spans with BT-54 girders.*

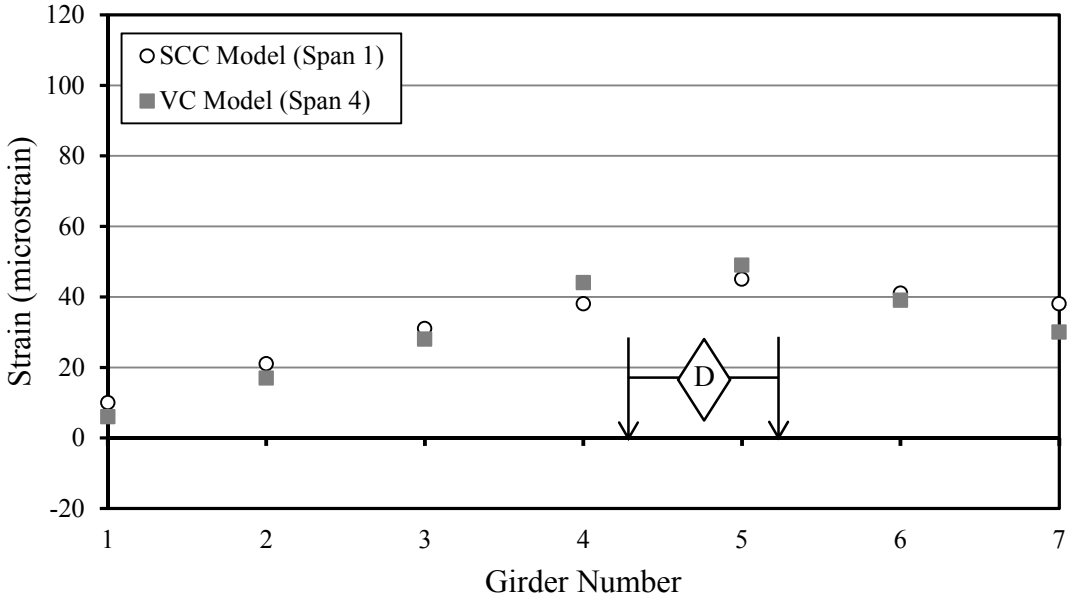

Figure C-7. *Strain results from load-truck-position D on spans with BT-54 girders.*

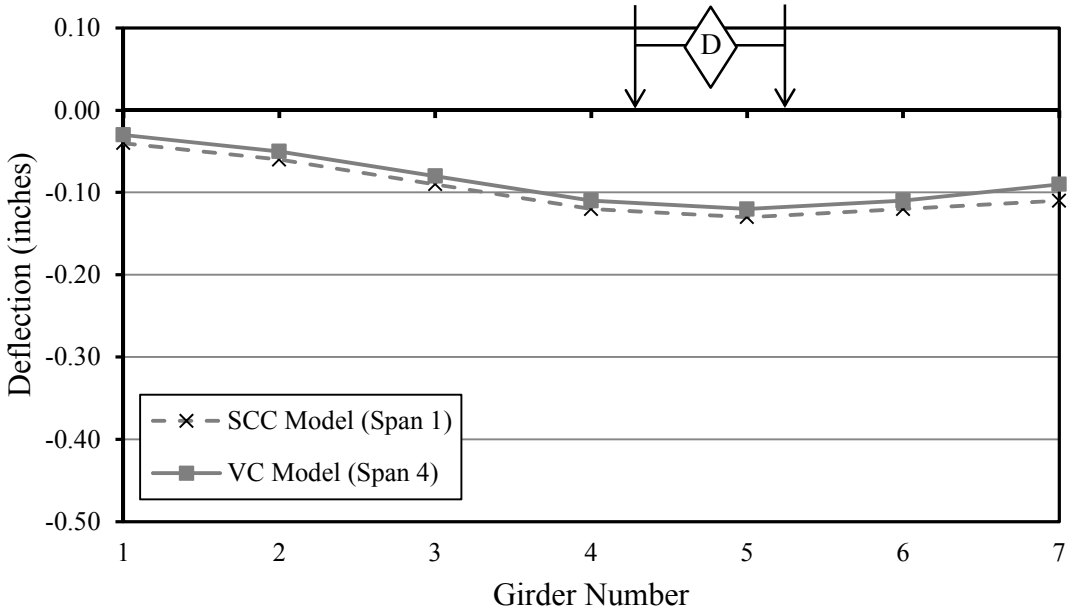

Figure C-8. *Deflection results from load-truck position D on spans with BT-54 girders.*

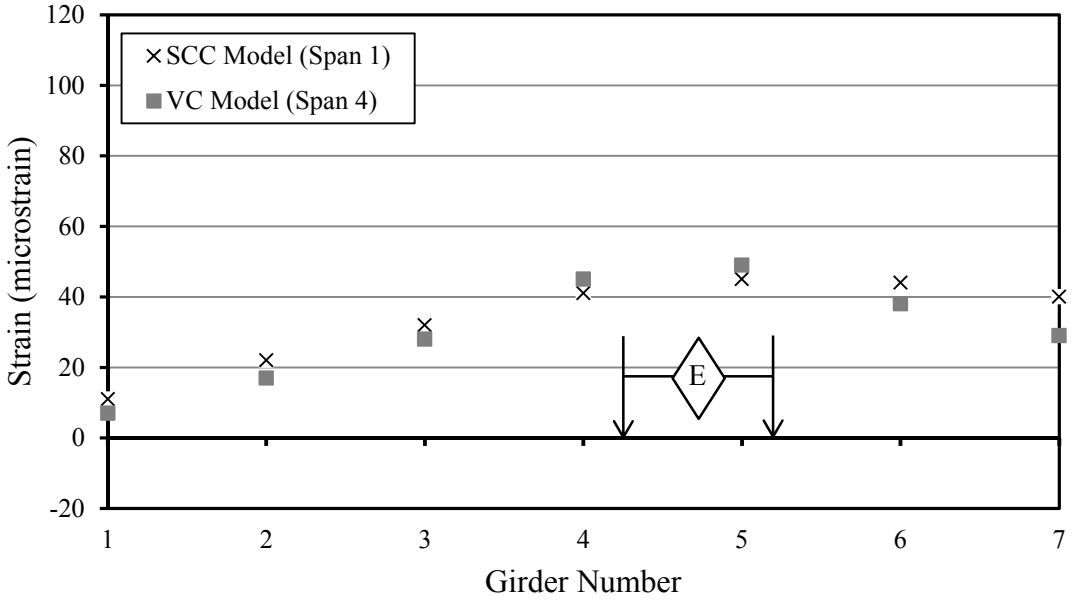

Figure C-9. *Strain results from load-truck-position E on spans with BT-54 girders.*

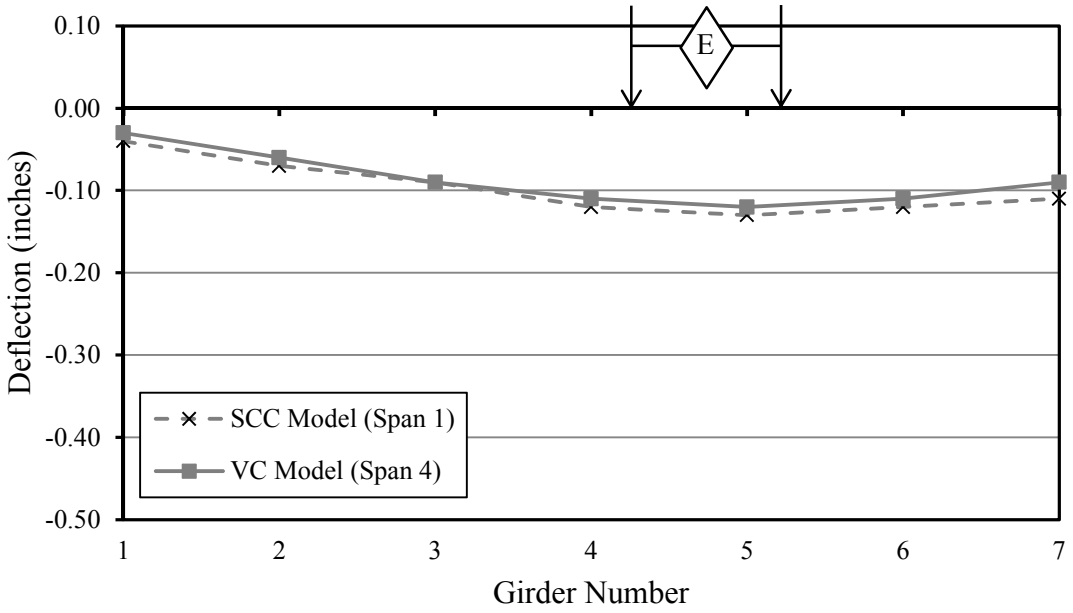

Figure C-10. *Deflection results from load-truck position E on spans with BT-54 girders.*

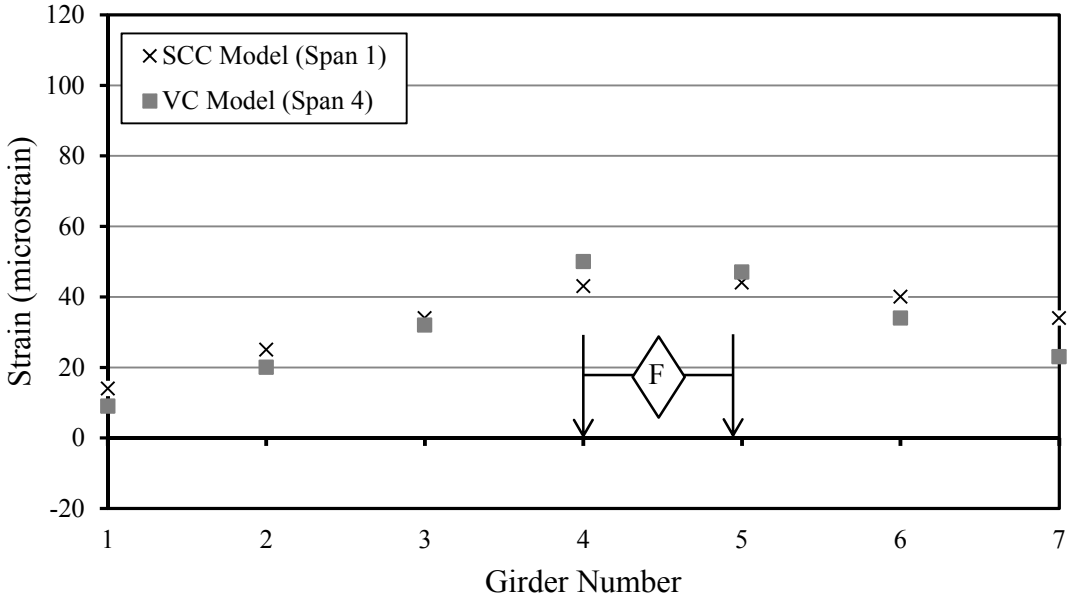

Figure C-11. *Strain results from load-truck-position F on spans with BT-54 girders.*

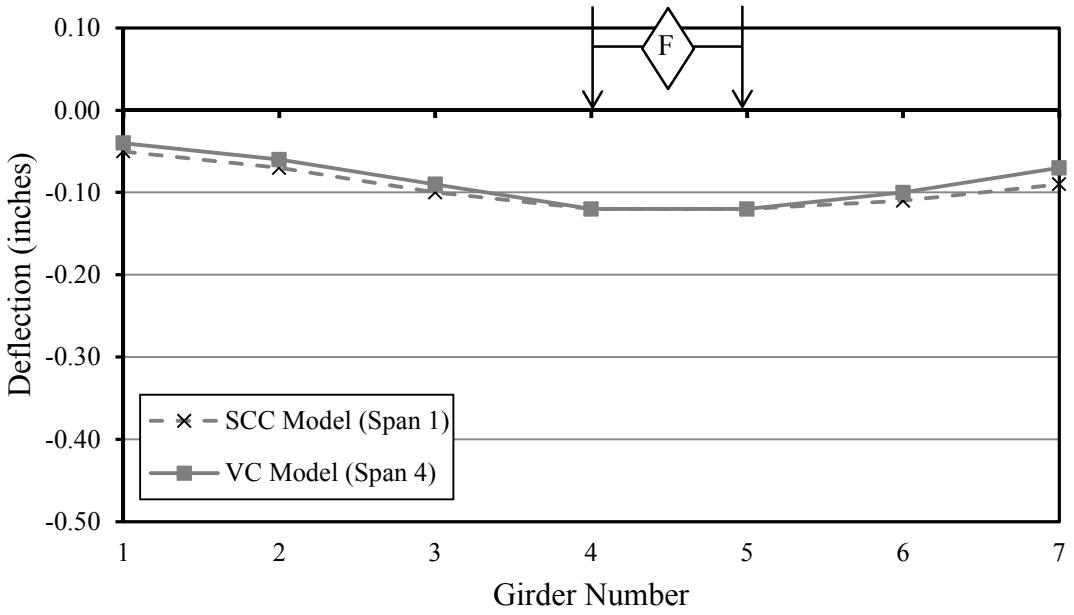

Figure C-12. *Deflection results from load-truck position F on spans with BT-54 girders.*

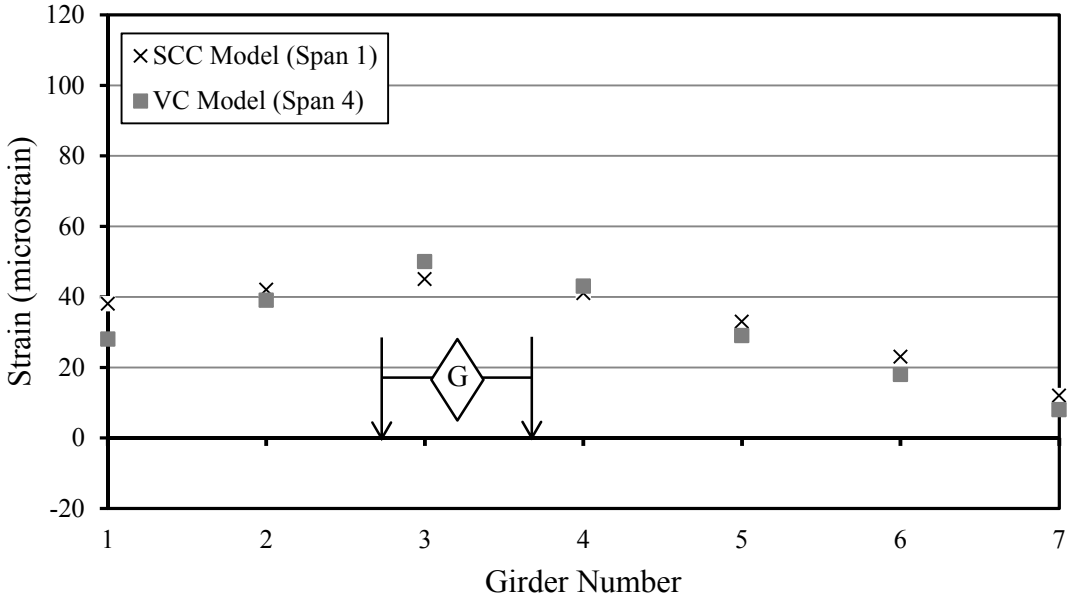

Figure C-13. *Strain results from load-truck-position G on spans with BT-54 girders.*

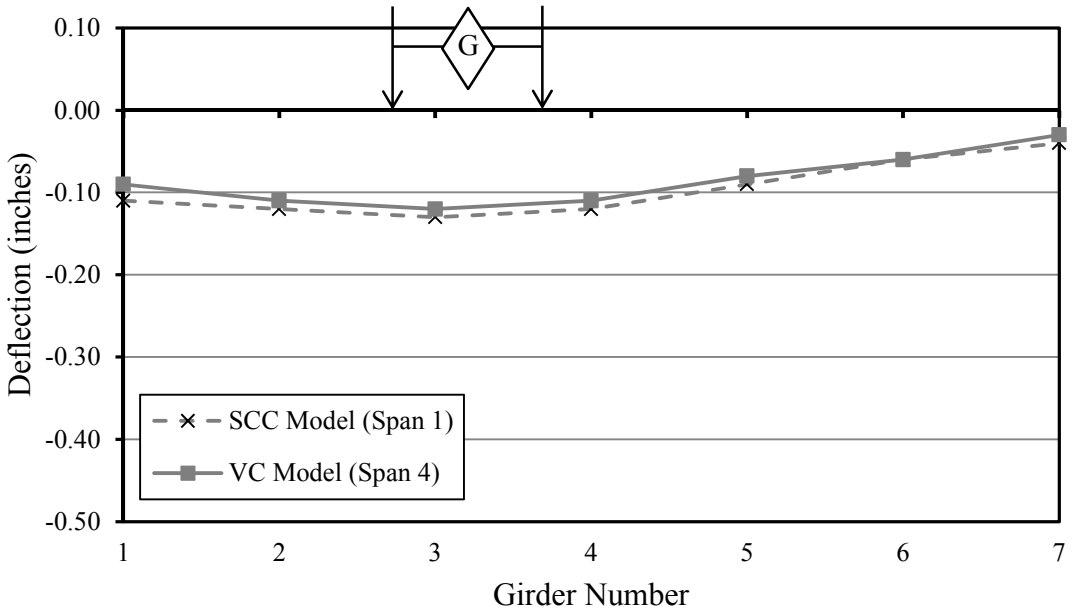

Figure C-14. *Deflection results from load-truck position G on spans with BT-54 girders.*

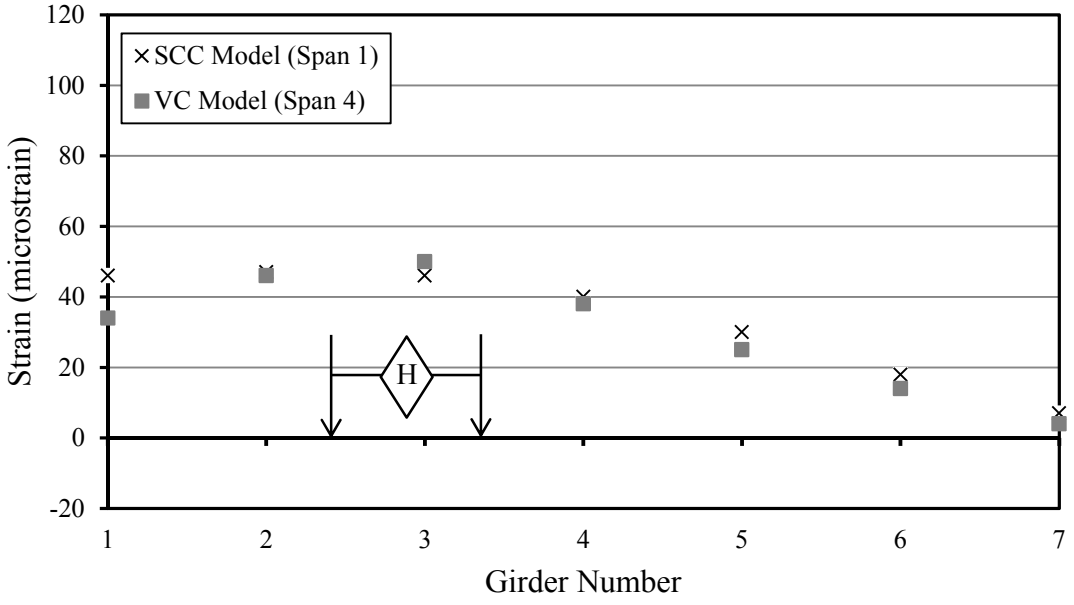

Figure C-15. *Strain results from load-truck-position H on spans with BT-54 girders.*

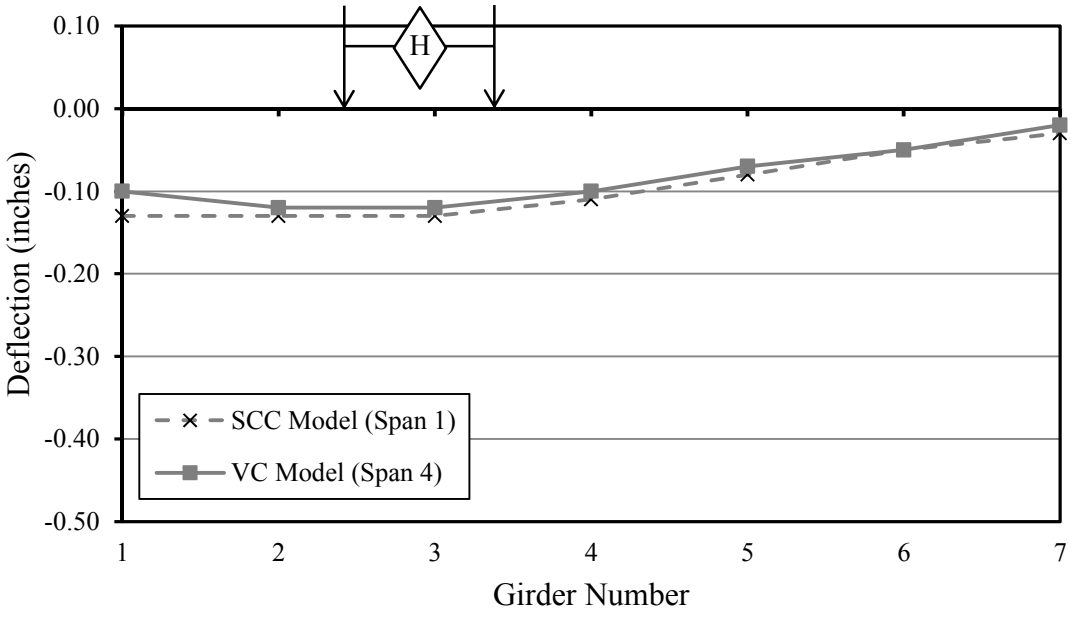

Figure C-16. *Deflection results from load-truck position H on spans with BT-54 girders.*

Table C-2. *CSiBridge modeler analysis results for spans 2 and 3 of the bridge model with barriers and adjusted web walls.*

	S2 G1		**S2 G2**		**S2 G3**		**S2 G4**		**S2 G5**		**S2 G6**		**S2 G7**	
Load Truck Position	SCC													
	Defl.	Strain	Defl.	Strain	Defl.	Strain	Defl.	Strain	Defl.	Strain	Defl.	Strain	Defl.	Strain
	in.	με	in.	με	in.	με	in.	με	in.	με	in.	με	in.	με
A	0.03	-9	-0.01	0	-0.06	11	-0.11	24	-0.16	40	-0.23	62	-0.29	85
B	0.02	-8	-0.02	2	-0.06	12	-0.11	25	-0.16	41	-0.22	62	-0.28	81
C	0.02	-7	-0.02	4	-0.06	13	-0.11	26	-0.16	42	-0.22	61	-0.27	76
D	-0.06	11	-0.08	19	-0.11	28	-0.13	37	-0.15	45	-0.15	42	-0.15	36
E	-0.06	12	-0.08	19	-0.11	28	-0.14	38	-0.15	45	-0.15	41	-0.15	35
F	-0.07	15	-0.09	23	-0.12	31	-0.14	40	-0.14	43	-0.14	36	-0.13	30
G	-0.15	36	-0.15	40	-0.15	44	-0.13	40	-0.11	28	-0.08	19	-0.06	11
H	-0.17	42	-0.17	45	-0.15	46	-0.13	37	-0.10	25	-0.07	15	-0.04	7
	S3 G1		**S3 G2**		**S3 G3**		**S3 G4**		**S3 G5**		**S3 G6**		**S3 G7**	
Load Truck Position	VC													
	Defl.	Strain	Defl.	Strain	Defl.	Strain	Defl.	Strain	Defl.	Strain	Defl.	Strain	Defl.	Strain
	in.	με	in.	με	in.	με	in.	με	in.	με	in.	με	in.	με
A	0.02	-6	-0.01	2	-0.05	9	-0.09	18	-0.13	32	-0.18	49	-0.24	68
B	0.01	-5	-0.02	2	-0.05	9	-0.09	19	-0.13	33	-0.18	49	-0.23	65
C	0.01	-3	-0.02	3	-0.05	11	-0.09	20	-0.13	33	-0.18	49	-0.22	61
D	-0.05	9	-0.07	16	-0.09	23	-0.11	31	-0.13	37	-0.13	33	-0.12	28
E	-0.05	10	-0.07	16	-0.09	24	-0.11	31	-0.13	37	-0.12	33	-0.12	27
F	-0.07	14	-0.09	21	-0.10	28	-0.12	38	-0.12	32	-0.11	26	-0.09	21
G	-0.12	29	-0.13	33	-0.13	37	-0.12	33	-0.09	23	-0.07	15	-0.05	8
H	-0.14	35	-0.14	37	-0.13	38	-0.11	30	-0.08	20	-0.06	12	-0.03	6

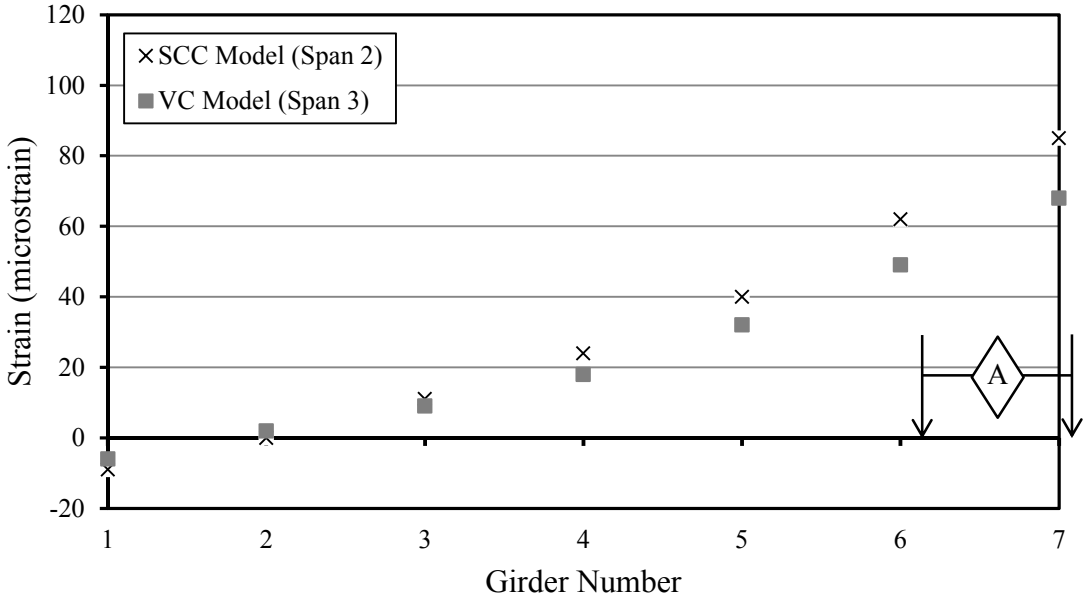

Figure C-17. *Strain results from load-truck-position A on spans with BT-72 girders.*

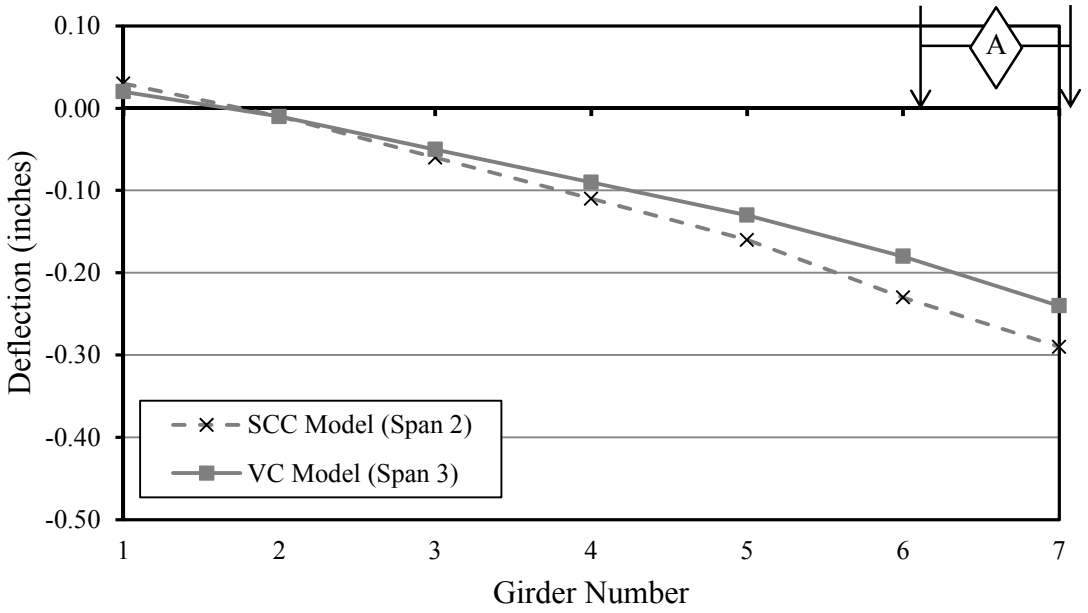

Figure C-18. *Deflection results from load-truck position A on spans with BT-72 girders.*

Figure C-19. *Strain results from load-truck-position B on spans with BT-72 girders.*

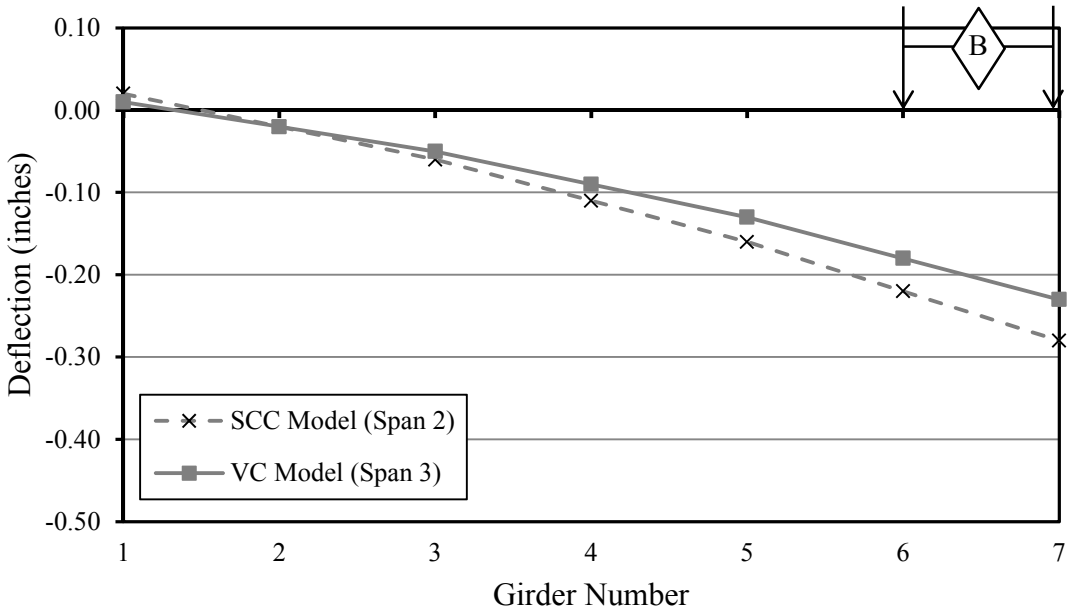

Figure C-20. *Deflection results from load-truck position B on spans with BT-72 girders.*

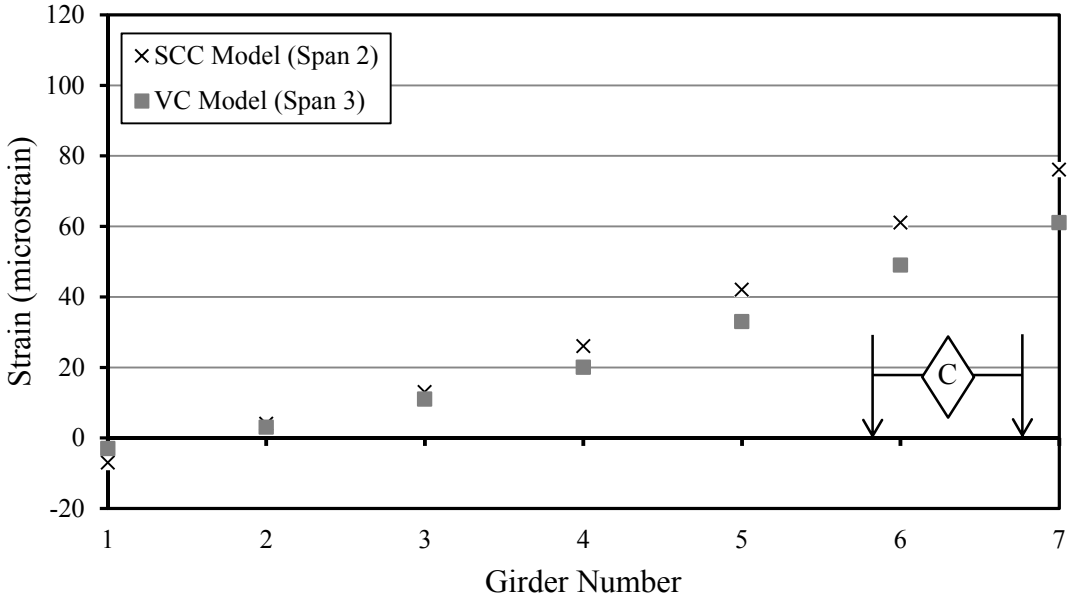

Figure C-21. *Strain results from load-truck-position C on spans with BT-72 girders.*

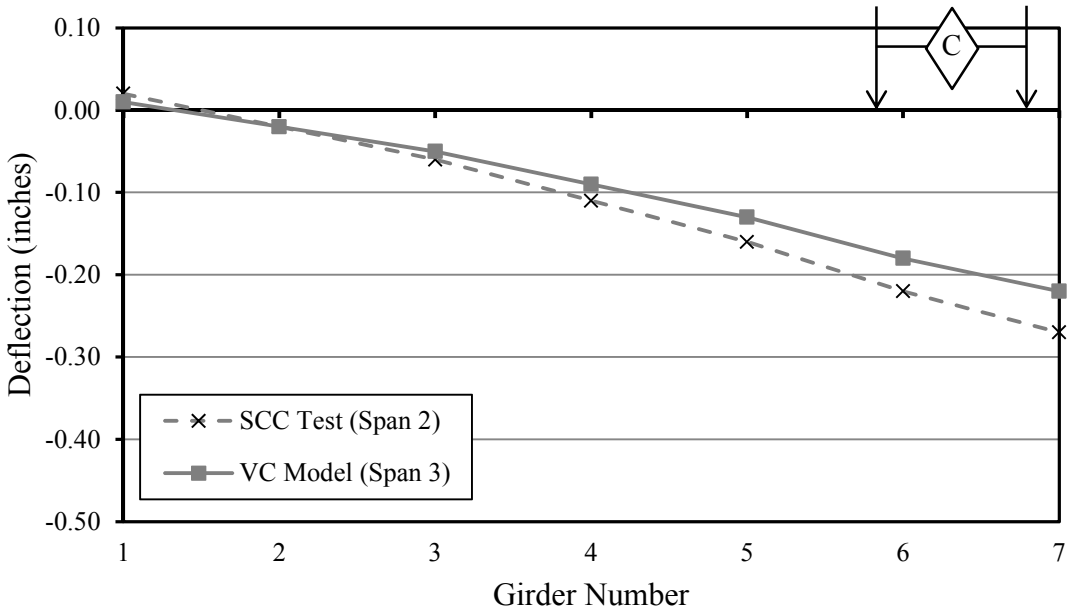

Figure C-22. *Deflection results from load-truck position C on spans with BT-72 girders.*

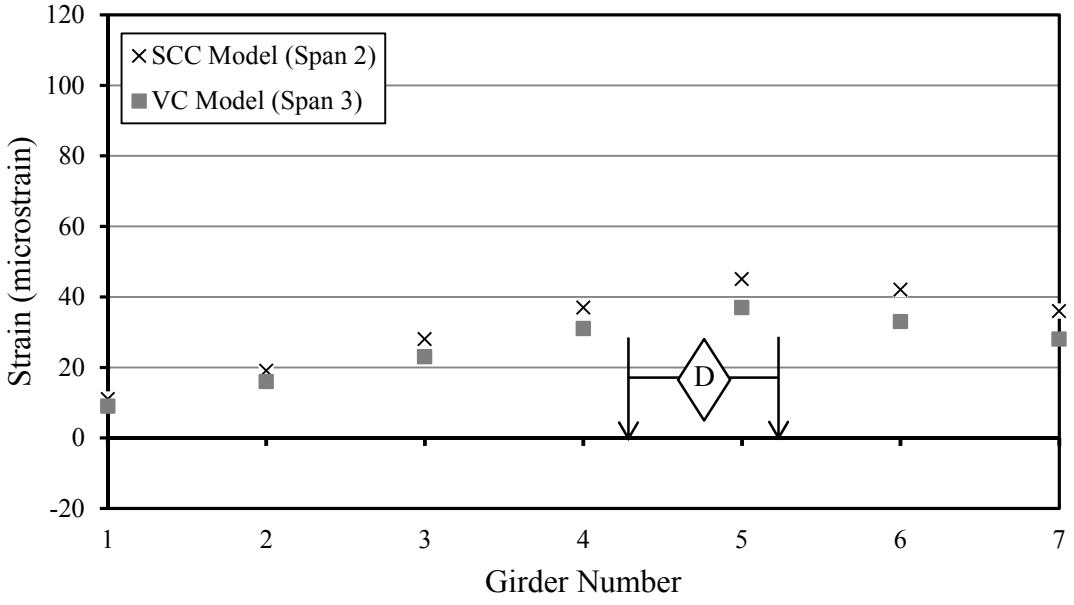

Figure C-23. *Strain results from load-truck-position D on spans with BT-72 girders.*

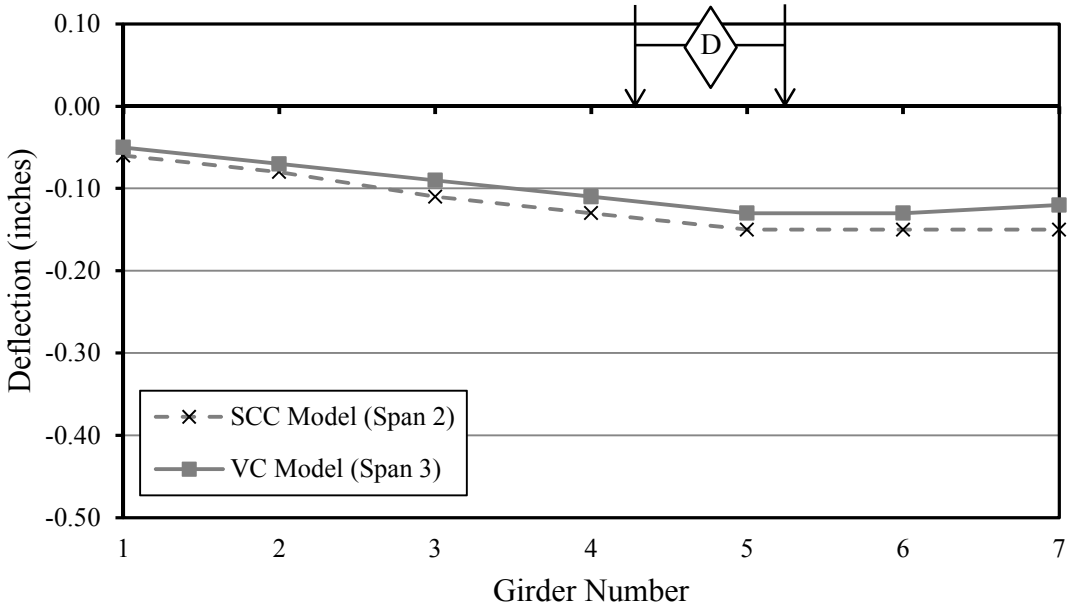

Figure C-24. *Deflection results from load-truck position D on spans with BT-72 girders.*

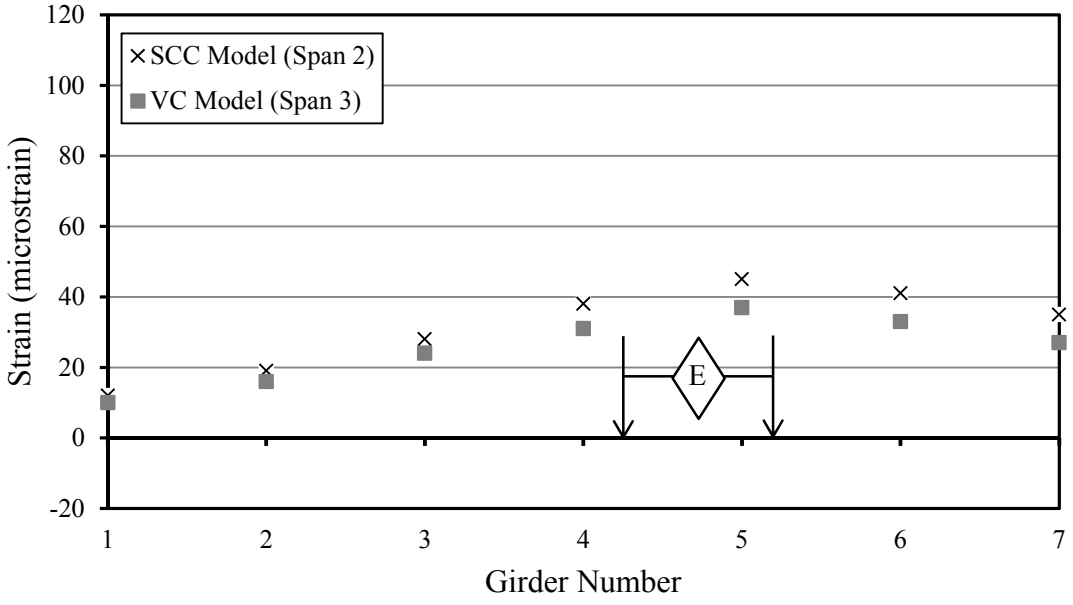

Figure C-25. *Strain results from load-truck-position E on spans with BT-72 girders.*

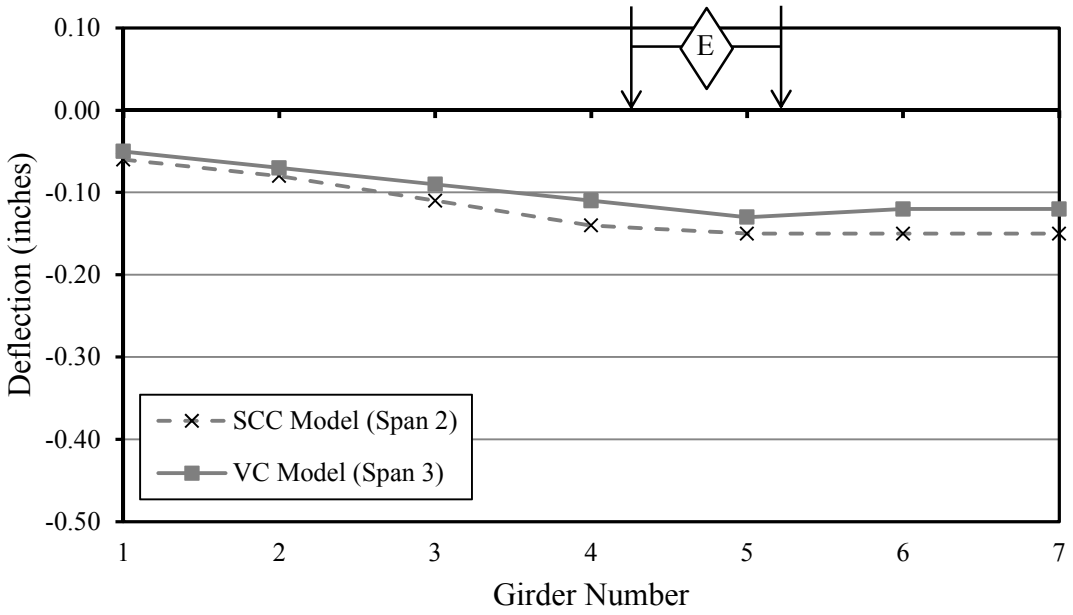

Figure C-26. *Deflection results from load-truck position E on spans with BT-72 girders.*

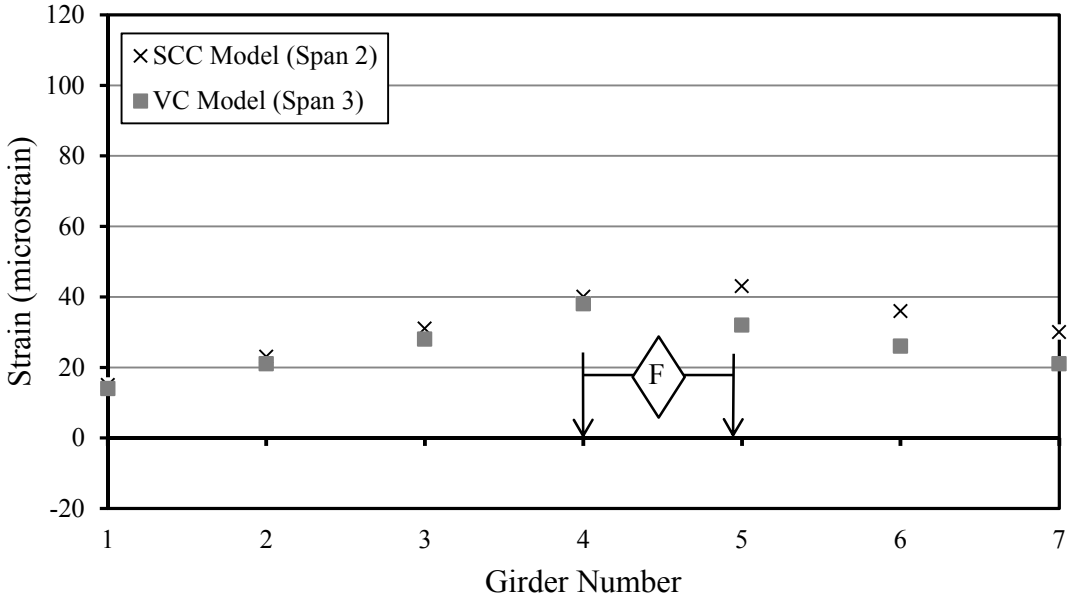

Figure C-27. *Strain results from load-truck-position F on spans with BT-72 girders.*

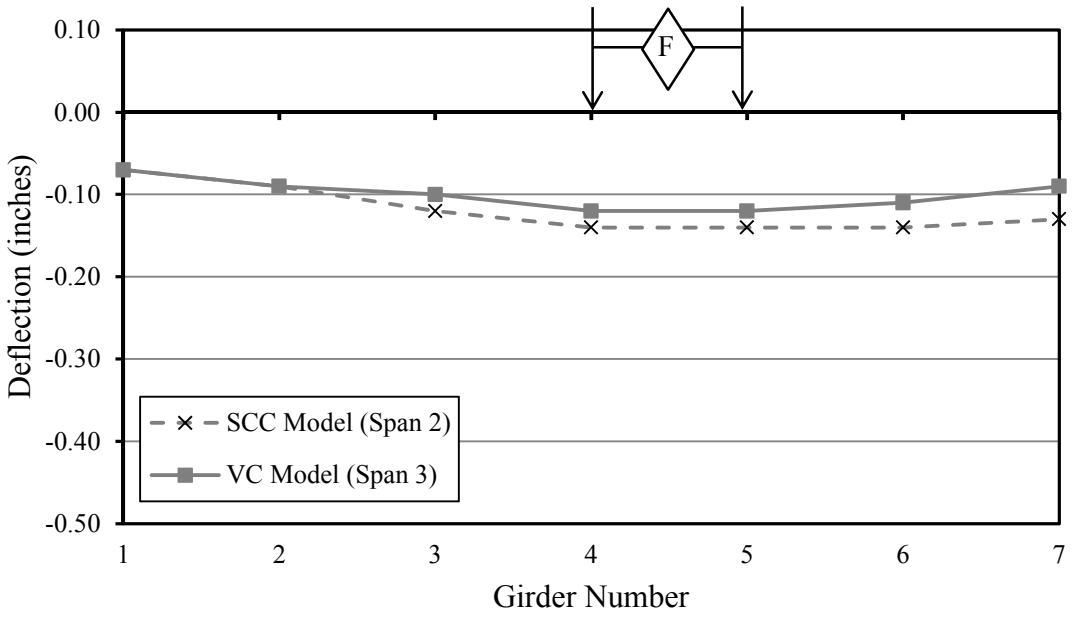

Figure C-28. *Deflection results from load-truck position F on spans with BT-72 girders.*

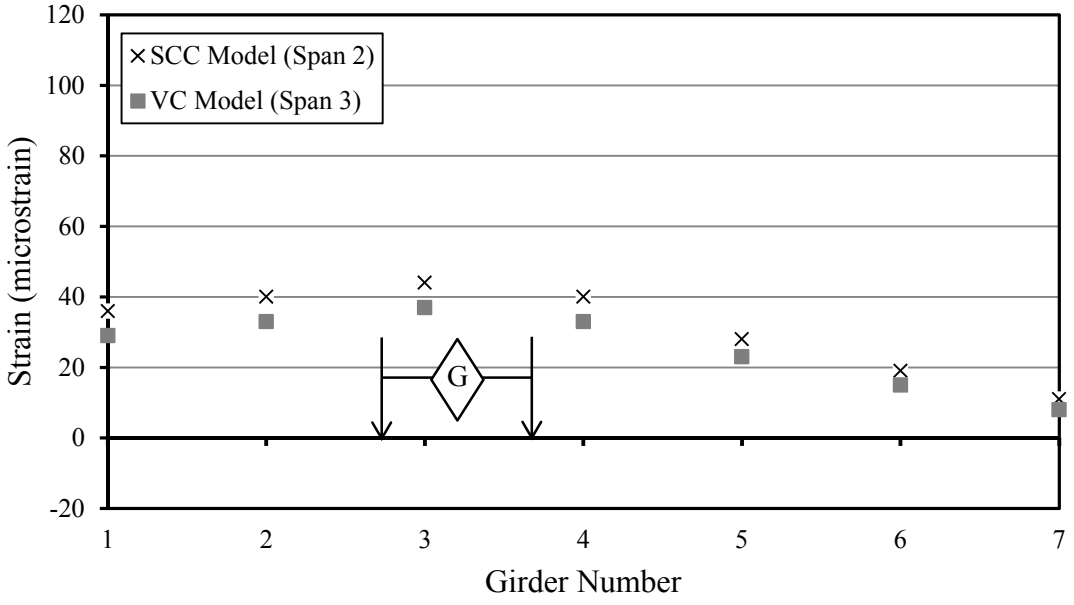

Figure C-29. *Strain results from load-truck-position G on spans with BT-72 girders.*

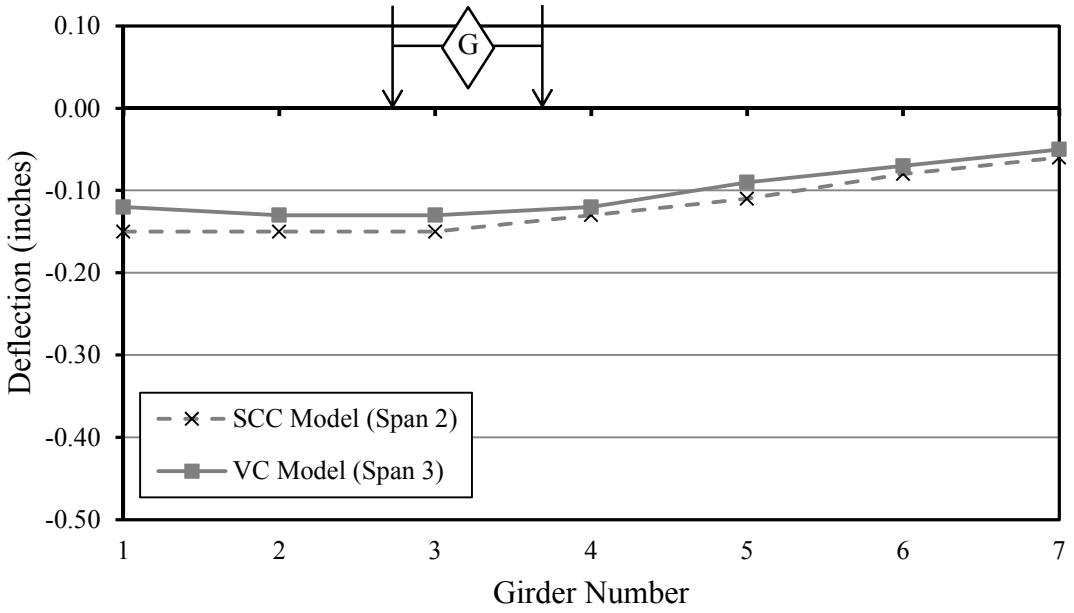

Figure C-30. *Deflection results from load-truck position G on spans with BT-72 girders.*

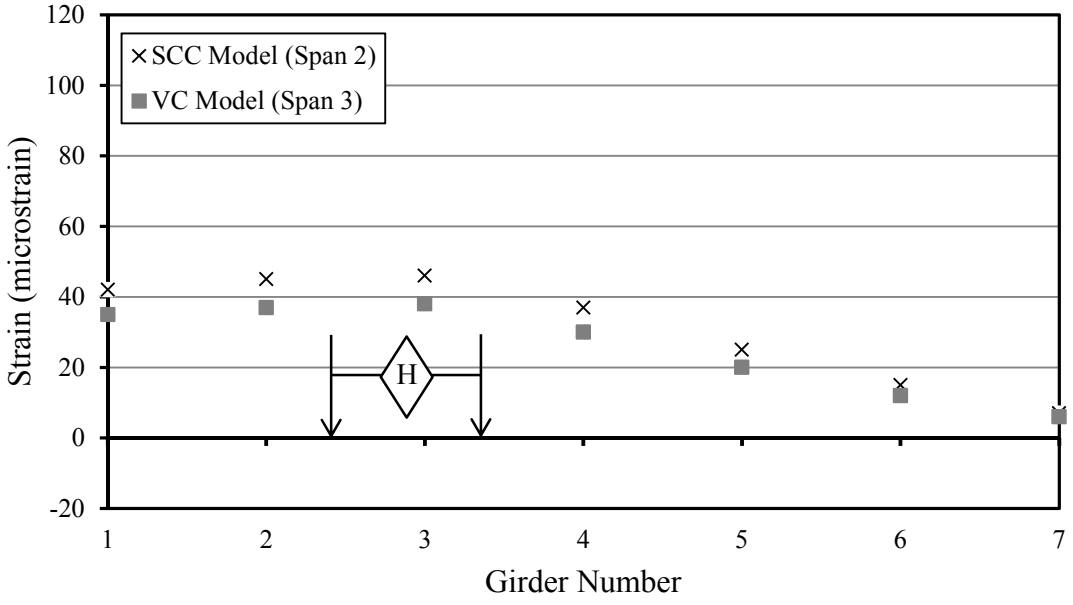

Figure C-31. *Strain results from load-truck-position H on spans with BT-72 girders.*

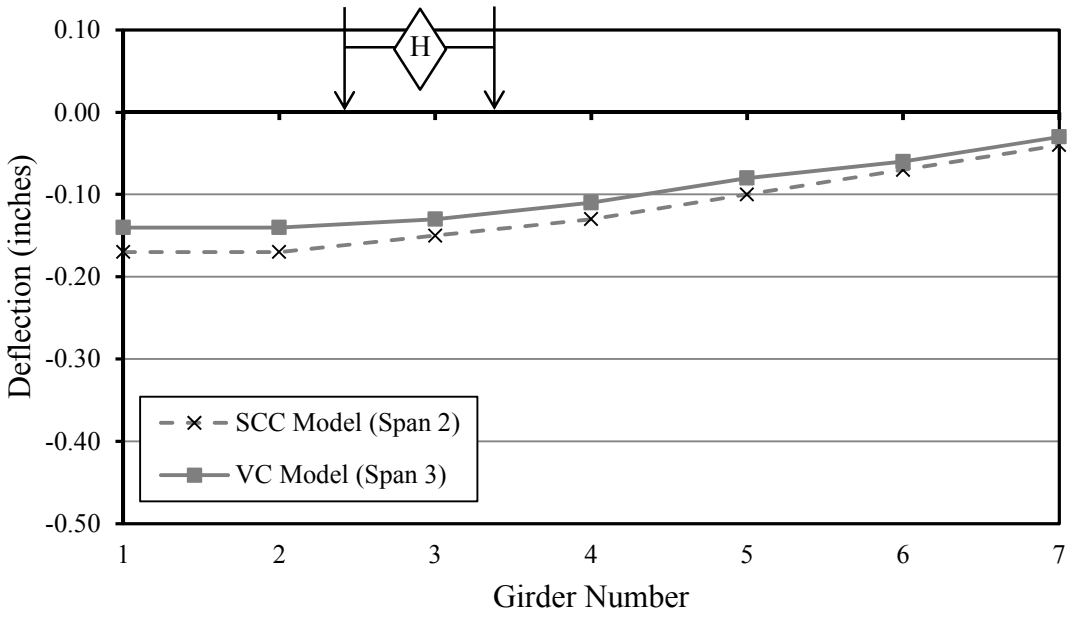

Figure C-32. *Deflection results from load-truck position H on spans with BT-72 girders.*

Appendix D:

CSiBridge Model Staggered Webwalls and without Barriers Results – Strains and Deflections

Table D-1. *CSiBridge modeler analysis results for spans 1 and 4 of the bridge model with staggered webwalls but without barriers.*

	S1 G1		**S1 G2**		**S1 G3**		**S1 G4**		**S1 G5**		**S1 G6**		**S1 G7**	
Load Truck Position	SCC													
	Defl.	Strain	Defl.	Strain	Defl.	Strain	Defl.	Strain	Defl.	Strain	Defl.	Strain	Defl.	Strain
	in.	με	in.	με	in.	με	in.	με	in.	με	in.	με	in.	με
A	0.04	-14	0	0	-0.04	12	-0.09	29	-0.15	50	-0.22	76	-0.3	105
B	0.03	-13	0.00	0	-0.05	14	-0.09	30	-0.15	50	-0.22	75	-0.29	101
C	0.03	-11	-0.01	2	-0.05	15	-0.10	31	-0.15	50	-0.21	73	-0.27	95
D	-0.04	10	-0.07	22	-0.10	33	-0.13	43	-0.14	48	-0.14	49	-0.14	47
E	-0.04	11	-0.07	23	-0.10	33	-0.13	43	-0.14	49	-0.14	49	-0.14	46
F	-0.06	15	-0.08	27	-0.11	36	-0.13	45	-0.14	47	-0.13	44	-0.12	39
G	-0.13	44	-0.14	47	-0.14	48	-0.13	44	-0.10	35	-0.07	24	-0.04	12
H	-0.16	52	-0.16	52	-0.14	49	-0.12	42	-0.09	31	-0.06	19	-0.03	7
	S4 G1		**S4 G2**		**S4 G3**		**S4 G4**		**S4 G5**		**S4 G6**		**S4 G7**	
Load Truck Position	VC													
	Defl.	Strain	Defl.	Strain	Defl.	Strain	Defl.	Strain	Defl.	Strain	Defl.	Strain	Defl.	Strain
	in.	με	in.	με	in.	με	in.	με	in.	με	in.	με	in.	με
A	0.02	-8	-0.01	0	-0.04	10	-0.08	23	-0.14	43	-0.21	76	-0.29	102
B	0.02	-7	-0.01	2	-0.04	11	-0.09	25	-0.14	44	-0.21	77	-0.28	97
C	0.02	-6	-0.01	3	-0.05	13	-0.09	26	-0.14	46	-0.2	74	-0.26	90
D	-0.03	9	-0.06	19	-0.10	31	-0.13	48	-0.14	54	-0.14	46	-0.12	38
E	-0.04	9	-0.06	19	-0.10	31	-0.13	49	-0.14	54	-0.14	45	-0.12	37
F	-0.05	11	-0.08	23	-0.11	35	-0.13	53	-0.14	52	-0.12	39	-0.10	30
G	-0.11	35	-0.13	44	-0.14	54	-0.13	46	-0.10	32	-0.07	20	-0.04	9
H	-0.14	43	-0.14	52	-0.14	54	-0.12	41	-0.09	28	-0.05	16	-0.03	6

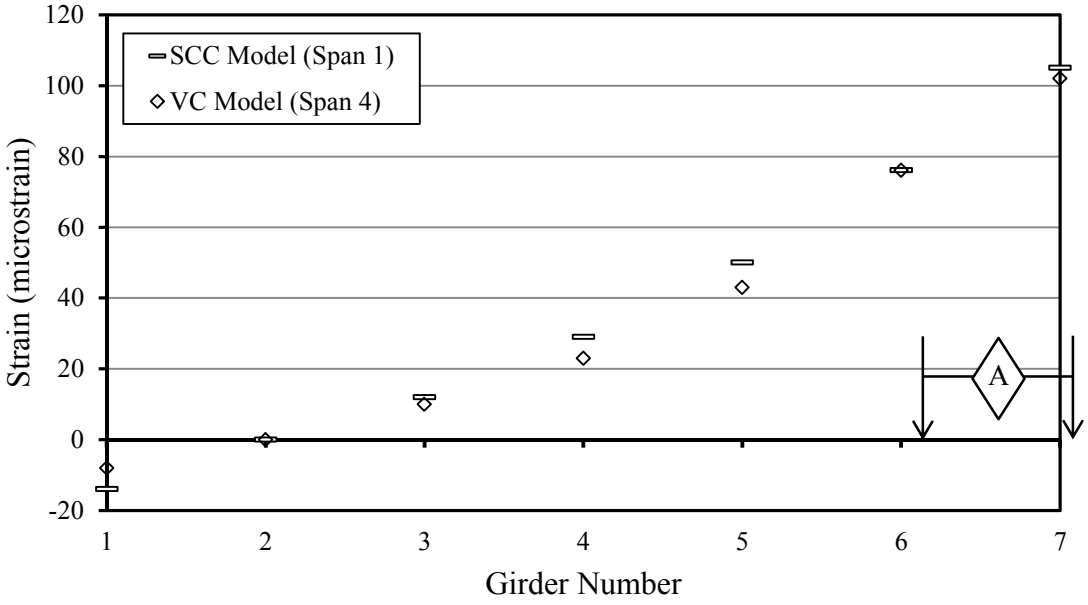

Figure D-1. *Strain results from load-truck-position A on spans with BT-54 girders.*

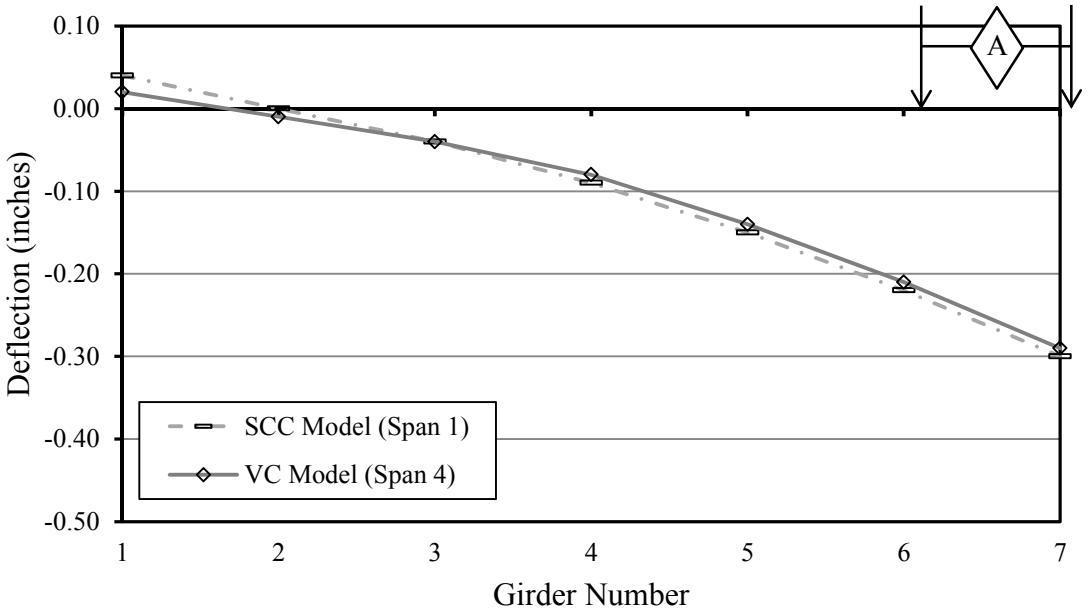

Figure D-2. *Deflection results from load-truck position A on spans with BT-54 girders.*

Figure D-3. *Strain results from load-truck-position B on spans with BT-54 girders.*

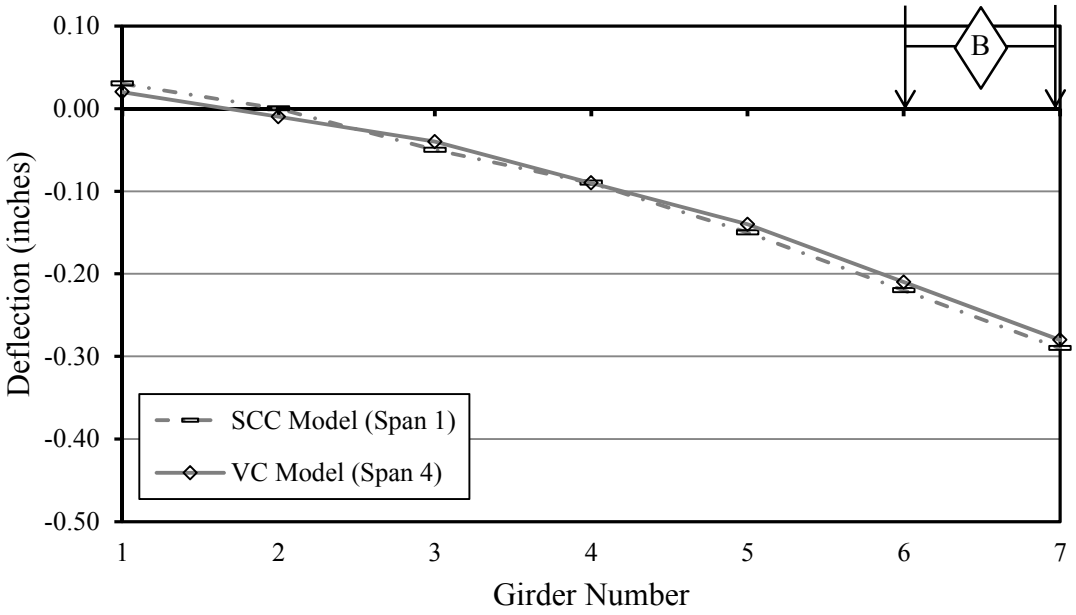

Figure D-4. *Deflection results from load-truck position B on spans with BT-54 girders.*

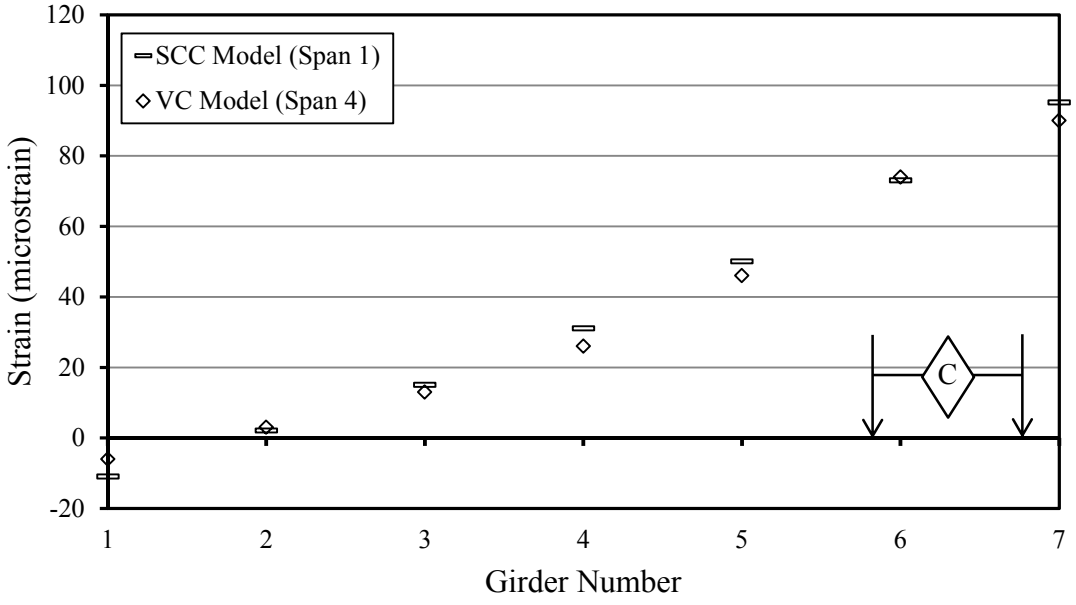

Figure D-5. *Strain results from load-truck-position C on spans with BT-54 girders.*

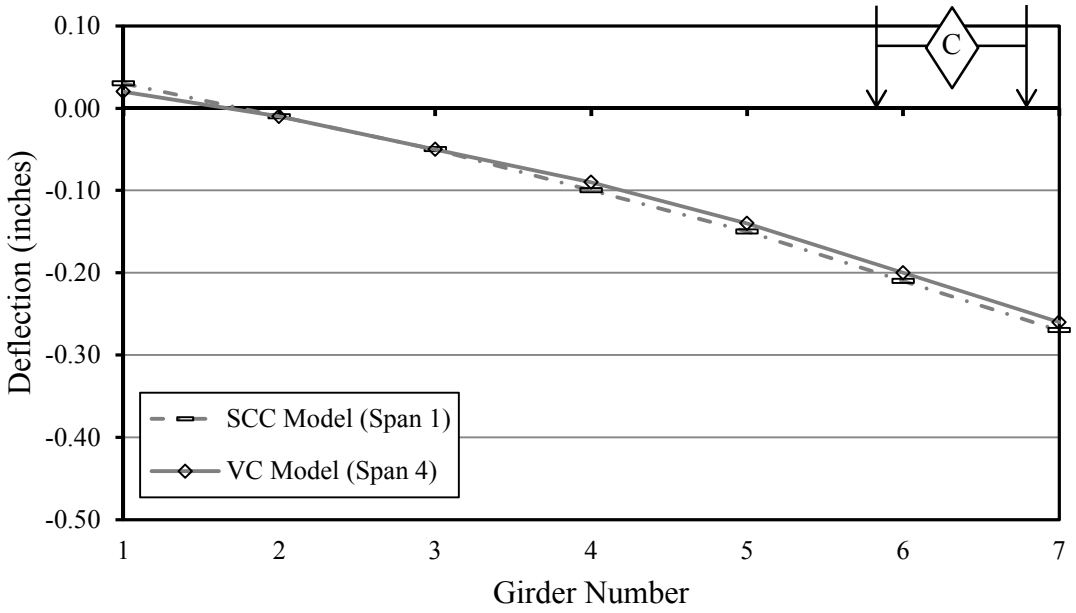

Figure D-6. *Deflection results from load-truck position C on spans with BT-54 girders.*

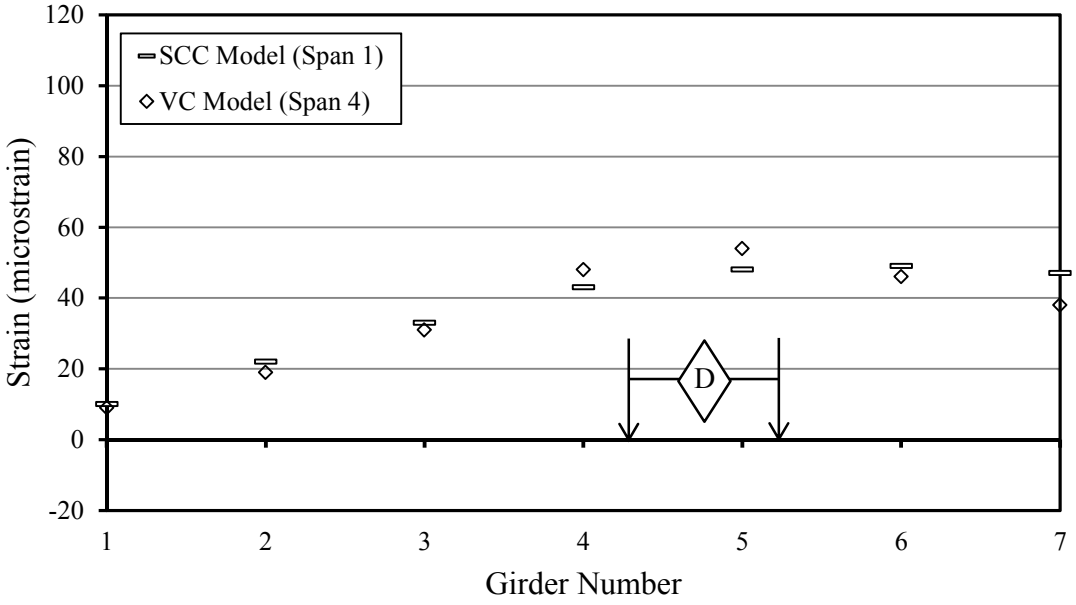

Figure D-7. *Strain results from load-truck-position D on spans with BT-54 girders.*

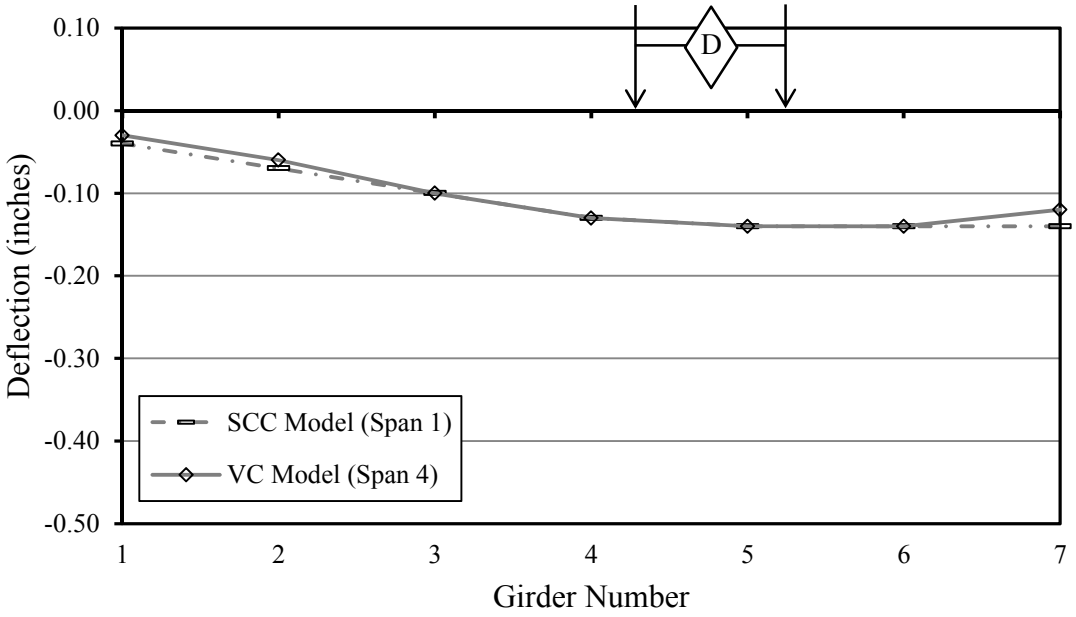

Figure D-8. *Deflection results from load-truck position D on spans with BT-54 girders.*

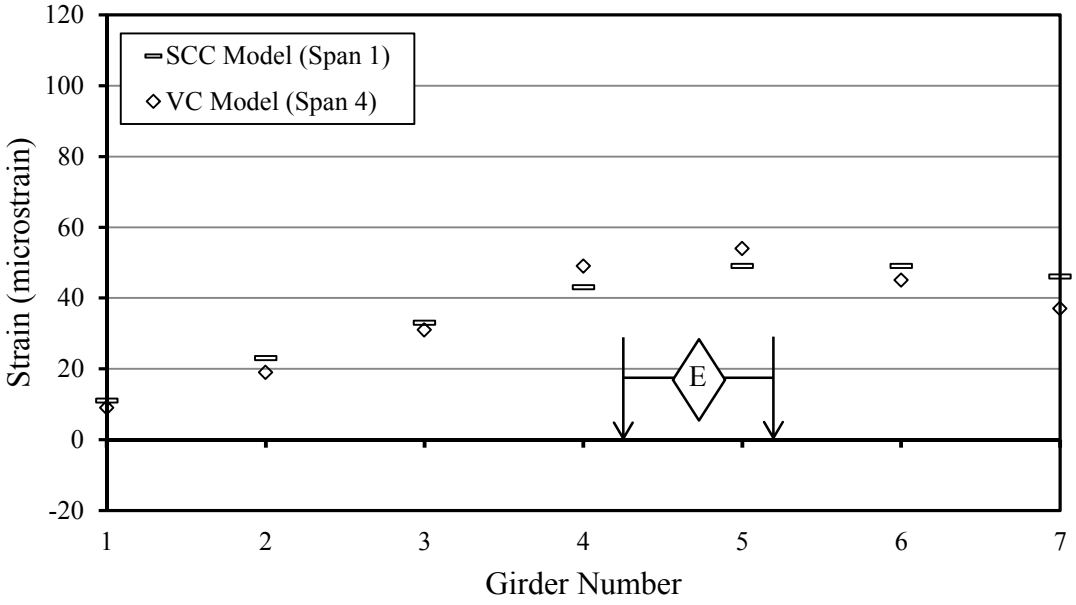

Figure D-9. *Strain results from load-truck-position E on spans with BT-54 girders.*

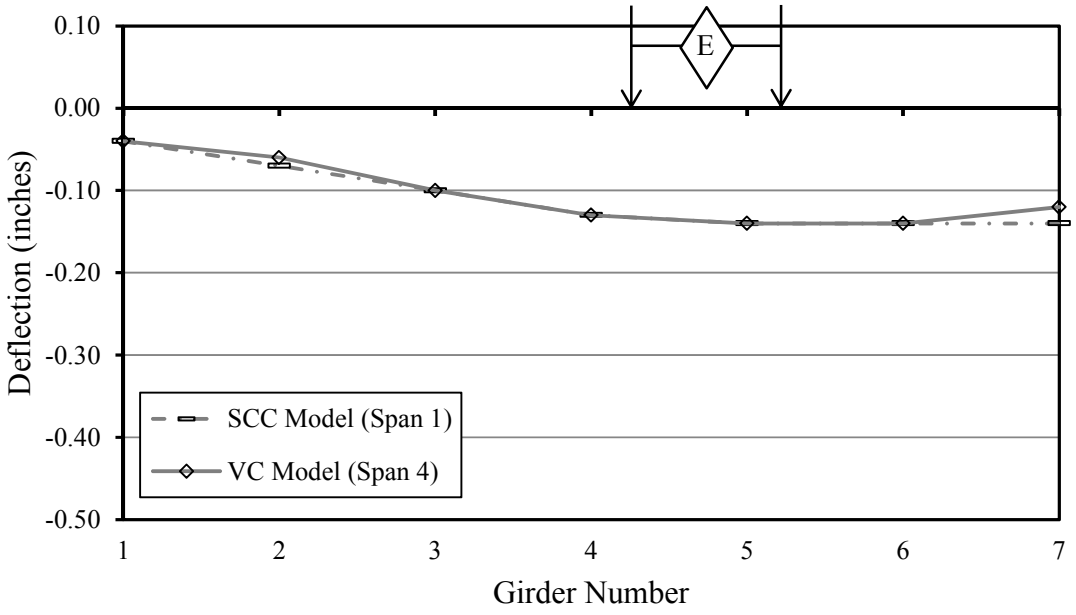

Figure D-10. *Deflection results from load-truck position E on spans with BT-54 girders.*

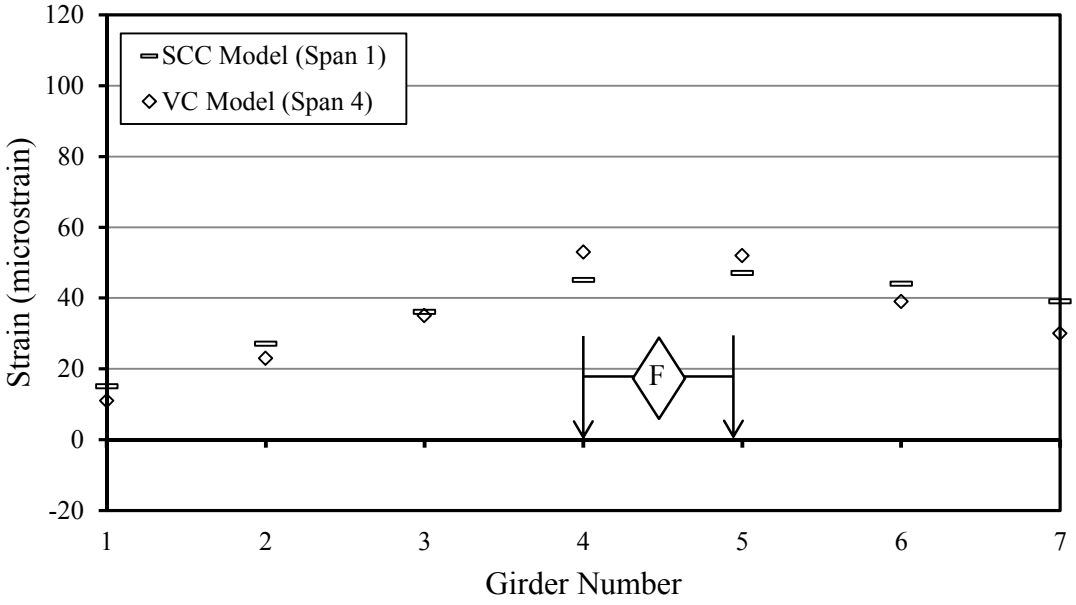

Figure D-11. *Strain results from load-truck-position F on spans with BT-54 girders.*

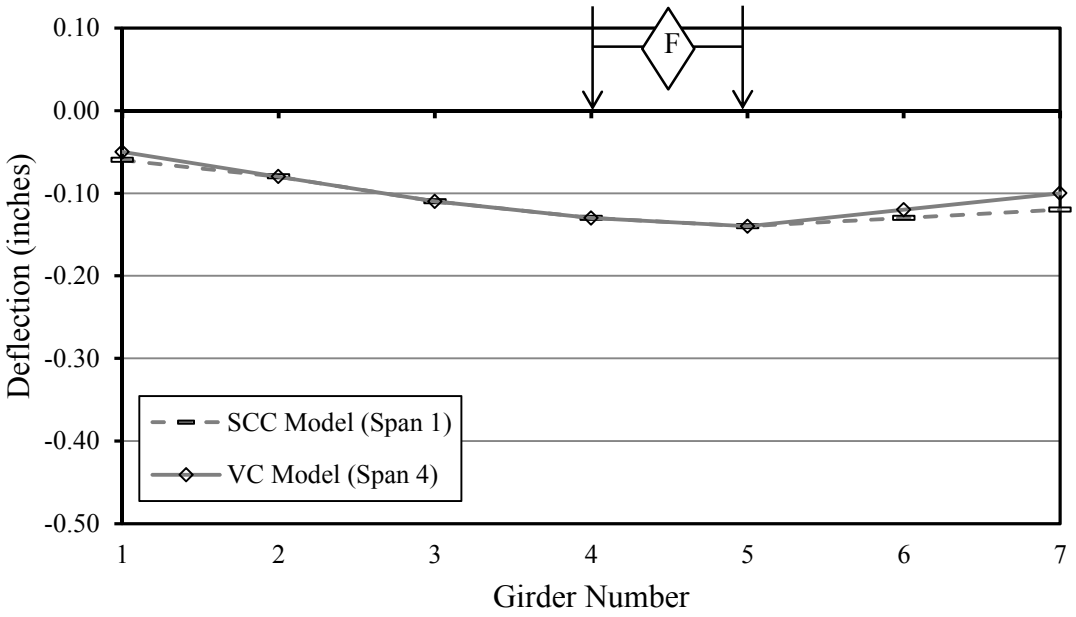

Figure D-12. *Deflection results from load-truck position F on spans with BT-54 girders.*

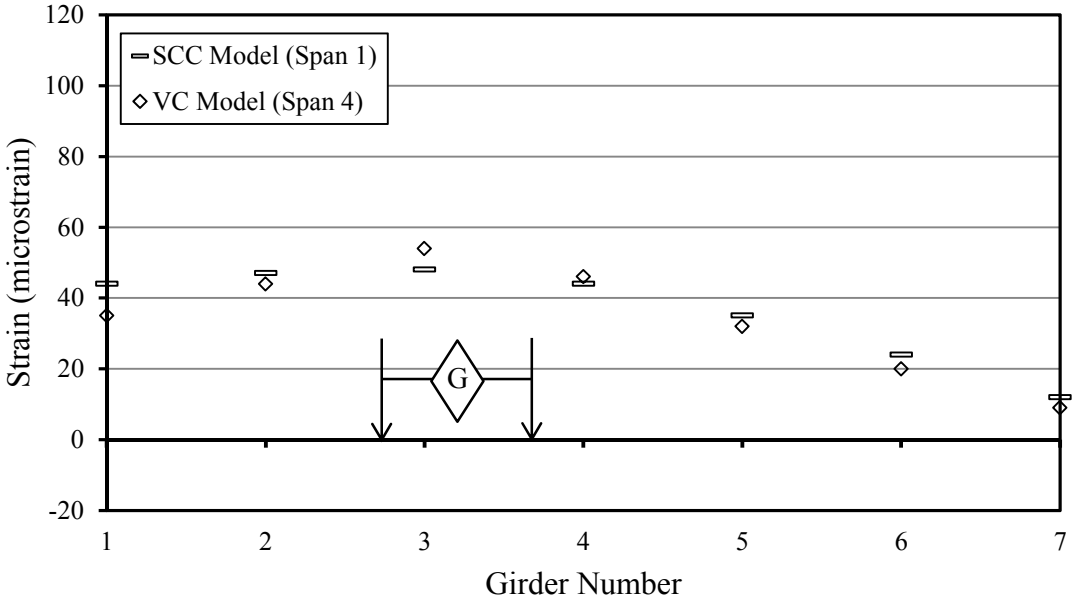

Figure D-13. *Strain results from load-truck-position G on spans with BT-54 girders.*

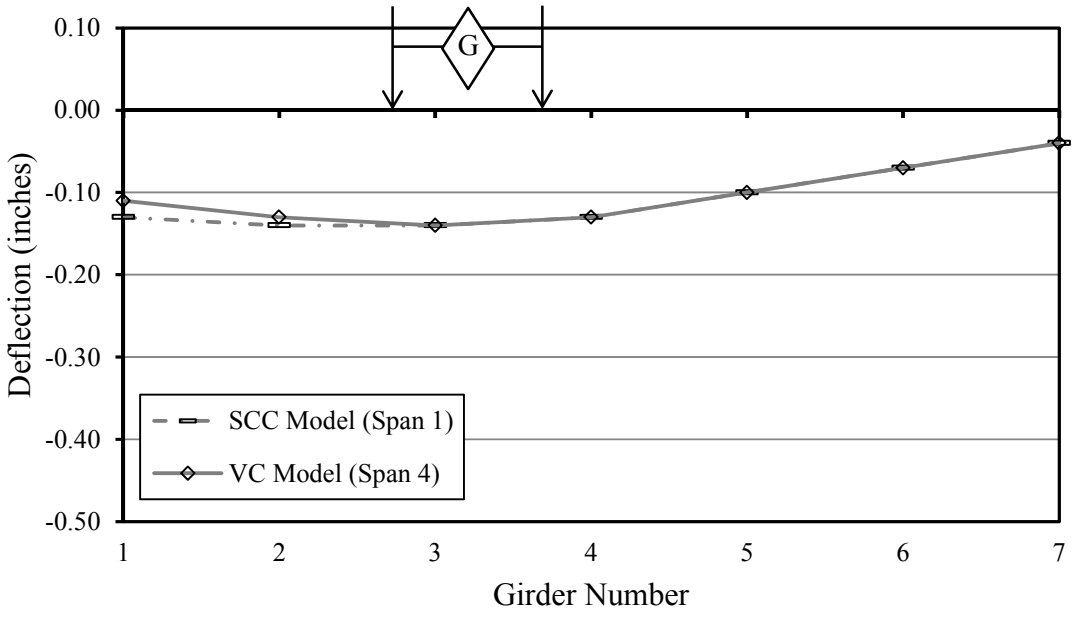

Figure D-14. *Deflection results from load-truck position G on spans with BT-54 girders.*

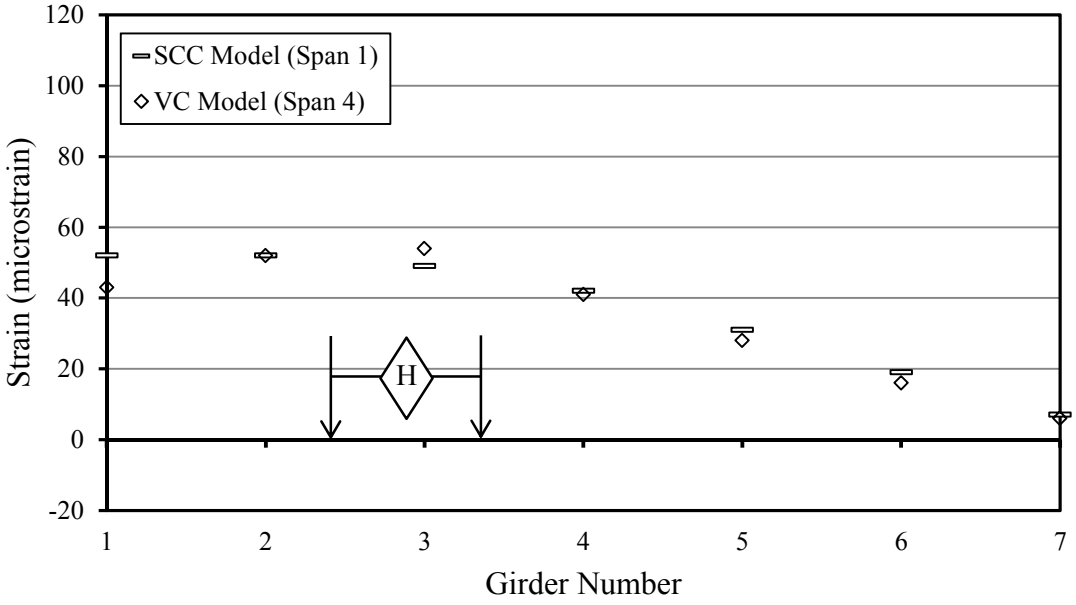

Figure D-15. *Strain results from load-truck-position H on spans with BT-54 girders.*

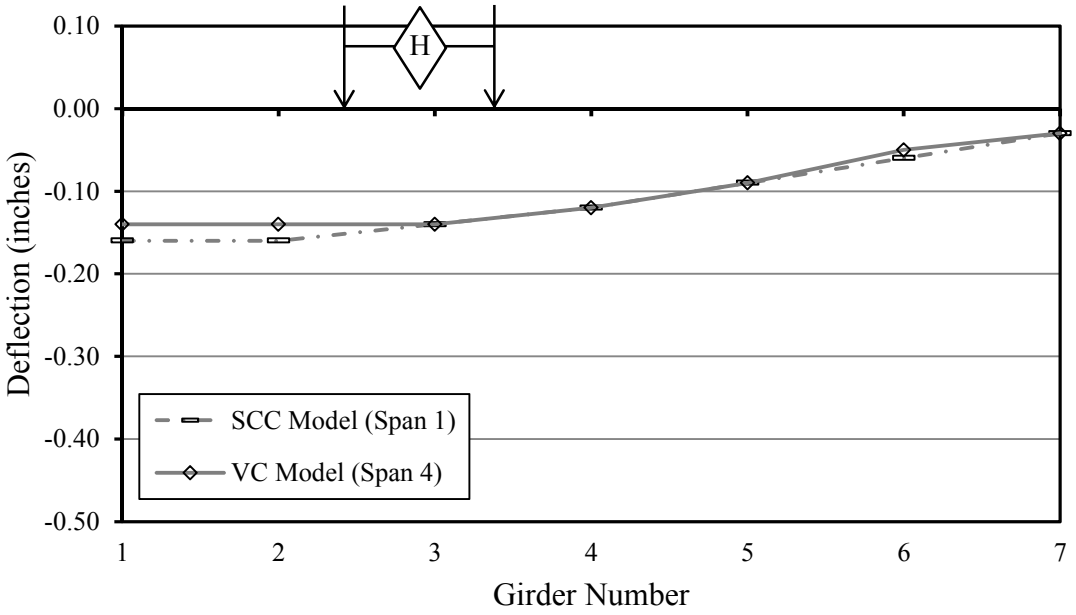

Figure D-16. *Deflection results from load-truck position H on spans with BT-54 girders.*

Table D-2. *CSiBridge modeler analysis results for spans 2 and 3 of the bridge model with staggered webwalls but without barriers.*

	S2 G1		**S2 G2**		**S2 G3**		**S2 G4**		**S2 G5**		**S2 G6**		**S2 G7**	
Load Truck Position	SCC													
	Defl.	Strain	Defl.	Strain	Defl.	Strain	Defl.	Strain	Defl.	Strain	Defl.	Strain	Defl.	Strain
	in.	με	in.	με	in.	με	in.	με	in.	με	in.	με	in.	με
A	0.05	-13	0.00	0	-0.06	11	-0.13	26	-0.2	45	-0.28	69	-0.36	96
B	0.04	-11	-0.01	0	-0.07	12	-0.13	27	-0.2	46	-0.27	69	-0.35	92
C	0.03	-10	-0.02	1	-0.07	14	-0.13	28	-0.19	46	-0.27	68	-0.33	86
D	-0.06	11	-0.09	20	-0.12	30	-0.15	39	-0.17	48	-0.18	45	-0.19	41
E	-0.07	12	-0.09	20	-0.12	30	-0.15	40	-0.17	48	-0.18	44	-0.18	40
F	-0.08	16	-0.11	24	-0.13	33	-0.16	42	-0.16	45	-0.16	39	-0.16	34
G	-0.18	40	-0.18	44	-0.17	47	-0.15	42	-0.12	29	-0.09	20	-0.06	12
H	-0.21	47	-0.20	49	-0.18	49	-0.15	39	-0.11	26	-0.08	16	-0.04	8
	S3 G1		**S3 G2**		**S3 G3**		**S3 G4**		**S3 G5**		**S3 G6**		**S3 G7**	
Load Truck Position	VC													
	Defl.	Strain	Defl.	Strain	Defl.	Strain	Defl.	Strain	Defl.	Strain	Defl.	Strain	Defl.	Strain
	in.	με	in.	με	in.	με	in.	με	in.	με	in.	με	in.	με
A	0.03	-7	-0.01	2	-0.06	11	-0.11	23	-0.17	38	-0.24	57	-0.31	80
B	0.03	-4	-0.02	3	-0.06	12	-0.11	23	-0.17	38	-0.23	57	-0.30	76
C	0.02	-3	-0.02	4	-0.07	13	-0.11	24	-0.17	39	-0.23	56	-0.28	71
D	-0.07	-13	-0.09	19	-0.11	27	-0.14	35	-0.15	42	-0.16	38	-0.16	33
E	-0.07	13	-0.09	19	-0.12	27	-0.14	35	-0.15	42	-0.16	37	-0.16	32
F	-0.09	18	-0.11	24	-0.13	31	-0.14	43	-0.14	36	-0.13	30	-0.12	24
G	-0.17	36	-0.17	39	-0.16	42	-0.14	37	-0.11	26	-0.09	17	-0.06	10
H	-0.19	42	-0.18	43	-0.17	43	-0.14	35	-0.10	23	-0.07	14	-0.04	6

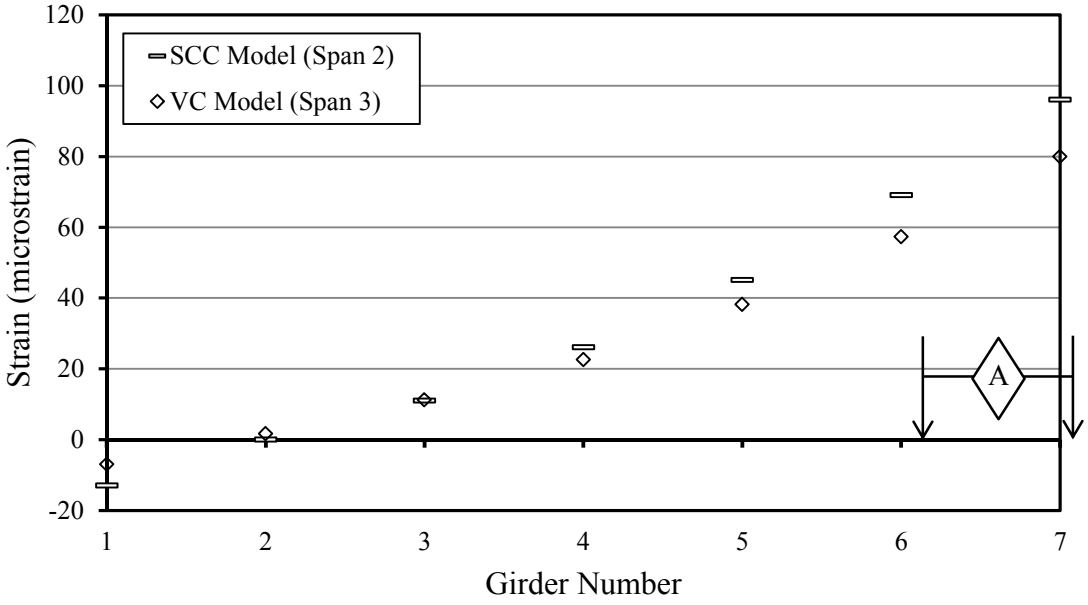

Figure D-17. *Strain results from load-truck-position A on spans with BT-72 girders.*

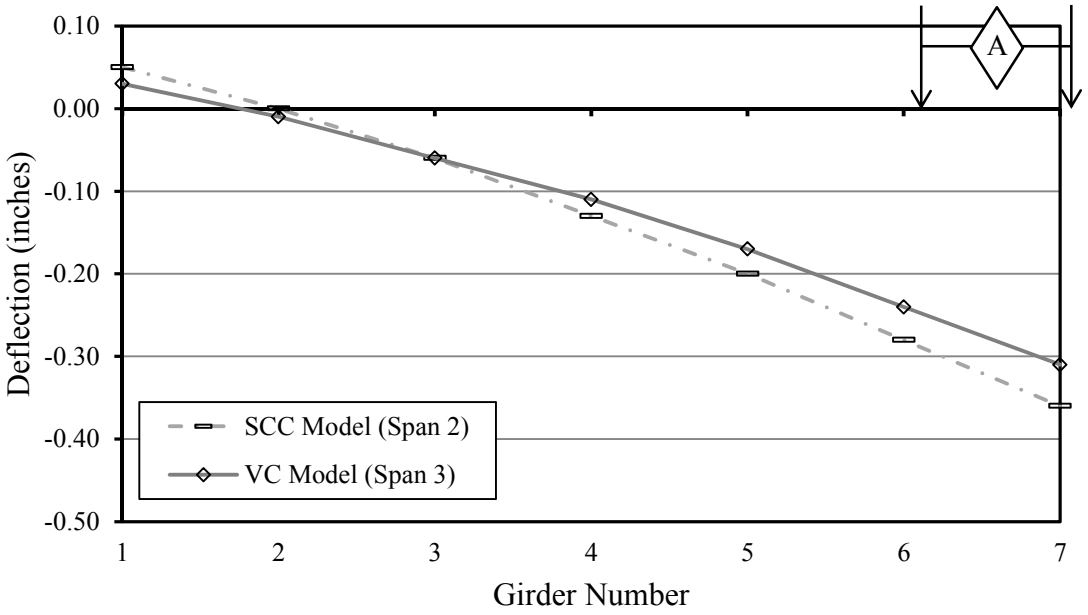

Figure D-18. *Deflection results from load-truck position A on spans with BT-72 girders.*

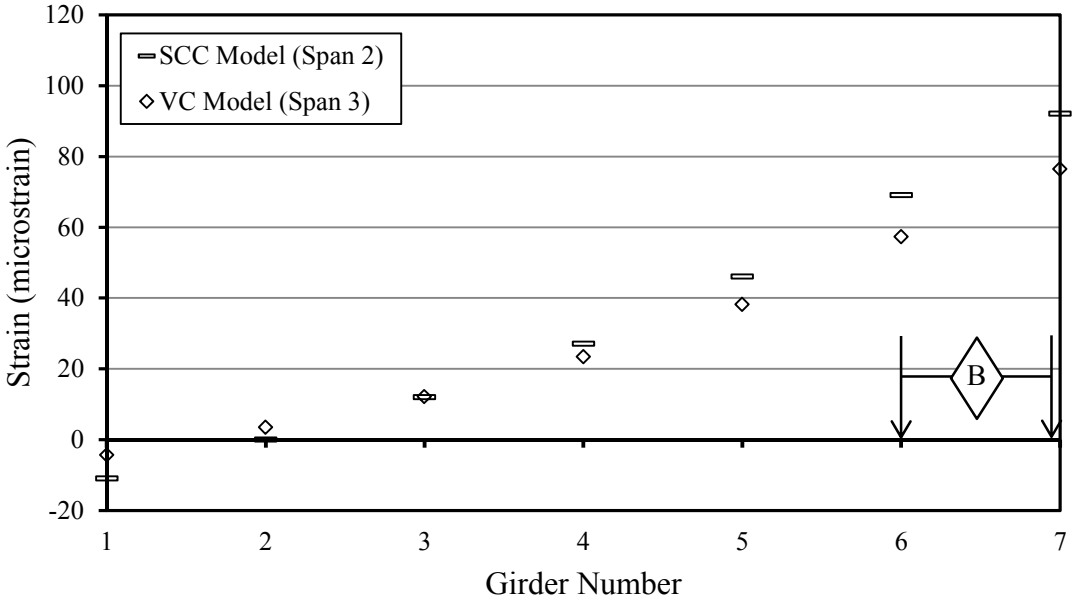

Figure D-19. *Strain results from load-truck-position B on spans with BT-72 girders.*

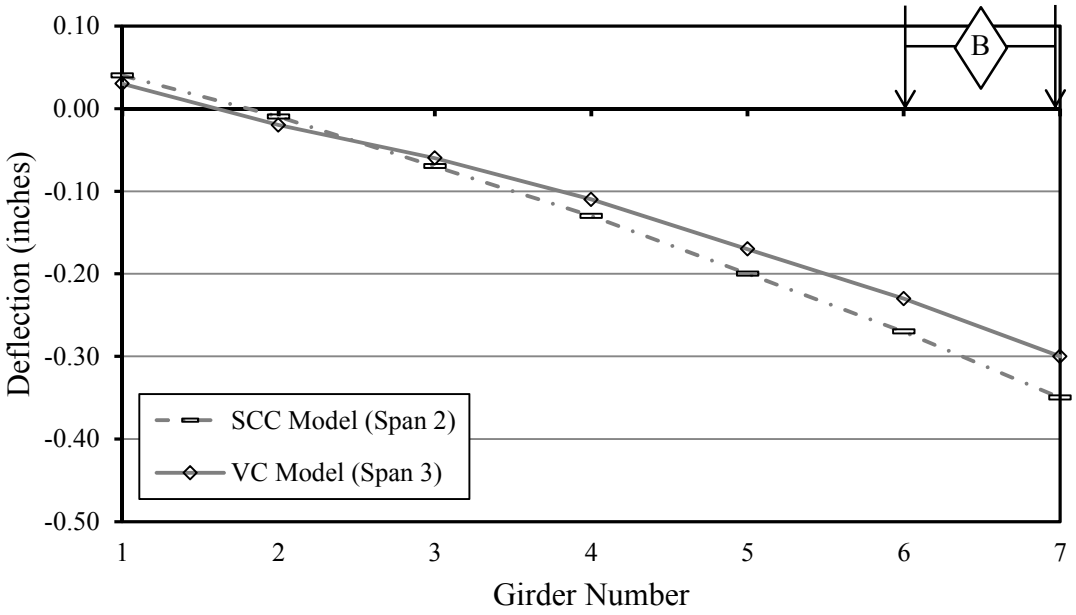

Figure D-20. *Deflection results from load-truck position B on spans with BT-72 girders.*

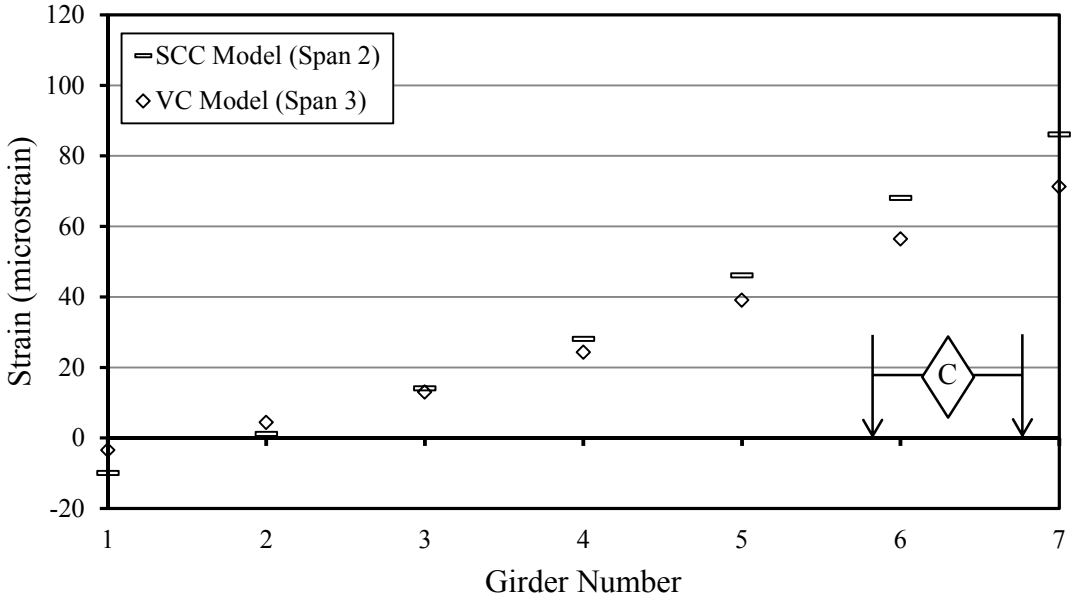

Figure D-21. *Strain results from load-truck-position C on spans with BT-72 girders.*

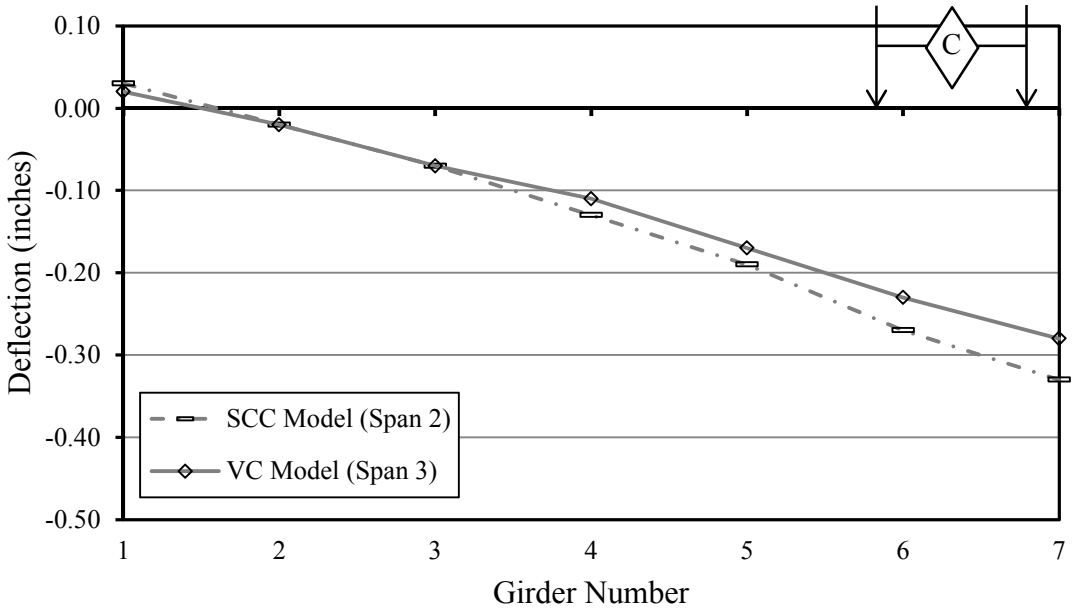

Figure D-22. *Deflection results from load-truck position C on spans with BT-72 girders.*

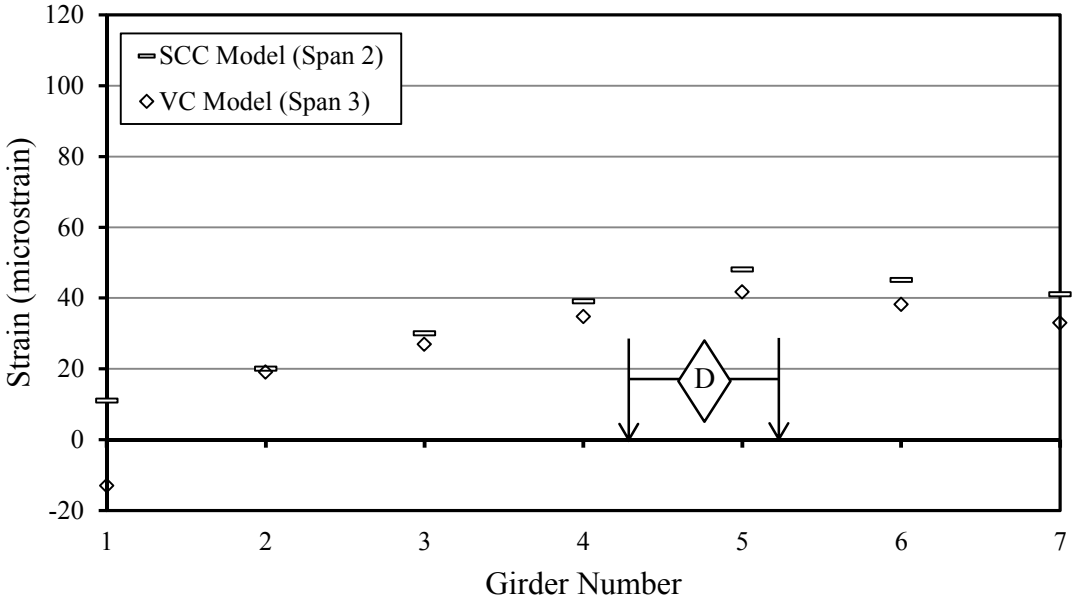

Figure D-23. *Strain results from load-truck-position D on spans with BT-72 girders.*

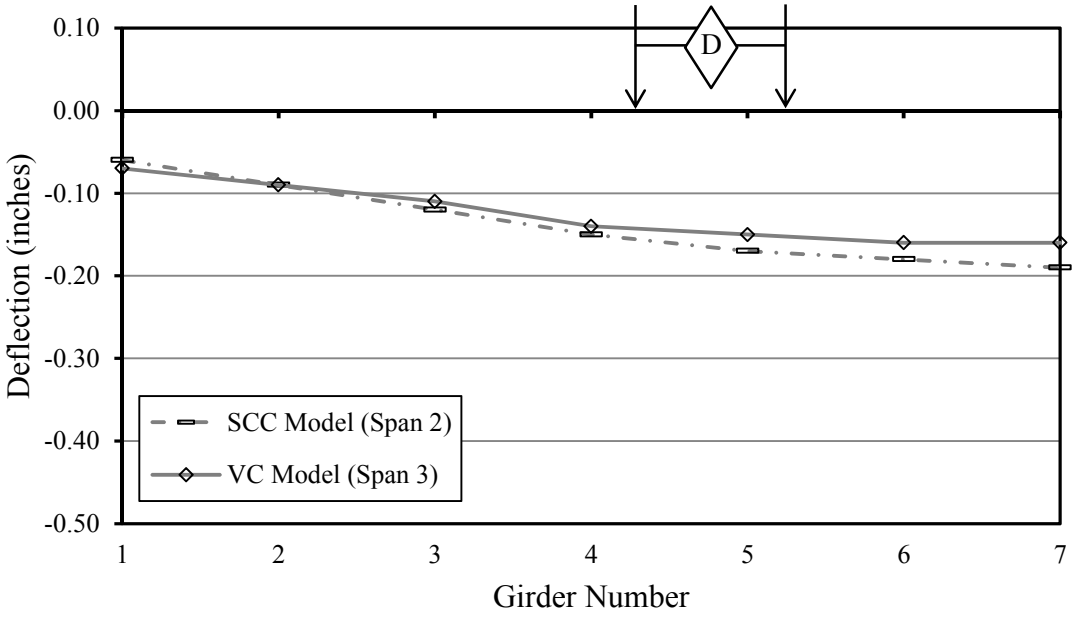

Figure D-24. *Deflection results from load-truck position D on spans with BT-72 girders.*

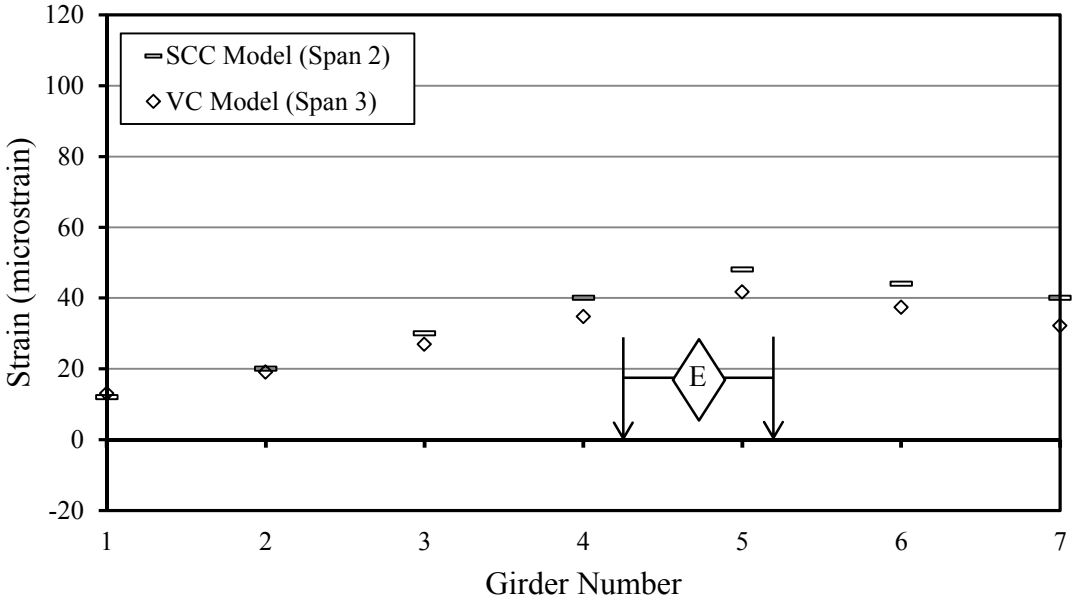

Figure D-25. *Strain results from load-truck-position E on spans with BT-72 girders.*

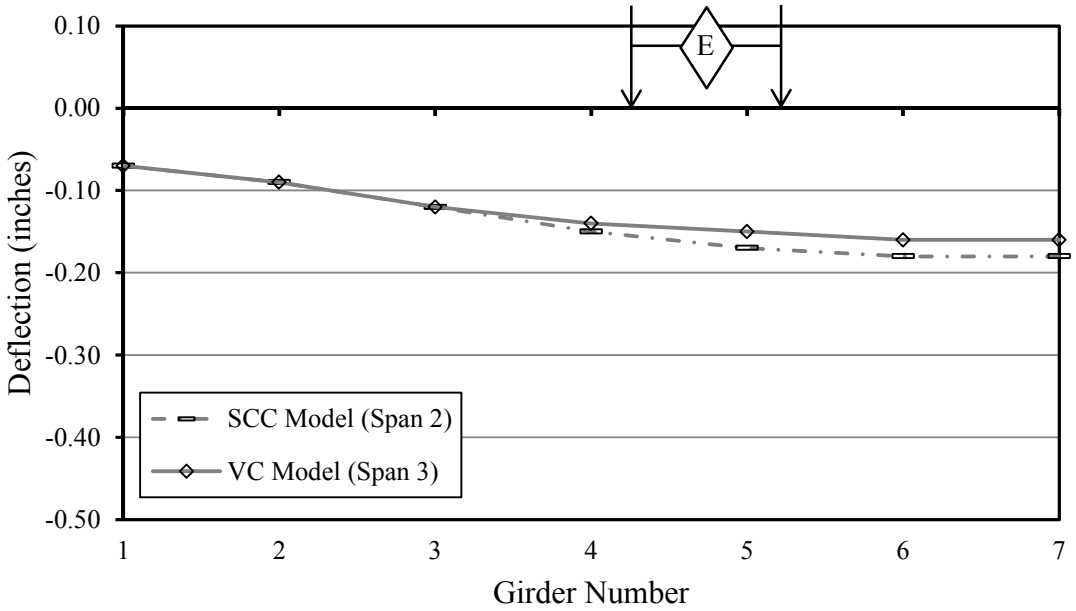

Figure D-26. *Deflection results from load-truck position E on spans with BT-72 girders.*

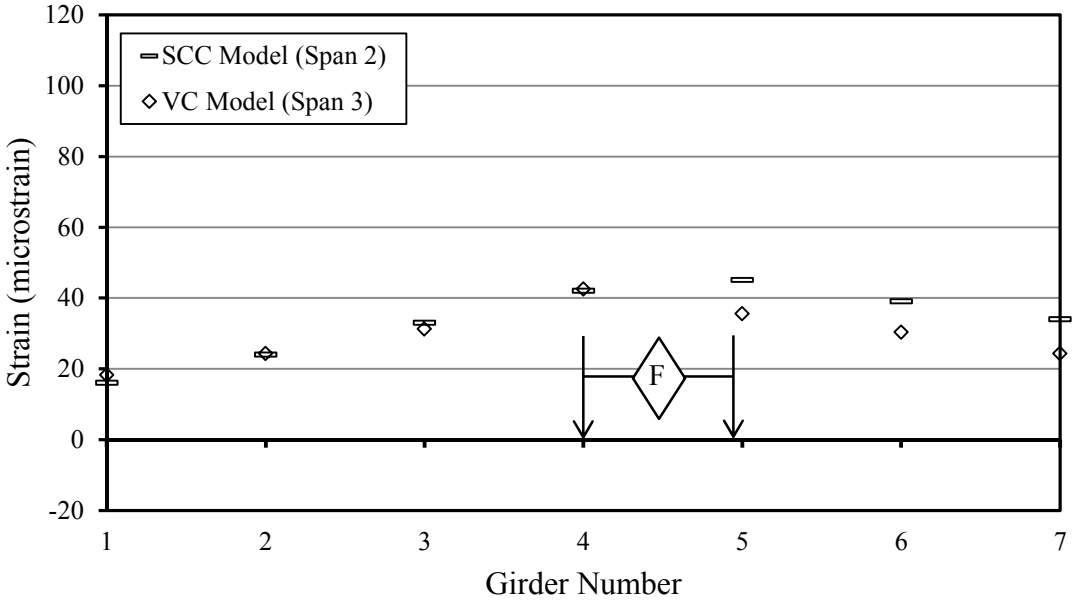

Figure D-27. *Strain results from load-truck-position F on spans with BT-72 girders.*

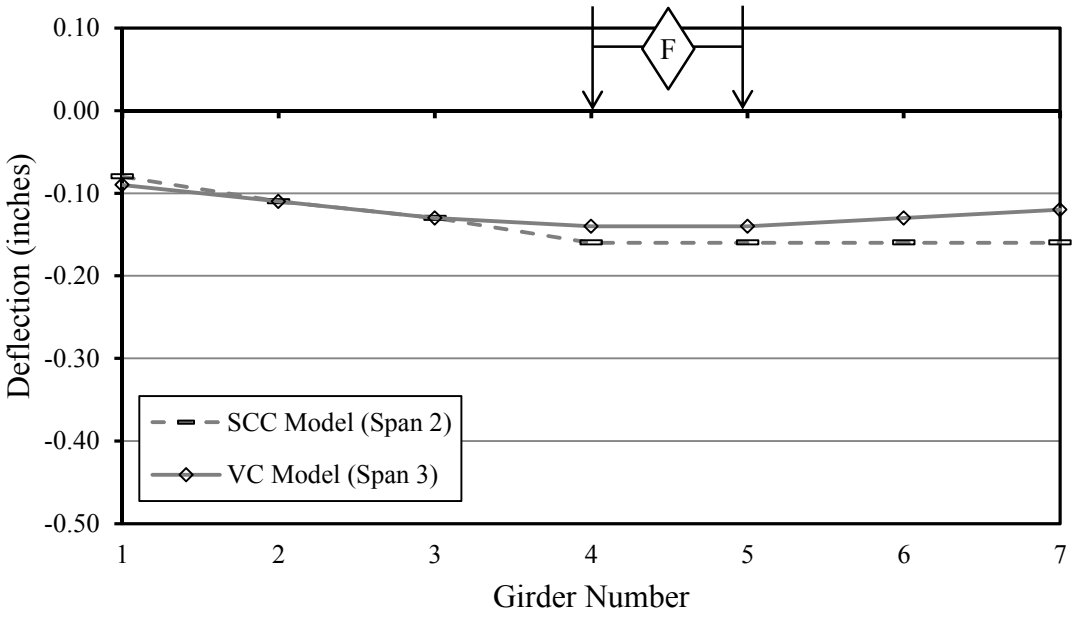

Figure D-28. *Deflection results from load-truck position F on spans with BT-72 girders.*

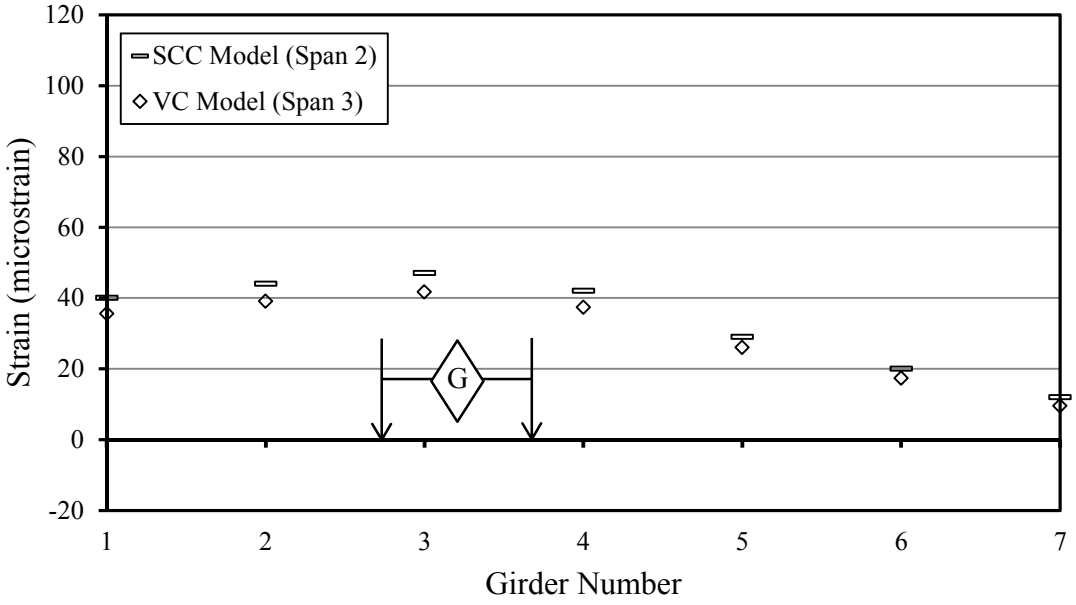

Figure D-29. *Strain results from load-truck-position G on spans with BT-72 girders.*

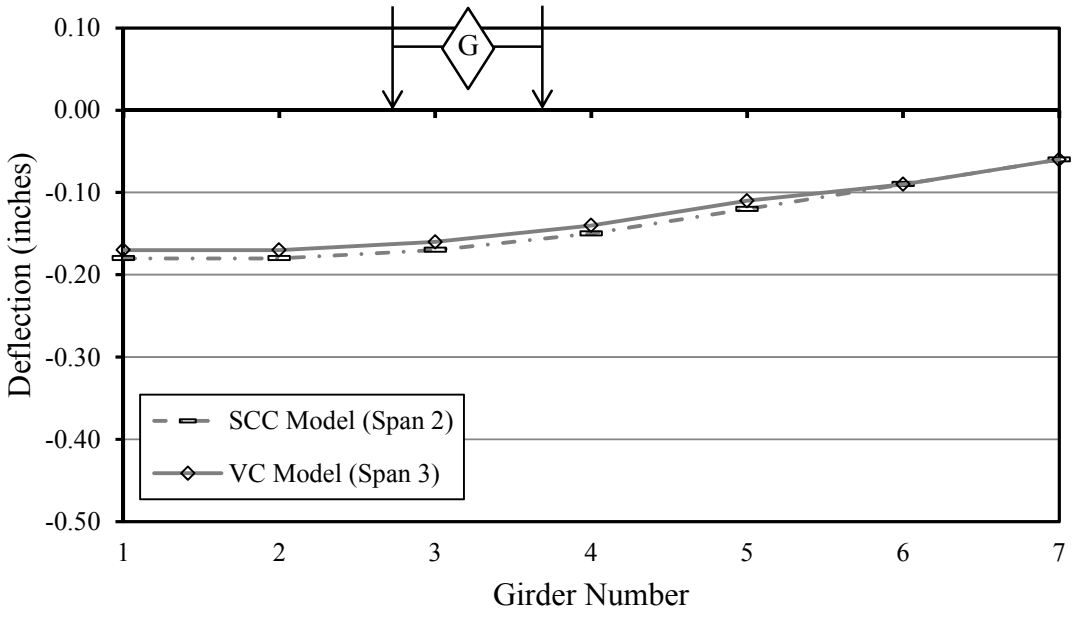

Figure D-30. *Deflection results from load-truck position G on spans with BT-72 girders.*

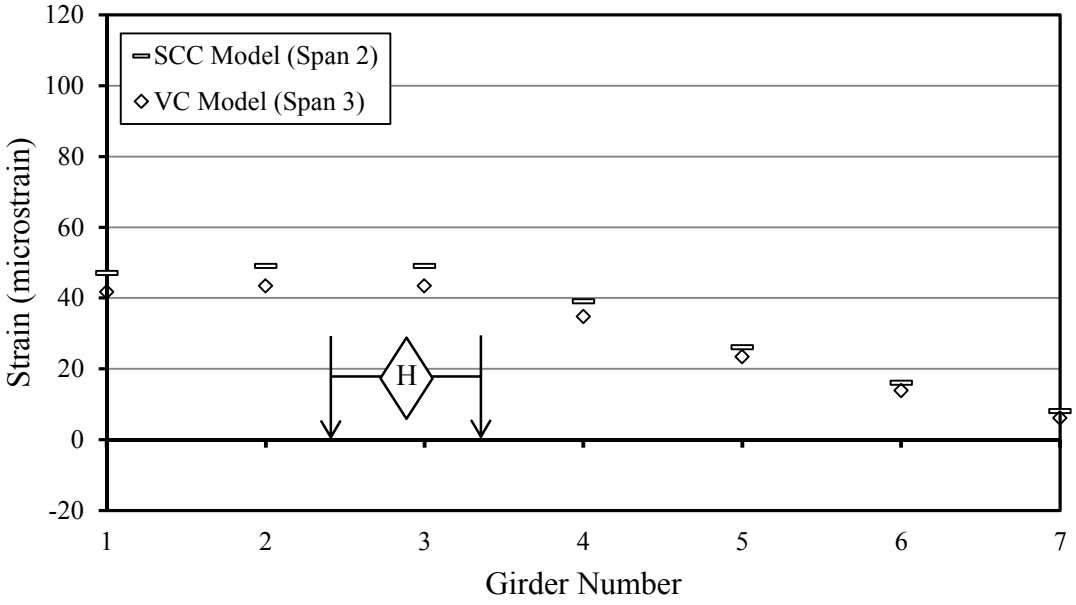

Figure D-31. *Strain results from load-truck-position H on spans with BT-72 girders.*

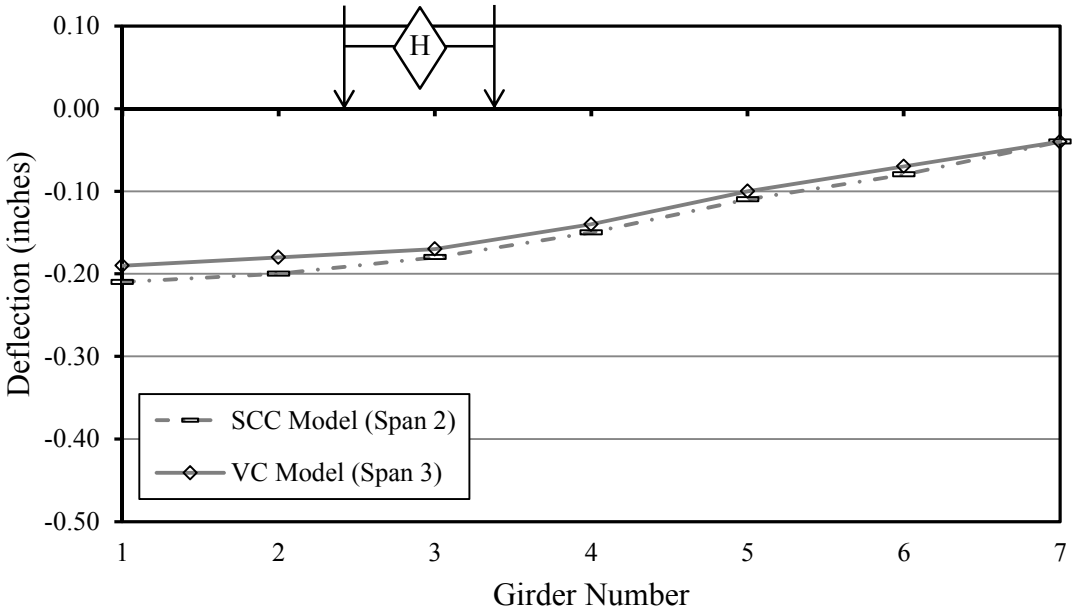

Figure D-32. *Deflection results from load-truck position H on spans with BT-72 girders.*

Appendix E:

CSiBridge Model with Simplified Webwalls but without Barriers Results—Strains and Deflections

Table E-1. *CSiBridge modeler analysis results for spans 1 and 4 of the bridge model with staggered webwalls but without barriers.*

	S1 G1		**S1 G2**		**S1 G3**		**S1 G4**		**S1 G5**		**S1 G6**		**S1 G7**	
Load Truck Position	SCC													
	Defl.	Strain	Defl.	Strain	Defl.	Strain	Defl.	Strain	Defl.	Strain	Defl.	Strain	Defl.	Strain
	in.	με	in.	με	in.	με	in.	με	in.	με	in.	με	in.	με
A	0.05	-20	0.00	-2	-0.05	15	-0.10	33	-0.16	55	-0.22	77	-0.29	98
B	0.04	-18	0.00	0	-0.05	16	-0.10	34	-0.16	54	-0.22	74	-0.28	96
C	0.03	-15	-0.01	2	-0.05	17	-0.10	35	-0.16	54	-0.21	71	-0.27	92
D	-0.05	14	-0.07	24	-0.10	33	-0.12	40	-0.14	43	-0.14	48	-0.15	52
E	-0.05	15	-0.07	25	-0.10	34	-0.12	40	-0.14	43	-0.14	47	-0.15	51
F	-0.06	21	-0.08	29	-0.10	36	-0.12	39	-0.13	42	-0.13	44	-0.13	44
G	-0.14	51	-0.14	49	-0.13	43	-0.12	39	-0.10	33	-0.07	25	-0.05	15
H	-0.17	60	-0.16	53	-0.14	45	-0.12	37	-0.09	30	-0.06	20	-0.03	9
	S 4 G1		**S 4 G2**		**S 4 G3**		**S4 G4**		**S4 G5**		**S4 G6**		**S4 G7**	
Load Truck Position	VC													
	Defl.	Strain	Defl.	Strain	Defl.	Strain	Defl.	Strain	Defl.	Strain	Defl.	Strain	Defl.	Strain
	in.	με	in.	με	in.	με	in.	με	in.	με	in.	με	in.	με
A	0.05	-22	0.01	-4	-0.04	12	-0.09	31	-0.15	51	-0.22	73	-0.29	94
B	0.05	-20	0.00	-3	-0.04	13	-0.09	31	-0.15	51	-0.21	70	-0.28	92
C	0.04	-17	0.00	0	-0.05	15	-0.10	32	-0.15	50	-0.21	67	-0.26	88
D	-0.04	12	-0.07	22	-0.09	31	-0.11	36	-0.13	40	-0.14	45	-0.14	49
E	-0.04	13	-0.07	23	-0.09	31	-0.11	36	-0.13	40	-0.14	44	-0.14	48
F	-0.06	19	-0.08	27	-0.10	34	-0.12	36	-0.12	39	-0.12	41	-0.12	41
G	-0.14	49	-0.14	46	-0.13	40	-0.11	36	-0.09	31	-0.07	22	-0.05	12
H	-0.16	57	-0.15	50	-0.14	42	-0.11	34	-0.08	28	-0.05	18	-0.03	6

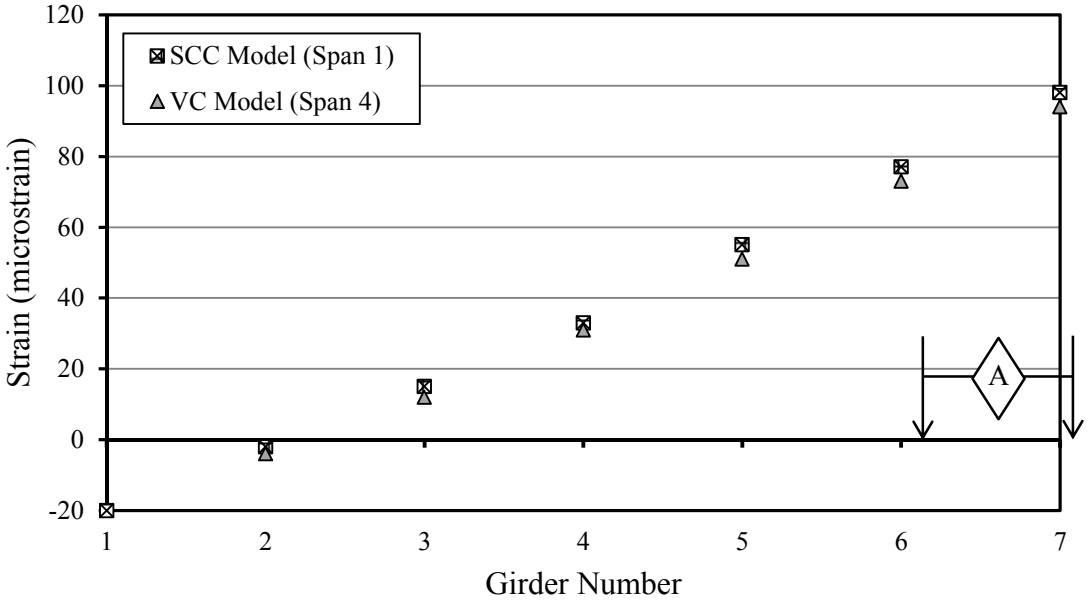

Figure E-1. *Strain results from load-truck-position A on spans with BT-54 girders.*

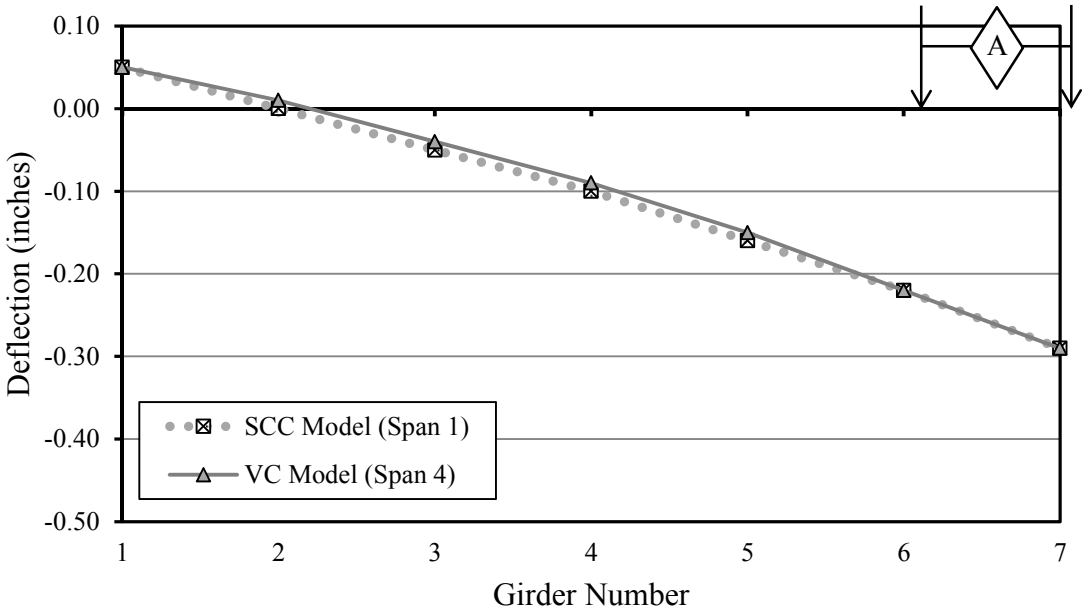

Figure E-2. *Deflection results from load-truck position A on spans with BT-54 girders.*

Figure E-3. *Strain results from load-truck-position B on spans with BT-54 girders.*

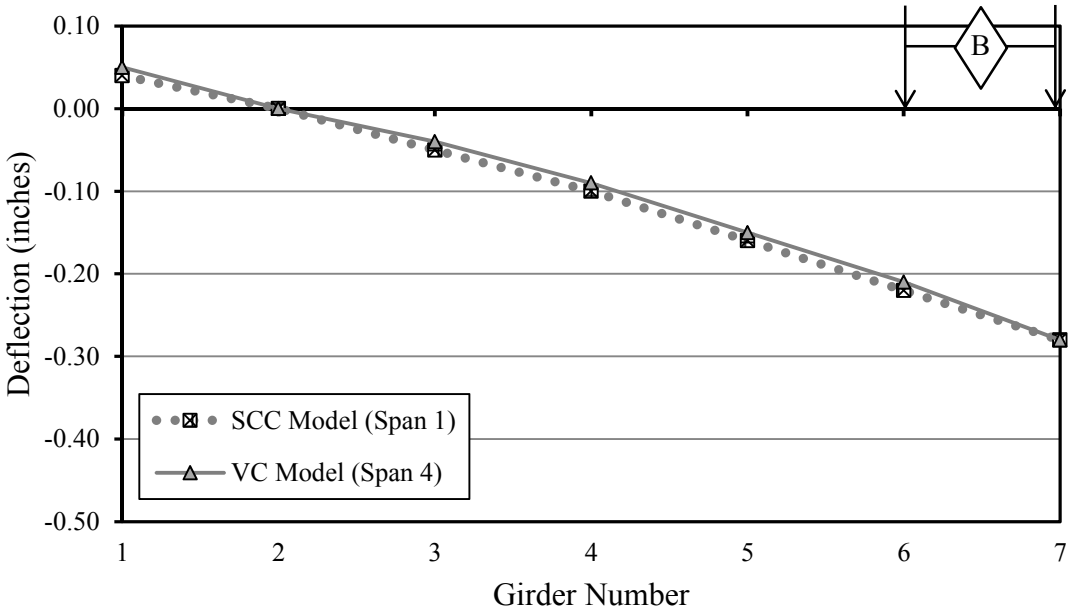

Figure E-4. *Deflection results from load-truck position B on spans with BT-54 girders.*

Figure E-5. *Strain results from load-truck-position C on spans with BT-54 girders.*

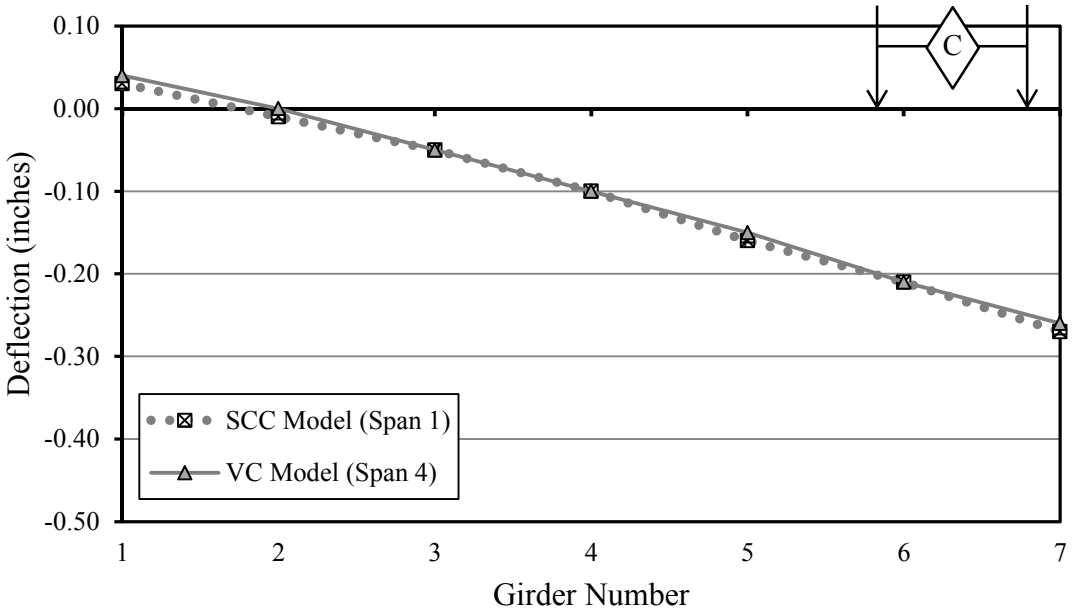

Figure E-6. *Deflection results from load-truck position C on spans with BT-54 girders.*

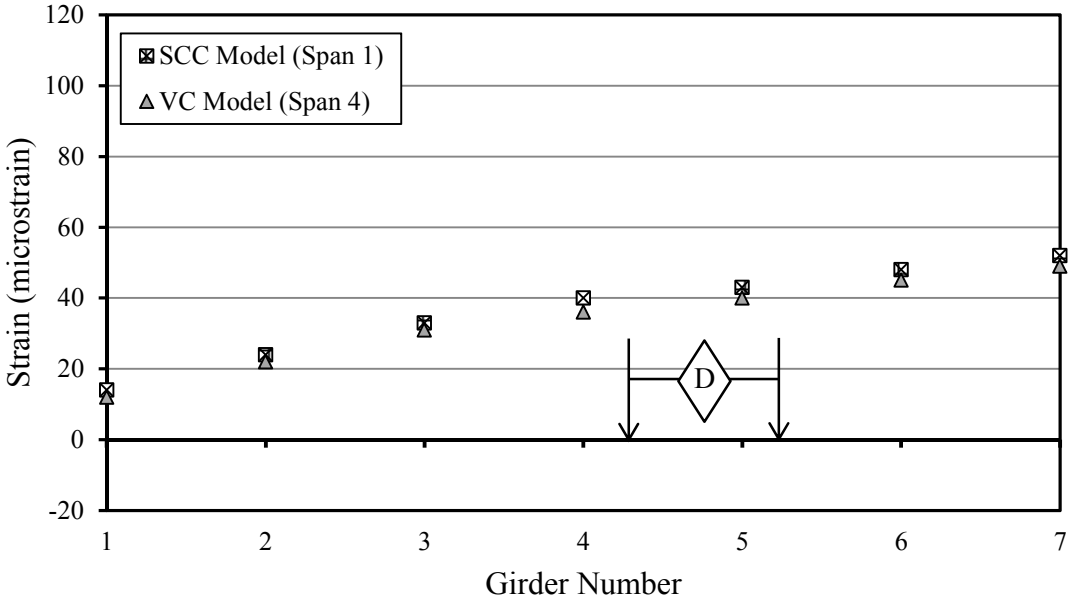

Figure E-7. *Strain results from load-truck-position D on spans with BT-54 girders.*

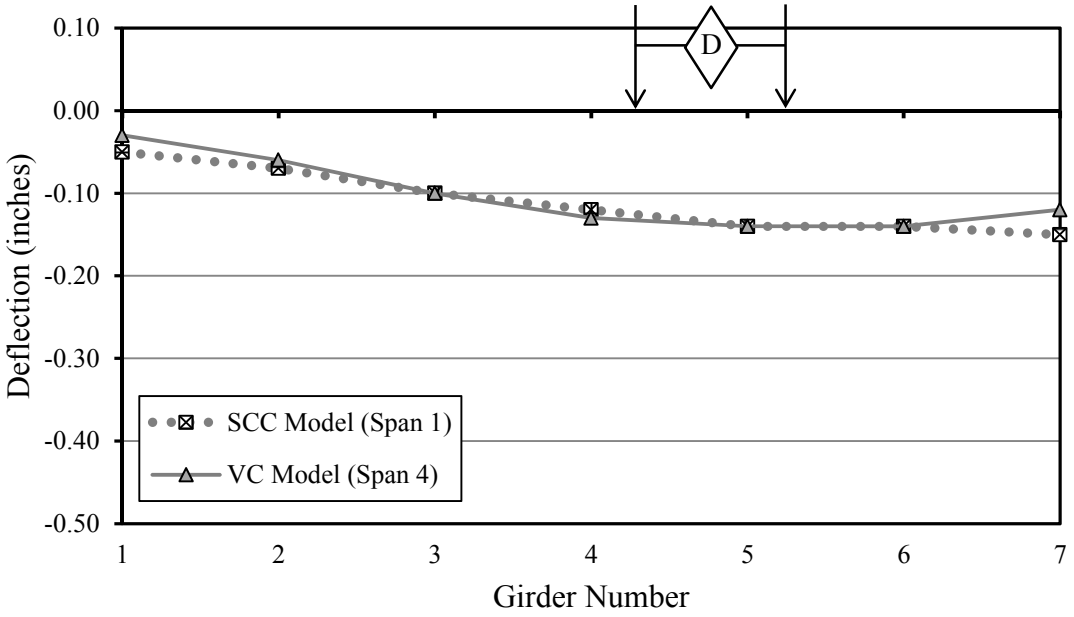

Figure E-8. *Deflection results from load-truck position D on spans with BT-54 girders.*

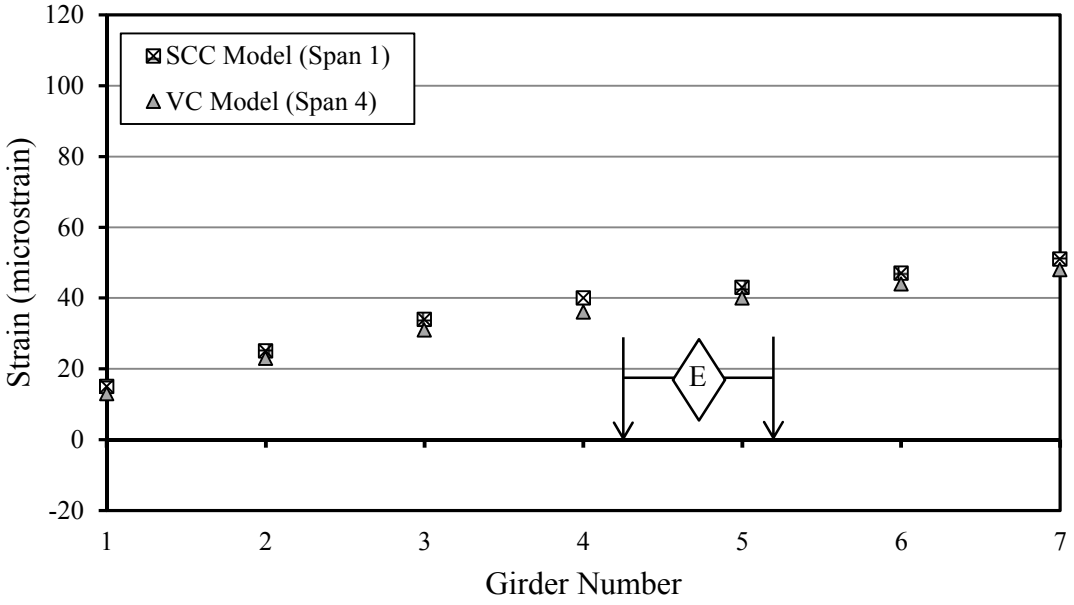

Figure E-9. *Strain results from load-truck-position E on spans with BT-54 girders.*

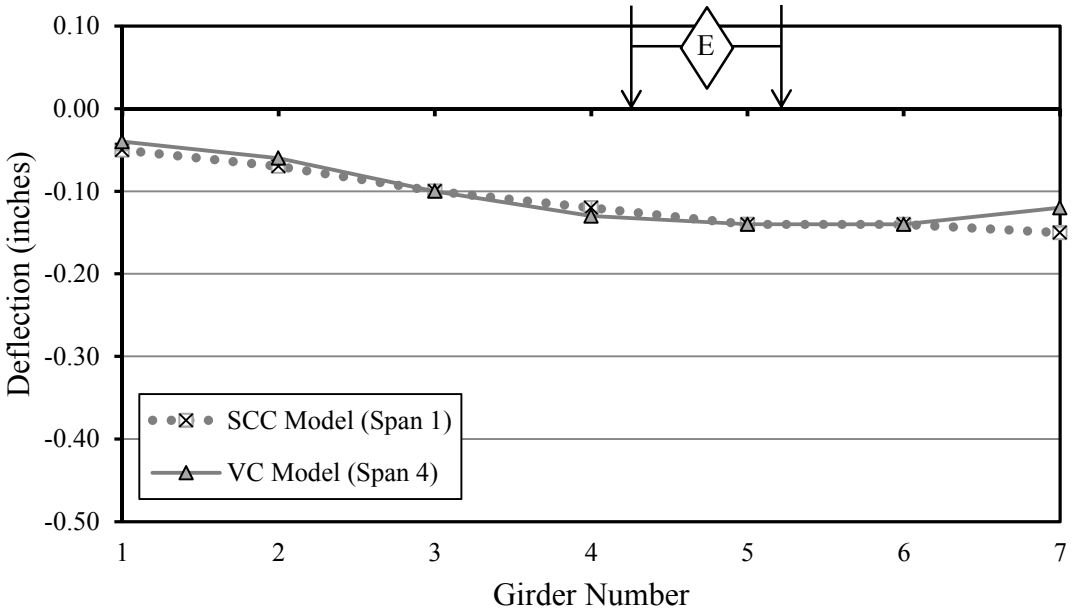

Figure E-10. *Deflection results from load-truck position E on spans with BT-54 girders.*

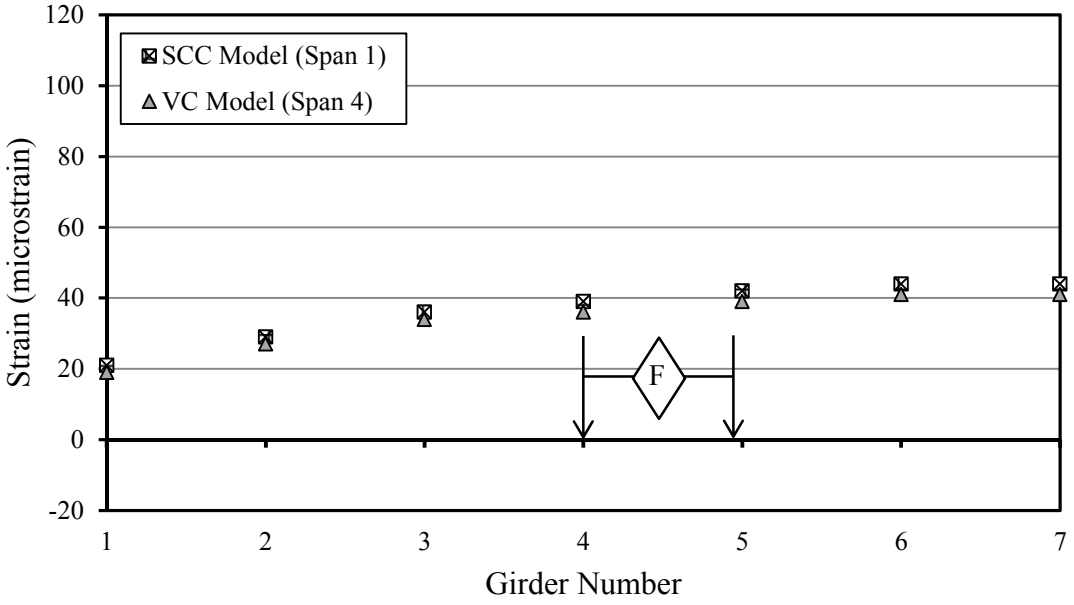

Figure E-11. *Strain results from load-truck-position F on spans with BT-54 girders.*

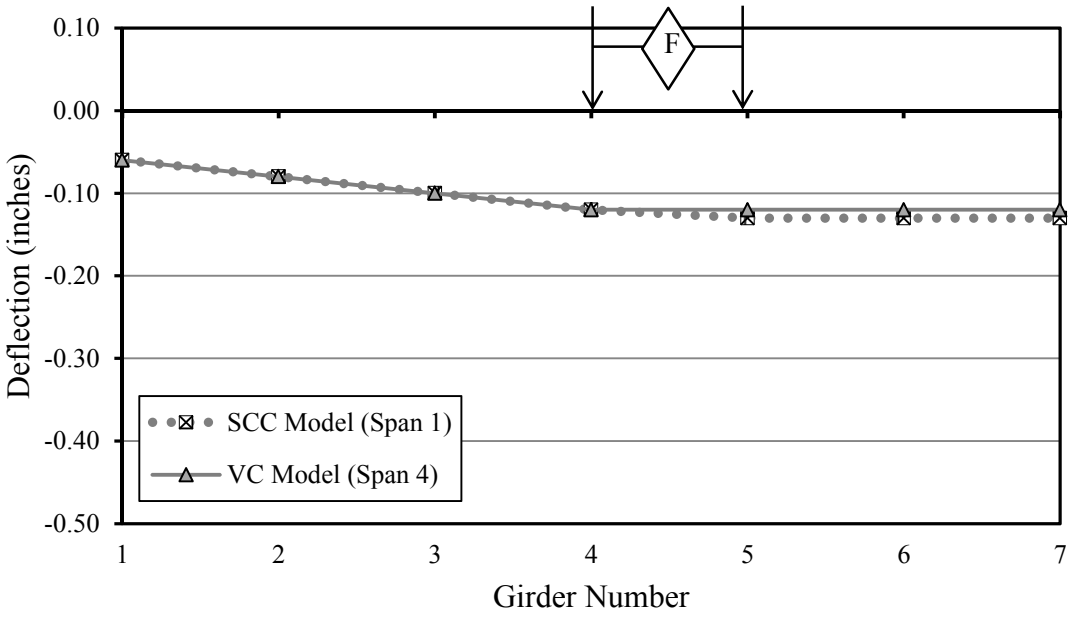

Figure E-12. *Deflection results from load-truck position F on spans with BT-54 girders.*

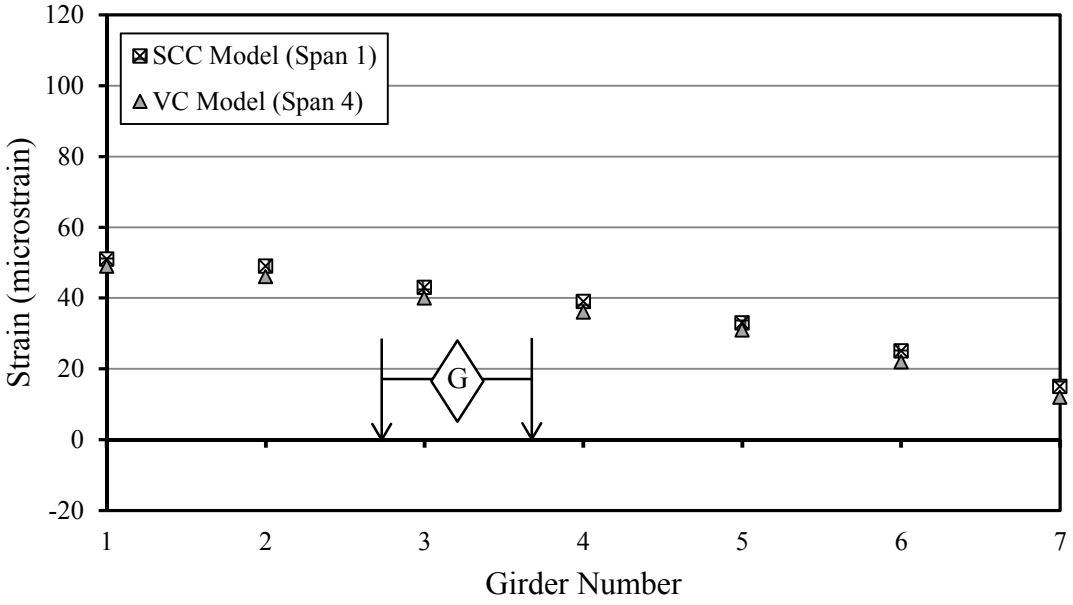

Figure E-13. *Strain results from load-truck-position G on spans with BT-54 girders.*

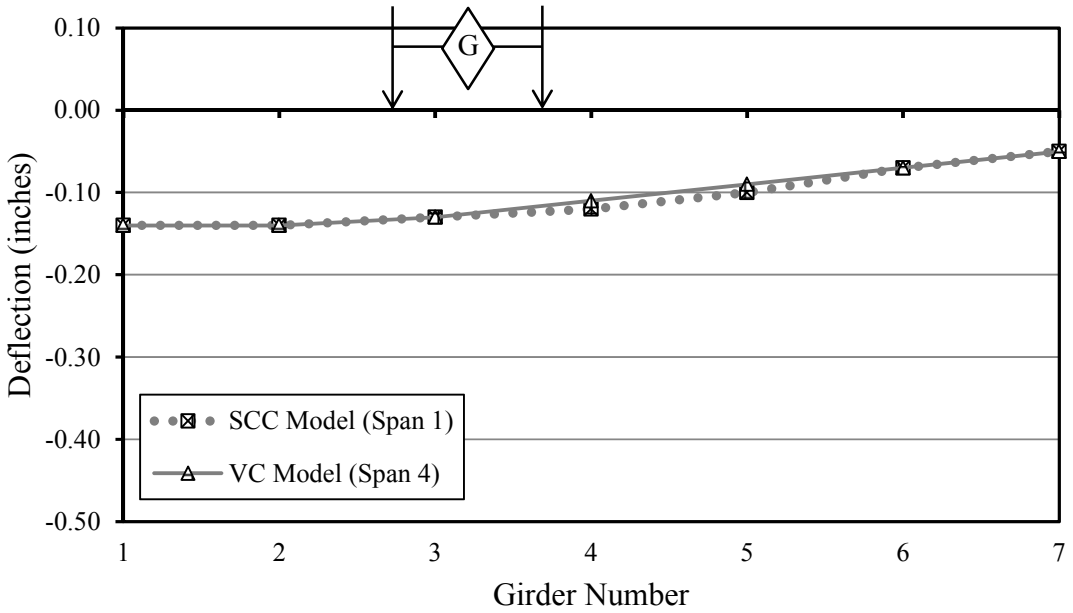

Figure E-14. *Deflection results from load-truck position G on spans with BT-54 girders.*

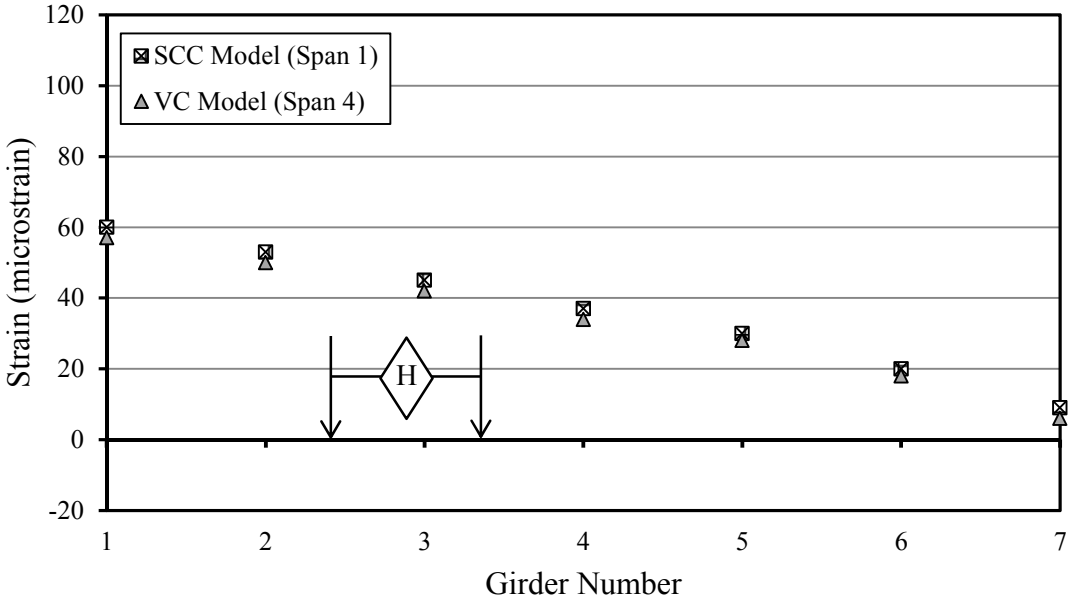

Figure E-15. *Strain results from load-truck-position H on spans with BT-54 girders.*

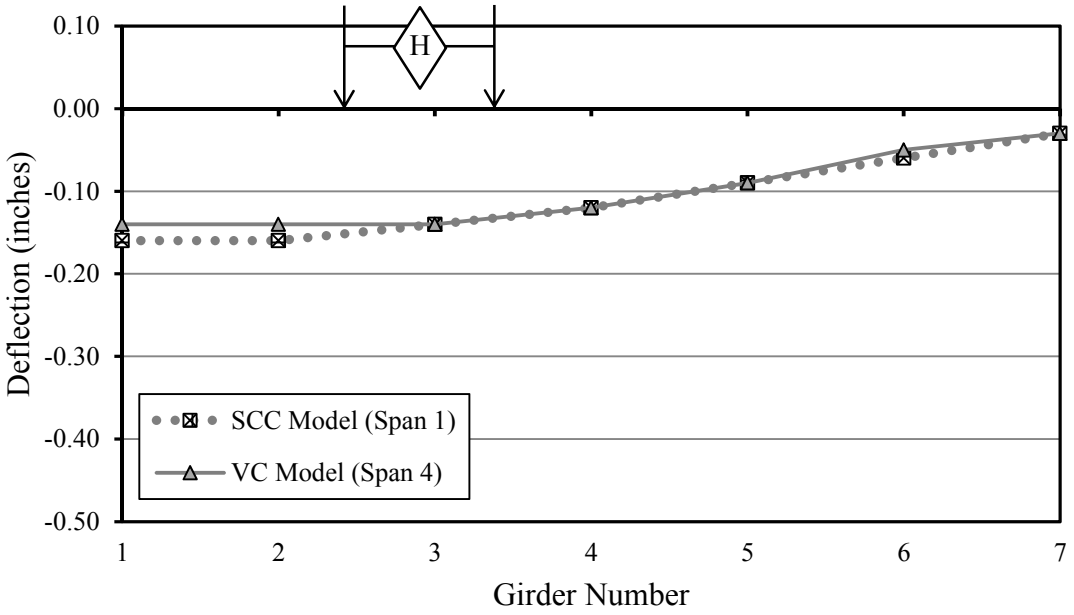

Figure E-16. *Deflection results from load-truck position H on spans with BT-54 girders.*

Table E-2. *CSiBridge modeler analysis results for spans 1 and 4 of the bridge model with staggered webwalls but without barriers.*

	S2 G1		**S2 G2**		**S2 G3**		**S2 G4**		**S2 G5**		**S2 G6**		**S2 G7**	
Load Truck Position	SCC													
	Defl.	Strain	Defl.	Strain	Defl.	Strain	Defl.	Strain	Defl.	Strain	Defl.	Strain	Defl.	Strain
	in.	με	in.	με	in.	με	in.	με	in.	με	in.	με	in.	με
A	0.07	-20	0.00	-3	-0.07	14	-0.13	31	-0.21	51	-0.28	71	-0.36	92
B	0.06	-18	0.00	-1	-0.07	15	-0.14	32	-0.20	50	-0.28	69	-0.35	89
C	0.05	-15	-0.01	0	-0.07	16	-0.14	32	-0.20	50	-0.27	67	-0.33	86
D	-0.07	14	-0.09	22	-0.12	30	-0.14	36	-0.16	41	-0.18	45	-0.20	49
E	-0.07	15	-0.10	22	-0.12	30	-0.14	36	-0.16	41	-0.18	44	-0.20	48
F	-0.09	20	-0.11	26	-0.13	32	-0.14	36	-0.16	40	-0.16	41	-0.17	41
G	-0.20	48	-0.18	45	-0.16	40	-0.14	36	-0.12	30	-0.09	22	-0.07	15
H	-0.22	56	-0.20	50	-0.17	43	-0.14	35	-0.11	27	-0.08	18	-0.05	9
	S3 G1		**S3 G2**		**S3 G3**		**S3 G4**		**S3 G5**		**S3 G6**		**S3 G7**	
Load Truck Position	VC													
	Defl.	Strain	Defl.	Strain	Defl.	Strain	Defl.	Strain	Defl.	Strain	Defl.	Strain	Defl.	Strain
	in.	με	in.	με	in.	με	in.	με	in.	με	in.	με	in.	με
A	0.07	-20	0.01	-4	-0.06	11	-0.12	27	-0.19	45	-0.27	64	-0.34	84
B	0.06	-18	0.00	-3	-0.06	12	-0.12	28	-0.19	45	-0.26	63	-0.33	81
C	0.05	-15	-0.01	0	-0.07	13	-0.13	28	-0.19	44	-0.25	60	-0.31	78
D	-0.06	12	-0.09	19	-0.11	26	-0.13	32	-0.15	37	-0.17	40	-0.18	43
E	-0.07	13	-0.09	20	-0.11	26	-0.13	32	-0.15	37	-0.17	40	-0.18	42
F	-0.09	17	-0.10	23	-0.12	29	-0.13	32	-0.15	35	-0.15	36	-0.16	36
G	-0.18	43	-0.17	41	-0.15	36	-0.13	32	-0.11	26	-0.09	19	-0.06	12
H	-0.21	50	-0.19	45	-0.16	38	-0.13	31	-0.10	24	-0.07	15	-0.04	7

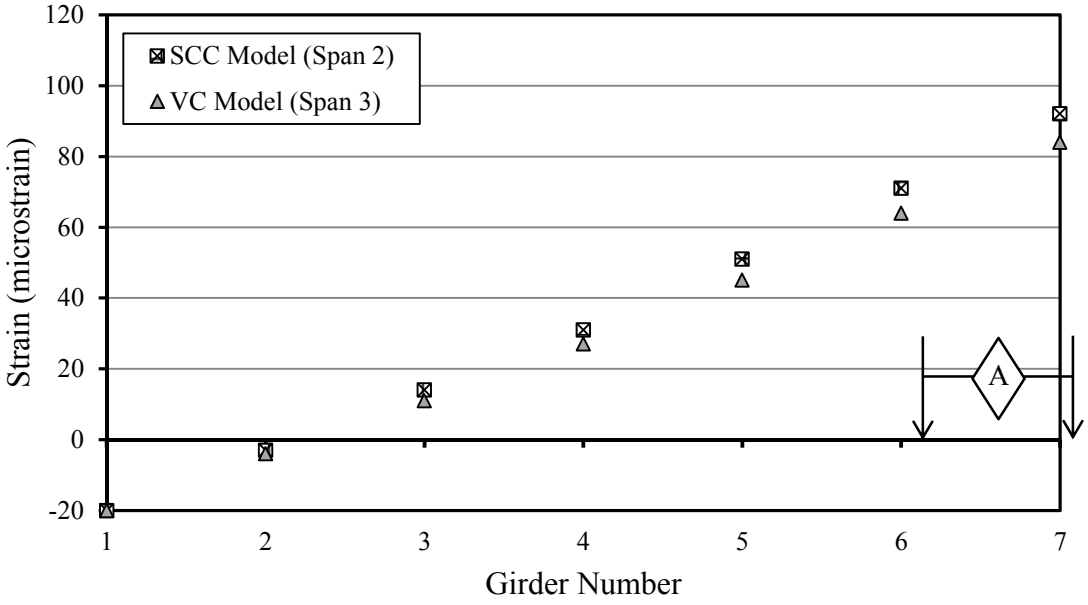

Figure E-17. *Strain results from load-truck-position A on spans with BT-72 girders.*

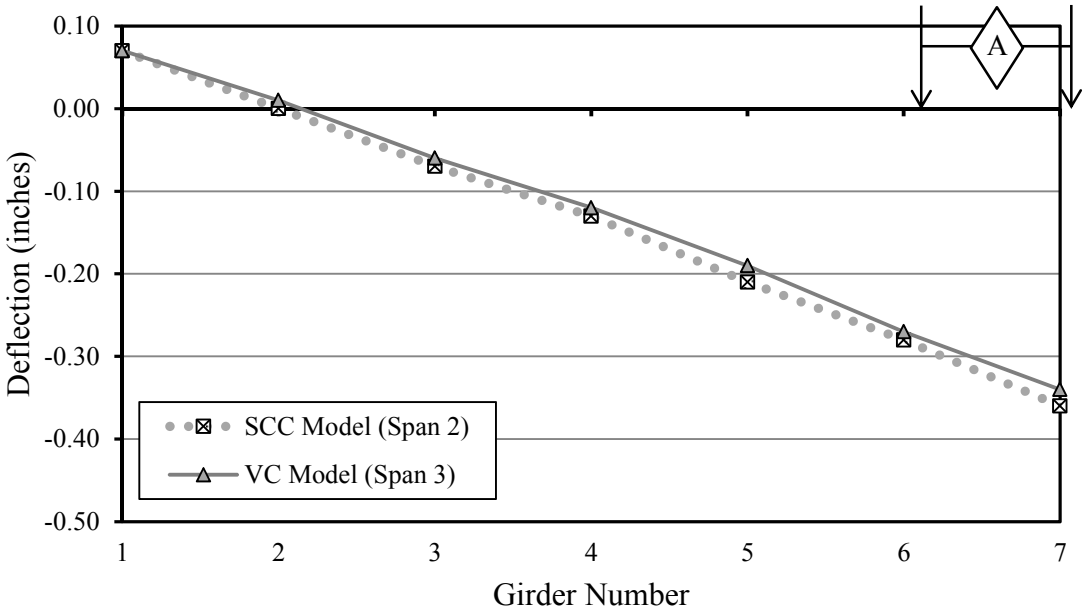

Figure E-18. *Deflection results from load-truck position A on spans with BT-72 girders.*

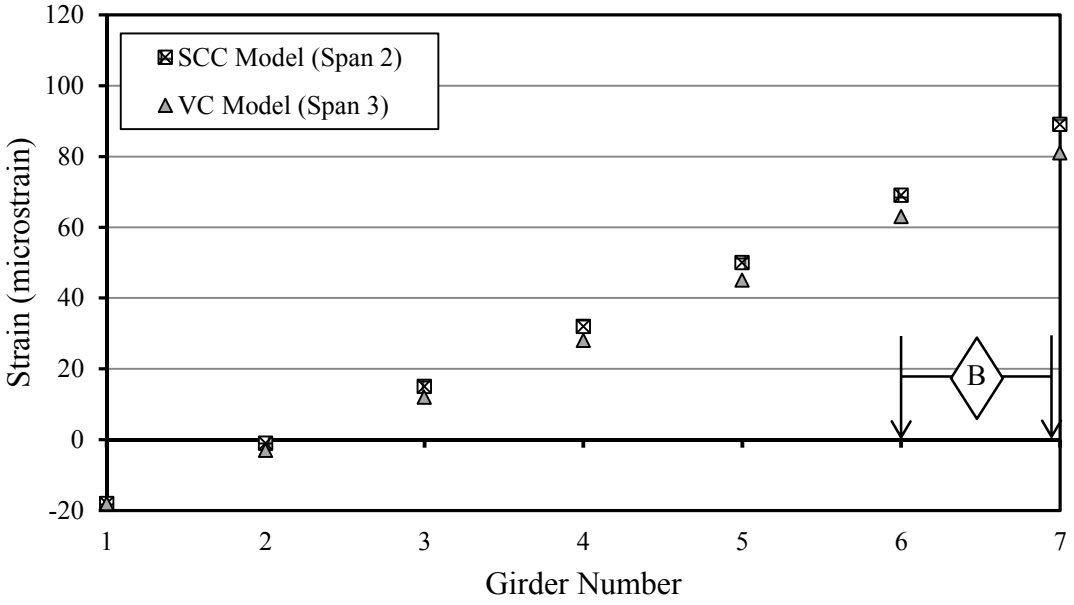

Figure E-19. *Strain results from load-truck-position B on spans with BT-72 girders.*

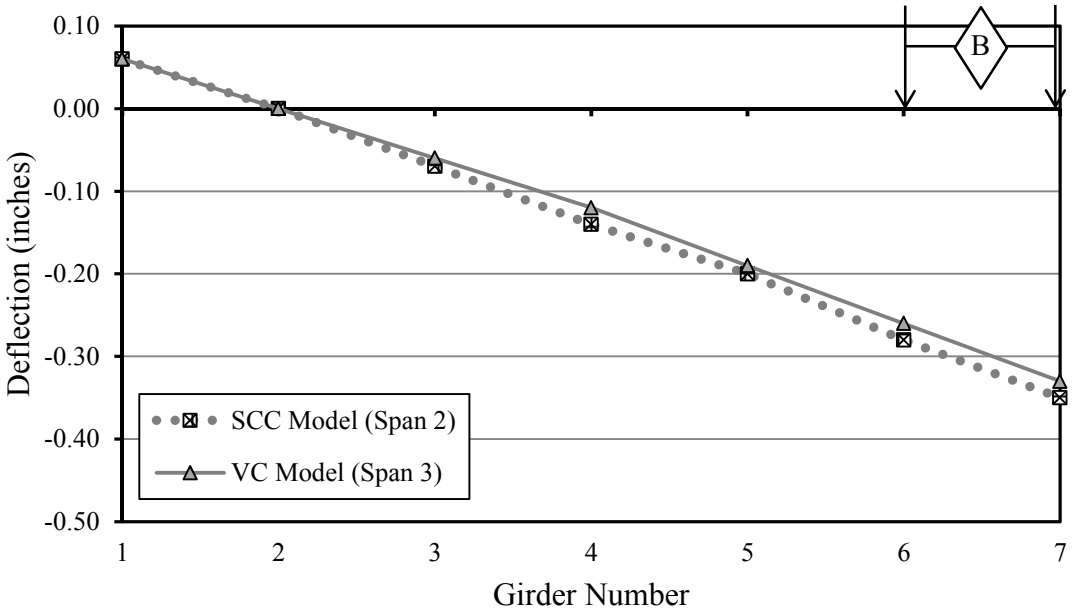

Figure E-20. *Deflection results from load-truck position B on spans with BT-72 girders.*

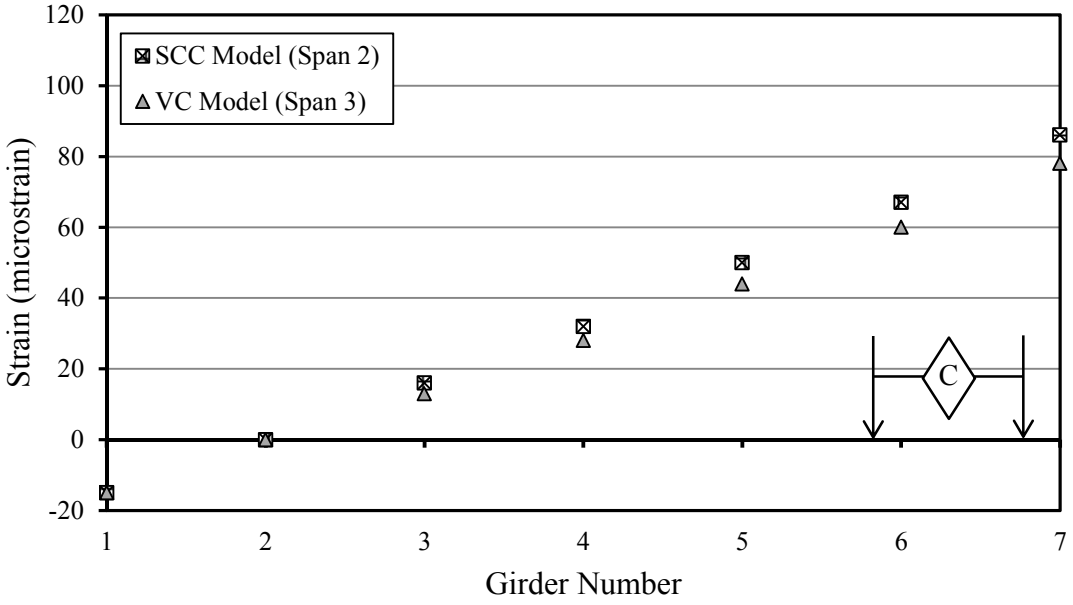

Figure E-21. *Strain results from load-truck-position C on spans with BT-72 girders.*

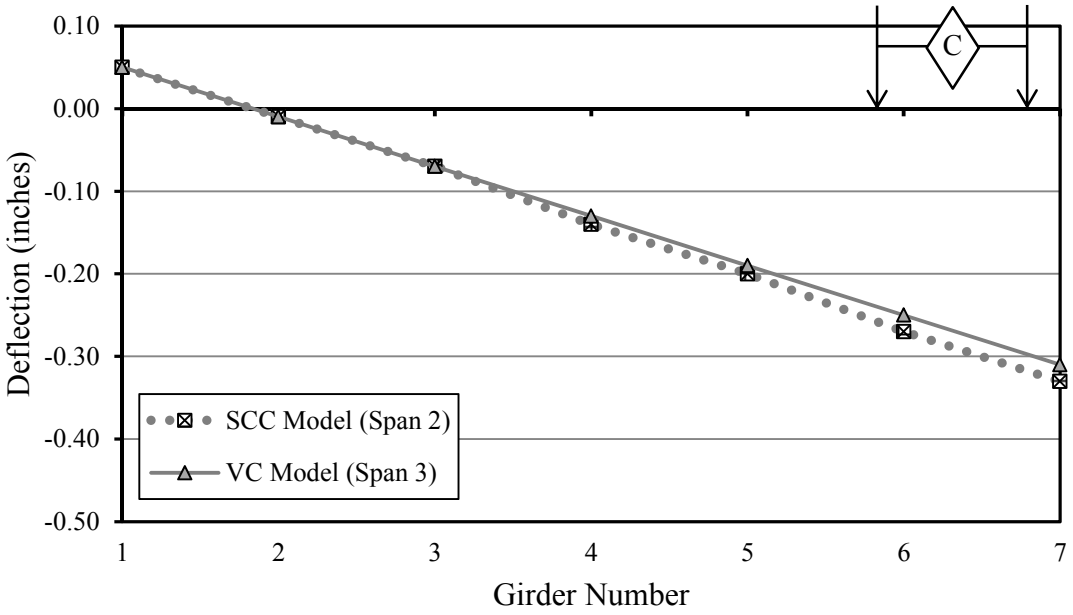

Figure E-22. *Deflection results from load-truck position C on spans with BT-72 girders.*

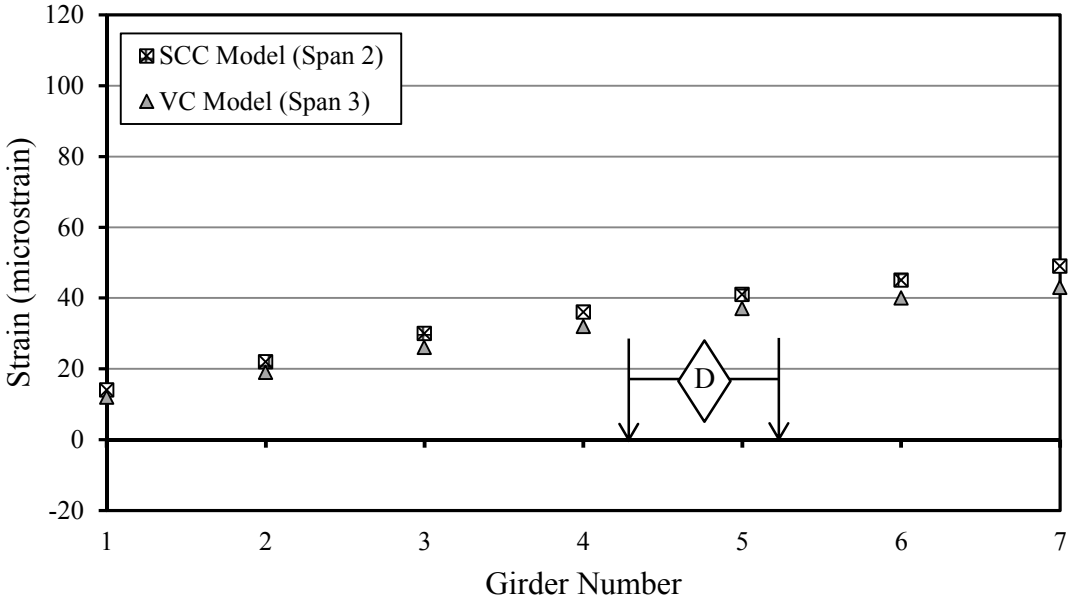

Figure E-23. *Strain results from load-truck-position D on spans with BT-72 girders.*

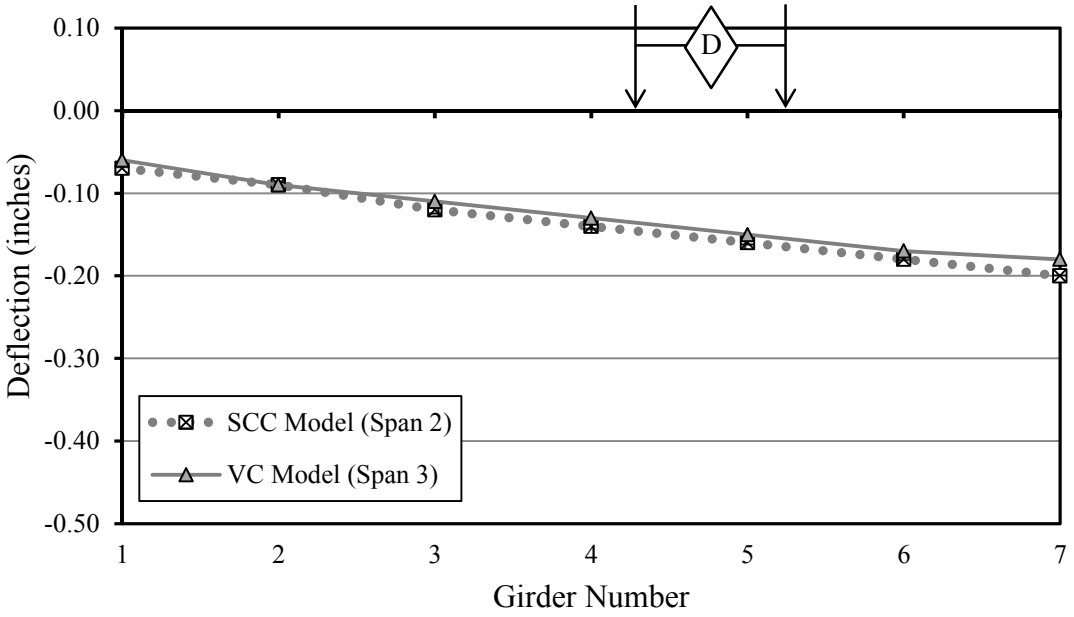

Figure E-24. *Deflection results from load-truck position D on spans with BT-72 girders.*

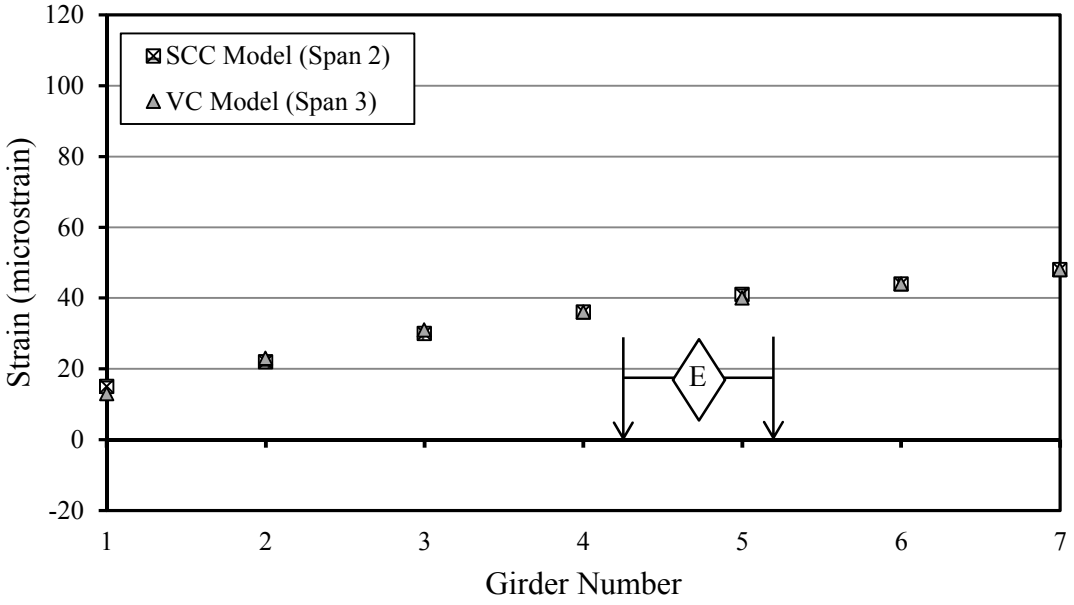

Figure E-25. *Strain results from load-truck-position E on spans with BT-72 girders.*

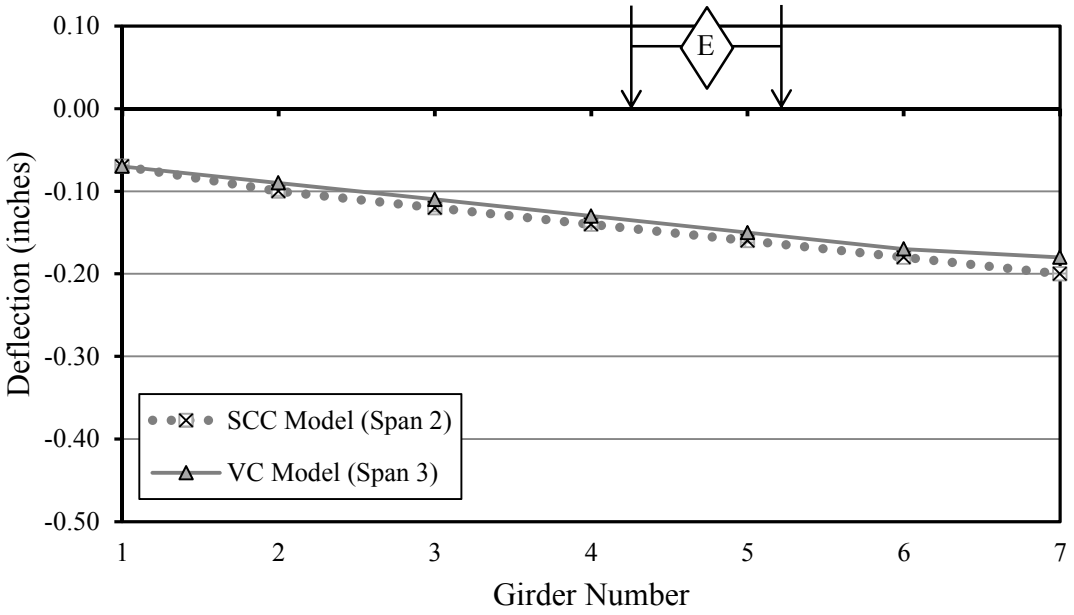

Figure E-26. *Deflection results from load-truck position E on spans with BT-72 girders.*

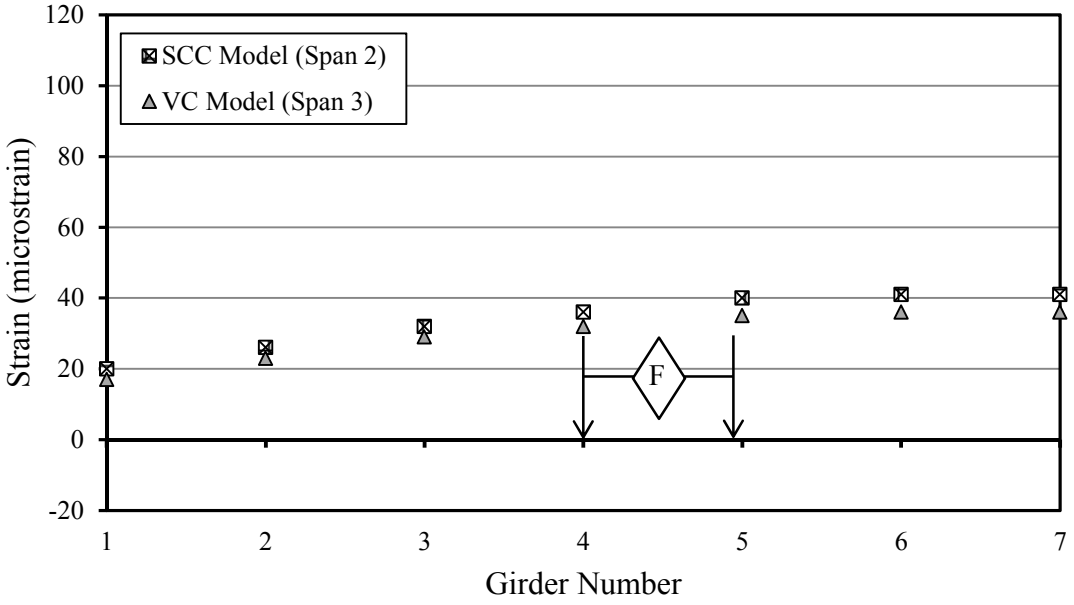

Figure E-27. *Strain results from load-truck-position F on spans with BT-72 girders.*

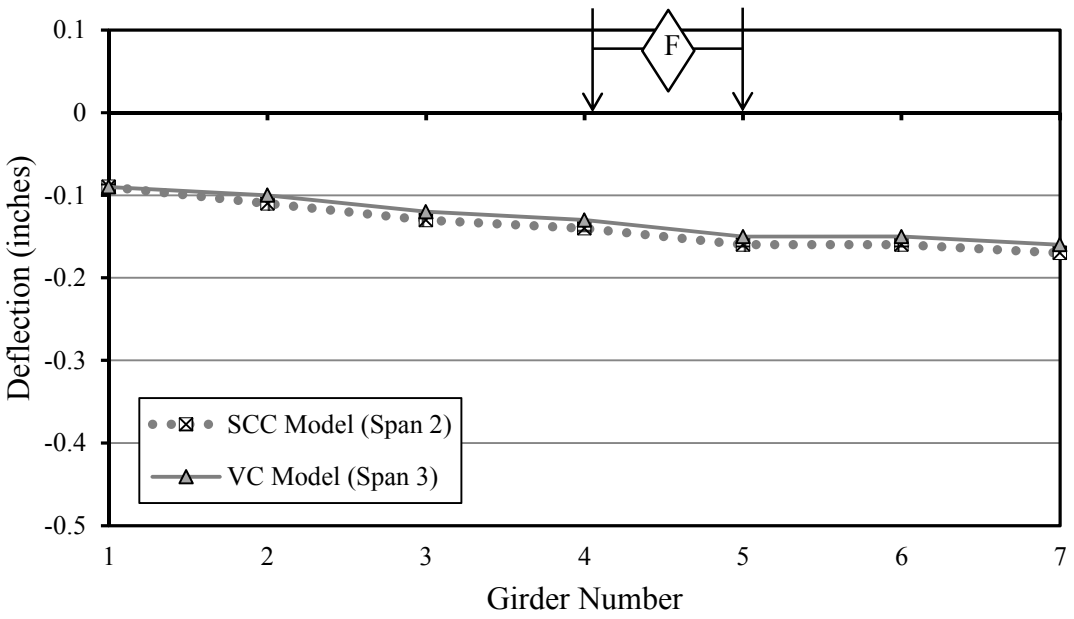

Figure E-28. *Deflection results from load-truck position F on spans with BT-72 girders.*

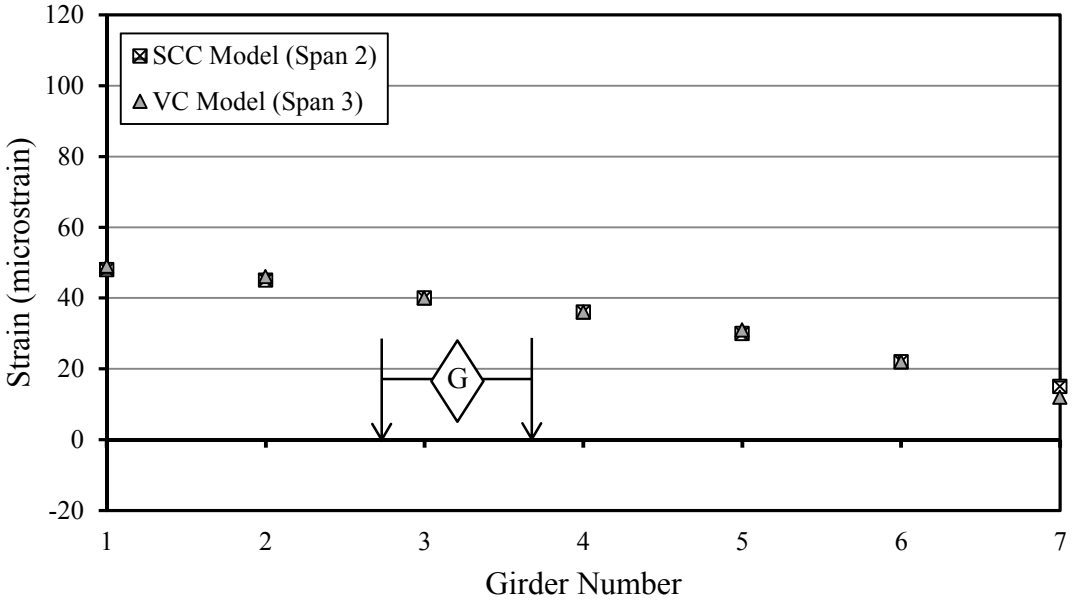

Figure E-29. *Strain results from load-truck-position G on spans with BT-72 girders.*

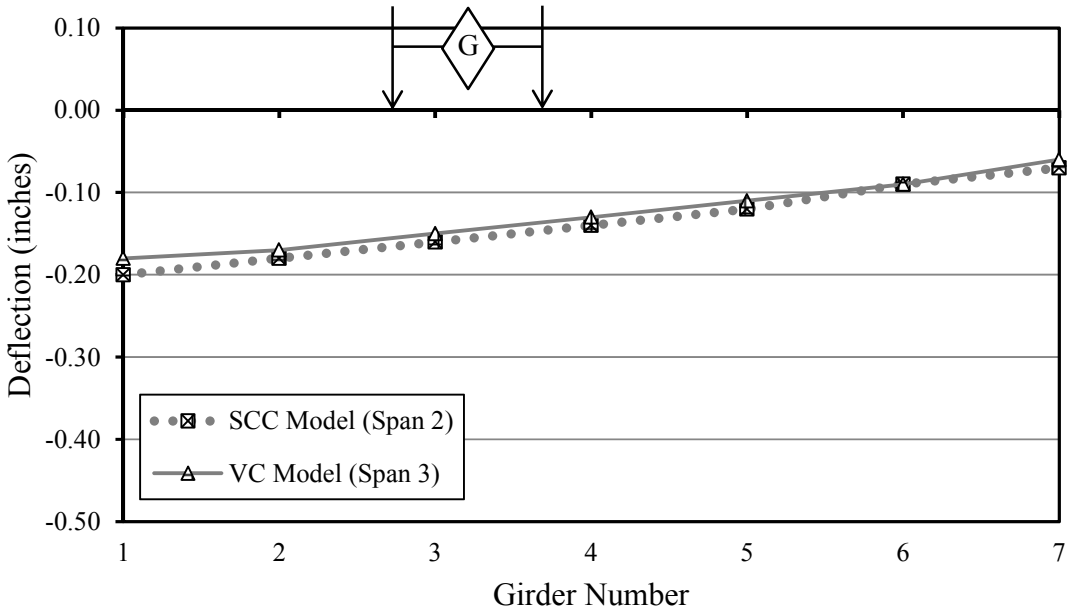

Figure E-30. *Deflection results from load-truck position G on spans with BT-72 girders.*

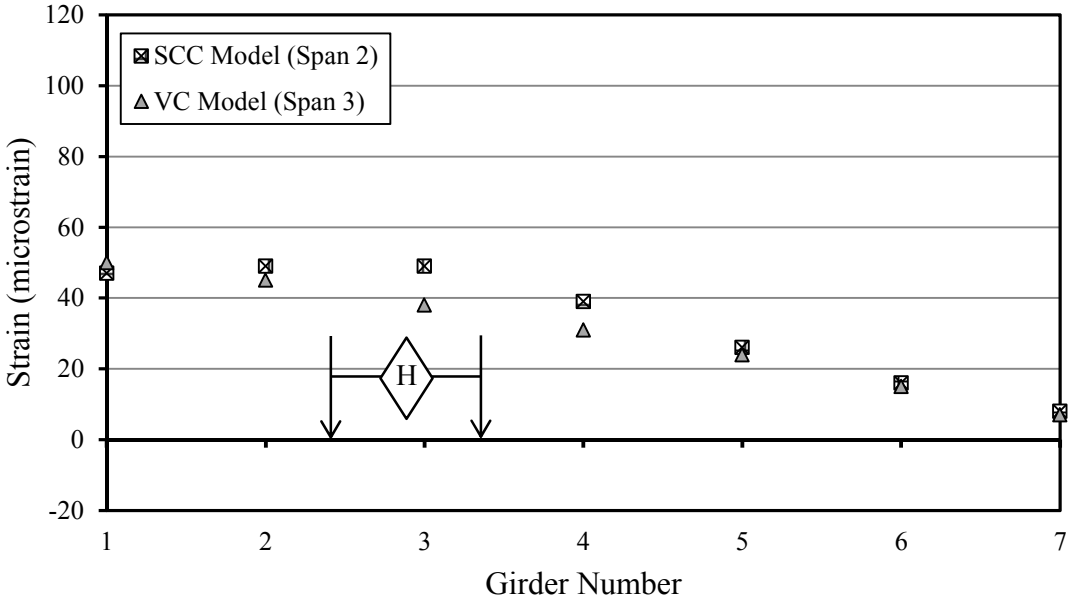

Figure E-31. *Strain results from load-truck-position H on spans with BT-72 girders.*

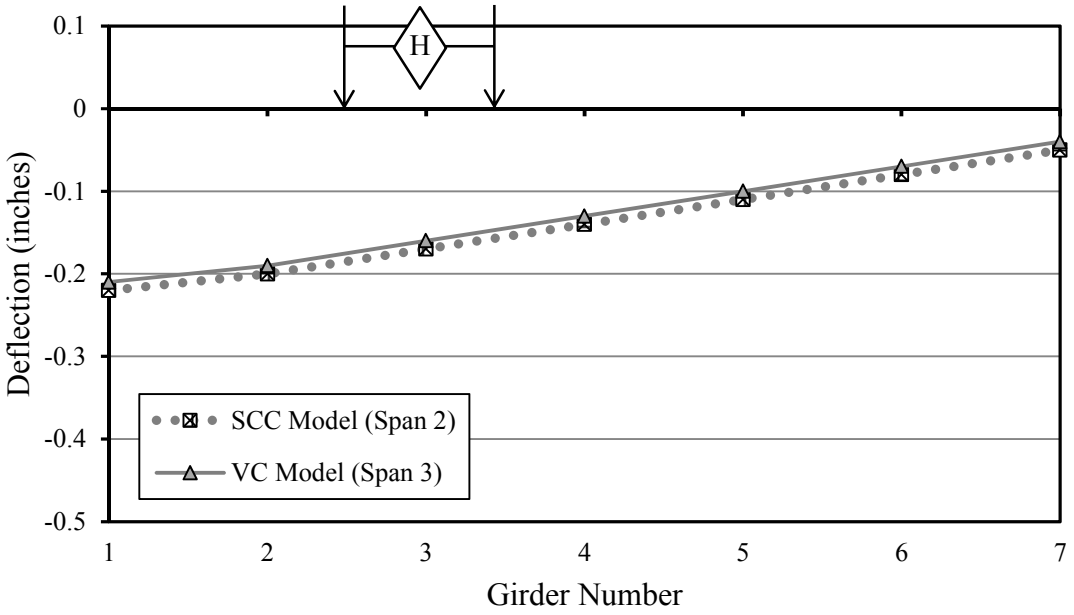

Figure E-32. *Deflection results from load-truck position H on spans with BT-72 girders.*

Appendix F:

AASHTO LRFD Section 4.6.2.2 – Load Distribution Comparisons

Table F-1. Expected strains, ε_g, calculated utilizing the equation in section 6.4.1.

	BT-54 Spans				BT-72 Spans			
	SCC (S1)		VC (S4)		SCC (S2)		VC(S3)	
	Int. με	Ext. με	Int. με	Ext. με	Int. με	Ext. με	Int. με	Ext. με
One lane Loaded (LRFD 4.6.2.2.2):	92	132	85	124	91	108	83	100
Two or more lanes loaded (LRFD 4.6.2.2.2):	128	108	118	102	130	87	119	82
One lane Loaded (LRFD C4.6.2.2.2d) (due to webwalls):		93		88		76		71
Two lanes Loaded (LRFD C4.6.2.2.2d) (due to webwalls):		119		112		97		90
Three lanes Loaded (LRFD C4.6.2.2.2d) (due to webwalls):		105		99		86		80

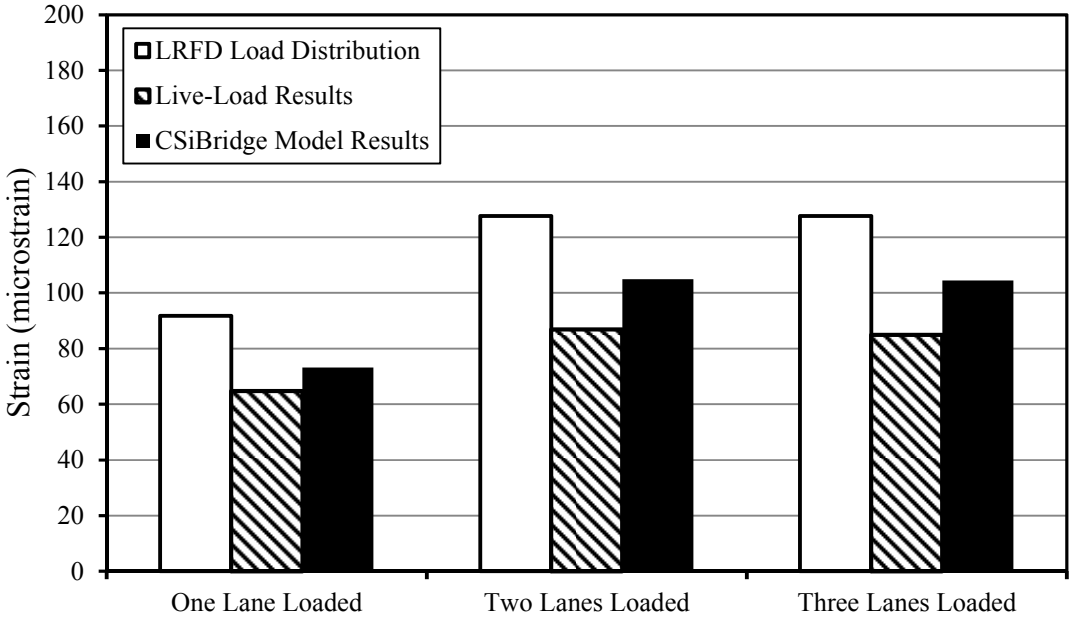

Figure F-1. *Span 1, Interior-girder, load-distribution comparisons utilizing AASHTO LRFD load distribution factors converted to strain.*

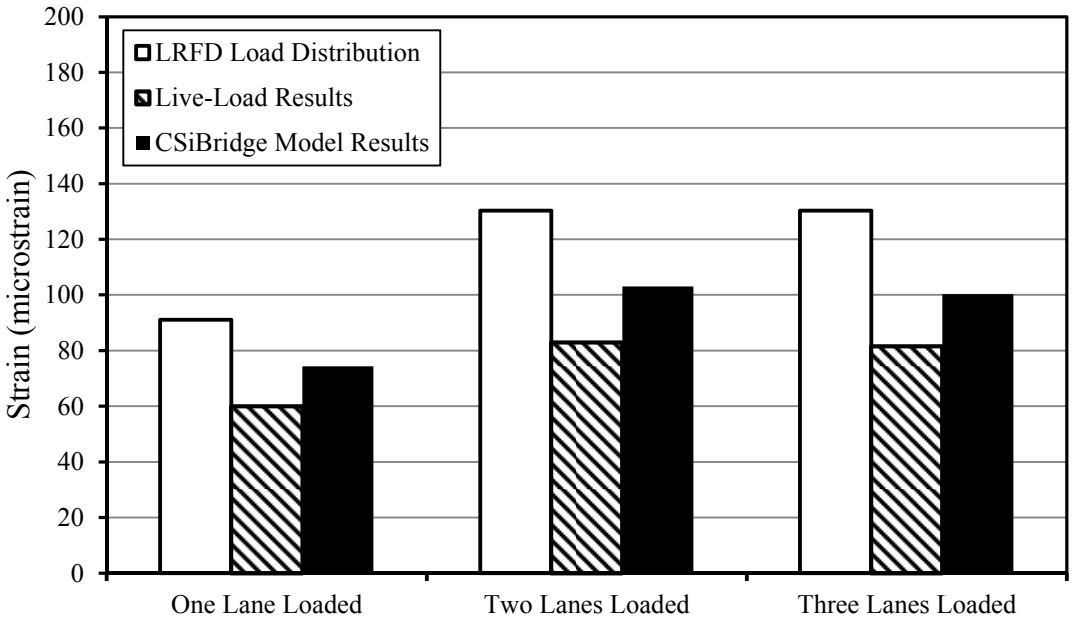

Figure F-2. *Span 2, Interior-girder, load-distribution comparisons utilizing AASHTO LRFD load distribution factors converted to strain.*

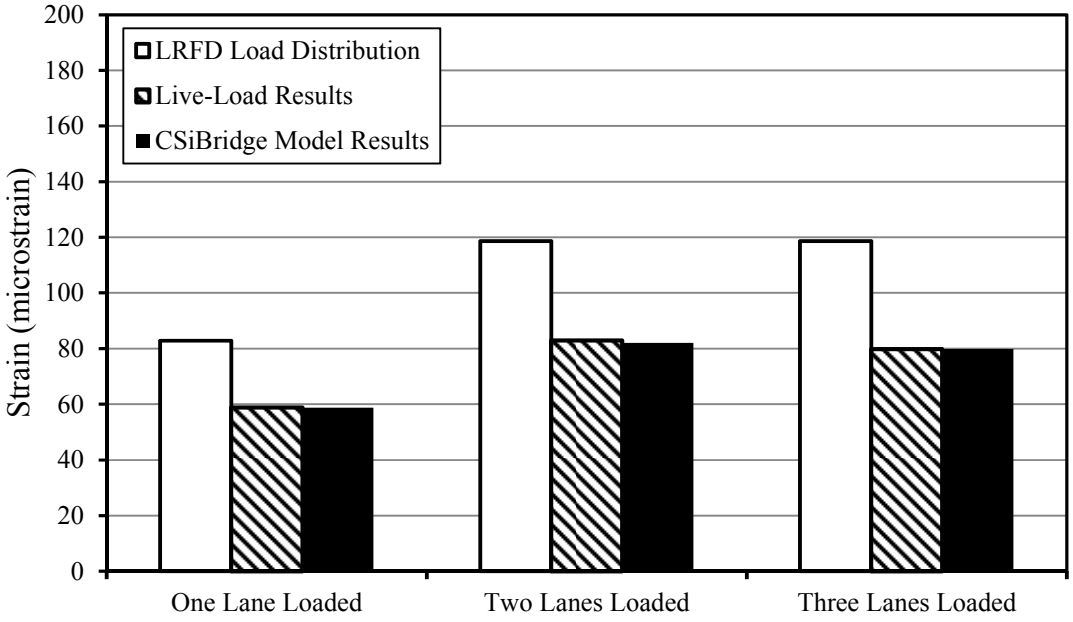

Figure F-34. *Span 3, Interior-girder, load-distribution comparisons utilizing AASHTO LRFD load distribution factors converted to strain.*

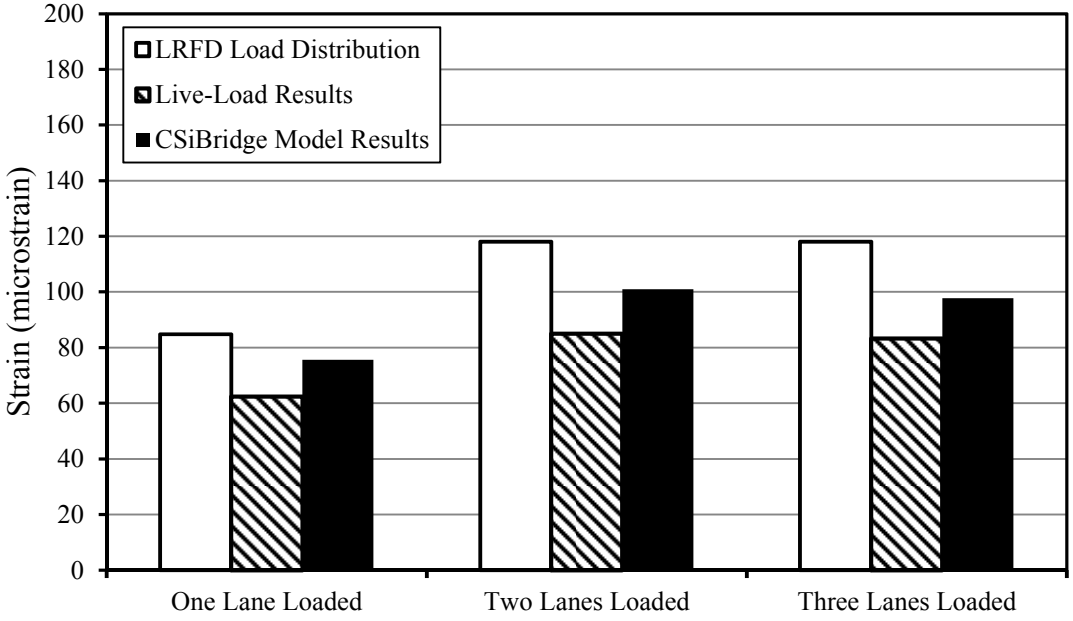

Figure F-4. *Span 4, Interior-girder, load-distribution comparisons utilizing AASHTO LRFD load distribution factors converted to strain.*

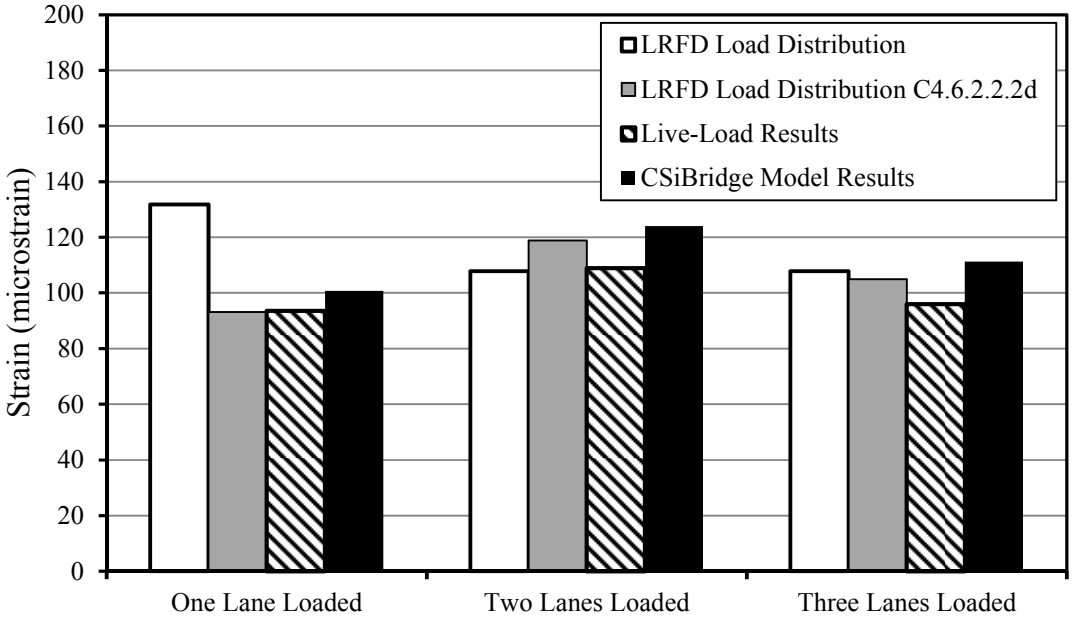

Figure F-5. *Span 1, Exterior-girder, load-distribution comparisons utilizing AASHTO LRFD load distribution factors converted to strain.*

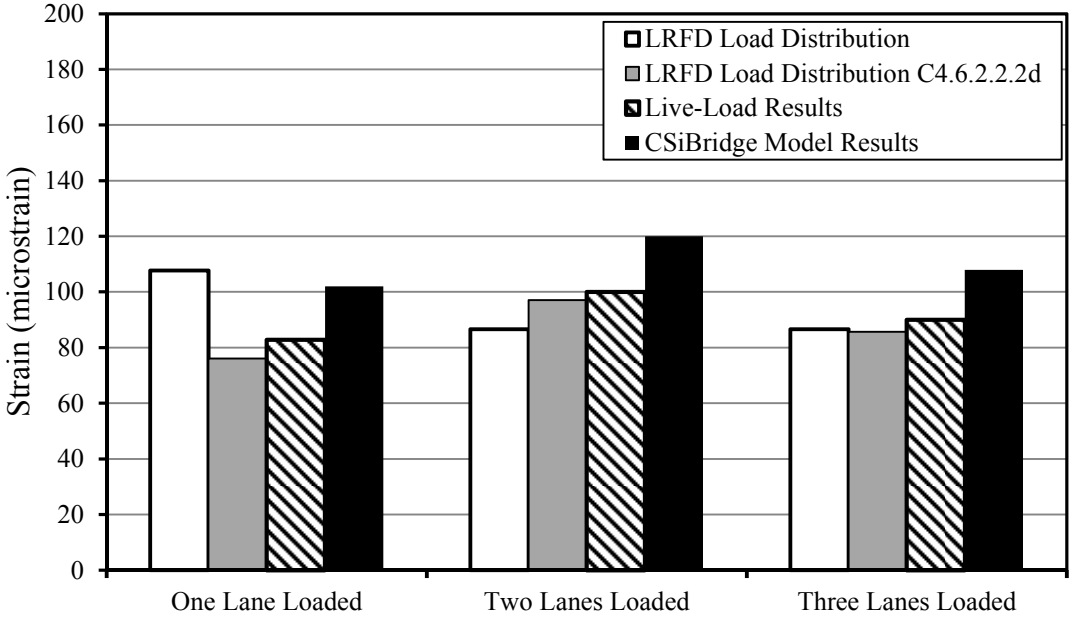

Figure F-6. *Span 2, Exterior-girder, load-distribution comparisons utilizing AASHTO LRFD load distribution factors converted to strain.*

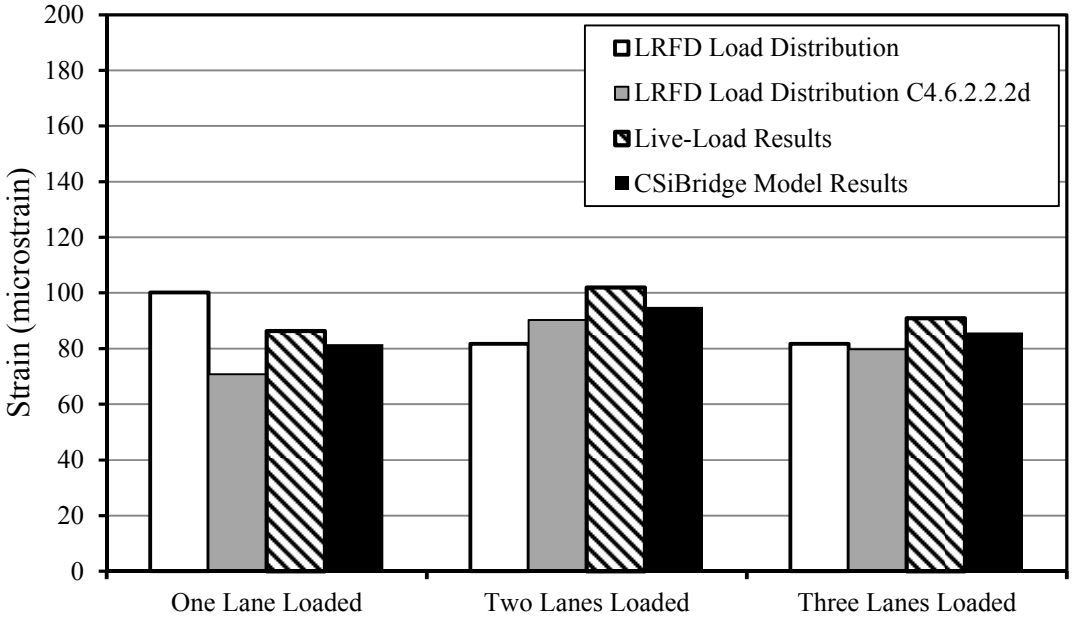

Figure F-7. *Span 3, Exterior-girder, load-distribution comparisons utilizing AASHTO LRFD load distribution factors converted to strain.*

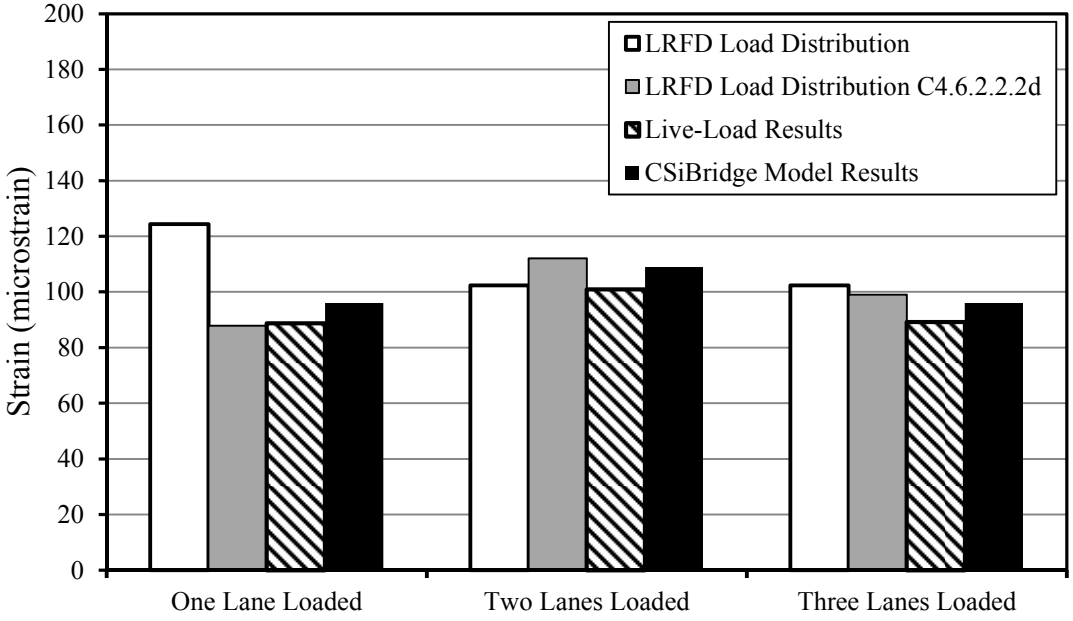

Figure F-8. *Span 4, Exterior-girder, load-distribution comparisons utilizing AASHTO LRFD load distribution factors converted to strain.*

Appendix G:

Load Test Results to Determine Performance after One Year of Service

Table G-1. Span 1 (SCC) results from load tests 1 and 2.

	S2 G1		**S2 G2**		**S2 G3**		**S2 G4**		**S2 G5**		**S2 G6**		**S2 G7**	
Load Truck Position	Load Test 1													
	Defl.	Strain	Defl.	Strain	Defl.	Strain	Defl.	Strain	Defl.	Strain	Defl.	Strain	Defl.	Strain
	in.	με	in.	με	in.	με	in.	με	in.	με	in.	με	in.	με
A	0.02	-7	0.00	0	-0.03	9	-0.07	19	-0.12	37	-0.17	54	-0.22	78
E	-0.02	8	-0.04	16	-0.07	24	-0.09	34	-0.10	35	-0.09	33	-0.09	31
H	-0.11	39	-0.12	37	-0.11	38	-0.09	29	-0.06	21	-0.04	13	-0.01	4
	S2 G1		**S2 G2**		**S2 G3**		**S2 G4**		**S2 G5**		**S2 G6**		**S2 G7**	
Load Truck Position	Load Test 2													
	Defl.	Strain	Defl.	Strain	Defl.	Strain	Defl.	Strain	Defl.	Strain	Defl.	Strain	Defl.	Strain
	in.	με	in.	με	in.	με	in.	με	in.	με	in.	με	in.	με
A	0.03	-7	0.00	0	-0.02	7	-0.05	17	-0.10	36		53	-0.21	79
E	-0.03	7	-0.05	16	-0.07	24	-0.10	35	-0.10	35		33	-0.09	31
H	-0.10	39	-0.11	38	-0.10	36	-0.09	30	-0.06	20		13	-0.01	4

Table G-2. Span 4 (VC) results from load tests 1 and 2.

	S4 G1		**S4 G2**		**S4 G3**		**S4 G4**		**S4 G5**		**S4 G6**		**S4 G7**	
Load Truck Position	Load Test 1													
	Defl.	Strain	Defl.	Strain	Defl.	Strain	Defl.	Strain	Defl.	Strain	Defl.	Strain	Defl.	Strain
	in.	με	in.	με	in.	με	in.	με	in.	με	in.	με	in.	με
A	0.03	-7	0.03	1	-0.02	8	-0.05	19	-0.11	35	-0.14	52	-0.19	74
E	-0.03	9		18	-0.08	26	-0.12	37	-0.12	38	-0.11	34	-0.12	27
H	-0.12	40	-0.12	38	-0.13	38	-0.11	29	-0.08	23	-0.06	13	-0.02	4
	S4 G1		**S4 G2**		**S4 G3**		**S4 G4**		**S4 G5**		**S4 G6**		**S4 G7**	
Load Truck Position	Load Test 2													
	Defl.	Strain	Defl.	Strain	Defl.	Strain	Defl.	Strain	Defl.	Strain	Defl.	Strain	Defl.	Strain
	in.	με	in.	με	in.	με	in.	με	in.	με	in.	με	in.	με
A	0.02	-7	0.00	2	-0.02	8	-0.07	20	-0.10	36		54	-0.20	76
E	-0.02	8		17	-0.07	24	-0.10	36	-0.11	37		33	-0.09	33
H	-0.10	39		37	-0.12	38	-0.10	28	-0.07	23		13	-0.02	4

Table G-3. Span 2 (SCC) results from load tests 1 and 2.

	S2 G1		**S2 G2**		**S2 G3**		**S2 G4**		**S2 G5**		**S2 G6**		**S2 G7**	
Load Truck Position	Load Test 1													
	Defl.	Strain	Defl.	Strain	Defl.	Strain	Defl.	Strain	Defl.	Strain	Defl.	Strain	Defl.	Strain
	in.	με	in.	με	in.	με	in.	με	in.	με	in.	με	in.	με
A	0.05	-11	0.01	0	-0.05	11	-0.09	20	-0.15	35	-0.21	50	-0.27	69
E	0.05	12	-0.07	18	-0.10	23	-0.12	28	-0.14	31	-0.14	34	-0.15	31
H	0.18	41	-0.17	38	-0.15	32	-0.12	25	-0.09	19	-0.07	13	-0.03	6
	S2 G1		**S2 G2**		**S2 G3**		**S2 G4**		**S2 G5**		**S2 G6**		**S2 G7**	
Load Truck Position	Load Test 2													
	Defl.	Strain	Defl.	Strain	Defl.	Strain	Defl.	Strain	Defl.	Strain	Defl.	Strain	Defl.	Strain
	in.	με	in.	με	in.	με	in.	με	in.	με	in.	με	in.	με
A	0.05	-9	0.00	0	-0.05	9	-0.09	22	-0.15	35	-0.20	50	-0.28	70
E	-0.06	12	-0.07	17	-0.10	22	-0.12	29	-0.13	32	-0.13	35	-0.14	32
H	-0.19	41	-0.15	39	-0.14	31	-0.11	24	-0.09	19	-0.06	13	-0.03	6

Table G-4. Span 3 (VC) results from load tests 1 and 2.

	S3 G1		**S3 G2**		**S3 G3**		**S3 G4**		**S3 G5**		**S3 G6**		**S3 G7**	
Load Truck Position	Load Test 1													
	Defl.	Strain	Defl.	Strain	Defl.	Strain	Defl.	Strain	Defl.	Strain	Defl.	Strain	Defl.	Strain
	in.	με	in.	με	in.	με	in.	με	in.	με	in.	με	in.	με
A	--	-9	0.00	0	-0.05	10	-0.1	20	-0.15	31	-0.22	49	-0.27	72
E	--	11	-0.08	18	-0.11	24	-0.12	30	-0.16	34	-0.15	34	-0.18	30
H	--	38	-0.17	41	-0.15	38	-0.13	27	-0.09	18	-0.06	12	-0.04	6
	S3 G1		**S3 G2**		**S3 G3**		**S3 G4**		**S3 G5**		**S3 G6**		**S3 G7**	
Load Truck Position	Load Test 2													
	Defl.	Strain	Defl.	Strain	Defl.	Strain	Defl.	Strain	Defl.	Strain	Defl.	Strain	Defl.	Strain
	in.	με	in.	με	in.	με	in.	με	in.	με	in.	με	in.	με
A	--	-10	--	--	--	8	--	21	--	33	--	47	--	73
E	--	11	--	--	--	20	--	29	--	28	--	32	--	35
H	--	37	--	--	--	33	--	28	--	19	--	13	--	8

Note: None of the values in the table were manipulated according to Chapter 6 Section 3.
-- = No value recorded due to missing or malfunctioning gauge.

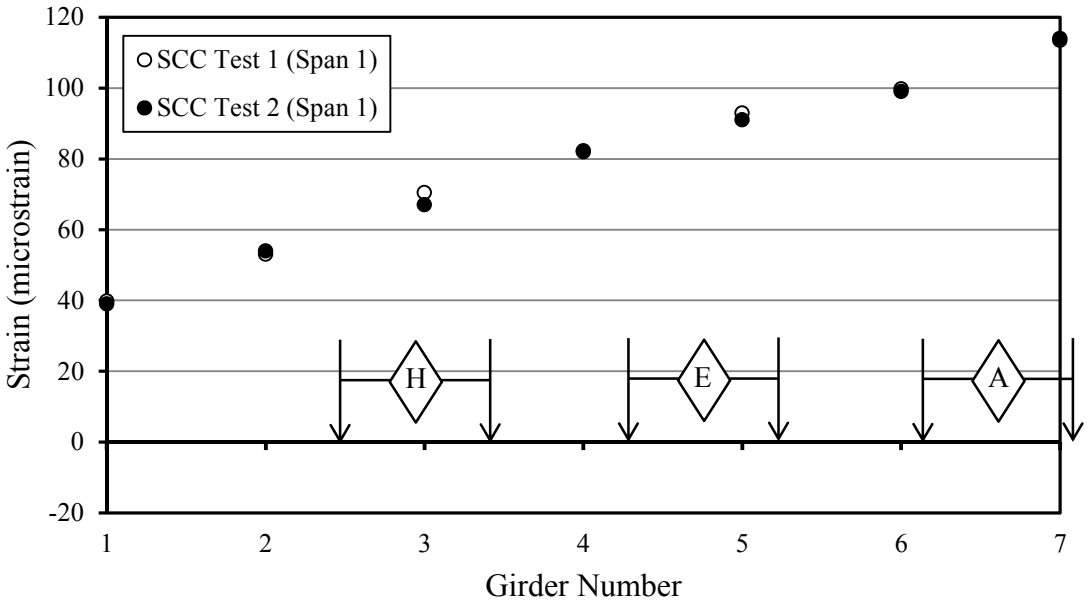

Figure G-1. *Bottom-surface strains from the superposition of three trucks (A+E+H) on span 1 of the bridge from both the first and second load tests.*

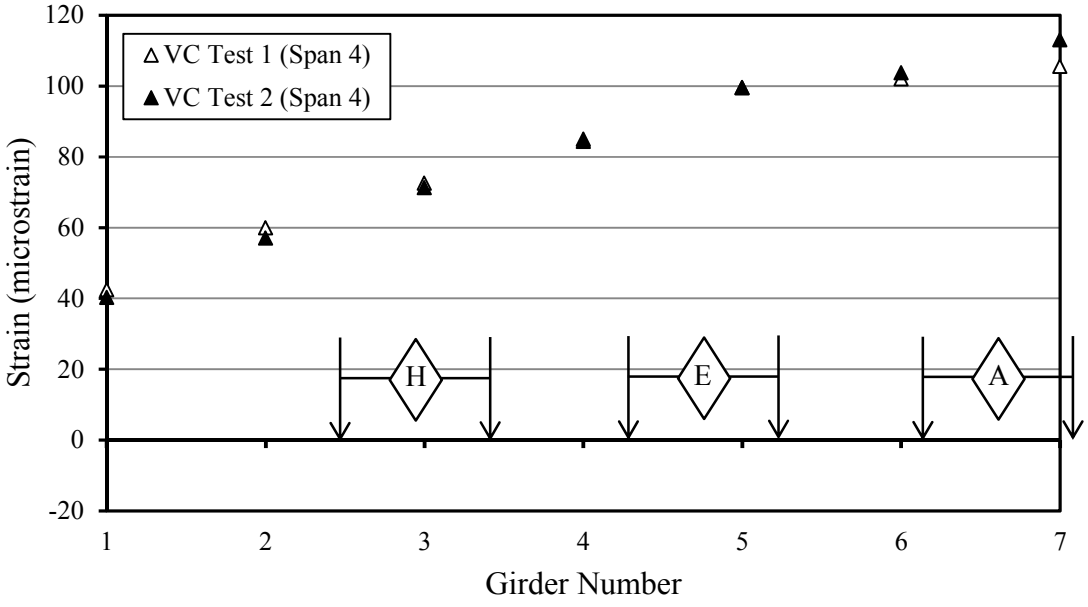

Figure G-2. *Bottom-surface strains from the superposition of three trucks (A+E+H) on span 4 of the bridge from both the first and second load tests.*

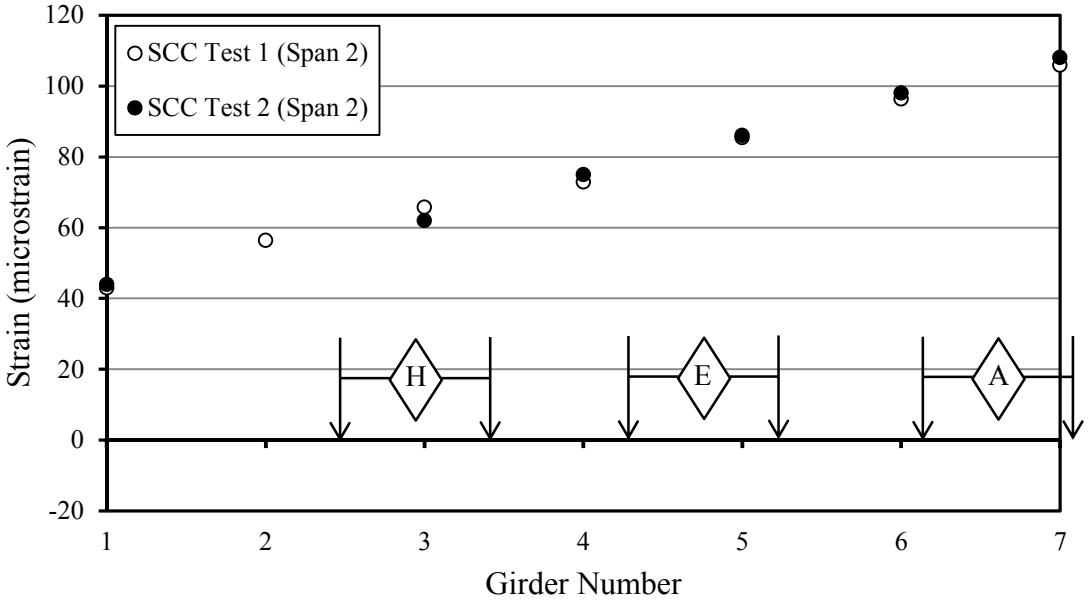

Figure G-3. *Bottom-surface strains from the superposition of three trucks (A+E+H) on span 2 of the bridge from both the first and second load tests.*

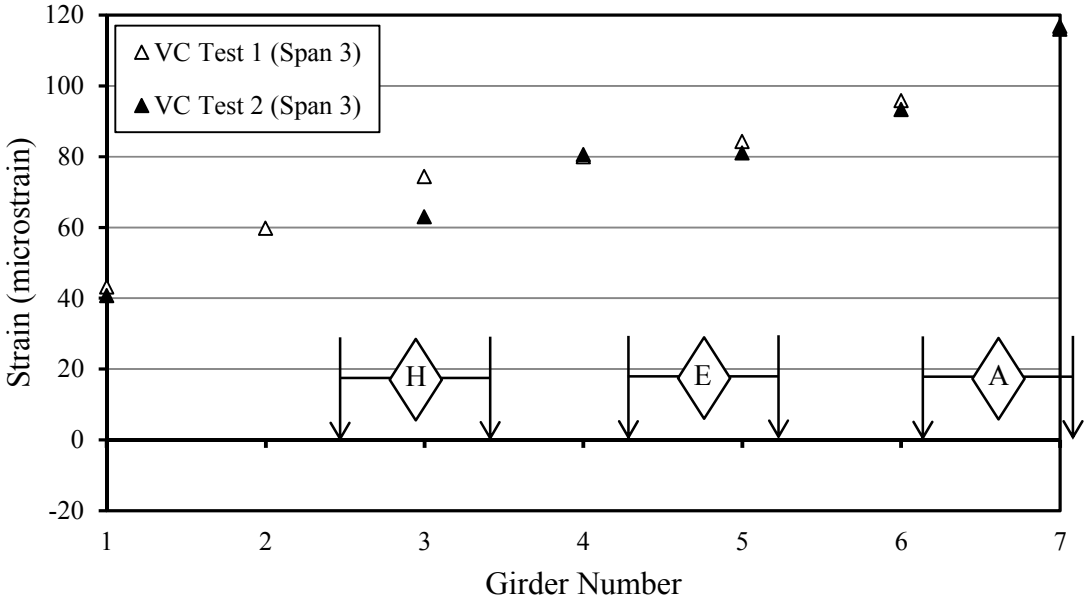

Figure G-4. *Bottom-surface strains from the superposition of three trucks (A+E+H) on span 3 of the bridge from both the first and second load tests.*